Experimental Study and Numerical Modeling of Diffusion and Reaction Behaviour

in

Cement-based Composites under Sulphate Attack

by

Chiqian Ou

A thesis submitted in partial fulfillment of the requirements for the degree of

Master of Science

In

Structural Engineering

Department of Civil and Environmental Engineering

University of Alberta

ABSTRACT

This thesis describes several approaches evaluating the resistance of cement-based composites under adverse external-sourced sulfate attack. The conventional approach of evaluation by means of measuring expansion was discussed in comparison with the sulfate diffusion, which was quantified as a function of depth. A numerical model was established to simulate the diffusion-reaction behavior of sulfate ingress with the results of sulfate diffusion. Particularly, a visual assessment on sulfate diffusion by image analysis was originally developed by the author. The results from visual assessment were corroborated to the results from expansion measurement and numerical model.

Besides CSA Types GU and HS cement, a 30:70 blend of fly ash and cement Type GU was also examined. The specimens so produced were immersed in a sulfate solution as per ASTM C1012 and retrieved variously after 7, 14, 28, 56 and 84 days of exposure. A control group was set with the specimens submerged in water environment in comparison.

As expected, Type HS cement performed best with minimum expansion and sulfate ingress, as well as the sulfate diffusion area detected in image analysis. On the other hand, the Type GU cement showed lower expansion and sulfate ingress in comparison to the fly ash blended binder. Although bearing identical porosity, the blended binder had the smallest median pore size. Therefore, the sulfate ingress and consequent ettringite production likely cracks the blended system more than the other two. Significantly, after longer durations of sulfate exposure, the blended system showed higher tensile strength which implies a healing of cracks through ettringite formation whereas sulfate exposure had limited effect to the compressive strength of all the binders examined.

ACKNOWLEDGEMENTS

TABLE OF CONTENTS

LIST OF FIGURES

LIST OF TABLES

LIST OF SYMBOLS

Chapter 3:

ΔL=change in length at *x* age, %

L$_x$=comparator reading of specimen at *x* age--reference bar comparator reading at *x* age,
L$_i$=initial comparator reading of specimen-reference bar comparator reading, at the same time,
L$_g$=nominal gauge length, or 250 mm [10 in.] as applicable.
C = compressive strength, MPa [psi],
P = maximum applied load indicated by the testing machine, N [lbf]
D = diameter of the compressive cylinder, mm [in.].

T = split tensile strength, MPa [psi],

l = length of the splitting tensile cylinder, mm [in.]

d = diameter of the splitting tensile cylinder, mm [in.].

GU = General Use type cement

HS = High Sulfate Resistance type cement

IC = InterCem type cement

W/S = specimen exposed to water/sulfate (unexposed/exposed)

#W = age of the specimen when testing, i.e. 1W=1week.

Chapter 4:

H_L= the thickness of layer in drill hole (mm)

D = diameter of the drill bit/drill hole (mm)

A = area of the drill hole (mm)

A$_{ai}$ = actual vertical area at any layer of drill hole (2D model)

A$_{ei}$ = equivalent vertical area at any layer of drill hole (2D model)

b_{i1}, b_{i2} = two measured depths of hole wall at *i* layer (mm)

a_i = measured maximum depth in the center of hole at *i* layer (mm)

x_i = depth from surface to the equivalent centroid at *i* layer (mm)

$\zeta = 0.9$, Coefficient containing operation loss

$V = 4 \cdot A \cdot h$, Volume of 4 holes with depth of *h*

R = the radius of the drill bit/drill hole (mm)

H = the height of the drill bit tip (mm)

$\bar{x} = \left(3/4\right) \cdot H$, the distance from body center to the bottom of circular cone

$A_b = \pi \cdot R^2 / 4$, the bottom area of drill hole (mm^2)

X_{Li} = equivalent extraction depth at i layer (mm)

$H_i = a_i - (b_{i1} + b_{i2})/2$, height of circular cone at i layer (mm)

$h_i = \left(b_{i1} + b_{i2}\right)/2$, the depth of cylindrical hole at i layer (mm)

$i \in [1, N]$, $N \rightarrow$ Number of layers

Chapter 5:

$Weight_1$ = the weight of Gooch crucible unit

$Weight_2$ = the weight of Gooch crucible unit with $BaSO_4$ precipitate

$Weight_P$ = the weight of extracted sample of each layer

C_s = sulfate molar concentration in titrated sample (mol / m^3)

$n_{SO_4^{2-}} / n_{BaSO_4}$ = amount-of-substance of precipitated sulfate (mol)

$V_{c.m.}$ = volume of powdered sample per layer (mm^3)

m_{BaSO_4} = weight of barium sulfate precipitate obtained per layer (g)

$m_{c.m.}$ = weight of powdered sample per layer (g)

$\rho_{c.m.}$ = density of cement mortar sample (g/mm^3)

Chapter 6:

D = Diffusion Coefficient of Matrix [m^2/sec]

C = Sulfate Concentration in the matrix [mol/m^3]

C_S = Sulfate Concentration in the environment/at the edge [mol/m^3]

t = Exposure duration [day]

$U_{i,j}$ = Sulfate concentration at i time, j distance in the matrix [mol/m^3]

Δt = time step in the finite difference methods [day]

Δx = space step in the finite difference methods [mm]

Δt = time step in the finite difference methods [day]

$erf(x)$ = error function employed for exact solution

i = space at any location within $L = 2n$

j = time at any location within $T = m$

$[A_U]$ = initial matrix of implicit iteration

$\{U_{,j}\}$ = Vector contain concentrations at j time

$[A_U']$ = modified [n×n] matrix from initial one

$\{U_{IM/CN}\}$ = compensated [n×1] order vector for modified matrix

$[B_U]$ = the second matrix established in Crank-Nicolson method

r = the iteration coefficient defined as $r = D \cdot \dfrac{\Delta t}{(\Delta x)^2}$ in FDM

Chapter 7:

λ = Reaction Proportional Coefficient

C = Concentration of Tricalcium Aluminate C_3A

$Z = U - \lambda \cdot C$

1   INTRODUCTION

1.1 BACKGROUND

General Statement. Concrete deterioration due to sulfate attack is one of the most severe durability problems. This type of deterioration is noted in the structures exposed to sulfate-bearing soils and groundwater. Though concrete deterioration due to sulfate attack is reported from many countries, the mechanisms of sulfate attack have not been thoroughly investigated. Sulfate attack on concrete is a complex process including chemical reactions. Many factors, such as cement type, sulfate attack type, sulfate concentration and exposure duration may affect the sulfate resistance (Al-Dulaijan et al. 2003).

The strategy of this thesis is to evaluate the resistance to external sulfate attack of cement-based structure by means of identifying sulfate diffusion inside the structure or specimen after sulfate exposure. On the other hand, the diffusion depth of external sulfate was designed to be obtained through experiments, which manifests the resistance to external sulfate diffusion of the examined cement-based composites. The determination of sulfate diffusion after sulfate exposure is the main work in this thesis. Experimental program was developed to retrieve the sulfate profiles as a function of diffusion depth. Furthermore, the visual assessment was created to identify the maximum diffusion depth under sulfate exposure. The diffused sulfate content and the diffusion depth, selected as the evaluation indicators of sulfate resistance in this work, are introduced to calibrate the numerical model that is created to predict the cracking development and service life of cement-based structures. With the mechanical properties, tensile stress-strain response in this case, and air-void networks of the cement-based composites, the numerical model is able to predict the cracking depth after varying durations of sulfate exposure, which helps engineers to better understand the service life of cement-based structure or concrete cover.

Mechanism of the Sulfate Attack Process. During varied types of sulfate attack, expansion caused by ettringite formation is the most widely recognized mechanism of sulfate attack in literature (Wang 1994). However, some researchers indicated that the gypsum formation during sulfate attack might be expansive whereas it is not considered in this study (Tian and Cohen 2000). The study by Santhanam M et al. (Santhanam et al. 2002) suggested that the expansion of mortars in sodium sulfate solution follows a two-stage process. In the initial stage, Stage 1, there is little expansion. This is followed by a sudden and rapid increase in the expansion in Stage 2. This work is intended to include these mechanisms into a numerical model that describes the diffusion reaction process.

Cement-based Composites and Mineral Admixtures. The effect of pozzolanic admixtures to the sulfate attack resistance has been studied. It is widely accepted that the replacement of fly ash and silica fume effectively improved the resistance of the mortar to the sulfuric acid and sulfate solution attack (Torii and Kawamura 1994). High fly ash content concrete with replacement level of 50% was steadily gaining the compressive strength, and no detectable deterioration was observed. Chemical analysis data also showed that the excellence of high fly ash content concrete in the sulfate resistance was attributed primarily to the prevention of ingress of sulfate ions into concrete, resulting in little formation of gypsum and/or ettringite in concrete (Torii et al. 1995). In this work, a blended binder IC with 30% fly ash replacement and 70% CSA Type GU cement was examined for its resistance to sulfate attack as well as the mechanical properties.

Simulation through Numerical Model. Numerical models simulated for sulfate attack process were developed by researches. The numerical model established in this study is broadly based on the approximation method developed by Tixier R, Mobasher B (Tixier and Mobasher 2003; Tixier and Mobasher 2003). However, strain expansion was employed

in the model to fit the experimental results. Study by Sun C et al. (Sun et al. 2013) conducted the sulfate concentration as the indicator to fit the numerical model. An experimental study was perfromed by Sun C on the diffusion of sulfate ions in concrete. In this study, the mechanism of sulfate attack developed by Tixier R, Mobasher B was used in the numerical model as the fundamental theory of sulfate diffusion.

Visual Assessment on External Sulfate Attack. The existing evaluation approaches upon external sulfate attack are either mechanical-based or chemical-based considering the volumetric expansion or chemical composition in the cement-based system. A convenient visual assessment on sulfate attack was preliminarily developed by the author by means of capturing and analyzing the images of cross section. New technologies are necessary for quick assessment on durability issue of external sulfate attack.

It is expected that the data base that results from this study will lead to a better understanding of the sulfate attack resistance of cement-based composites in general, and the factors influencing the sulfate diffusion in particular. This study should also make it possible to develop a more reliable analytical numerical model to predict the crack initiation of cement-based composites under adverse sulfate-rich environment.

1.2   PROBLEM STATEMENT

The effect of mineral admixtures contained in cement-based composites has been the subject of intensive study for decades. Limited information has been generated so far on the numerical simulation of diffusion reaction behavior during sulfate attack, especially by varying exposure durations to external sulfate environment. As a result, many fundamental questions, such as the following, remained unanswered:

Problems upon cement-based composites.

■ Why the CSA Type HS (high sulfate resistant) cement is highly preferred for the concrete structures exposed to external sulfate attack? Is it physically or chemically resistant to sulfate diffusion, or physicochemical?

■ How does the fly ash admixture affect the sulfate resistance of cement-based composites? Does the fly ash facilitate the resistance to external sodium sulfate attack?

Problems upon simulation through numerical model.

■ How to develop the diffusing-based numerical model including chemical reactions inside cement-based composites?

■ What kind of approximation method is preferred to simulate the diffusion-reaction behavior under external sulfate attack?

■ What parameters in the model are supposed to be revised when fitting experimental data to the model?

■ How to calculate the volumetric change caused by the ettringite production and the strain-stress response as affected by external sulfate attack?

This study addresses the above questions in detail to lead to a better and more reliable understanding of the factors affecting the resistance to sulfate attack of cement-based composites.

1.3 RESEARCH OBJECTIVES

In order to fill the knowledge gaps identified above, the objectives of this study are:

■ To evaluate the mechanical properties and air-void networks of chosen cement-based composites both exposed to sulfate environment and immersed in water.

■ To evaluate the sulfate attack resistance conventionally by means of measuring the length changes/expansions.

■ To precisely extract the powdered samples at defined depth inside cement-based composites after varying exposure durations to sulfate environment.

■ To develop the sulfate determination method and precisely get the sulfate concentrations in the extracted powdered samples.

■ To establish the basic numerical model employing Finite Difference Method (FDM) and compare the accuracy of several approximation methods.

■ To include chemical reactions during sulfate attack process into the numerical model and fit the experimental sulfate concentration results to the finalized model.

■ To develop the volumetric expansion due to ettringite production and achieve the service life prediction of cement-based composites based on the expansive strain-stress response. (if possible)

■ To develop, or discover novel evaluation approaches of sulfate attack. If possible, investigate the link to the numerical model.

1.4 SCOPE OF THE STUDY

This thesis is intended to address the following:

- Conventionally measure the length change of prismatic specimen and mechanical properties after varying exposure durations to sulfate environment.

- Experimentally detect the sulfate concentration at defined depth inside the cylindrical specimen by titration experiment inside extracted sample after varying exposure durations to sulfate environment.

- Establish the numerical model on diffusion reaction behavior under external sulfate attack and fit to the experimental results.

- Develop the visual evaluation on sulfate diffusion by image analysis.

1.5 SIGNIFICANCE OF THE STUDY

Resistance to external sulfate attack of cement-based composites has been the subject of many studies but not much data is available on the diffusion reaction behavior of sulfate ingress, and the effect of various factors on the to the sulfate attack resistance.

This research project was designed primarily to bridge gaps between the experimental sulfate concentration and numerical model as ascertained during the literature review, especially the understanding of the various factors influencing not only the resistance to sulfate attack but the mechanical properties.

Further, the investigation on the color variation inside captured images caused by external sulfate diffusion reveals that image analysis is supposed to be a convenient and reliable

evaluation approach on sulfate attack. In particular, two analyzing method were developed with detailed mechanism of diffusion depth identification.

In addition, the established numerical model is defined as the fundamental part of the simulation for service life prediction of cement-based composites, which has been well studied in the collaboration research.

1.6 THESIS ORGANIZATION

This thesis is organized into nine chapters and two appendices.

Chapter 1 provides the general introduction to this study, the problem statement, objective, scope and the research significance.

Chapter 2 reviews and discusses in detail the published literature on various aspects of evaluation approaches, numerical simulation, cement-based composites, and the presence of pozzolanic admixture. The literature on the physical properties, expansion measurements, evaluation techniques, numerical model and the microstructure have been dealt with in detail. The chapter examines the theoretical models used for sulfate attack process, and also identifies their limitations.

Chapter 3 describes physical properties and shrinkage performances of three examined cements subjected to sulfate-rich environment. Besides CSA Types GU and HS, a 30:70 blend of fly ash and cement Type GU was also examined. The specimens so produced were immersed in a sulphate solution as per ASTM C1012 and retrieved variously after 7, 14, 28, 56 and 84 days of exposure. The length change, porosity, compressive and splitting tensile strengths were retrieved in comparison with unexposed case. Although bearing identical porosity, the blended binder had the smallest median pore size.

Chapter 4 describes an originally developed method for powdered sample extraction by varying depths inside hardened cement samples. Additionally, the simulation of drilled layer and equivalent depth of each layer were achieved after powdered samples were extracted. The extraction depth was controlled either manually or automatically, which depended on the research purpose. Specifically, impact hand drill and concrete drill bit of 1 inch diameter were employed for extraction in this study. And the thickness of each layer extracted was controlled between 2 mm to 4 mm for high precision of equivalent depth and the maximum depth extracted was 12 mm. This method has its potential to provide powdered samples with precise locations inside cement or concrete structures in research area of durability issues like sulfate attack, chloride corrosion and carbonation. Extracted powder can be grinded to finer granularity depending on the research purposes.

Chapter 5 describes the titration experiment for sulfate content inside powdered samples extracted. The titration experiment in this study was developed for dissociative sulfate concentration inside cement mortar samples. Powdered samples were tested and extracted with different depths from the surface exposed to sulfate environment. Sulfate was detected by barium chloride solution and precipitate barium sulfate was weighed then. The sulfate diffusion was quantified as a function of depth, and this was incorporated into a numerical model to determine the extent of expansion in the cement based system.

Chapter 6 establishes the basic non-reaction diffusion model by three numerical simulating methods. The fundamental diffusion mechanism of sulfate attack conformed to the Fick's Second Law that explains the process of ion diffusion in homogeneous matrix. However, the sulfate attack inside cement-based composites consists of complicated reactions with inherent compounds and it was hardly to evaluate the precision of selected approximation methods involved with these reactions. The scheme of this chapter was to firstly investigate

the accuracy of various finite methods through non-reaction diffusion and further develop the diffusion-reaction process upon several selected approximation approaches.

Since the non-reaction diffusion was mathematically solved by Error Function Solution, the simulating precisions of examined methods could be discussed in comparison with the exact solution. In this manner, only the external sulfate concentration and diffusion coefficient were taken under consideration as the parameters in the present modeling. The errors caused by finite difference methods were investigated for further development of sulfate attack modeling.

Chapter 7 describes the specific numerical model involved with chemical reactions, which was extended from the physical diffusion model as demonstrated in Chapter 6. Explicit stencil of finite difference methods was chosen for its high simulating precision and convergence. Sulfate ingress from external environment, after consumed by the internal compositions, was obtained through improved model in order to fit the experimental results from titration experiments. In addition, the effects caused by several parameters in the modeling were discussed and compared. As a result, some revisions were proposed and the numerical modeling was calibrated considering the real diffusion conditions.

Chapter 8 describes the visual assessment of sulfate diffusion by analyzing the captured image of cross section. Two evaluation approaches were developed based on the color variation inside cement-based composites under sulfate attack. Firstly, area Ratio Method was developed to calculate the diffusion depth by means of comparing the diffused and undiffused areas based on the color contrast. Additionally, grayscale Variation Method was developed based on the grayscale variations along diameters inside the captured image. A

fuzzy synthetic evaluation model was introduced to assess the scale variation. The results obtained by these two approaches were compared and sulfate diffusion depth was retrieved.

Chapter 9 firstly draws the conclusions based on current findings upon several evaluation methods on resistance to sulfate attack. Besides, the limitations of these approaches were listed for the purpose of further applications. In the end, future research on cement-based composites, numerical modeling, and visual assessment was sketched considering the potentials and limitations of this thesis.

2 LITERATURE REVIEW

2.1 INTRODUCTION

In this chapter, the relevant literature for cement-based composite, its constituent materials, mechanical properties, diffusion-reaction mechanisms, and simulating models under adverse sulfate attack are reviewed. In addition, previous research on chemical analysis in cement-based composites during sulfate attack is also discussed for the ettringite production.

2.2 FACTORS INFLUENCING THE SULFATE RESISTANCE

2.2.1 WATER-TO-CEMENT RATIO

The effect of water-to-cement ratio and mix proportion to the sulfate attack resistance has already been studied for decades. Study by Sahmaran M et al. reveals that the effect of w/c ratio was more pronounced for the low sulfate resistant cements with higher C_3A amounts, while the blended cements were less affected by an increase in the w/c ratio (Sahmaran et al. 2007). High C3A content cement, such as CSA type GU cement, was examined to be more susceptible to sulfate attack with higher water-to-cement ratio.
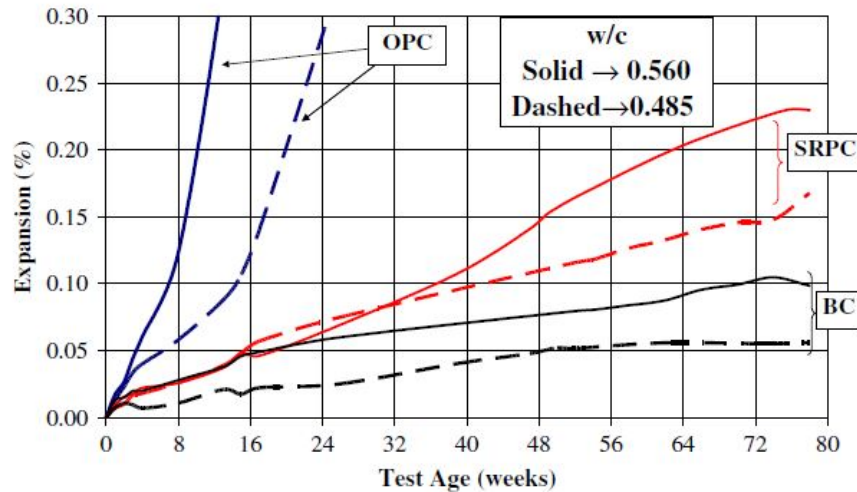
Figure 2.1 Expansion of mortar bars (Sahmaran et al. 2007)

As shown in Figure 2.1 Expansion of mortar bars (Sahmaran et al. 2007), ordinary Portland cement (OPC), sulfate resistant Portland cement (SRPC) and a blend cement (BC) with natural pozzolan and fly ash were examined for length changes subjected to sulfate attack with two varied water-to-cement ratio of 0.560 and 0.485.

Similarly in this study, the water-to-cement ratio was chosen to 0.485 in order to make sure that the prismatic specimen was not deteriorated due to adverse sulfate attack.

2.2.2 C_3A AND GYPSUM CONTENT

According to the chemical reactions inside cement-based composite subjected to sulfate attack, the inherent C_3A and Gypsum content was studied as the main compound that governed the maximum ettringite production.

The mechanism of adverse sulfate attack to cement-based composites has been studied in detail by civil and material researchers. Expansion caused by ettringite formation is the most widely recognized mechanism of sulfate attack in literature. The chemical reactions inside Portland cement prior to hardening are listed:

$$C_3A + 3C\bar{S}H_2 + 26H = C_6A\bar{S}_3H_{32} \qquad (2.1)$$

However, if all the gypsum is consumed before the entire C_3A has reacted, then ettringite transforms to another form of calcium aluminate sulfate:

$$2C_3A + C_6A\bar{S}_3H_{32} + 4H = 3C_4A\bar{S}H_{12} \qquad (2.2)$$

The formation of monosulfate occurs because in most cements, there is not sufficient gypsum provided to consume all the C_3A into ettringite. The monosulfate, however, remains a potential risk of ettringite re-formation in the presence of further sulfate ions, for example, the external sulfate attack.

$$C_4A\bar{S}H_{12} + 2C\bar{S}H + 16H = C_6A\bar{S}_3H_{32} \qquad (2.3)$$

The transformation from monosulfate to ettringite is a highly expansive reaction as explained in the numerical modeling. Besides, some researchers mentioned that the formation of gypsum during sulfate attack also leads to expansion. (Tian and Cohen 2000) The reaction of gypsum formation is listed below:

$$Na_2SO_{4\ (external)} + Ca(OH)_2 \leftrightarrow CaSO_{4\ (gypsum)} + NaOH \qquad (2.4)$$

Ordinary Portland cement like general use type cement in this study, contains high C_3A content that is likely to form monosulfate during hardening. High sulfate resistant cement that has lower C_3A content leads to less monosulfate production. It reduces the risk of expansion when exposed to external sulfate attack.

During the period of exposure, sulfate ingress from external environment reacts with internal monosulfate and leads to volumetric expansion. In accordance with the development of numerical simulation, sulfate concentration was introduced as a featured indicator to evaluate the resistance to sulfate attack. The infiltration depth of external sulfate, as affected by exposure durations and cement types, was intended for qualitative evaluation and further data fitting to the numerical modeling.

Chemically, research by Tixier R, Mobasher B applied the series of chemical reactions into numerical modeling, Two reactants, C_3A and SO_3 (represented of gypsum in cement-based composites), were chosen and the reactions were rearranged. These three main components in several forms of calcium aluminate phases in a hydrated cement paste were considered: C_4AH_{13}, $C_4A\bar{S}H_{12}$ and residual anhydrous C_3A. The relative proportions of the components are evaluated from the C_3A, gypsum content of the cement, the cement dosage, and the degree of hydration.

The three compounds may react with sulfate ingress according to one of the following reactions (Tixier and Mobasher 2003; Tixier and Mobasher 2003),

$$C_4AH_{13}+3C\bar{S}H_2+14H \rightarrow C_6A\bar{S}_3H_{32}+CH \qquad (2.5)$$

$$C_4A\bar{S}H_{12}+2C\bar{S}H_2+16H \rightarrow C_6A\bar{S}_3H_{32} \qquad (2.6)$$

$$C_3A+3C\bar{S}H_2+26H \rightarrow C_6A\bar{S}_3H_{32} \qquad (2.7)$$

These reactions are lumped in a global sulfate phase-aluminate phase reaction as following,

$$CA + \lambda C\overline{S}H_2 + nH \rightarrow C_6A\overline{S}_3H_{32} \qquad (2.8)$$

Where CA signifies an equivalent grouping of the reacting calcium aluminates, and λ and n represent the weighted average stoichiometric coefficient of the lumped reaction for $C\overline{S}H_2$ and H respectively, obtained from the coefficients of the individual reaction. The value of λ represents the degree of initial hydration and C_3A consumption during external sulfate exposure. Accordingly, the chemical reactions during sulfate attack were combined to Eq. (2.8) that only the C3A and gypsum contents were considered as the factors that influenced the ettringite production.

Two featured cements, CSA Type GU (general use) and HS (high sulfate resistant) were chosen to evaluate their resistance to external sulfate attack. It was provided by the cement supplier that Type GU contains higher C3A content where Type HS contains extremely lower C3A content. Besides, a 30:70 blend of fly ash and cement Type GU was also examined for its sulfate resistance with mineral admixtures.

2.2.3 POZZOLANIC ADMIXTURES

The pozzolanic admixtures, such as fly ash, slag, and silica fume, are widely used as the replacement of Portland cement in order to improve the mechanical properties. It was found by Torii K et al. (Torii et al. 1995) that, from the measurements of expansion that the 50 % replacement by fly ash was very effective in the improvement of the sulfate resistance of concrete. It has been studied by Sahmaran M et al. (Sahmaran et al. 2007) that all blended cements examined containing natural pozzolanic admixtures and/or fly ash have a notable reduction in expansion at all test ages. Expansion reduction was drastic in mortars with fly ash cements.

The effect of replacement of silica fume and fly ash on resistance to sulfate attack was studied by past researchers (Torii and Kawamura 1994). The laboratory test data showed that the replacement of cement by fly ash and silica fume effectively improved the resistance of the mortar to the sulfate attack due to the high impermeability and low calcium hydroxide content in the mortar. Analysis indicated that the expansion of plain mixes were associated with the formation of both ettringite and gypsum. On the other hand, all fly ash mixes showed a good resistance to a 10 % Na_2SO_4 solution at an early stage of exposure up to 1 year since the replacement by fly ash reduced the calcium hydroxide and alumina-bearing hydrates which are most vulnerable to the sulfate attack. Furthermore, all silica fume mixes did not expand independently of the replacement percentage by silica fume during 3 years of exposure. The visual condition of these silica fume mortars was also excellent.

Results from the study by Irassar E et al. (Irassar et al. 1996) showed that mineral admixtures improved the sulfate resistance when the concrete is buried in the soil. However, concretes with high content of mineral admixtures exhibit a greater surface scaling over soil level due to the sulfate salt crystallization. The mineral admixtures used for partial replacement of ordinary Portland cement showed a greater sulfate resistance than plain concrete in the buried zone judged by visual, mechanical and mineralogical characteristics.

2.3   MECHANICAL PROPERTIES OF CEMENT-BASED COMPOSITES

2.3.1 Length Change Measurement

Based on the ASTM C1012 specification that assesses the expansion of prisms subjected to sulfate attack, the length change measurement was widely and conventionally employed to evaluate the sulfate resistance of cement-based composites (Sahmaran et al. 2007).

The adverse effects of sulphate attack on cement-based composites have been studied from the perspective of ettringite formation, gypsum and C_3A content. The sulphate resistance of conventional cement-based composites is evaluated by length change and is reflected by their mechanical response. However, the qualitative evaluation of sulphate resistance on length measurement presents the resultant change, not the mechanism of sulphate ingress from external environment (Mamun and Bindiganavile 2011).
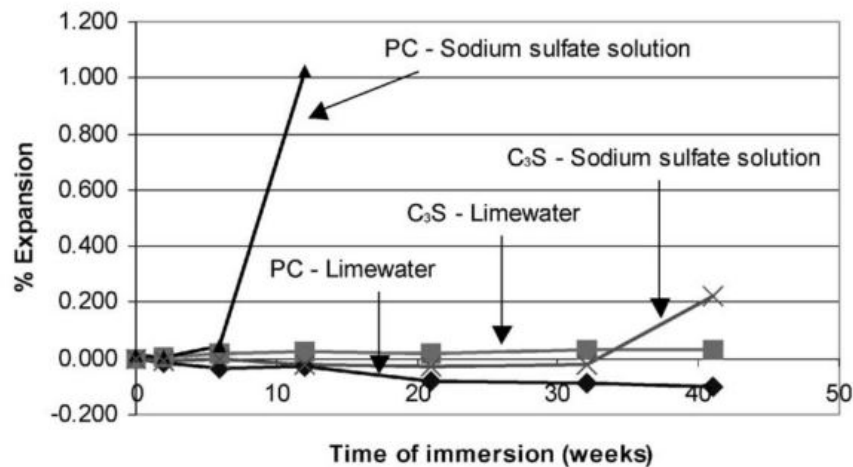
Figure 2.2. Expansion data for PC and C_3S mortars (Santhanam et al. 2003)

Study by past researchers reported that the expansion data for the Portland cement (PC) mortars stored in the limewater and sodium sulfate solutions. The PC mortars stored in sodium sulfate solution showed a high degree of expansion between the 6th and 12th week of exposure as shown in Figure 2.2. Compared with the length change of cement only contained C_3S (C_3S), Portland cement (PC) containing C_3A was more likely to expand when subjected to sulfate environment. Complete disintegration of the specimens occurred after about 16 weeks of immersion (Santhanam et al. 2003).

2.3.2 COMPRESSIVE AND SPLITTING TENSILE STRENGTH

The effect of adverse sulfate attack on compressive response was studied by previous researchers (Torii et al. 1995). It was reported that external sulfate attack had limited influence on the compressive strength of ordinary.
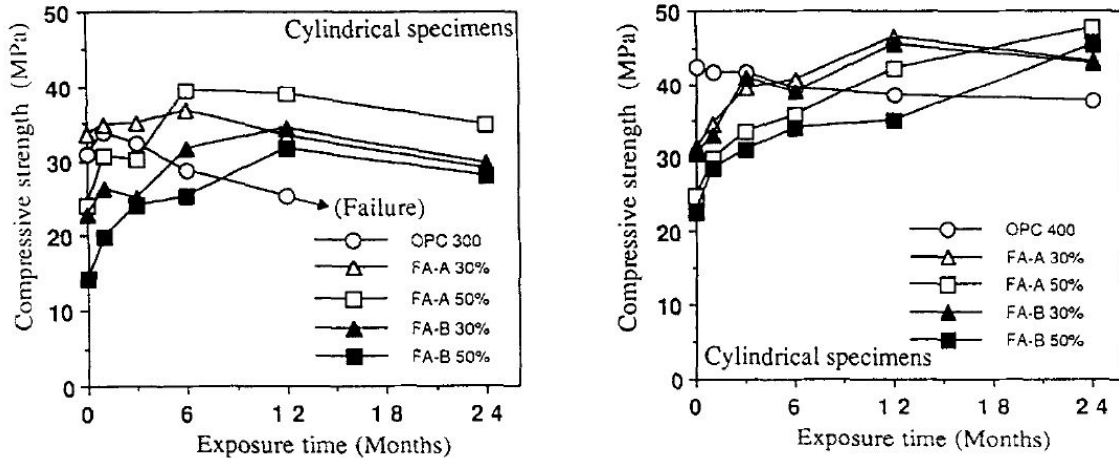
Figure 2.3. Changes in compressive strength of the concrete with the binder content of 300 kg/m^3 and 400 kg/m^3 (Torii et al. 1995)

Figure 2.3 shows changes in the compressive strength of the concrete with the binder content of 300 and 400 kg/m^3 with the exposure time, respectively. During the exposure to the 10 % Na$_2$SO$_4$ solution. the compressive strength of OPC concrete with the cement content of 300 kg/m^3 gradually decreased after 3 months of exposure, which was about 80 % relative to the 28-day old compressive strength at 1 year of exposure time, while the reduction in compressive strength in OPC concrete with the cement content of 400 kg/m^3 was not so significant even at 2 years of exposure time.

All fly ash concretes had the compressive strength greater than the 28- day old compressive strength independently of the binder content and the replacement level by fly ash when they were exposed to the 10 % Na$_2$SO$_4$ solution for 2 years. Especially, high fly ash content

concrete with the binder content of 400 kg/m^3 and with the replacement level of 50 % showed an excellent resistance to the sulfate attack, their compressive strength being successively gaining with the exposure time (Torii et al. 1995).

Results of compressive strength in the study by Mamun and Bindiganavile reveals that the outcome of sulphate exposure on the compressive strength of cement-based foams is not as significant as the effect on the flexural response (Mamun and Bindiganavile 2011).

Broadly based on the ASTM C39/39M specification that assesses the compressive response of cement-based specimens, the compressive strength of cylindrical specimens either immersed in sulfate solutions or submerged in water environment was obtained after varying durations.

Presently, the effect of adverse sulfate attack on splitting tensile response of cement-based composites was not well studied by past research. During the sulfate attack, the formation of ettringite and gypsum may cause volumetric expansion that leads to micro cracks in the specimen. The effect of sulfate attack on tensile strength was supposed to be investigated in comparison with the effect on compressive strength. In this program, splitting tensile strength was investigated upon three cement-based binders.

2.4 MICROSTRUCTURE OF THE CEMENT-BASED COMPOSITES

2.4.1 AIR-VOID NETWORKS

Air-Void Characteristics of cement-based composites after sulfate exposure was measured by existing methods such as Mercury Intrusion Porosimetry (MIP), and Scanning Electron Microscope (SEM).

MIP Test was applied by researcher K Torii et al. to obtain the total pore volume and pore size distribution that described the permeability of examined cement-based composites.

The results showed that in pore size distribution curves of ordinary Portland cement (OPC) concrete, there was a remarkable increase of volume of pores with the diameter greater than 0.1 pm during 2 years of exposure. This may be due primarily to the relaxation in the texture of cement paste and/or interfacial zone around aggregates due to the formation of expansive reaction products. However, in pore size distribution curves of high fly ash content concretes, the peak of pore size distribution shifted toward the finer diameter along with the decrease in total pore (Torii et al. 1995). The replacement of finer fly ash may fill the porosity inside the specimen that enhanced the impermeability of cement-based composite. Accordingly, MIP was also applied in this work in order to retrieve the pore size distribution and total capillary porosity of cement-based composites after exposure to sulfate environment. Besides, the porosity measured by MIP experiment was intended to calculate the strain change due to formation of ettringite during sulfate attack.

2.4.2 VOLUMETRIC EXPANSION

The volumetric expansion of cement-based specimen subjected to sulfate attack was investigated by researchers and it was mainly attributed to the production of ettringite and monosulfate. Study by researchers (Tian and Cohen 2000) reported that the formation of gypsum during sulfate attack may cause expansion.

It is suggested that the formation of gypsum could be expansive when subjected to sulphate attack. The research by Santhanam et al. (Santhanam et al. 2003) reveals that there is a possible link between the amount of gypsum formation and measured expansion.

On the other hand, it was studied by researchers that the formation of above productions was the partial reason of the expansion. The pore size distribution and porosity in the cement-based composite may affect the expansive results as well.

2.5 EXPERIMENTAL INVESTIGATION ON SULFATE DIFFUSION

2.5.1 EXISTING EVALUATION TECHNIQUES

Conventionally, it is suggested to evaluate the resistance to sulfate attack by means of measuring the length change of prismatic specimens. However, research by Sahmaran M et al. (Sahmaran et al. 2007) showed that the prismatic specimens cracked after 52 weeks of sulfate expousre so that the expansion cannot be measured by this evaluation method. Besides, the expansion measured cannot explain the complicated chemical reactions during the sulfat exposure.

Analysis on chemical compositions after sulfate exposure is widely employed by researchers by means of X-Ray Diffraction (XRD), X-Ray Fluorescence (XRF), and Scanning Electron Micrograph (SEM). Study by Mamun M, Bindiganavile V (Mamun and Bindiganavile 2011) reveals that upon exposure to sulfates, the empty cells are filled with ettringite by means of SEM and XRD. While this results in expansive cracking in the heavier composites, it manifests as self-healing in the lightest mix, which results in higher strength and flexural toughness factors.

SEM was widely employed to detect the ettringite and gypsum formation due to the sulfate attack. Research by K Torii et al. reported that, through the SEM analysis, it appeared that the formation of large amounts of gypsum may contribute to the softening and scaling of surface layers of concrete, and subsequently to accelerate the deterioration of concrete due to the sulfate attack. It was also suggested by SEM analysis that the formation of gypsum as well as ettringite might play an important role in the process of deterioration of concrete due to the sulfate attack (Torii et al. 1995). This SEM analysis was applied to understand the mechanism of sulfate attack inside cement-based composites. Gypsum and ettringite can be detected through SEM analysis to identify the main production due to the sulfate

diffusion. However, the SEM analysis was qualitative and had limited relationship to the recently-developed numerical models on sulfate attack.

In the recent decades, sulfate diffusion inside the cement-based composites from external was evaluated though X-Ray Diffraction (XRD) analysis by past researchers (Irassar et al. 1996; Wang 1994). Gypsum and ettringite were found through XRD analysis to be the main part of the products of the chemical reaction because of the penetration of the sulfate solution into the specimen (Wang 1994).

Mamun and Bindiganavile employed X-ray diffraction analysis and Scanning electron micrographs to detect the ettringite formation in cement-based foams subjected to adverse sulfate attack. The formation of ettringite was detected by both XRD analysis and SEM as shown in Figure 2.4 and Figure 2.5. Results of Scanning electron micrographs and X-ray diffraction revealed that upon exposure to sulphate, the empty cells are filled with ettringite. While this results in expansive cracking in the heavier composites, it manifests as self-healing in the lightest mix, which results in higher strength and flexural toughness factors (Mamun and Bindiganavile 2011).
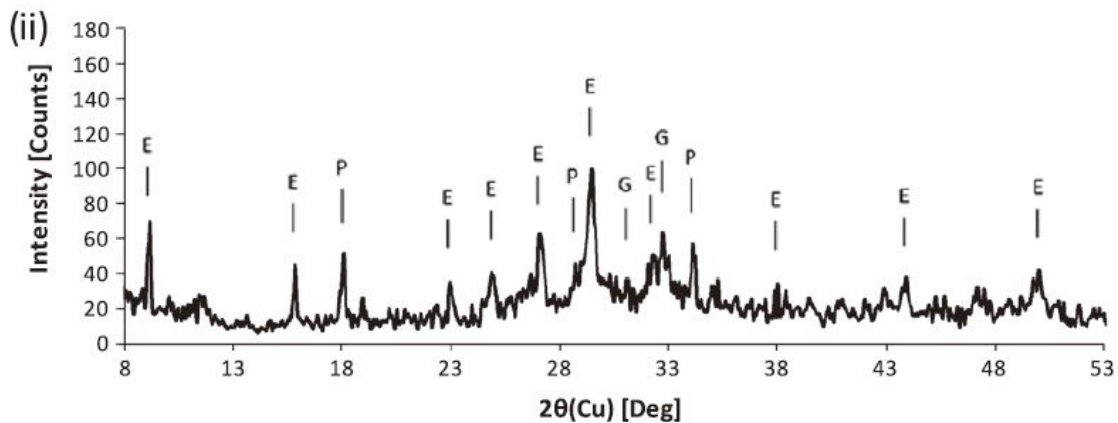
Figure 2.4. X-ray diffraction of cement-based foams exposed to sulphate for 30 days. C = Calcite, E = Ettringite, G = Gypsum, P = Portlandite (Mamun and Bindiganavile 2011)
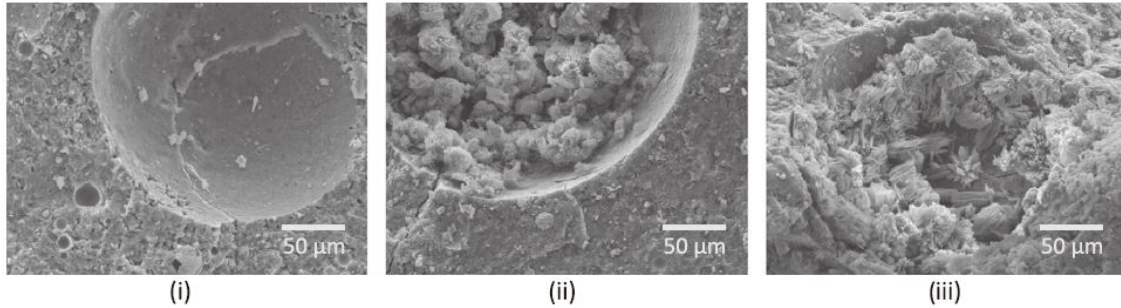
Figure 2.5. Scanning electron micrograph (1000X) showing the densification in cement-based foams exposed to sulphate: (i) 0-days; (ii) 30-days; (iii) 90-days (Mamun and Bindiganavile 2011)

2.5.2 PROCEDURE DESIGN

The research direction on sulfate attack in this study focused on the investigation on diffusion of sulfate ingress inside the cement-based composites.

At present, there is no standard sample extraction method extracting powdered samples inside the cement-based composite. In particular, it is hardly to precisely extract sample within defined depth along the direction of external sulfate diffusion.

In terms of existing physical extraction approaches, mechanical grinding, drilling and smashing were considered as applicable techniques for sampling inside cement mortar specimens. Study by researchers (Sun et al. 2013) reported that the sulfate concentrations at different depths in the specimens were obtained by using a method of drilling. However, the equivalent extraction depth of powdered sample was not explained in the literature.

On the other hand, precise area of sampling is necessary based on the research requirement. Consequently, extraction by drilling is preferred since it is a direct method to collect powdered samples in defined regions.

Past researchers (Torii et al. 1995) studied on the sulfur trioxide content in the specimen after exposure to sulfate environment. However, the sulfur trioxide content (SO_3) measured at surface layers within 20 mm from the surface in cylindrical specimens could not reveal the sulfate diffusion along the depth. The results obtained by above study explained that the

sulfate solution deeply penetrated into the concrete through small cracks after surface cracks had occurred, manifested as the SO_3 content detected in the depth of 20 mm (Torii et al. 1995).

Research by Sun et al. also retrieved the sulfate concentrations at varied depths in specimen through chemical experiment. The chemical method of EDTA complexometric titration (GB/T13025.8-1991) was used to measure the sulfate content in the specimens. After the concentrations at different depths and at different times were obtained, the ionic distribution profile for each time in the specimen was plotted in Figure 2.6 (Sun et al. 2013). However, the minimum depth extracted was 6 mm from the specimen surface that may not reveal the variations of sulfate diffusion very close to the surface.
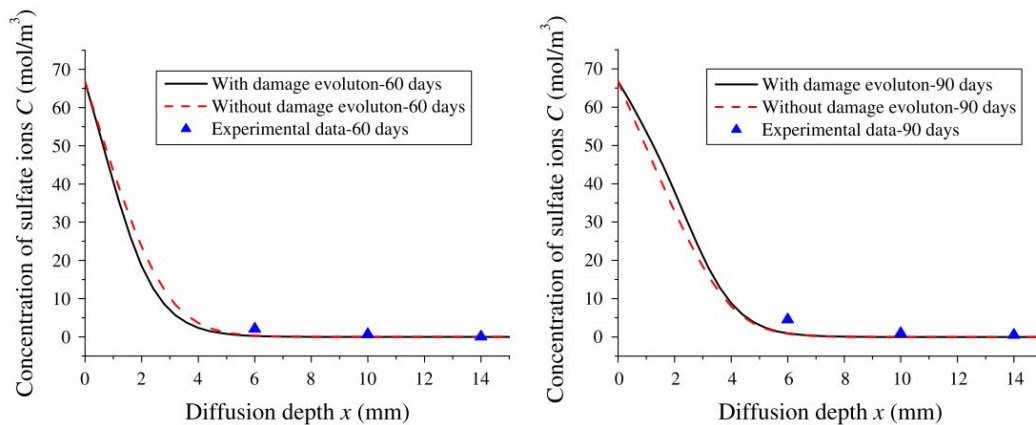
Figure 2.6. Sulfate concentration profiles in specimens at 60/90 days of exposure (Sun et al. 2013)

The main task of the titration experiment in this program was to identify and quantify the sulfate contents inside the cylindrical specimens within defined depth. Much more sulfate contents were supposed to be detected near the specimen surface since the variation of sulfate ingress might be larger in that region. Further, Portland cements comprised gypsum in the blends and that might affect the sulfate content titrated if the gypsum has not been completely consumed prior to the sulfate exposure.

Presently, several ASTM standards mention chemical analysis methods in cement-based composites. However, detailed experiment procedures and conditions are unavailable in these standards, such as temperatures, durations, devices and chemicals. Based on the chemical analysis method explained in ASTM C114 standard, sulfate can be determined by barium chloride solution after the powdered samples being decomposed in hydrochloric acid.

Broadly based on the ASTM C114 and C265 standards that assess the chemical composites inside cement-based materials, fundamental experiment procedures were determined in this study. More detailed procedures are supposed be developed to obtain the precise sulfate concentration in the specimen.

Procedures are not demonstrated in detail, experimental conditions, such as temperatures and durations, are not completely defined that in the specification. For instance, as recommended in ASTM C114 standard, heating environment and sample grinding are required if necessary but the heating temperature and grinding sieve are not determined in the standard.

Furthermore, the standard advises to dilute the solution to 50mL and digest for 15 min at a temperature just below boiling whereas the exact temperature is still not defined. It was recognized by the author that the standard test method in ASTM C114 specification was not practical when applying titration experiment.

As demonstrated in the ASTM C114 standard in terms of sulfate compositions:

"To 1 g of the sample add 25mL of cold water and, while the mixture is stirred vigorously, add 5mL of HCl. If necessary, heat the solution and grind the material with the flattened end of a glass rod until it is evident that decomposition of the cement is complete. Dilute the solution to 50mL and digest for 15 min at a temperature just below boiling. Filter through a

medium-textured paper and wash the residue thoroughly with hot water. Dilute the filtrate to 250mL and heat to boiling. Add slowly, drop wise, 10mL of hot barium chloride (100g/L) and continue the boiling until the precipitate is well formed. Digest the solution for 12 to 24 h at a temperature just below boiling. Take care to keep the volume of solution between 225 and 260mL and add water for this purpose if necessary. Filter through a retentive paper, wash the precipitate thoroughly with hot water, place the paper and contents in a weighed platinum crucible, and slowly char and consume the paper without inflaming. Ignite at 800 to 900 ℃, cool in a desiccator and weigh." (ASTM C114-13 (2013))

More detailed standard procedures are required to determine the sulfate content by above titration experiment.

2.6   NUMERICAL SIMULATION ON SULFATE ATTACK

2.6.1 Physical Diffusion

In order to study the diffusion-reaction behavior of cement-based composites subjected to adverse sulfate attack, numerical modeling was highly preferred and widely used (Tixier and Mobasher 2003; Tixier and Mobasher 2003). The fundamental diffusion mechanism of sulfate attack conformed to the Fick's Second Law that explained the mechanism of ion diffusion in homogeneous matrix. However, the sulfate attack inside cement-based composites consisted of complicated reactions with inherent compounds and it was hardly to evaluate the precision of selected approximation methods involved with these reactions. The scheme of this study was to firstly investigate the accuracy of various finite methods through non-reaction (physical) diffusion and further develop the diffusion-reaction process upon several selected approximation approaches.

Non-reaction diffusion model, widely employed by researchers (Chalee et al. 2009; Song et al. 2009) to simulate the chloride penetration to cement-based materials, was preliminarily

applied in this chapter to compare the errors caused by finite difference methods. Since the non-reaction diffusion was mathematically solved by Error Function Solution, the simulating precisions of examined methods could be discussed in comparison with the exact solution. In this manner, only the external sulfate concentration and diffusion coefficient were taken under consideration as the parameters in the present modeling. The errors caused by approximate methods were investigated for further development of sulfate attack modeling. The diffusion model involved with complicated reactions was demonstrated in detail in the next chapter of data fitting through the favorable finite difference methods decided in this study.

In this study the experimental data were used to generate a model for predicting the sulfate diffusion profile without chemical reactions of cement-based composites in adverse sulfate environment by applying Fick's second law (Crank 1979) as shown in Eq. (2.9):

$$\frac{\partial C}{\partial t} = \frac{\partial}{\partial x}\left(D\frac{\partial C}{\partial x}\right) \tag{2.9}$$

If the diffusion coefficient D does not change with the concentration C, Eq. (2.9) can be presented:

$$\frac{\partial C}{\partial t} = D\frac{\partial^2 C}{\partial x^2} \tag{2.10}$$

Fick's Second Law explains that, when applying non-steady diffusion inside homogeneous matrix, at the distance of x, the rate of concentration variation to time equals to the negative rate of diffusion flux to the distance.

The diffusion coefficient D in Eq. (2.9, 2.10) is a quantified parameter that represents the matrix resistance to the external ion diffusion. In previous study, experimental data obtained

from titration were introduced to determine the diffusion coefficient D of each examined composite.

The simulation of chloride diffusion was based on the Fick's second law and achieved by means of several finite difference methods. Study by Chalee W et al. (Chalee et al. 2009) revealed that some revisions on the numerical model were supposed to be taken under consideration such as the boundary concentration when exposed to seawater.

2.6.2 PHYSICOCHEMICAL DIFFUSION

Recently, numerical model on the sulfate attack process has been developed by several researchers. A diffusion model simulated for sulfate attack was developed by Sun C et al. (Sun et al. 2013) with the experimental results of sulfate concentration detected inside concrete. The model developed was still based on the Fick's second law, and the diffusion equation of sulfate ions can be expressed as follows:

$$\frac{\partial C}{\partial t} = \frac{\partial}{\partial x}\left(D_{eff}\frac{\partial C}{\partial x}\right) - k \cdot C \cdot U_{CA}$$

Figure 2.7. Diffusion equation of sulfate ions (Sun et al. 2013)

$$U_{CA} = C_{C_3A}^0 \cdot \left(1 - h_\alpha + \frac{1}{2}\beta h_\alpha + \beta h_\alpha \cdot e^{-\frac{1}{6}kCt}\right)e^{-\frac{1}{3}kCt}$$

Figure 2.8. Expression of CA content (Sun et al. 2013)

$$h_\alpha = 1 - 0.5 \cdot [(1 + 1.67\tau)^{-0.6} + (1 + 0.29\tau)^{-0.48}]$$

Figure 2.9. Expression of hydration degree of cement (Sun et al. 2013)

where C is the concentration of sulfate ions in the unit volume of concrete, x is the distance from the surface, t is the time, D_{eff} is the effective diffusion coefficient of sulfate ions in

concrete, k is the reaction rate between sulfate and cement hydrated products, U_{CA} is the concentration of calcium aluminates, defined by Figure 2.8, C_{C3A} is the initial content of C_3A in concrete, b is the initial content of gypsum, h_a is the hydration degree of cement related to hydration time s, defined by Figure 2.9. The second term in the right hand side of Figure 2.7 was a dissipative source term of sulfate ions, indicating a second-order chemical reaction between calcium aluminates and sulfate ions.

A more detailed numerical model on sulfate attack simulation was developed by Tixier R and Mobasher B that includes the chemical reactions during sulfate attack process as mention above. The three compounds may react with sulfate ingress according to one of the following reactions (Tixier and Mobasher 2003; Tixier and Mobasher 2003),

$$C_4AH_{13}+3C\overline{S}H_2+14H \rightarrow C_6A\overline{S}_3H_{32}+CH \qquad (2.11)$$

$$C_4A\overline{S}H_{12}+2C\overline{S}H_2+16H \rightarrow C_6A\overline{S}_3H_{32} \qquad (2.12)$$

$$C_3A+3C\overline{S}H_2+26H \rightarrow C_6A\overline{S}_3H_{32} \qquad (2.13)$$

These reactions are lumped in a global sulfate phase-aluminate phase reaction as following,

$$CA+\lambda C\overline{S}H_2+nH \rightarrow C_6A\overline{S}_3H_{32} \qquad (2.14)$$
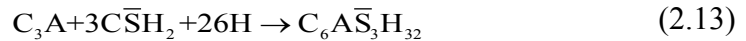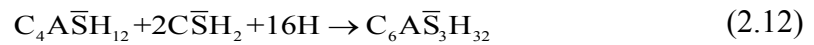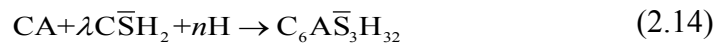
Broadly based on the Fick's Second Law as demonstrated in physical diffusion model, the numerical model involved with chemical consumption on sulfate ingress was developed by Tixier and Mobasher in order to obtain the sulfate profiles as affected by the diffusion depth.

$$CA + q\overline{S} \rightarrow C_6A\overline{S}_3H_{32}$$
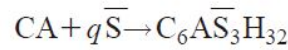
$$\frac{dM_{SO_4}}{dT} = -kM_{SO_4}M_{CA}; \quad \text{or} \quad \frac{dM_{CA}}{dT} = -\frac{k}{q}M_{SO_4}M_{CA}$$

Figure 2.10. Partial Differential Equation of CA and SO$_4$ (Tixier and Mobasher 2003)

with M = molar concentration; T = time; and k representing the rate constant. Assuming Fick's law of diffusion and the absence of convection, the following equations are obtained by substituting the variables: U and C, with $U = M_{SO4}$, $C = M_{CA}$, and X the distance,

$$\frac{\partial U}{\partial T} = D\frac{\partial^2 U}{\partial X^2} - kUC$$

$$\frac{\partial C}{\partial T} = -\frac{kUC}{q}$$

Figure 2.11. Rearranged PDEs of sulfate concentration (Tixier and Mobasher 2003)

Accordingly, the sulfate concentration after chemical consumption was obtained by solving above partial differential equations through finite difference methods. The sulfate profiles were retrieved and plotted in Figure 2.12. Note that when considering the chemical reactions inside the cement-based composites, the sulfate concentration profiles (solid) were lower than the profiles (dashed) of physical diffusion. After chemical consumption of external sulfates by inherent C$_3$A, the sulfate concentrations remained were supposed to be lower. This was also the main objective of numerical simulation in the author's program.
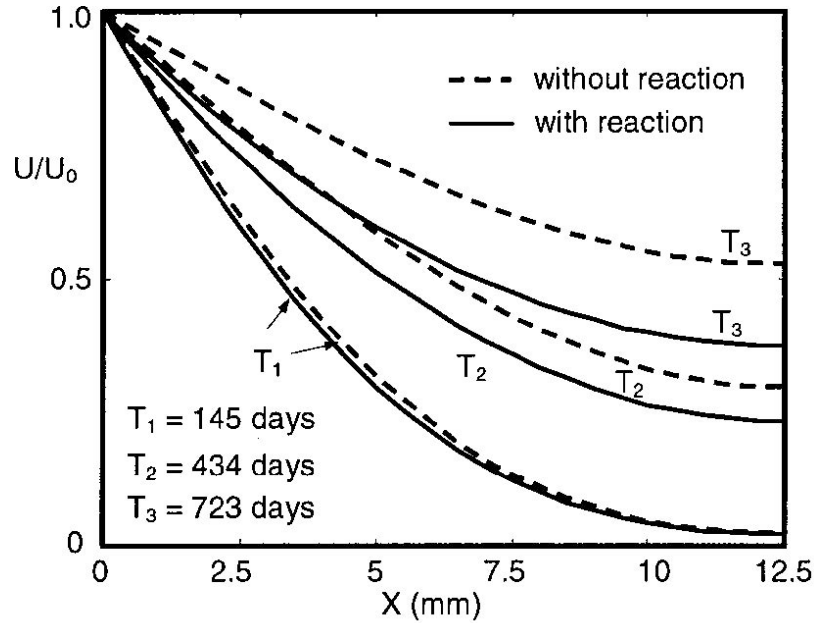
Figure 2.12. Effect of first-order chemical reaction on concentration profiles obeying Fick's law—1D case (Tixier and Mobasher 2003)

2.6.3 THE LINK BETWEEN EXPERIMENTAL RESULTS AND NUMERICAL MODEL

In accordance with the research studied by Tixier R and Mobasher B, the diffusion reaction model developed employed the experimental expansion-time data in comparison with the results obtained by numerical model. The developed numerical model consisted of volumetric expansion based on the reaction as per Eq. (2.8) in order to calculate the strain change of the specimen.

As demonstrated above, the sulfate concentration was obtained by previous researchers (Sun et al. 2013) and applied to fit the numerical model simulated for sulfate attack process. It was suggested to employ the sulfate concentration as the indicator to verify the precision of numerical model.

2.7   VISUAL ASSESSMENT

2.7.1 EXISTING VISUAL EVALUATION

Visual observation: The external condition of specimens was judged by a visual rating based on the rating system. Due to the characteristics of the attack, specimens were evaluated at top and bottom-half height. For each concrete a photograph of a representative specimen was taken at each annual inspection. (Irassar et al. 1996).

Figure 2.13. Visual rating system of sulfate attack (Irassar et al. 1996)

As shown in Figure 2.13, the visual rating system was roughly based on the appearance of cylindrical specimens to evaluate the resistance to sulfate attack. The rating system only depended on the area of exposed aggregates on sample surface and it was hardly to determine the percentage of the area. However, this rating system was a perceptible evaluation method and was not quantitative.

2.7.2 IMAGE ANALYSIS

Image analysis on durability issues of cement-based composites has been developed by researchers, particularly in the research area of carbonation and Interfacial Transition Zone (ITZ) measurement. However, there is very little information in related literature on the visual assessment on sulfate attack resistance by image analysis. In addition, Analysis on images of cement-based composites was conventionally achieved through SEM test as mentioned above. Laboratory conditions and particular devices are required for this kind of analysis. Accordingly, more convenient evaluation on the cement-based images is needed.

3 MIX PROPORTIONS AND PHYSICAL PROPERTIES

3.1 INTRODUCTION

The adverse effects of sulphate attack on cement-based composites have been studied from the perspective of ettringite formation, gypsum and C_3A content. The sulphate resistance of conventional cement-based composites is evaluated by length change and is reflected by their mechanical response. However, the qualitative evaluation of sulphate resistance on length measurement presents the resultant change, not the mechanism of sulphate ingress from external environment (Mamun and Bindiganavile 2011). It is suggested that the formation of gypsum could be expansive when subjected to sulphate attack. The research by Santhanam et al. (Santhanam et al. 2003) reveals that there is a possible link between the amount of gypsum formation and measured expansion.

The effect of adverse sulfate-rich environment on cement-based materials was evaluated through their mechanical performances such as shrinkage performances and physical properties after varying durations of exposure. The main task of the research in this chapter was to comprehensively analyze the properties of InterCem cement, with a 30:70 blend of fly ash and cement type GU, compared with High Sulfate Resistance (HS) Type and General Use (GU) Type cement.

In order to capture the changes due to the submersion in liquid environment, the experiments in this study occurred in two groups per cement type, one of which would be submerged in water and another that would be exposed in a sulfate-rich solution with a certain PH ratio. Length change, porosity, compressive and splitting tensile strength were examined under sulfate attack conforming to related ASTM specifications with specific intervals of exposure in comparison with unexposed specimens.

3.2 MATERIAL PREPARATIONS

The creation of specimens was governed by testing requirements, availability of molds and availability of materials and operated in the concrete laboratory in University of Alberta. Specimens were chosen to be made out of mortar due to materials available. CSA type HS, GU cements and fine aggregates listed below were commercially sourced and the InterCem blend was provided by the industrial partner.

Table 3.1. Sample sizes and amounts of designed experiments

Tests required:	
Length Change	(12 25x25x285mm bar specimens per cement type)
Compression	(33 75x150mm cylinder specimens per cement type)
Split Tensile	(33 50x100mm cylinder specimens per cement type)

Table 3.2. Available molds employed in this study

Molds available:
15 Cylinders @ 75mm diameter 150mm height (75x150mm)
20 Cylinders @ 50mm diameter 100mm height (50x100mm)
6-8 Prisms @ 25x25x285mm

Table 3.3. Required fine aggregates and cements

Materials available:
Fine aggregate
Sizes 3.4/2.4/1.0
Cement
General Use (GU)/ High Sulfate Resistance (HS)/ InterCem (IC)

Table 3.4. The mix proportions of cement mortar samples

- Cement to sand ratio = 1 : 2.75	
- Water to cementitious ratio = 0.485	
- Sand distribution:	
3.4	65%
2.4	20%
1.0	15%

Table 3.5. The amounts of materials used per liter

Example 1L batches are as follow:			
GU/HS		InterCem	
Sand	1.4944kg	Sand	1.4734kg
3.4	0.97136kg	3.4	0.95771kg
2.4	0.29888kg	2.4	0.29468kg
1.0	0.22416kg	1.0	0.22101kg
Cement	0.5434kg	Cement	0.5358kg
Water	0.2636kg	Water	0.2599kg

Creation of specimens was carried out in three batches for each cement type, one for the group that would be submerged in water, one for the group that would be submerged in sulfate solution and the last one for the zero exposure specimens that would be going through destructive testing (compressive and splitting tensile strength). The main reason for separation into the three batches is the availability of molds. Curing lasts 28 days, this allowed all testing to be done during week days so no special permissions would be required to work on weekends.

3.3 EXPERIMENTAL SCHEMES

3.3.1 EXPOSURE CONDITION AND TESTING SCHEDULE

Testing Schedule. All three mixes were cast at a manufacturing unit into prismatic and cylindrical molds and were cured for 4 weeks in standard curing condition (temperature 23 centigrade and relative humidity 95%) in humidity room. The exposure time 0 Week (0W) mentioned in the study signified that samples were tested right away after 28 days curing. Length changes were measured using the length comparator with reference bar as per ASTM C1012 standard that access the drying shrinkage performance at the exposure intervals of 0, 1, 2, 4, 8 and 12 weeks.

Compressive strengths and split-tensile strengths were examined as per ASTM C39 and C496 standards at the same exposure intervals as length change measurements and then plotted. An investigation of control groups, exposing specimens to water environment, were evaluated as comparison in order to capture the changes due to the submersion in liquid environment.

Exposure Condition. The sulfate attack environment simulated in this study was provided by 11L and 68L plastic containers with higher concentration sodium sulfate solution. The sulfate solution consisted of 50g anhydrous sodium sulfate per liter that was identical to 352 molars per cubic meter as defined in accordance with ASTM C1012 Standard (C1012/1012M-13 (2013)). This solution required a pH within the range of 6.0 to 8.0; using tap water a pH between 7.50 and 7.80 was consistently produced.

Same samples were submerged in water environment with the same volume as sulfate solution and employed as control groups of unexposed condition. It also required a solution to specimen volume ratio between 3.5 and 4.5, this ratio was maintained in both the water and sulfate solutions.

Storage and Container. For the 11L plastic containers storing length change prisms (see Figure 3.1), a constant volume of 5 liters of sodium sulfate solution was chosen as it minimizes sulfate usage while still submerging the specimens, two layers were placed with three prisms for each layer; for the 68L containers (destructive tests) a ratio of 3.61 was chosen because the amount of solution required starts at 50L and drops by exactly 10L per test date.

Figure 3.1. 11L container storing six length change bar specimens

3.3.2 LENGTH CHANGE MEASUREMENT

Apparatus. *Prism molds,* it is required to prepare the specimen molds in accordance as per Specification ASTM C490 Practice (C490/490M-11 (2011)) except the interior surfaces of the mold shall be covered with a release agent. Figure 3.2 shows the standard manufacturing molds for prismatic specimens and the same molds were employed in this work as shown in Figure 3.3.
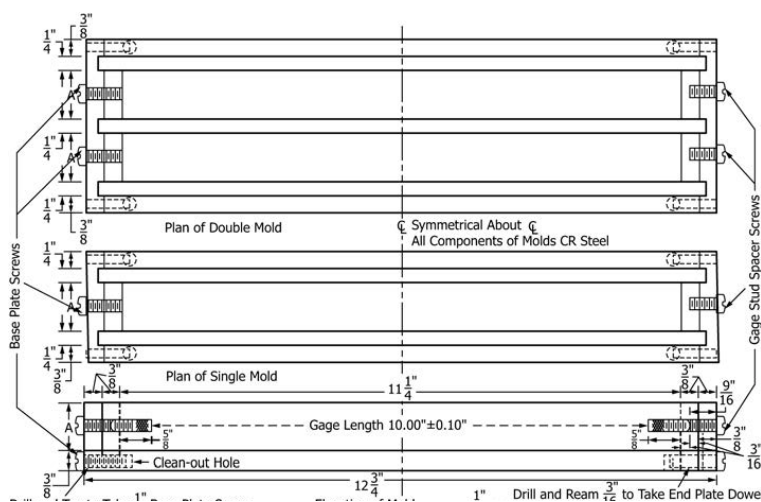
Figure 3.2. Standard molds for length change bar specimen (ASTM C490)

A release agent will be acceptable if it served as a parting agent without affecting the setting of the cement and without leaving any residue that will inhibit the penetration of water into the specimen. In this case, wax paper was used as the release agent for easier de-molding. Additionally, four units of prism molds were available so that eight prisms can be molded for each batch specimens.

Figure 3.3. Bar molds used and length change bar specimen after de-molding

Figure 3.4. Length comparator employed for length change measurement

Length Comparator, for determining length change of specimens, shall be designed to accommodate the size of specimen employed and to provide or permit a positive means of contact with the gauge studs and the convenient and rapid obtaining of comparator readings.

The length comparator used conformed to ASTM C1012 standard (C1012/1012M-13 (2013)) and was calibrated prior to each testing. Note that two metal tips of prism were rubbed by tissue paper after taking out from liquid as the remaining water drops would affect the length change measurements.

Calculation. The length of reference bar was measured prior to the specimen measurements. And it was re-measured after testing to make sure the apparatus work properly. The reference bar was used in the comparator to correct for changes occurring to the comparator apparatus and gauge that affect length readings. The reference bar was always placed in the same orientation in the comparator apparatus to minimize changes in reading due to differences in contact surfaces. Frequent use of the reference bar can result in significant wear of the tips, which affects the indicated length of the bar. Appropriate steps should be taken to monitor reference bar condition and replace as needed.

Calculation the length change at any age as following:

$$\Delta L = \frac{L_x - L_i}{L_g} \times 100 \qquad (3.1)$$

Where:

ΔL=change in length at x age, %

L_x=comparator reading of specimen at x age--reference bar comparator reading at x age,

L_i=initial comparator reading of specimen-reference bar comparator reading, at the same time,

L_g=nominal gauge length, or 250 mm [10 in.] as applicable.

Calculate length change values for each bar to the nearest 0.001% and report averages to the nearest 0.01%.

3.3.3 COMPRESSIVE AND SPLIT-TENSILE PROPERTIES

Compressive Strength. This test method consisted of applying a compressive axial load to molded cylinders or cores at a rate which was within a prescribed range until failure occurs. The compressive strength of the specimen was calculated by dividing the maximum load attained during the test by the cross-sectional area of the specimen (C39/39M-14a (2014)).
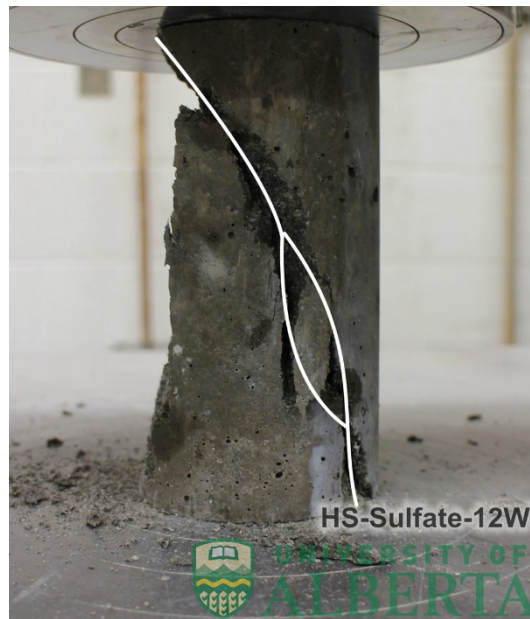
Figure 3.5. cylindrical sample with shear cracks after compressive test

Prior to testing, both ends of compression test specimens were ground to meet that tolerance, or capped. In this project, cylindrical specimens were ground at both ends by grinding machine prior to compressive experiments (see Figure 3.6 and Figure 3.7).

Figure 3.6. Grinding machine with three cylindrical samples

Figure 3.7. Grinded surface of cylindrical sample prior to test

The diameter used for calculating the cross-sectional area of the test specimen shall be determined to the nearest 0.25 mm [0.01 in.] by averaging two diameters measured at right angles to each other at about mid-height of the specimen.

The specimen tested has a length to diameter (L/D) ratio of 2.0 that a correction factor is not

necessary in accordance with ASTM standard C39/C39M (C39/39M-14a (2014)). Calculation the compressive strength at any age as follow:

$$C = \frac{4P}{\pi D^2}$$
(3.2)

Where:

C = compressive strength, MPa [psi],

P = maximum applied load indicated by the testing machine, N [lbf], and

D = diameter of the cylinder, mm [in.].

Most of the cylinders were crushed with normal fracture curves. However, there were two specimens tested with unreasonable compressive strength after one week exposed, the data of these two specimens were not taken under consideration.

Splitting Tensile Strength. This test method consisted of applying a diametric compressive force along the length of a cylindrical concrete specimen at a rate that is within a prescribed range until failure occurs. This loading induces tensile stresses on the plane containing the applied load and relatively high compressive stresses in the area immediately around the applied load. Tensile failure occurs rather than compressive failure because the areas of load application were in a state of tri-axial compression, thereby allowing them to withstand much higher compressive stresses than would be indicated by a uniaxial compressive strength test result. (C496/C496M-11 (2011))

The maximum load sustained by the specimen was divided by appropriate geometrical factors to obtain the splitting tensile strength. Calculation the split tensile strength at any age as following:

$$T = \frac{2P}{\pi l d} \qquad (3.3)$$

Where:

T = split tensile strength, MPa [psi],

P = maximum applied load indicated by the testing machine, N [lbf],

l = length, mm [in.], and

d = diameter, mm [in.].
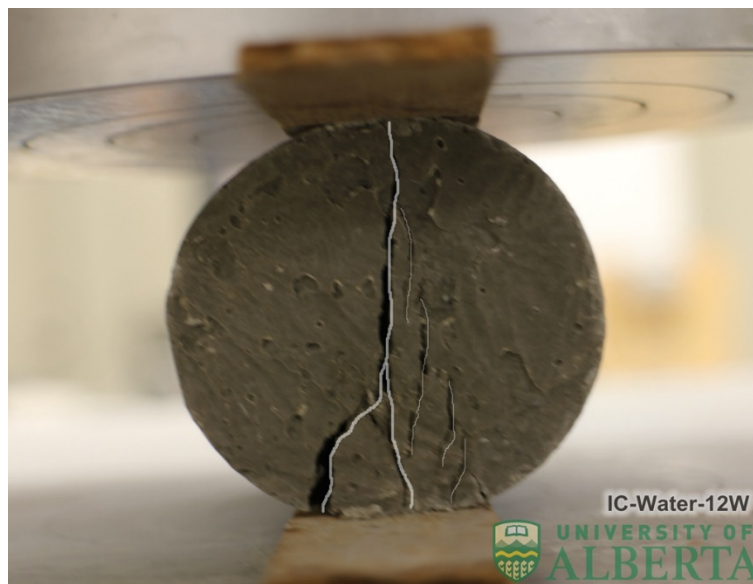
Figure 3.8. Specimen positioned in testing machine for determination of splitting tensile strength

3.3.4 MERCURY INTRUSION POROSIMETRY (MIP) TEST

Mercury Intrusion Porosimetry (MIP) test were employed in this work for the capillary porosity and pore size distribution after sulfate exposure. The cubic sample, as shown in Figure 3.9, was obtained inside the cylinder after 12 weeks exposure for each binder. Note

that the porosity evolved with exposure duration but only the specimens after 12-week exposure were investigated for their porosities.
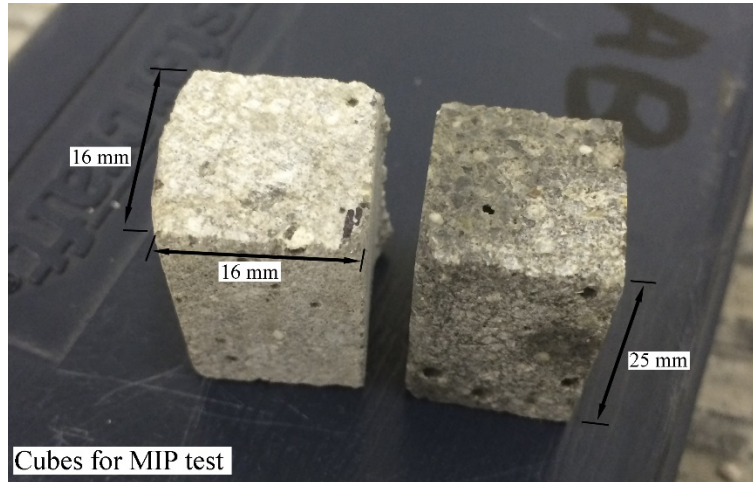
Figure 3.9. Cubes cut from cylindrical specimens after 12-week exposure

3.4   RESULTS AND DISCUSSIONS

3.4.1 SHRINKAGE PROPERTIES

The length changes of bar specimens directly revealed the shrinkage performances at specific durations when exposed to adverse sulfate environment. Six bar specimens were molded for length change measurements respectively. However, there were extra two GU type prisms in unexposed condition (eight prisms in total) in case of cracking damage when de-molding.
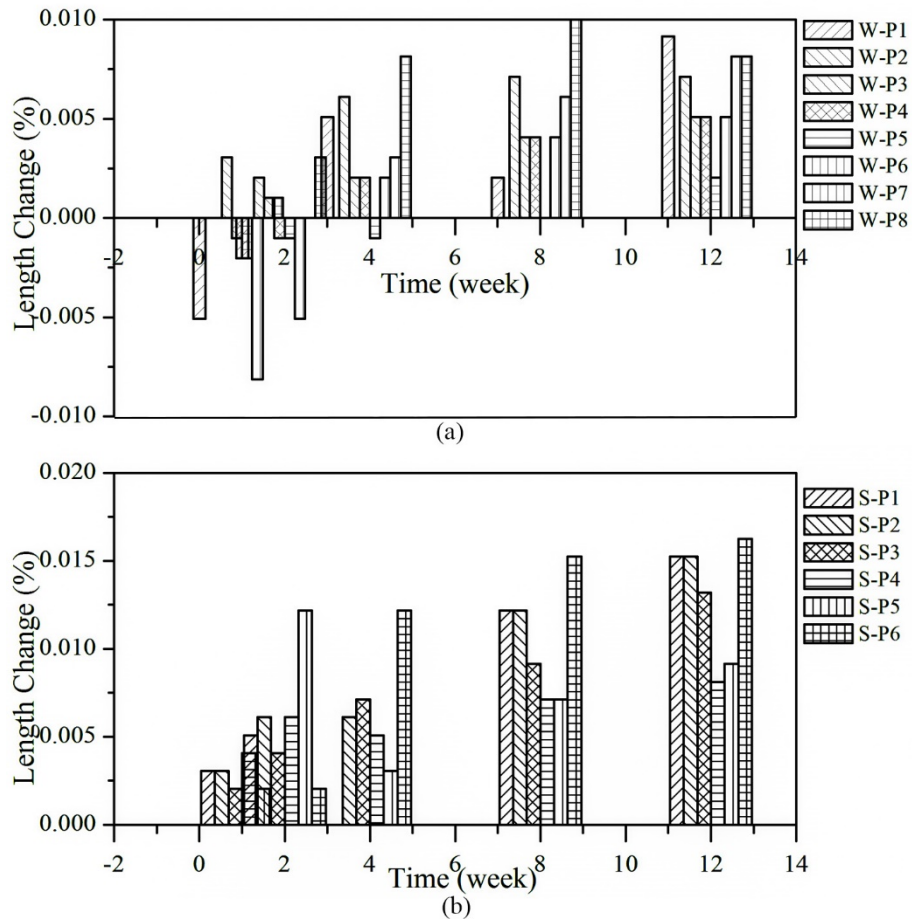
Figure 3.10. Length change of Type GU as affected by duration in: (a) water; (b) sulfate exposure

Some of the GU type specimens shrink when submerged in water environment within 1 week and started to expand after the second week (2W) (see Figure 3.10). Within 12 weeks, the length changes of GU type prisms under sulfate attack are greater than those submerged in water. It is likely that the cement was not completely hydrated at the first week but bar specimens produced ettringite attributed to sulfate ingress that leads to length change increments.
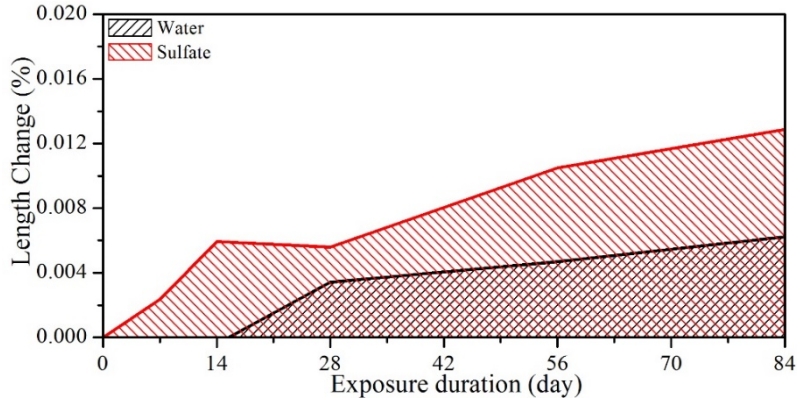
Figure 3.11. Average length change of Type GU specimen as affected by exposure duration

Comparing to the unexposed ones, bar specimens under adverse sulfate attack showed larger average length changes at any durations within 12 weeks. The maximum length change is around 0.012% for the exposed ones and 0.005% for the unexposed ones (see Figure 3.11).
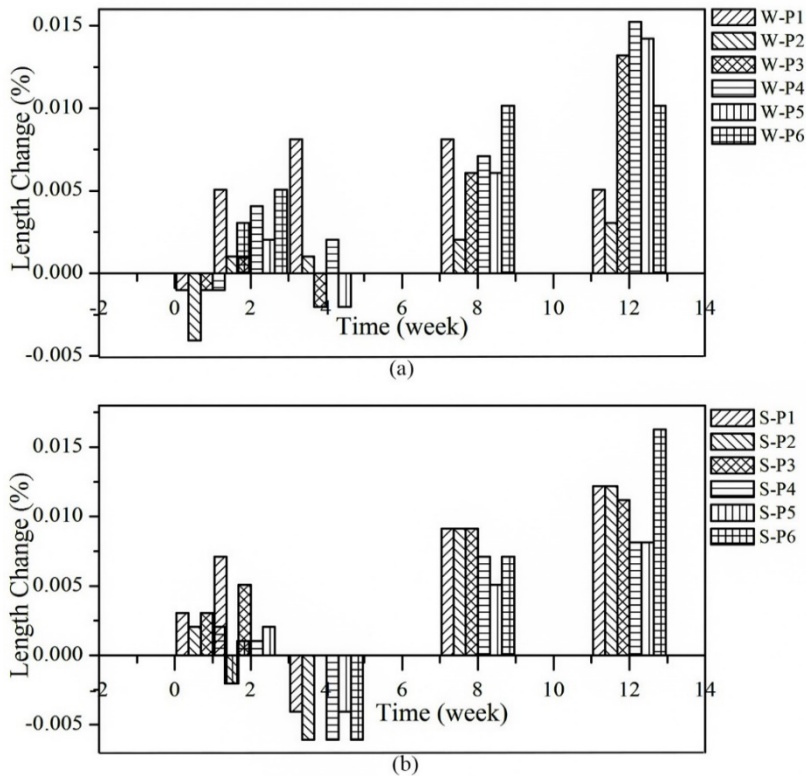
Figure 3.12. Length change of Type HS as affected by duration in: (a) water; (b) sulfate exposure

Neglecting the negative data at the fourth week of exposure, the length changes evolved with duration in both exposed and unexposed cases. The adverse sulfate environment has few effect to the shrinkage performance of Type HS specimens, as evident from the very *close* length changes in both cases (see Figure 3.13). The maximum length change is around 0.01%.
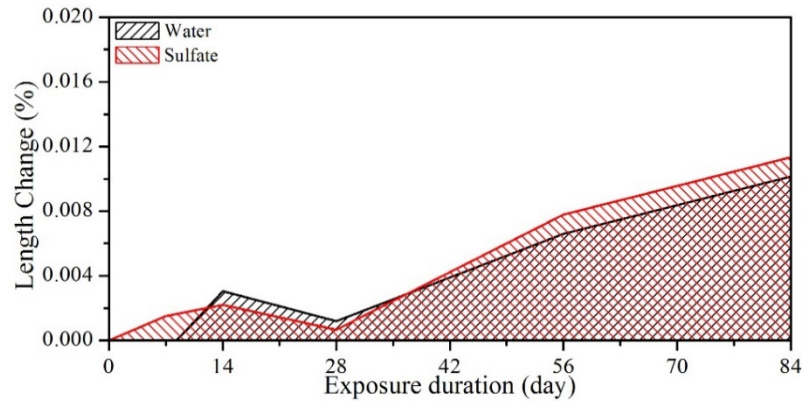
Figure 3.13. Average length change of Type HS specimen as affected by exposure duration
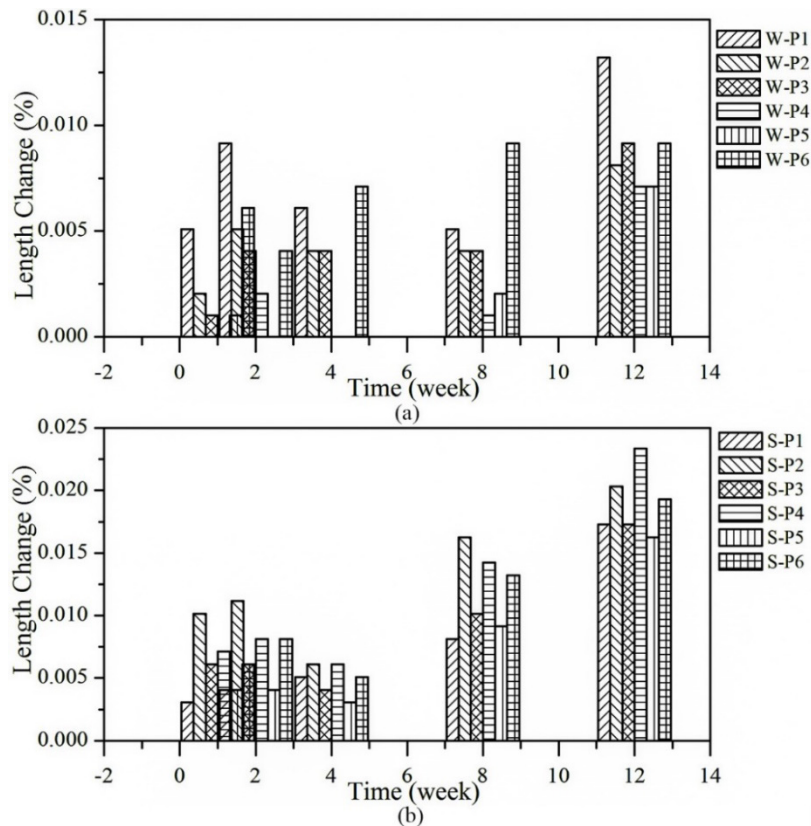
Figure 3.14. Length change of IC blend as affected by duration in: (a) water; (b) sulfate exposure
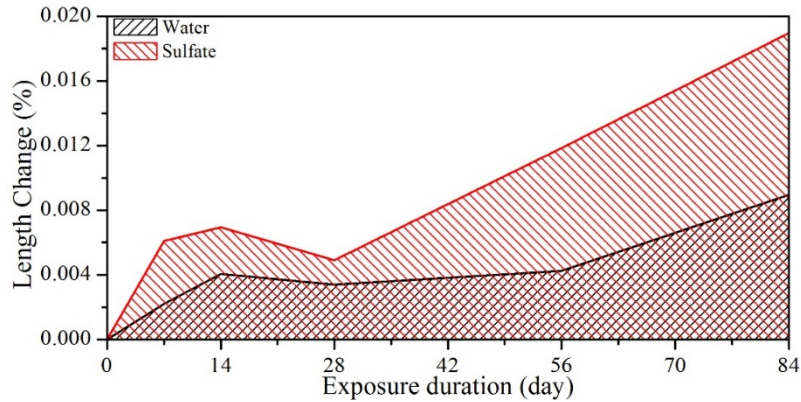
Figure 3.15. Average length change of IC specimen as affected by exposure duration

Based on the length change measurements, IC type prismatic specimens expanded with time in both exposed and unexposed cases (see Figure 3.14). Compared with the unexposed bar specimens, specimens submerged in sulfate solution performed significantly larger average length changes within planned durations. The maximum length change is around 0.019% for the exposed ones and 0.009% for the unexposed ones (see Figure 3.15).

The length changes slightly increased with time when exposed to water environment for all three type bar specimens. However, when subjected to sulfate attack, the length increments of GU and IC type specimens were significantly higher comparing to unexposed ones. Prismatic specimens using IC type binder, containing 70% GU type cement and 30% fly ash replacement, registered greater length increments (0.019%) than those using GU type cement (0.012%).

The blended binder containing fly ash (IC) showed the maximum expansion at all durations of exposure. Specimens with Type HS cement on the other hand had minimum expansion. However, Sahmaran and Kasap (Sahmaran et al. 2007) noticed that a binder similar to Type GU showed specimen disintegration after 26 weeks. Whereas in the present study the

specimens did not disintegrate, there were visible cracks on the surface of the prisms, most notably on the IC blended mix. It is suggested by Santhanam and Cohen (Santhanam et al. 2002) that the expansion of mortars immersed in sodium sulfate solution follows a two-stage process. Whereas there was little expansion in the initial stage that is, up to four weeks of immersion. A significant increase in expansion was witnessed beyond four weeks.

3.4.2 COMPRESSIVE PROPERTIES

Compressive strengths were plotted respectively by cement types and exposure conditions within 12 weeks of testing duration. Three cylindrical specimens were tested conforming to ASTM C39M standard. Besides, experimental errors were obtained for every specimen examined with a comparison to the averaged compressive strength.
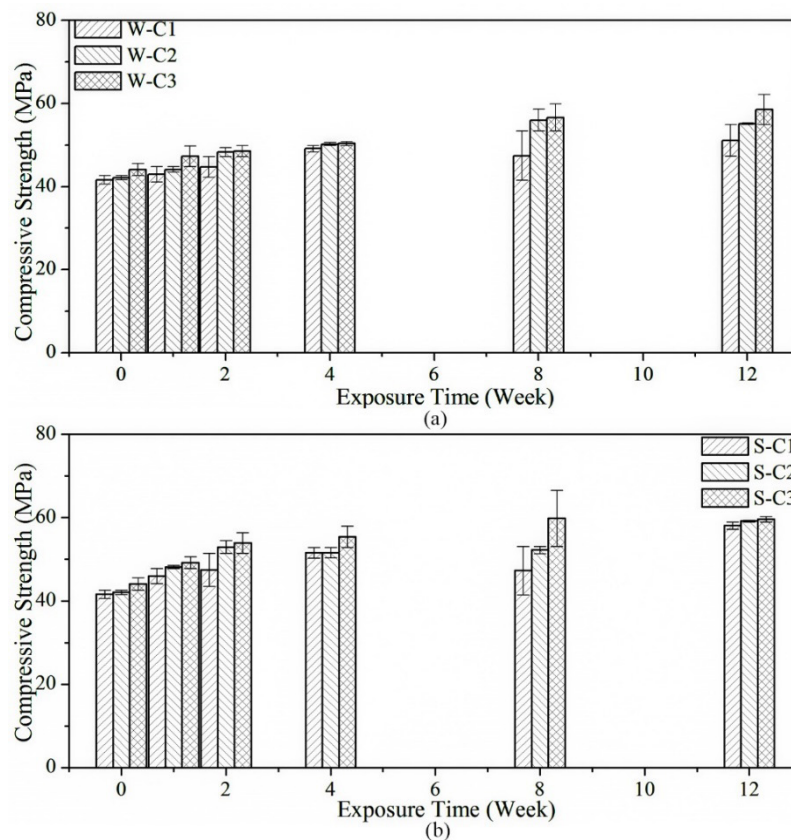
Figure 3.16. Compressive strength of Type GU as affected by duration in: (a) water; (b) sulfate exposure

The compressive strengths of GU type cylinders registered a slight growth with time in either exposed or unexposed cases (see Figure 3.16). Strengths were calculated between 40 MPa to 60 MPa. Cylinders exposed to sulfate solution (Sulfate) performed close compressive strengths to the unexposed ones (Water) (see Figure 3.17). The maximum compressive strengths were 58.9 MPa (Sulfate) and 54.9 MPa (Water) within 12 weeks.
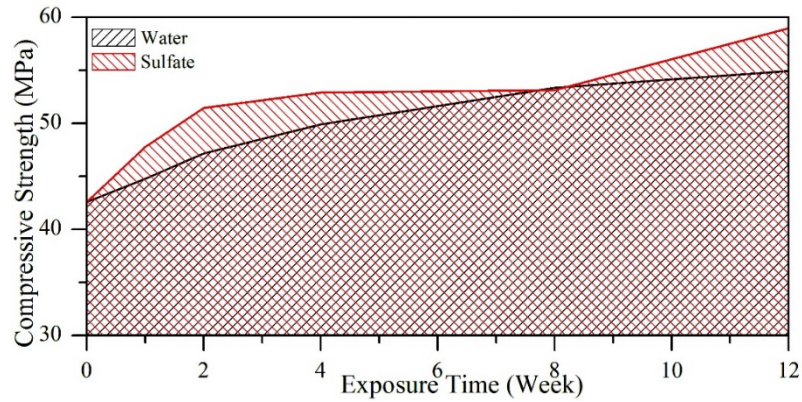
Figure 3.17. Average compressive strength of Type GU specimen as affected by exposure duration
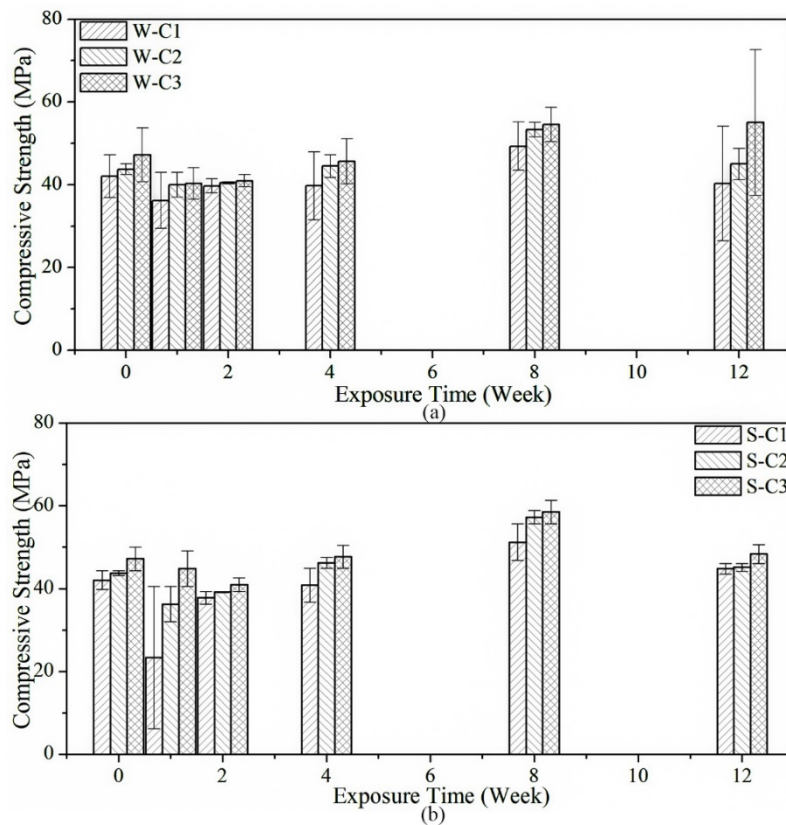
Figure 3.18. Compressive strength of Type HS as affected by duration in: (a) water; (b) sulfate exposure
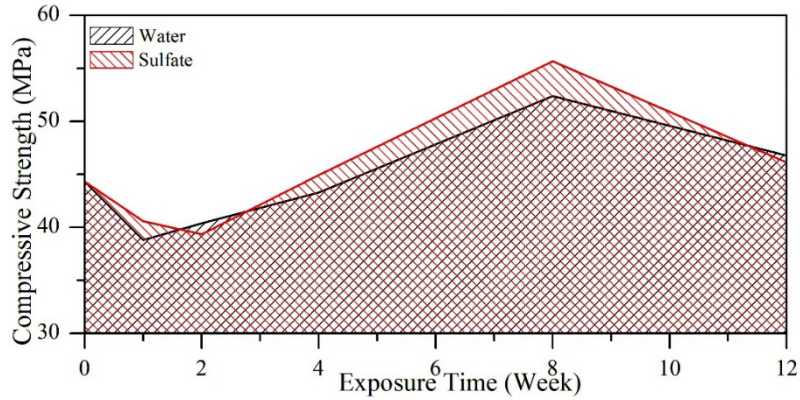
Figure 3.19. Average compressive strength of Type HS specimen as affected by exposure duration

HS type cylinders submerged in sulfate solution registered very close compressive strengths with a comparison those of unexposed ones. The maximum strength is 55.7 MPa (exposed) and 52.4 MPa (unexposed) that appeared at the 8th week for both cases (see Figure 3.19).
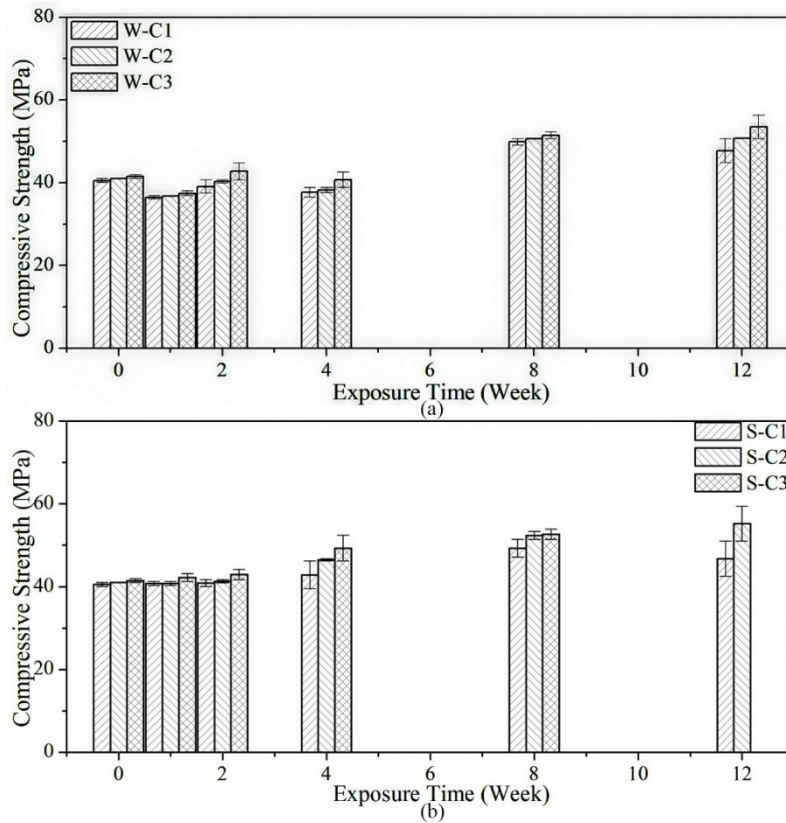
Figure 3.20. Compressive strength of IC blend as affected by duration in: (a) water; (b) sulfate exposure
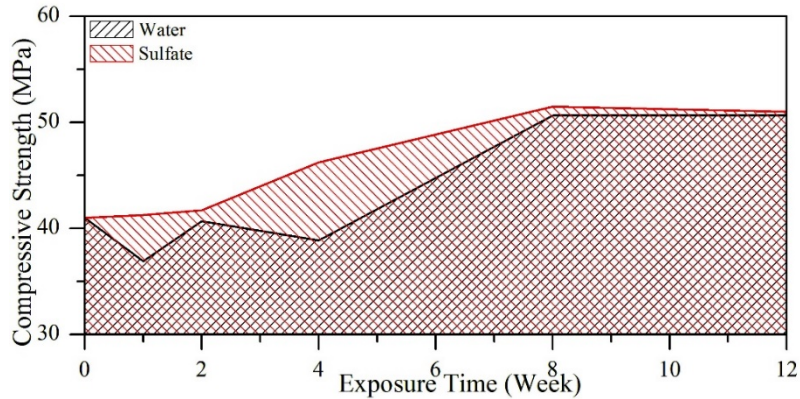
Figure 3.21. Average compressive strength of blend IC specimen as affected by exposure duration

An investigation on the compressive strengths of InterCem specimens were explained with very similar performance between exposed and unexposed ambient conditions (See Figure 3.20). The compressive strengths of IC type cylinders increased with time during the first eight weeks of exposure. Figure 3.21 presents the averaged compressive strengths as affected with exposure time and the maximum compressive strength is 50.9 MPa obtained from exposed ones and 50.6 MPa from unexposed ones after 12 weeks.

To sum up, the effect of adverse sulfate attack was not considerable in terms of the compressive strengths experienced during the whole experiments. Compressive strength responses were hardly distinguished between exposed and unexposed conditions within 12 weeks. Cylindrical specimens of three mixes achieved slight growths in compressive strengths. GU type cylinders reached the maximum strength increments, which is 38.5% higher than 0 week's strength under sulfate attack and 28.9% when submerged in water within 12 weeks. Further, the average maximum strength of GU type cylinder was also higher than the other two mixes. InterCem type cylinders with 30% fly ash replacement by weight were examined to have the lowest compressive strength. In accordance with the dry shrinkage property, short-term external sulfate attack (12 weeks) was not significant to affect the compressive strength of the specimens tested.

3.4.3 SPLITTING TENSILE PROPERTIES
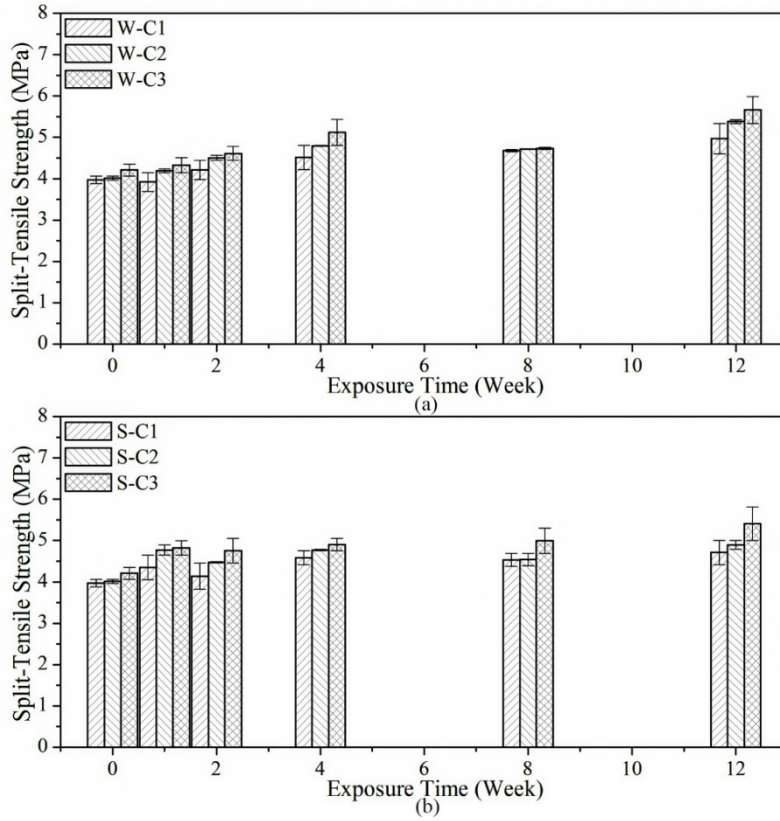
Figure 3.22. Split-tensile strength of Type GU as affected by duration in: (a) water; (b) sulfate exposure
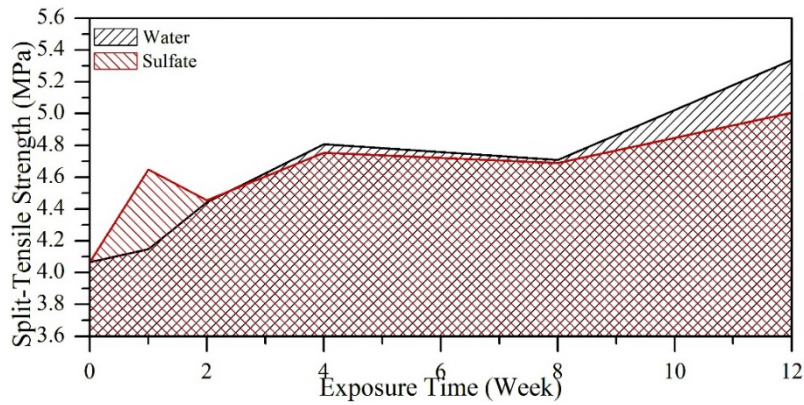
Figure 3.23. Average split-tensile strength of Type GU specimen as affected by exposure duration

Similar to the compressive strength responses, GU type cylinders achieved slight growth win split-tensile strength during experiment (see Figure 3.22). Adverse sulfate attack had little influence to the split-tensile strength of GU type samples (see Figure 3.23).
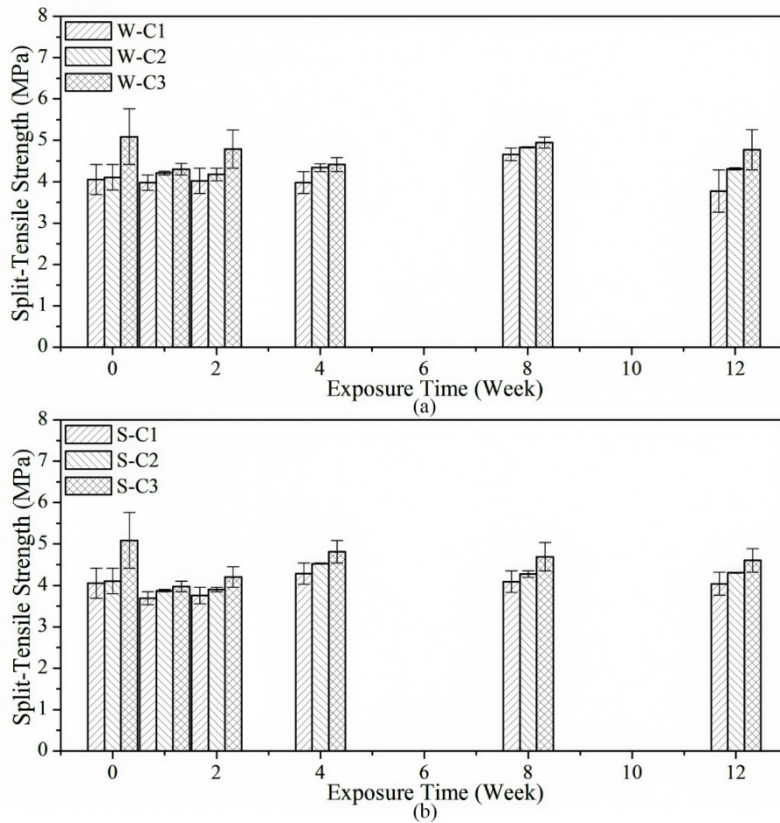
Figure 3.24. Split-tensile strength of Type HS as affected by duration in: (a) water; (b) sulfate exposure
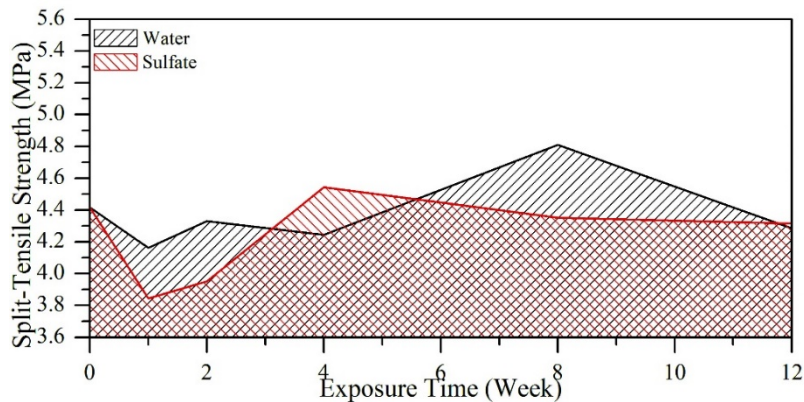
Figure 3.25. Average split-tensile strength of Type HS specimen as affected by exposure duration

In like manner, either time or external sulfate attack had little effect to the split-tensile strength of HS type specimens within 12 weeks (see Figure 3.24, Figure 3.25).
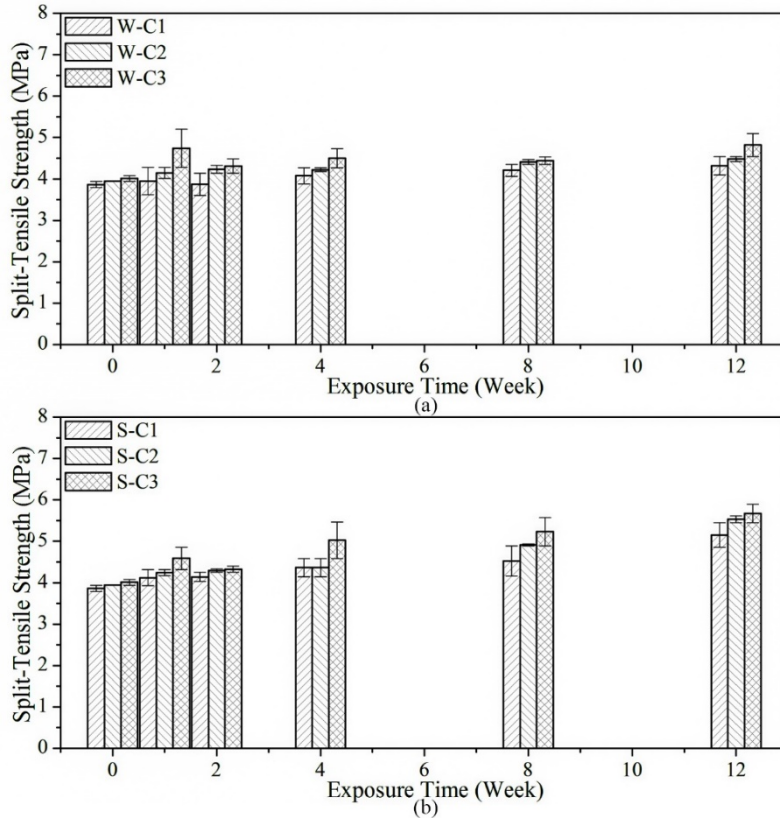
Figure 3.26. Split-tensile strength of IC blend as affected by duration in: (a) water; (b) sulfate exposure
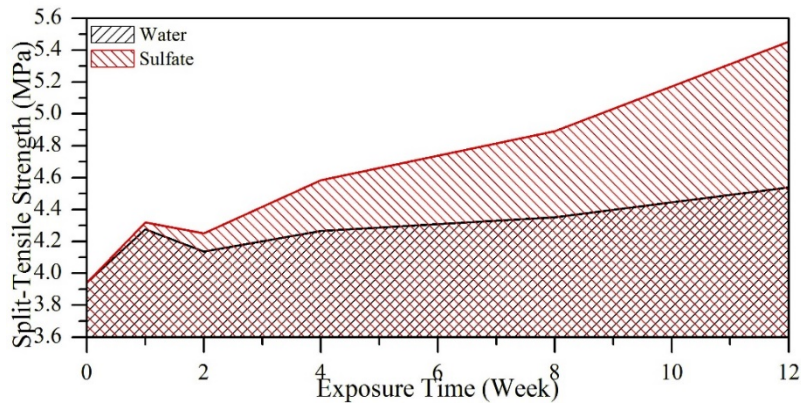
Figure 3.27. Average split-tensile strength of blend IC specimen as affected by exposure duration

When immersed in water, the split-tensile strengths of IC type specimens increased from 3.94 MPa to 4.54 MPa. The specimens subjected to adverse sulfate attack, however, had significantly higher improvement of in the split-tensile strength from 3.94 MPa to 5.45 MPa (see Figure 3.26, Figure 3.27). Compared to the responses of Type GU and HS specimens, specimens cast by InterCem blend were corroborated to be more sensitive to chemical environment in terms of split-tensile response.

In conclusion, external sulfate environment, sodium sulfate solution in this work, had greater improvement to the split-tensile strength of IC type samples than those of GU type and HS type. IC type specimens under sulfate attack performed much higher split-tensile strengths comparing to the ones submerged in water. But the split-tensile strengths in both exposed and unexposed cases were very close within 12 weeks for GU and HS type cylinders. As commented before, it was different from the responses of compressive strength that external sulfate environment merely enhanced the split-tensile strength of IC type specimens.

Consequently, IC type cylinders were examined to have highest average split-tensile strength after 12 weeks exposure among three type mixes. The maximum average split-tensile strength of IC sample was 5.45 MPa that was 38.4% higher than 0 week's strength when exposed to sulfates, and 4.54 MPa that was 15.2% higher when immersed in water.

3.4.4 COMPRESSIVE-SPLIT TENSILE RELATIONSHIP

The relationship between compressive and split-tensile responses was developed after results were obtained for different cement types and exposure conditions.
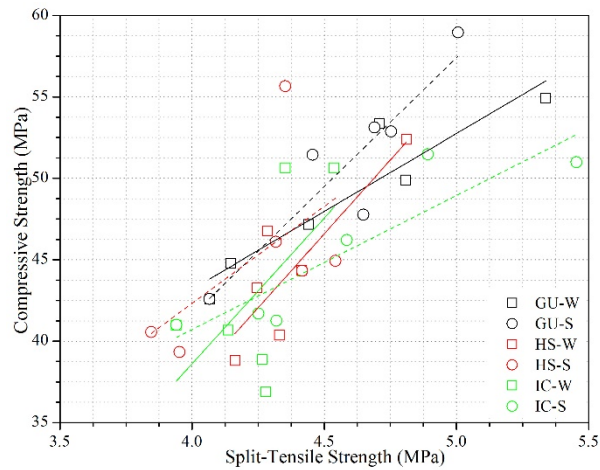
Figure 3.28. Relationship of compressive and split-tensile stengths by cement types

As shown in Figure 3.28, the relationship was simulated to linear response respectively by cement types and exposure conditions. The linear slopes were captured and listed in Table 3.6 below.

Table 3.6. Slopes of the relationship between compressive and split-tensile responses

Exposure cases	Binder		
	Type GU	Type HS	Blend IC
Sulfate	9.557	11.916	8.228
Water	15.816	18.128	17.884
Water/Sulfate	1.655	1.521	2.173

It is to be noted that from the slope results listed, external sulfate environment reduced the compressive-to-split tensile ratio of all type mixes tested within 12 weeks, which means that specimens performed lower compressive strengths with the same split-tensile responses when subjected to sulfate attack, or namely, sulfate environment dramatically improved the split-tensile strengths under same compressive responses.

On the other side, when submerged in water, HS type specimens were evaluated to have the *highest* compressive-to-tensile ratio of 18.1 while IC type specimens had slightly lower ratio

of 17.9. The ratio of HS type cement remained the highest among three tested cements when exposed to sulfate environment but the ratio of IC type blend changed to the lowest of 8.2. It is likely that adverse sulfate environment had featured but constant effect to the mechanical properties of GU and HS type cements, as evident from water/sulfate ratios. While the effect of sulfate attack on InterCem blend remained a concern based on the varying performances of mechanical properties.

3.4.5 POROSITY AND PORE SIZE DIAMETER

Table 3.7. Parameters of the Air-Void Network as Measured by Mercury Intrusion Porosimetry

Parameter	Binder		
	Type GU	Type HS	Blend IC
Porosity (%)	13.6	14.1	13.1
Total Pore Area (m²/g)	3.33	4.66	12.08
Median Pore Diameter (Å)	457	348	74
Tortuosity	6.8	18.7	6.3
Bulk Density (g/mL)	2.15	2.12	2.14
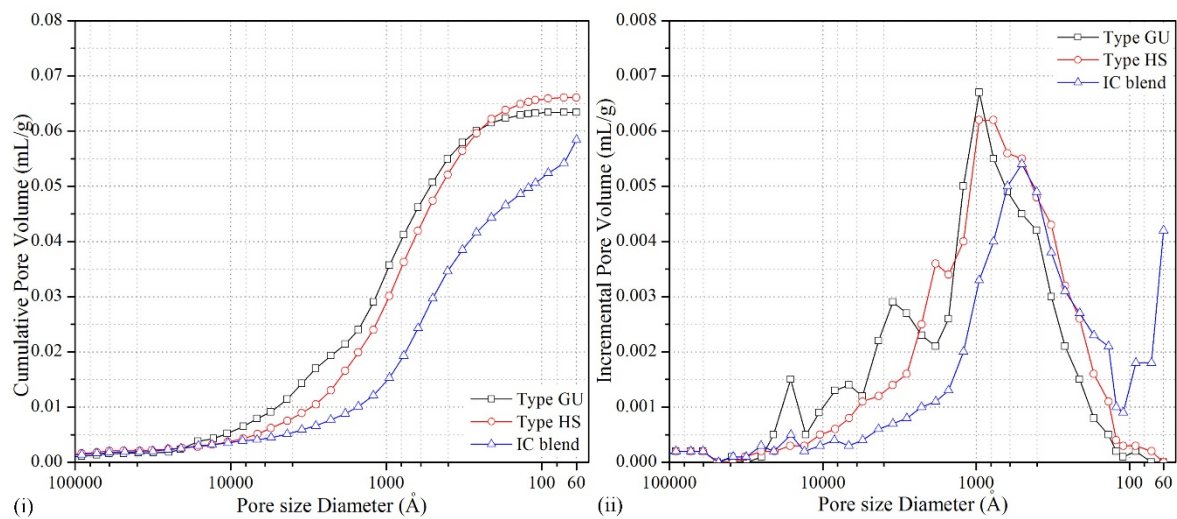
Figure 3.29. Pore Size Frequency (i) and Pore Size Distribution (ii) for Mixes *before* Sulfate Exposure

Clearly, as shown in Figure 3.29, there is a higher pore fraction in the smaller size diameters for the blended binder IC, as compared with the specimens with the other two binders. This suggests the following stages of sulfate attack: Firstly, the presence of fly ash delays the onset of strength. However, by 28 days maturity, all three mixes showed about the same compressive and tensile strength. Note further that at this age, the median pore size was much smaller in the IC binder mix compared to the other two. Now, upon exposing to sulphate attack, it is clear that the production of expansive ettringite breaks apart the microstructure. This is more manifest in the IC mix with smaller pore size compared to the Type GU cement mix. Therefore, there is a perceptible rise in the compressive and tensile strength of Type GU mix at 30 day exposure. The relative larger pores can accommodate the expansive ettringite.

On the other hand, the blended IC mix registers higher strength after longer durations of exposure to sulphate. This may be explained through a healing mechanism whereby, the microstructure first cracks due to sulphate attack and thereafter heals due to the continued formation of ettringite. Mamun and Bindiganavile (Mamun and Bindiganavile 2011) illustrated a similar phenomenon in controlled low strength cement based foam. If the pore size accommodates the formation of ettringite, it will strengthen the matrix whereas if the pore size is relatively small, the matrix will crack open. However, continued exposure and the availability of reactive agents (in this case, C_3A; $\bar{S}$ and CH) leads to filling up of these cracks which manifests as a strength recovery and may even exceed the pre-exposure strength. The results presented in this paper were used to develop a numerical model that predicts the onset of cracking in cement based composites upon sulphate exposure.

3.5 CURRENT FINDINGS

■ The effect of sulfate exposure on compressive and tensile response of cement based systems is not as reflective of damage as evident from the length change measurements. As expected the mix with Type HS cement showed minimum change in length upon exposure, whereas the fly ash blended IC binder exhibited the largest change in length.

■ It was recognized by the author that there was no perceptible difference in length changes of HS type specimens between exposed and unexposed conditions (0.01%) that means sulfate environment had little effect to shrinkage performance, particularly when using HS type cement. Resultant length increments were attributed to the production of ettringite that contributes to the volume expansion inside specimens.

■ The air-void network as quantified using Mercury Intrusion Porosimetry illustrates that although the total porosity was identical, the median pore size with the IC binder is 5-6 times smaller than that with the Types GU and HS cement. Therefore, the formation of ettringite in the former results in expansion and allows deeper sulfate ingress. However, it is likely that continued exposure to sulfate results in a healing that manifests in higher strength at 12 weeks exposure.

3.6 SUGGESTIONS AND FUTURE WORK

■ **Modulus of elasticity.** For the purpose of service life prediction, it is recommended to have compressive stress-strain experiment on cylindrical samples. The modulus of elasticity from stress-strain response enable us to obtain volumetric change due to the production of ettringite. The change of compressive elastic modulus is critical to the expansion stress after varying durations of exposure. Besides, the tensile stress-strain response is also suggested in this study although the tensile elastic modulus can be calculated by the compressive elastic modulus.

■ **Curing Conditions.** InterCem blend, comprising 30% of fly ash and 70% of CSA type GU cement, was examined to be more susceptible to sulfate environment with short-term exposure of 12 weeks. Whereas cement-based blend with fly ash admixture is supposed to achieve higher resistance to adverse sulfate attack. Some researchers has corroborated fly ash of improvement to sulfate attack resistance as longer as 24 months of exposure (Al-Dulaijan et al. 2003). The deterioration of InterCem blend when exposed to sulfate environment may be attributed to the short-term curing of 28 days, in which the effect of fly ash replacement is not completely reinforced. Longer curing duration prior to exposure, more than 28 days experienced in this work, is highly suggested in comparison with the short-term curing.

■ **Flexural Strength.** To completely analyze the physical properties of tested materials under adverse sulfate attack, flexural strength shall be investigated conforming to related ASTM specifications.

4   SAMPLE   EXTRACTION   AND   EQUIVALENT   DEPTH CALCULATION

4.1   INTRODUCTION

4.1.1 OBJECTIVES

Sulfate content is employed as a direct feature that indicates the severity of sample damage under adverse sulfate attack. It is required to obtain the sulfate contents inside the cement samples after exposure and a physical extraction method is preferred in this project to collect independent powdered samples at defined depths from the surfaces. Particularly, titration experiment is planned for sulfate content correlated to defined locations in this work in accordance with ASTM C114 standard (C114-13 (2013)). In addition, precise equivalent depths of extracted samples are also required for sulfate content determination in the numerical modeling. Similar extraction method has never been developed nor mentioned in related publications or journals for purpose of precise sampling inside cement based materials.
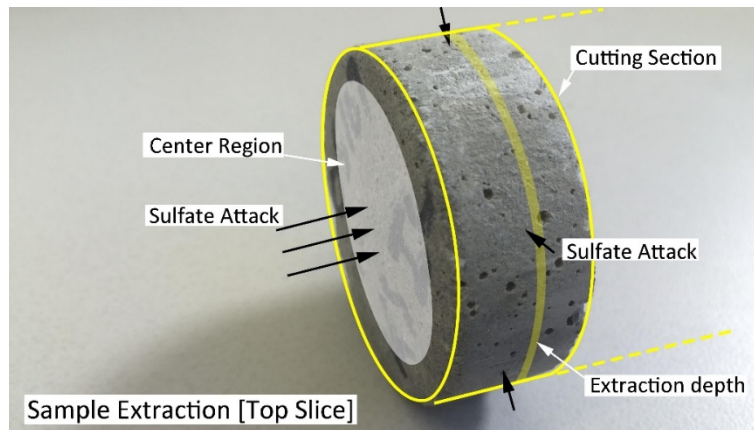
Figure 4.1. Objective to extract samples by infiltration depths

Figure 4.1 presents the sulfate attack environment and the defined extraction area in the middle of cylinder surface. Considering the exposure conditions introduced in this work, the broadside of cylindrical specimen is subjected to approximately one dimensional sulfate

attack, whereas the curved surface is difficult to be fixed or drilled. Two end pieces, with the thickness of 15 mm and 10 mm, are exposed to sulfate attack from both broadside and end face.

The peripheral area of end piece is subjected to two-dimensional sulfate attack from both broadside and end face. To avoid the effect of two-dimensional diffusion in the peripheral area of round shape, target area is limited inside the center of cylinder surface, which is highlighted in Figure 4.1. In addition, the weight of extracted sample depends on the requirement of chemical analysis.

4.1.2 METHOD SELECTION

In order to extract powdered samples inside cylinders, several existing methods are appropriate such as mechanical grinding, drilling and smashing. The grinding machine grinds the whole cylinder surface with defined thickness while smashing obtains the internal samples randomly and variously. Study by Sun et al. reported that very similar powdered samples were extracted for titration experiment whereas detailed extracting procedures were not mentioned in the publications (Sun et al. 2013).

As mentioned, central area of both end surfaces is identified as one-dimensional diffused area under sulfate attack. Central area is preferred for sample extraction in this exposure condition. Extraction is supposed to be within the highlight center area as shown in Figure 4.1 ensuring that all the samples obtained are subjected to one-dimensional sulfate attack. On the other hand, precise area of sampling is necessary based on the research requirement. Consequently, extraction by drilling is preferred since it is a direct method to collect powdered samples in defined regions. Whereas there is little information in the literature on the sample extraction inside cement-based specimens for chemical analysis, nor in the

related ASTM standards. Further, detailed procedures and calculation steps were developed and finalized in this study.

4.2   TOOL PREPARATION

As mentioned in the introduction, extraction by drilling was introduced to obtain powdered samples of defined area inside specimens. Owing to the very limited data existing to explain the method of extraction, preliminary experiment scheme was chosen considering the availability of tools and convenience of operation.

In general, samples were firstly drilled on a stable workbench manually by electric hammer drill. As listed in Table 4.1, drill machine is specified to powerful hammer drill with concrete drill bit of varying sizes. The size of drill bit had not been determined after samples were extracted and weighed by trial experiment. Trial experiment was then executed with spare sample pieces following the preliminary scheme prior to formal experiments, and all the tools and materials were commercially sourced. Table 4.1 presents all the tools and materials required based on the preliminary scheme.

Personal Protective Equipment (PPE) was also required during the whole experiments. The drill experiments were executed in the construction laboratory at the University of Alberta.

Table 4.1. Required tools, devices and PPE during the drill experiments

Items	Model	Quantity	Items	Quantity
Portable hammer drill	Skil 7A hammer drill	1	Lab coat	1
Hammer drill bits	Bosch drill bit kit	1	Dusk mask	1
Fixtures	Adjustable clamps	4	Steel toe boots	1
Caliper		1	Safety glasses	1
Storage tubes	Falcon Tube	60	Earplug	20
Steel plate		1	Rubber gloves	20
Plastic restraint sleeve		1		

4.3 DRILLING TRIAL

4.3.1 PRELIMINARY SCHEME

Procedures. The objective of trial experiment was to collect powered samples with required quantity and then develop the detailed procedures for formal experiment. It was firstly specified to 1/2 inch diameter of drill bit and one position in the center of cylinder was chosen by drilling (see Figure 4.3). Due to the round shape of surface, it was hard to fix the piece while drilling. Hence two adjustable clamps were employed to fix the piece crisscross and to avoid horizontal movement. Besides, a plastic restrain sleeve was covered around the cylindrical piece in case of partial damage near the crosswise fixture. Thick cushion base was also placed under the specimens to mitigate the vibration caused by impaction.

It was calculated by Eq. (4.1) that the weight of powder sample drilled for 3 mm thickness layer by 1/2 inch drill bit was 0.912 gram. The density of tested cement mortar was measured between 2,300kg/m^3 − 2,400 kg/m^3.

$$m = \rho \cdot v = \rho \cdot A \cdot H_{L} = \rho \cdot \frac{\pi \cdot D^2}{4} \cdot H_{L} \qquad (4.1)$$

Where:

$\rho = 2{,}400\,kg/m^3$, Density of the cement mortar

H_{L} = the thickness of layer in drill hole (mm)

D = diameter of the drill bit/drill hole (mm)

A = area of the drill hole (mm)

As scheduled, powdered samples were taken out for sulfate content determination that was broadly based on ASTM C114 standard. It is suggested in ASTM C114 standard that the optimum weight of powder sample is around 2 grams. Thus more samples per layer were supposed to be collected by means of adding more drilling holes inside the same surface. The simulation on longitudinal section of drill trial was sketched by Google Sketch Up® and presented in Figure 4.2.
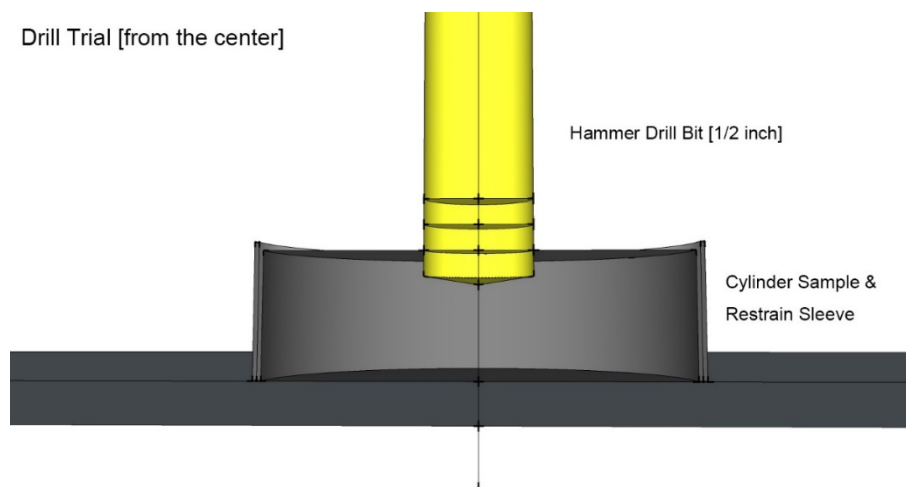
Figure 4.2. Simulation of drill trial from the center of sample surface

Calculation of Equivalent Extraction Depth. It was realized that in this case, the longitudinal section of drilled hole was not regular rectangle due to the tip shape of drill bit. Thus, to calculate the equivalent depth of each layer samples extracted, three depth were measured by caliper as presented in Figure 4.3.

The maximum depth (a_i) in the center, two edge depths $(b_{1i}$ and $b_{2i})$ were chosen to retrieve the actual area of longitudinal section. In this manner, the distance from the centroid to the surface (x_i), representing the equivalent depth of each layer, was calculated by Eq. (4.2) and Eq. (4.3) based on the identical area principle explained in Figure 4.3.
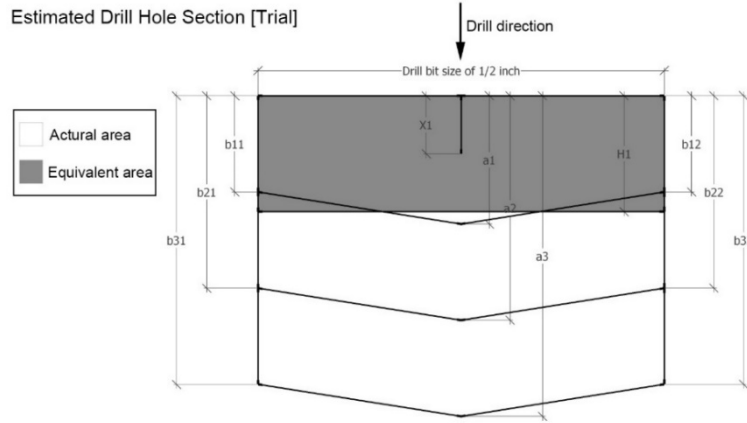
Figure 4.3. Estimated longitudinal section of drilled hole (3 layers in this case)

Note that two dimensional equivalent depths were retrieved for the sake of simple calculation in trial experiment. A comparison with 2D and 3D simulation was investigated later revealing that equivalent extraction depth deduced by 3D simulation was more precise to represent the location of extracted sample.

$$A_{ai} = \frac{b_{i1} + b_{i2}}{2} \cdot D + \frac{1}{2} \cdot \left(a_i - \frac{b_{i1} + b_{i2}}{2} \right) \cdot D \qquad (4.2)$$

$$A_{ei} = D \cdot H_i = 2 \cdot D \cdot x_i \qquad (4.3)$$

Where:

A_{ai} = actual vertical area at any layer of drill hole (2D model)

A_{ei} = equivalent vertical area at any layer of drill hole (2D model)

b_{i1}, b_{i2} = two measured depths of hole wall at i layer (mm)

a_i = measured maximum depth in the center of hole at i layer (mm)

x_i = depth from surface to the equivalent centroid at i layer (mm)

$i \in [1, N], N \rightarrow$ Number of layers

4.3.2 PROBLEMS ENCOUNTERED AND SOLUTIONS

Destruction. It is a potential issue that may occur in many kinds of physical extraction methods that specimens are likely to crack or fracture by machinery vibration.

In this experiment, when sample was fixed crosswise as shown in Figure 4.4, stress concentration appeared along the two crossed fixture lines. Moreover, the center of the round shape was also the center of stress. High-speed drilling in the center probably damaged the piece because of the stress concentration.
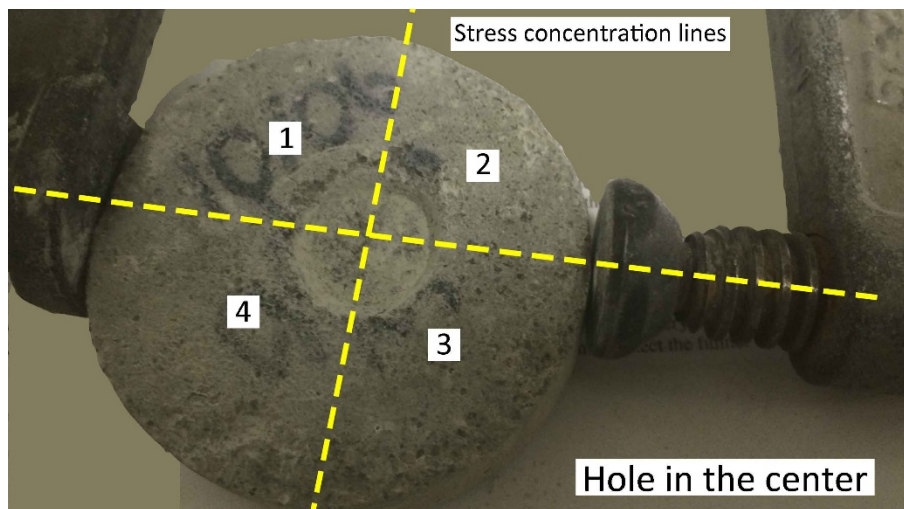
Figure 4.4. Stress concentration lines when fixed crosswise and drilled from center

During many trials of drilling in the center, samples cracked or even broke with the extraction depth only 7 mm out of 15 mm of the whole thickness (see Figure 4.5). However, when the extraction positions located inside the area 1, 2, 3 and 4 as shown in Figure 4.4, it succeeded to drill through the whole samples without damaging the integrity of the specimen. In addition, it was necessary to adjust the size of drill bit in view of the smaller drilling areas presented.
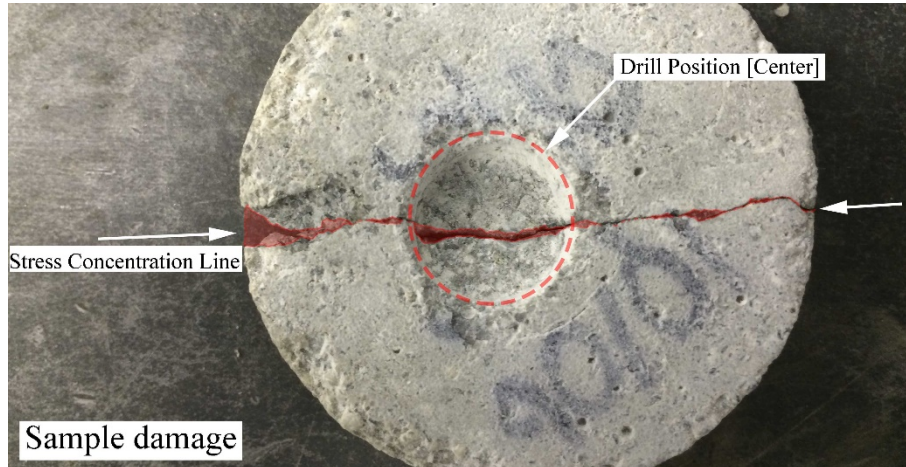
Figure 4.5. Sample damage when drilled on the stress concentration line

Figure 4.5 presents that the sample cracked to two pieces after being extracted for the first layer. Optimized drill positions outside the stress concentration line enabled us to even penetrate the whole piece. Figure 4.6 shows that four full holes were drilled through the whole sample of 15 mm thickness with the specimens un-cracked. The samples were integrally maintained after four holes were drilled inside the round surface.

The size of drill bit applied in the following figure was 3/8 inch that was the most applicable size in order to collect enough weight of powdered samples after trials and failures.
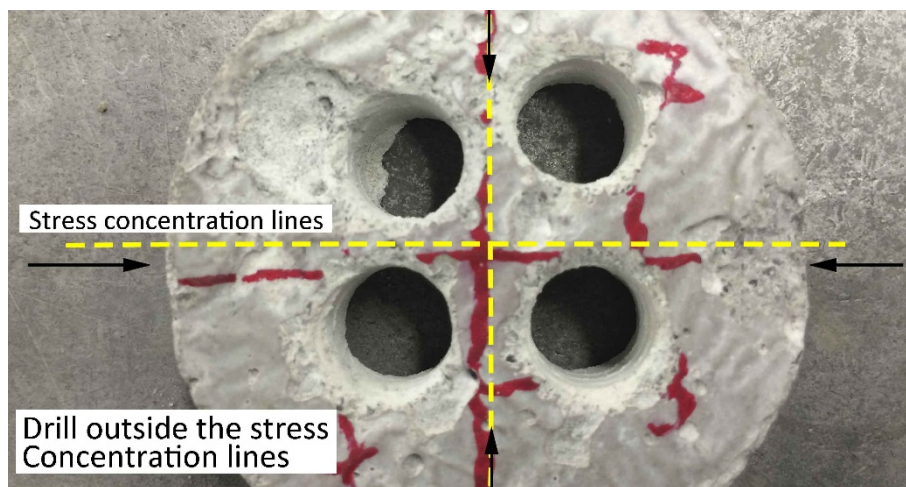
Figure 4.6. Bore holes drilled throughout the sample within desired locations

Contamination. As mentioned in the preliminary scheme, powdered samples were collected layer by layer when extracted from the specimen. The residual powder on the hole walls between adjacent layers may contaminate the collected powder. To avoid the contamination, two steps were developed including brushing and cleaning by compressed air.

In particular, it is suggested to brush the bore holes prior to compressed air cleaning after the powdered sample was collected and stored upon each layer. Compressed air was forced to completely clean each layer of drilled holes.

Besides, the residual powder on the hole walls was collected once and was weighed of 0.002 gram out of 2 grams of sample weight per layer in average. The contamination was evaluated of little effect hence the cleaning steps were required during formal experiments after the sample collection (see Figure 4.7).
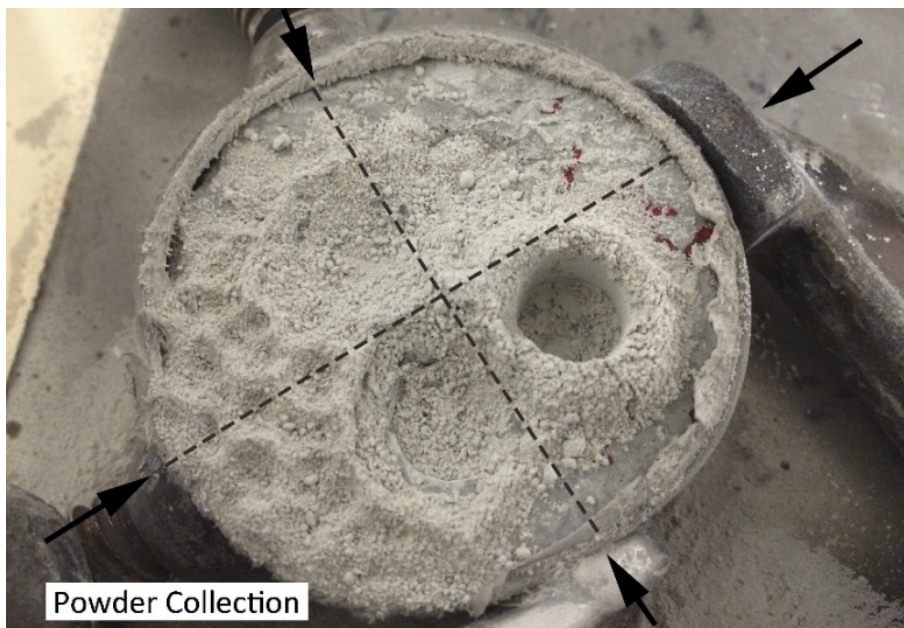
Figure 4.7. Powder sample distribution after drilling for one layer

4.4   FORMAL EXPERIMENTS

4.4.1 FIXTURE SETUPS

The fixture setup of the cylinder specimen affected the drill operation. Depending on what concluded after the extraction trial, four fixture clamps were used to fix pieces horizontally on the workbench: two clamps were for fixing the specimen crosswise and two clamps for fastening the unit tightly on the table. Figure 4.8 simulates the operating conditions while drilling. The restrain sleeve released the stress on fixed points, which reduced the possibility of sample damage under violent vibration.
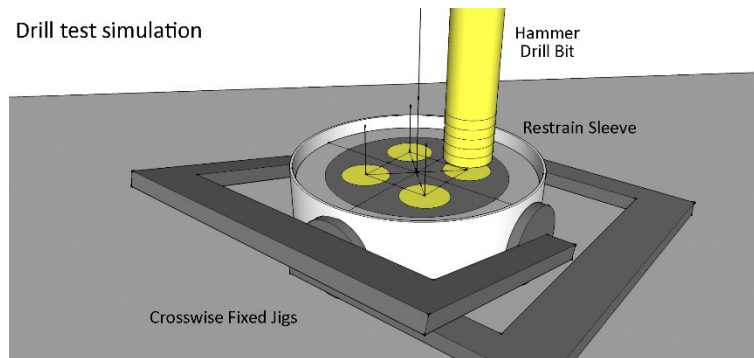
Figure 4.8. The simulation of drill test and fixture setup

During the formal experiments, a steel plate of 300 mm length and 200 mm width was placed under the sample as the cushion base. Other setups were kept the same as the simulation (see Figure 4.8 and Figure 4.9).
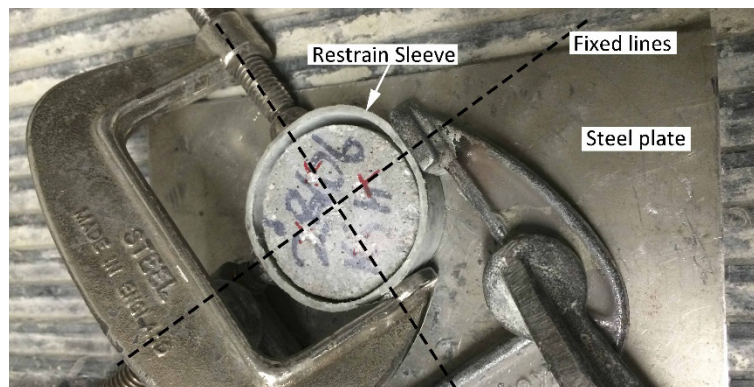
Figure 4.9. Fixture setup and fixed lines in formal experiments

4.4.2 Positions of Drilled Holes

Because of the insufficient powdered sample obtained by one drill hole during the trial experiment, four positions were chosen for extraction inside defined area as explained in Section 4.3. Figure 4.10 presents the planform view of drill positions inside the round surface. By using the 3/8 inch size drill bit, the distance between adjacent hole centers was controlled over 15 mm in view of the operating errors while drilling.

Based on the problems encountered in drill trial, selected drill positions were supposed to locate outside the crossed fixture lines. Four drill positions were distributed evenly in the center area and were labeled orderly from 1 to 4 for measuring convenience and identification (see Figure 4.10).
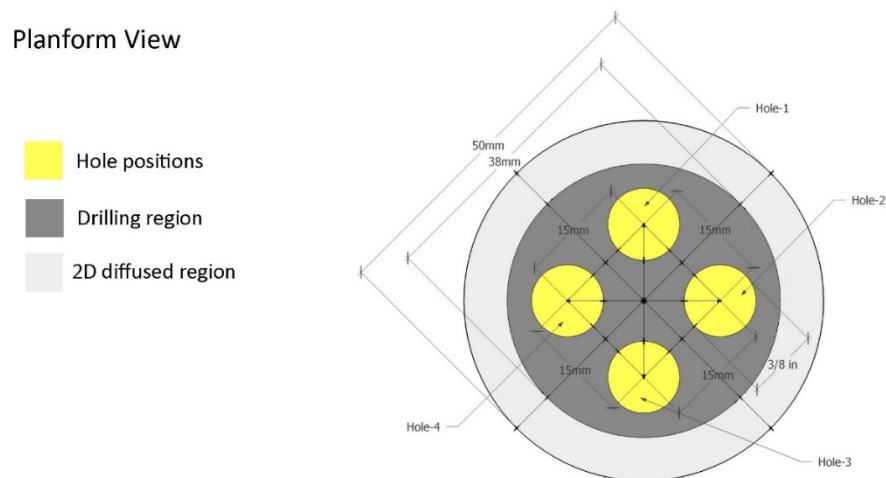
Figure 4.10. The Planform view of bore holes' positions inside sample surface

Drilling positions should locate in the dark gray area in Figure 4.10 since the peripheral area was determined as the portion subjected to two directional sulfate attack in this work. However, samples subjected to one dimensional sulfate diffusion were preferred in order to evaluate the severity of sulfate attack. For the simplicity of equivalent depth simulation, four holes were drilled perpendicularly to the surface by 3/8 inch drill bit. Powder was collected and stored afterwards.

4.4.3 DRILLING

As mentioned at the outset, two end pieces cut from cylindrical specimens are applicable for extraction. Specifically, top piece of each type specimen subjected to sulfate attack, with thickness of 15 mm, was chosen for extraction. Other pieces were reserved in case of damage of chosen piece.

The weight of powdered sample for each layer was recalculated considering operation loss as per Eq. (4.4).

$$m' = \zeta \cdot \rho \cdot v \qquad\qquad (4.4)$$

Where,

$\zeta = 0.9$, Coefficient containing operation loss

$\rho = 2{,}400 \, kg/m^3$, Density of the cement mortar

$V = 4 \cdot A \cdot h$, Volume of 4 holes with depth of h

It was recognized that powder did not splash out due to the revolving drill bit. In contrast, the air disturbance gathered powder around the drill bit, from which there was little powder loss during the operation. Drilling made it easier to collect powdered samples in this case. An estimation on the quantity of extracted samples based on Eq. (4.4) suggested that the thickness of each layer of extraction was expected to 2 mm for four positions per specimen. As the simulation presented in Figure 4.11, the applicable size of drill bit was chosen to 3/8 inch after trials and errors. However, in accordance with varying exposure durations, larger thickness from 2 mm to 4 mm per layer was decided in this work, owing to the concerning that sulfate concentration after short-term exposure may not be detected by chemical analysis if insufficient powdered sample was collected.
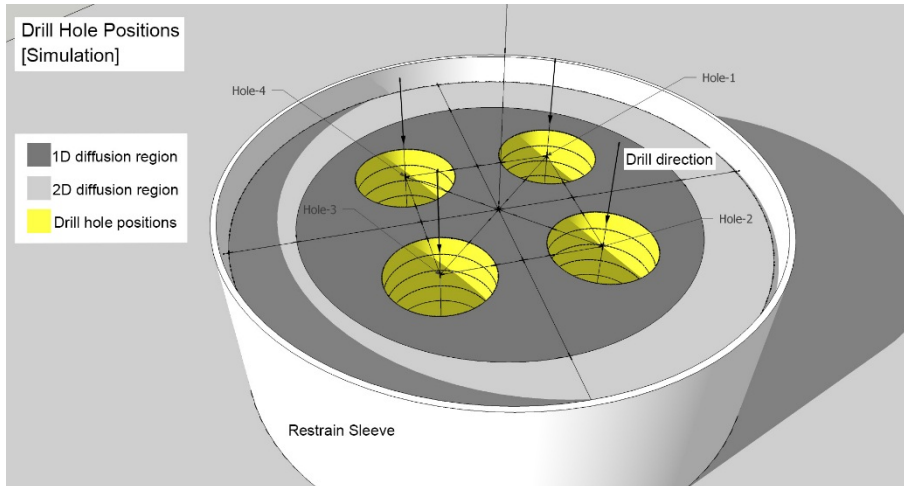
Figure 4.11. The 3D simulation of drilled holes and estimated layers
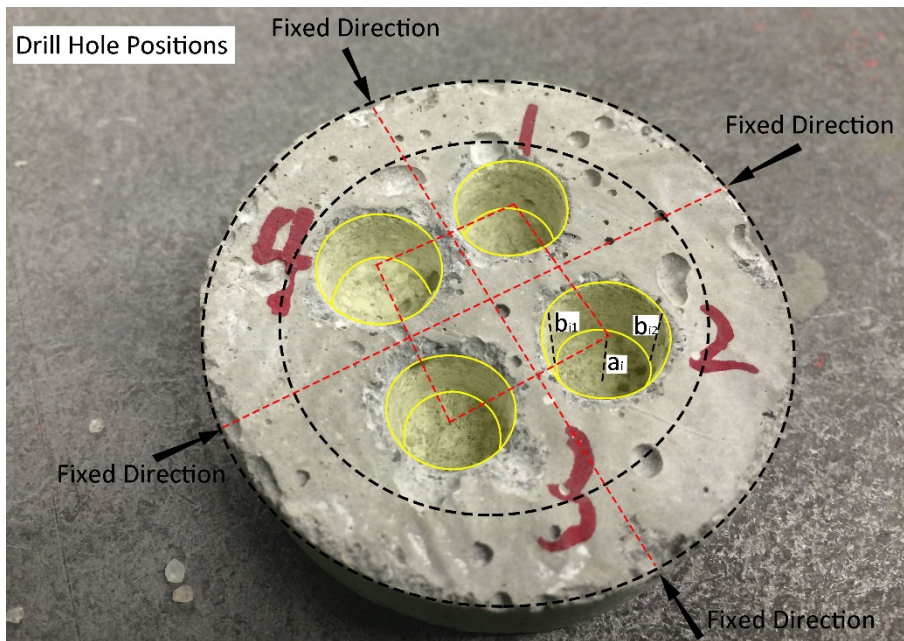
Figure 4.12. Analysis image on drilled samples with required measurements

The structure of specimen after extraction, as shown in Figure 4.12, was witnessed same as the simulation sketched beforehand in Figure 4.11, which was verified for the practicality and convenience of this extraction method. In fact, 4 or 5 layers of powder were extracted upon 4-week, 8-week and 12-week of exposure considering the deeper diffusion depths; 3 layers of powder were extracted for 1-week and 2-week exposure relatively.

4.4.4 SECTION ANALYSIS

During one experiment, drilled samples was cut so that the longitudinal section of drilling hole was then analyzed (see Figure 4.14). Apparently, the actual shape of longitudinal section in Figure 4.12 conformed to the shape in the simulation sketch in Figure 4.13. Three measured depths as described in Drilling Trial, b_{i1}, b_{i2} and a_i were obtained for each layer after extraction.

Figure 4.13 shows that the diamond drill bit (yellow color) was perpendicular to specimen surface when drilling. Sample in the first layer, closest to the surface, was firstly extracted and collected prior to extraction of the next layer.
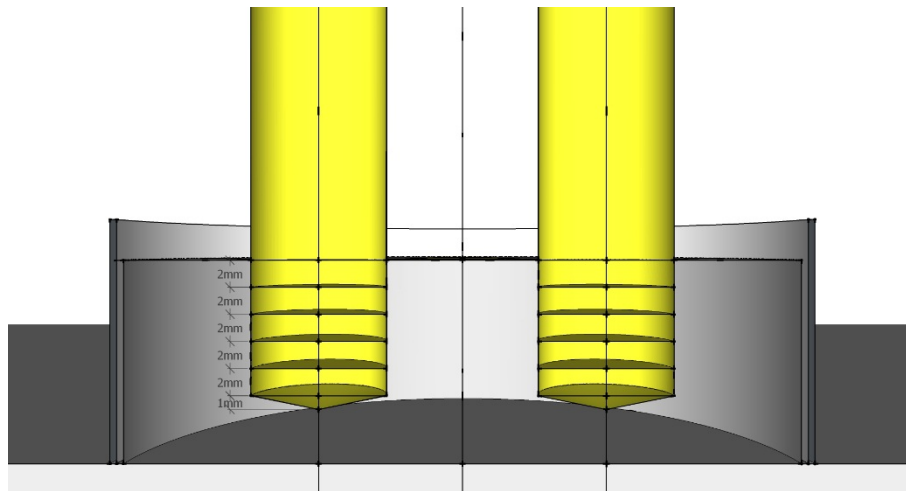
Figure 4.13. Simulation on vertical section of drilled holes and layers

Two dimensionally, it was recognized that the longitudinal section of extracted sample layer was a rectangle combined with a triangle. Whereas more precise equivalent extraction depth of layer was supposed to be determined by three dimensional analysis on drilled holes, which was presented in section Calculations in this chapter.
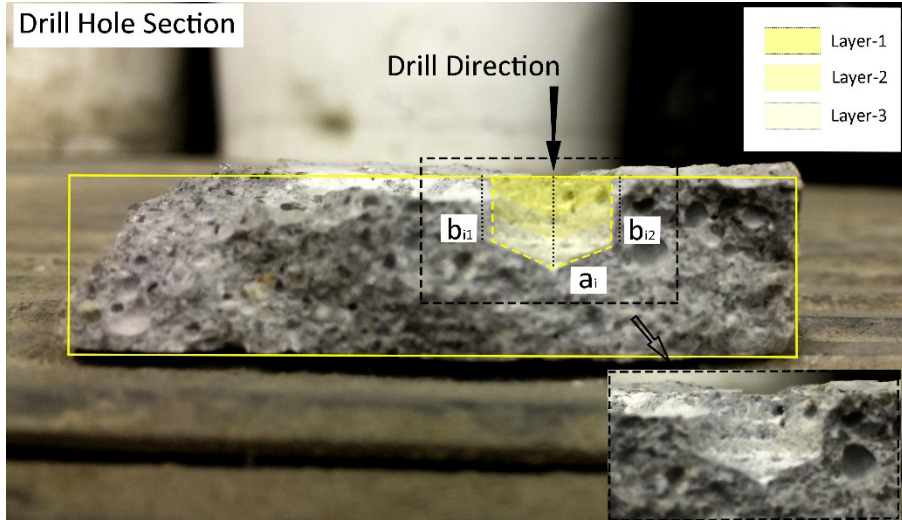
Figure 4.14. Analysis image on vertical section of drilled hole with required measurements

As analyzed in Figure 4.14, beside two depths, b_{i1} and b_{i2}, measured at the edge upon each layer, one depth in the center was also retrieved by caliper and was named as a_i. There were three layers extracted in the presented section with the maximum depth of 10.540 mm.

4.4.5 STORAGE

Figure 4.15 presents the plastic storage tubes for collected powdered samples. 10 mL sealed tube was employed to store each layer of powder sample in case of contamination. Stored powder samples were namely labelled for chemical experiments. In total, 59 powdered samples were stored by cement types, layers and exposure durations.

Figure 4.15. 10 mL labeled and sealed storage tubes for powder

4.5   CALCULATIONS

4.5.1 LAYER SECTIONS

The calculation in the preliminary scheme was two dimensional integration of longitudinal section. In reality, the drilled hole was three dimensional so that the calculation method should be developed considering the internal geometric size. Figure 4.16 presents the simulated 3D geometric shape of one drilled hole. Note that in this instance, the body center from 3D analysis was different from the centroid of 2D shape calculated in Drilling Trial. Based on the equal body moment inertia, the revised equivalent extraction depths were recalculated by integrating 3D geometric shapes.
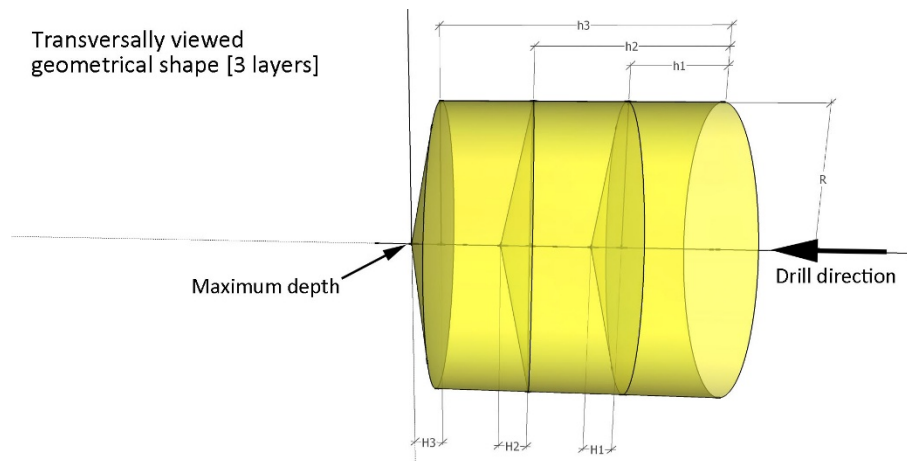
Figure 4.16. 3D simulation on transversally viewed geometrical shape of drilled hole

4.5.2 EQUIVALENT EXTRACTION DEPTHS

Circular Cone Integration. Note that the tip shape of drill bit was conical, the geometrical shape of drilled hole was column combined with a circular cone. Figure 4.17 presents the integral method of circular cone in order to obtain the body center of tip. In Figure 4.17, polar coordinates and rectangular coordinates systems were both employed calculating the equivalent extraction depths of each layer. As assumed, cement sample inside the circular cone was homogeneous for convenient calculation.
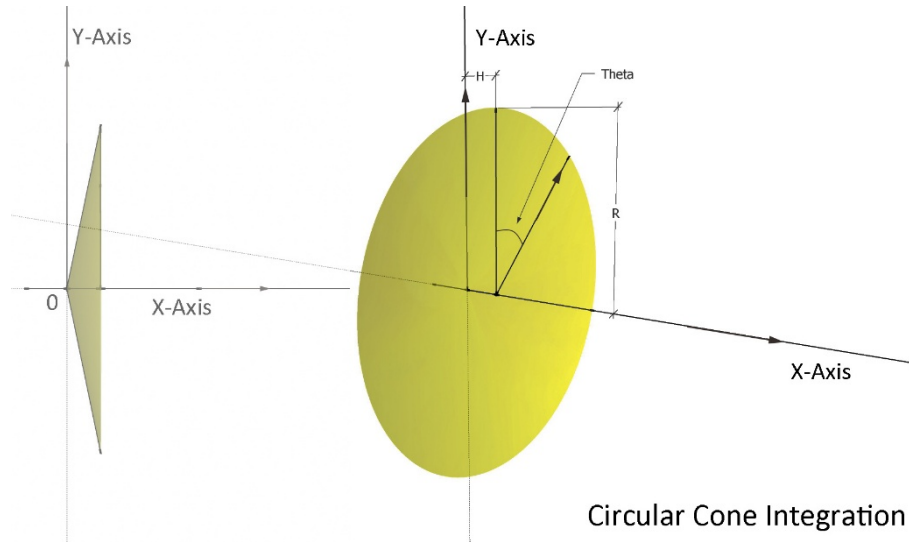
Figure 4.17. Integration of circular cone simulating the shape of drill bit tip

$$\left(\frac{1}{3} \cdot \pi \cdot R^2 \cdot H\right) \cdot \bar{x} = \int_0^H \int_0^{\frac{R}{H} \cdot x} \int_0^{2\pi} r \cdot x \, d\theta \, dr \, dx \qquad (4.5)$$

Where,

R = the radius of the drill bit/drill hole (mm)

H = the height of the drill bit tip (mm)

$\bar{x} = (3/4) \cdot H$, the distance from body center to the bottom of circular cone

First Layer Integration. When combined circular cone with the column, the body center was recalculated for the first layer of drilled hole. Figure 4.18 explains the relationship between measured parameters and calculated parameters. The thickness of cylinder, h_i was averaged by the two measured depths of b_{i1} and b_{i2}.

Also, the maximum measured depth of a_i was equal to cylinder thickness h_i plus the height of circular cone H_i. By using the equal-volume principle, the body center was obtained as per Eq. (4.6).
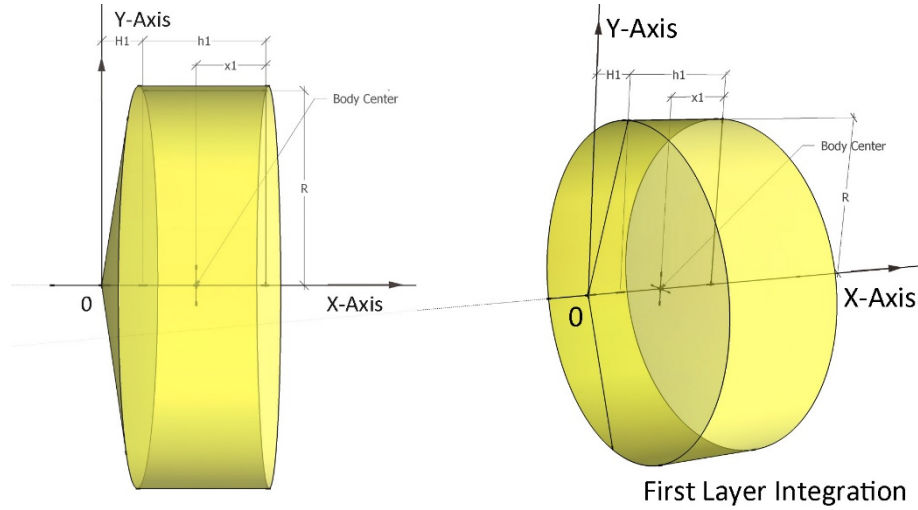
Figure 4.18. Integration of the first layer to determine the body center

For the first layer of drilled hole, the distance from the surface to the body center was calculated by equal inertia moment equation,

$$\frac{1}{3} \cdot H_1 \cdot A_b \cdot (\frac{H_1}{4} + \frac{h_1}{2}) = A_b \cdot (h_1 + \frac{H_1}{3}) \cdot (X_1 - \frac{h_1}{2}) \tag{4.6}$$

Where:

$H_1 = a_1 - (b_{11} + b_{12})/2$, the height of circular cone at the first layer (mm)

$h_1 = (b_{11} + b_{12})/2$, the depth of cylindrical hole at the first layer (mm)

$A_b = \pi \cdot R^2 / 4$, the bottom area of drill hole (mm^2)

$X_1 = X_{L1}$, the equivalent extraction depth at the first layer (mm)

So that the equivalent extraction depth of first layer was rearranged below:

$$X_{L1} = X_1 = \frac{H_1^2 + 4H_1 h_1 + 6h_1^2}{4H_1 + 12h_1} \tag{4.7}$$

The Second and Other Layer Integrations.
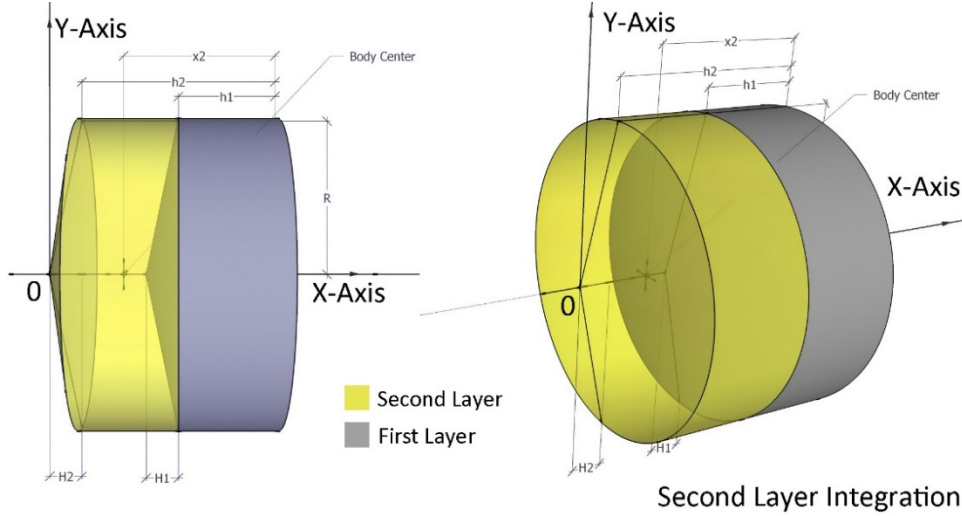
Figure 4.19. Integration of the second layer to determine the body center

The calculation for equivalent extraction depth of the second layer was deduced and listed:

$$A_b \cdot [\frac{1}{3} \cdot (H_2 - H_1) + (h_2 - h_1)] \cdot X_2 = \int_0^{H_2} \int_0^{\frac{R_x}{H_2}} \int_0^{2\pi} x \cdot rd\theta drdx$$

$$+ \int_{H_2}^{H_2+(h_2-h_1)} \int_0^R \int_0^{2\pi} x \cdot rd\theta drdx - \int_{(H_2-H_1)+(h_2-h_1)}^{H_2+(h_2-h_1)} \int_{H_1}^{\frac{R}{H_1}(x-(H_2-H_1)+(h_2-h_1))} \int_0^{2\pi} x \cdot rd\theta drdx \qquad (4.8)$$

The equivalent extraction depth of the second layer,

$$X_{L2} = \frac{(H_2^2 - H_1^2) + 4(H_2 h_2 - H_1 h_1) + 6(h_2^2 - h_1^2)}{4(H_2 - H_1) + 12(h_2 - h_1)} \qquad (4.9)$$

Where:

$H_2 = a_2 - (b_{21} + b_{22})/2$, the height of circular cone at the second layer (mm)

$h_2 = (b_{21} + b_{22})/2$, the depth of cylindrical hole at the second layer (mm)

$X_2 = X_{L2}$, the equivalent extraction depth at the second layer (mm)

$A_b = \pi \cdot R^2 / 4$, the bottom area of drill hole (mm^2)

As the geometric shape simulated in Figure 4.19 and the calculation of the second layer, depth of other layers can be deduced using equal body moment inertia. The equivalent extraction depth of any layer was presented in Eq. (4.10).

$$X_{Li} = \frac{(H_i^2 - H_{i-1}^2) + 4(H_i h_i - H_{i-1} h_{i-1}) + 6(h_i^2 - h_{i-1}^2)}{4(H_i - H_{i-1}) + 12(h_i - h_{i-1})} \tag{4.10}$$

Where:

X_{Li} = equivalent extraction depth at i layer (mm)

$H_i = a_i - (b_{i1} + b_{i2})/2$, height of circular cone at i layer (mm)

$h_i = (b_{i1} + b_{i2})/2$, the depth of cylindrical hole at i layer (mm)

4.5.3 PROGRAMING

To verify the expressions of equivalent extraction depths deduced above, programmable codes were developed by Mathematica and the results were exactly the same as shown in Figure 4.20.


```
In[39]:= (*Calculation for the equivalent drill depth by software Mathematica*)
        (*Layer-1*)
        I11 = Integrate[r*x, {x, 0, H1}, {r, 0, R*x/H1}, {theta, 0, 2*Pi}] +
            Integrate[r*x, {x, H1, H1 + h1}, {r, 0, R}, {theta, 0, 2*Pi}];
        I12 = (H1/3 + h1) * Pi * R^2 * (H1 + h1 - x1);
        Solve[I11 == I12, x1]
        (*Layer-2*)
        I21 = Integrate[r*x, {x, 0, H2}, {r, 0, R*x/H2}, {theta, 0, 2*Pi}] +
            Integrate[r*x, {x, H2, H2 + h2 - h1}, {r, 0, R}, {theta, 0, 2*Pi}] -
            Integrate[r*x, {x, H2 - H1 + h2 - h1, H2 + h2 - h1},
            {r, 0, R*(x - (H2 - H1 + h2 - h1))/H1}, {theta, 0, 2*Pi}];
        I22 = (h2 - h1 + (H2 - H1)/3) * Pi * R^2 * (H2 + h2 - x2);
        FullSimplify[Solve[I21 == I22, x2]]

Out[41]= {{x1 -> (6 h1^2 + 4 h1 H1 + H1^2)/(4 (3 h1 + H1))}}

Out[44]= {{x2 -> (6 h1^2 + 4 h1 H1 + H1^2 - 6 h2^2 - 4 h2 H2 - H2^2)/(4 (3 h1 + H1 - 3 h2 - H2))}}
```

Figure 4.20. Mathematica Program code for the equivalent extraction depths

When employing the drill experiments as demonstrated using standard drill bits with sharp tips specifically for concrete composites, calculating expressions for equivalent depths by above programing would be applicable.

4.6 ANALYSIS ON RESULTS

In this work, beside CSA type GU and HS cements, one blend named InterCem with 30% fly ash replacement of GU cement investigated by extraction method. In total, 59 groups of powdered samples were collected sorted by cement types, layers and exposure durations. One GU type specimen was extracted in trial, so that more layers were obtained than HS and InterCem specimens, which was presented below.

Table 4.2. Measured and calculated depths of HS type as affected by layers and exposures

	Layer	a_i (mm)	b_{i1} (mm)	b_{i2} (mm)	h (mm)	H (mm)	x (mm)
HSS-12	1	3.7050	2.5975	2.5775	2.5875	1.1175	1.4923
	2	6.0375	4.9275	4.9250	4.9263	1.1113	2.6549
	3	8.3100	7.0950	7.3550	7.2250	1.0850	3.7979
	4	11.9575	10.7050	11.0375	10.8713	1.0863	5.6196
HSS-8	1	3.7150	2.2350	2.5225	2.3788	1.3363	1.4317
	2	5.8800	4.3225	4.5225	4.4225	1.4575	2.4663
	3	8.3650	6.9725	7.0550	7.0138	1.3513	3.7393
	4	10.4850	9.3700	9.4125	9.3913	1.0938	4.8814
HSS-4	1	3.6275	2.0575	2.7875	2.4225	1.2050	1.4274
	2	6.3850	4.6725	5.4000	5.0363	1.3488	2.7523
	3	9.1375	7.8900	8.6950	8.2925	0.8450	4.2894
	4	11.2700	9.7700	10.6900	10.2300	1.0400	5.2912
HSS-2	1	3.7625	2.7625	2.5850	2.6738	1.0888	1.5298
	2	6.9425	5.3925	5.5275	5.4600	1.4825	2.9874
	3	10.8500	9.8675	9.9625	9.9150	0.9350	5.1157
HSS-1	1	3.2950	2.2500	2.2075	2.2288	1.0663	1.3046
	2	7.7825	6.8200	6.8950	6.8575	0.9250	3.5864
	3	10.3300	9.4650	9.4825	9.4738	0.8562	4.8817

Table 4.3 lists the measured depth and calculated parameters of InterCem® specimen by layers. It is to be noted that the height H_i was approximately equal to 1 mm that was same as the height measured on the drill bit. Further, b_{i1} and b_{i2} were very close that means the drill bit was approximately perpendicular to the sample surface.

Table 4.3. Measured and calculated depths of IC type as affected by layers and exposures

Group	Layer	a_i (mm)	b_{i1} (mm)	b_{i2} (mm)	h (mm)	H (mm)	x (mm)
ICS-12	1	3.7775	2.5100	2.5625	2.5363	1.2413	1.4904
	2	5.6100	4.2125	4.2650	4.2388	1.3713	3.8271
	3	8.0225	6.4100	6.9700	6.6900	1.3325	5.9144
	4	9.7175	8.7850	8.7250	8.7550	0.9625	8.0938
	5	12.1525	11.0000	10.8875	10.9438	1.2088	10.2177
ICS-8	1	3.3560	2.2200	2.1440	2.1820	1.1740	1.3018
	2	6.1650	4.8775	4.8125	4.8450	1.3200	3.9328
	3	9.4800	8.5625	8.7150	8.6388	0.8413	7.0942
	4	13.2800	12.2500	12.2500	12.2500	1.0300	10.7588
ICS-4	1	3.1275	1.7250	2.1450	1.9350	1.1925	1.1833
	2	5.2200	3.9525	4.3625	4.1575	1.0625	3.4186
	3	7.8500	6.8375	7.1350	6.9863	0.8638	5.8891
	4	10.1875	8.8875	9.3700	9.1288	1.0588	8.3840
ICS-2	1	3.7025	2.3450	2.7475	2.5463	1.1563	1.4794
	2	7.7750	6.7125	7.1350	6.9238	0.8513	5.0652
	3	10.5450	9.6850	10.1950	9.9400	0.6050	8.6709
ICS-1	1	5.3025	3.8700	4.0375	3.9538	1.3488	2.2136
	2	8.3025	6.9725	6.9475	6.9600	1.3425	5.9048
	3	10.6625	9.6075	9.8850	9.7463	0.9163	8.7208

As shown in Table 4.3, the maximum equivalent extraction depths of InterCem were from 8 mm to 10 mm and these depths were based on maximum infiltration depth calculated from numerical modeling. It is necessary to note that the measured depths of b_{i1}, b_{i2} and a_i were averaged by measurements of four bore holes. All the extraction depths would be used for the numerical modeling as the infiltration depths from sample surfaces in other parts of this study.
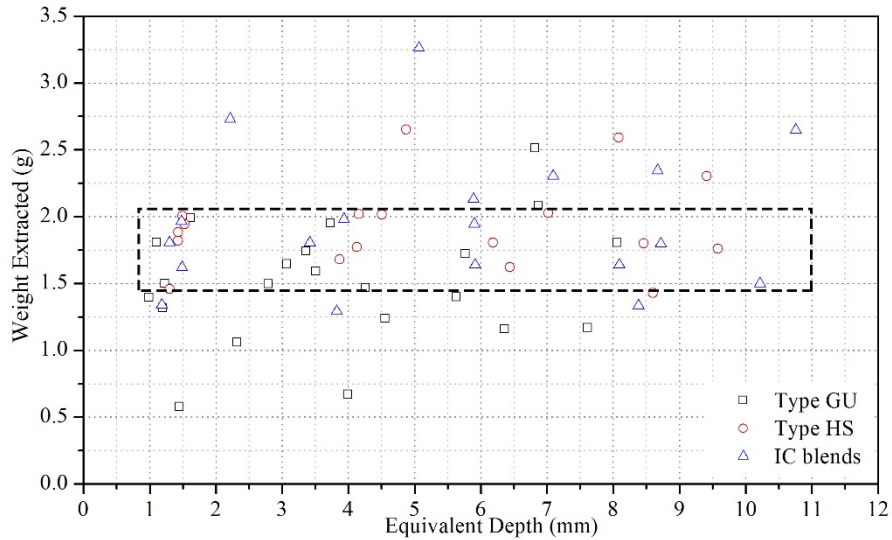
Figure 4.21. Sample weights as affected by equivalent extraction depths

Figure 4.21 plots the weights with equivalent extraction depths of all examined powdered samples. It is to be noted that most weights locate in range of 1.5 to 2.0 grams. Similar weights extracted by this method lead to high precision in chemical analysis.

4.7 POTENTIALS AND FUTURE WORK

4.7.1 POTENTIALS

The main objective of the method developed is to extract cement samples at defined area inside cast specimens. Powdered samples are required for chemical analysis. However, there is very little information in the literature on the practice of sample extraction inside cement-based materials. The present study is a detailed experimental investigation on the sampling practice in accordance with ASTM C114 standard.

In conclusion, with all procedures and calculations finalized, it is recommended that this method developed in this study is a favorable choice for the purpose of precise composition analysis. The results of extraction depths calculated are intended for sulfate attack identification with correlated sulfate contents.

4.7.2 FUTURE WORK

Note that in the present instance, extraction was easily operated by simple tools and materials.

The development of experimental equipment is necessary for various sizes of specimens and required extraction depths.

Automatically controlled drilling machines, such as table drill with depth controller, are preferred to simplify the procedures with higher extraction precision. If available, lager specimens are also preferred considering the size of drill bit and the powder weight collected.

5 SULFATE CONTENT DETERMINATION BY TITRATION EXPERIMENT

5.1 INTRODUCTION AND RATIONALE

5.1.1 INTRODUCTION

Sulfate concentration is one of the featured factor that indicates the resistance on adverse sulfate attack of cement-based materials. When the cement-based system was exposed to adverse sulfate-rich environment, external sulfates infiltrate into the structure through micro pores and cracks and might exist in these interspaces. Similar titration experiment was studied by Sun C but limited sulfate concentrations were obtained for muerical model (Sun et al. 2013).

The work presented consists of two parts: preliminary experimental processes were firstly investigated by trials; finalized procedures were developed broadly based on ASTM C114 standard and the results obtained from trials. In this work, CSA Type GU and HS cement were examined as well as the blend InterCem cement provided by industry partner. The InterCem cement has 30% replacement of fly ash and 70% type GU cement. Technique assistance was provided by the Kirst King-Jones' laboratory in biological department in University of Alberta. Devices for chemical analysis were supported by the Kirst King-Jones' laboratory as well as consumables. The titration was operated in the teaching laboratory of environmental engineering department in University of Alberta.

5.1.2 OBJECTIVE

The main objective of the experiment described is to identify and quantify the sulfate contents inside the cylindrical specimens within defined depth. With the exposure conditions set in this work, the source of sulfate content is by far through external ingress not through internal generation as envisaged in ASTM specifications. Portland cements

comprise gypsum in the blends and may affect the sulfate content titrated if the gypsum has not been completely consumed prior to the sulfate exposure.

The SO_3 content determination was mentioned in several ASTM standards that access the chemical composites in cement-based systems. However, detailed experiment procedures and conditions are unavailable in these standards, such as temperatures, durations, devices and chemicals. Methodologies were based on the ASTM C114 standard but improved for higher precision on concentration determination. The results presented in this paper were aimed to develop a numerical model that predicted the onset of cracking in cement based composites upon sulfate exposure. Besides, the sulfate concentrations detected were an indicator to evaluate the resistance to adverse external sulfate attack.

5.1.3 STANDARD TEST METHOD

As demonstrated in the ASTM C114 standard in terms of sulfate compositions,

"To 1 g of the sample add 25mL of cold water and, while the mixture is stirred vigorously, add 5mL of HCl. If necessary, heat the solution and grind the material with the flattened end of a glass rod until it is evident that decomposition of the cement is complete. Dilute the solution to 50mL and digest for 15 min at a temperature just below boiling. Filter through a medium-textured paper and wash the residue thoroughly with hot water. Dilute the filtrate to 250mL and heat to boiling. Add slowly, drop wise, 10mL of hot barium chloride (100g/L) and continue the boiling until the precipitate is well formed. Digest the solution for 12 to 24 h at a temperature just below boiling. Take care to keep the volume of solution between 225 and 260mL and add water for this purpose if necessary. Filter through a retentive paper, wash the precipitate thoroughly with hot water, place the paper and contents in a weighed platinum crucible, and slowly char and consume the paper without inflaming. Ignite at 800 to 900 ℃, cool in a desiccator and weigh."

As explained in ASTM C114 standard (C114-13 (2013)), sulfate can be determined by barium chloride solution after the powdered samples are decomposed in hydrochloric acid, sulfate is then precipitated from an acid solution of the cement with barium chloride. The precipitated is ignited and weighed as barium sulfate and the SO_3 equivalent is calculated. However, procedures are not demonstrated in detail, experimental conditions, such as temperatures and durations, are not completely defined that in the specification.

For instance, heating environment and sample grinding are required if necessary but the heating temperature and grinding sieve are not determined in the standard. Furthermore, the standard advises to dilute the solution to 50mL and digest for 15 min at a temperature just below boiling whereas the exact temperature is still not defined.

It was recognized by the author that the standard test method in ASTM C114 specification was not practical when applying titration experiment. Broadly based on these standards that assess the chemical composites inside cement-based composites, fundamental experiment procedures were determined in this study.

5.2   EXPERIMENT PREPARATION

Material and tool preparations were decided broadly as per ASTM standards as mentioned at the outset. The standard test methods for chemical analysis of hydraulic cement ASTM C114-13 (C114-13 (2013)) and the standard test method for water-extractable sulfate in hydrated hydraulic cement mortar ASTM C265-08 (C265-08 (2008)) reveal the general test requirements for chemical determination analysis. To improve the precision of titration experiment, all the devices and materials were provided by the biological department in the University of Alberta. In accordance with the sulfur trioxide determination in ASTM C114-13 standard, 37% chloride acid solution and 10% barium chloride solution were employed in this experiment. Both the chloride acid and barium chloride solution were commercially sourced from Fisher scientific.

5.2.1 EQUIPMENT, DEVICES AND MATERIALS

Table 5.1. Tools and devices required for the titration experiments

DEVICES	QUANTITY	DESCRIPTION
Fume hood	1	Operation with hydrochloric acid
Oven	2	Automatic temperature control
Heater	1	Heating water under boiling
Desiccator	3	Cooling down after oven-drying
Stirrer	9	Fisher brand standard stirrer
Electronic balance	1	accuracy of 0.1 milligram
Air pump device	1	vacuum air pump
Pipet 1	1	Max of 5 mL/ Accuracy of 0.001 mL
Pipet 2	1	Match to transfer pipette
Beaker	3	500 mL, 1000 mL and 2000 mL
Filtering flask	1	For air pump filtration
Standard flask	120	250 mL flask for reaction
Vacuum flask	60	250 mL flask for filtration
Tube holder	1	For the centrifugation tubes
Funnel	60	Glass funnel for reactants filtration
Gooch crucible	60	For air pump filtration

Table 5.2. Chemicals and consumables required for the titration experiments

CONSUMABLES	QUANTITY	DESCRIPTION
Storage tube	60	10 mL storage tube
Centrifugation tube	60	50 mL centrifugation tube
Aluminum Dish	80	Capacity of 20 mL
Pipet tip	60	Capacity from 1 mL to 5 mL
Transfer pipette	60	5mL, 15 mL, 25 mL and 30 mL
Filter paper	150	110 mm filter paper with fast speed
Micro-filter paper	100	Crucible matched filter paper
CHEMICALS		
Barium Chloride	1	4 L of 10% $BaCl_2 \cdot 2H_2O$ solution
Hydrochloric Acid	1	1 L of 37% HCl solution
Distilled water	Sufficient	Laboratory distilled water

5.2.2 PERSONAL PROTECTIVE EQUIPMENT (PPE)

As required during chemical experiment, Lab coats, rubber gloves, masks, glasses are compulsory during the experiment in the laboratory. Note that in this case, the weight of sample was around 2 grams so that the fingerprints on tools might affect the weighing. Rubber gloves were introduced during the whole experimental procedures to reduce the possibility caused by fingerprints.

5.3   MECHANISM INVOLVED IN SULFATE ATTACK

5.3.1 TITRATING REACTIONS

As mentioned before, Portland cement based materials subjected to external sulfate attack may have sulfates infiltrating through pores and cracks during the exposure. The powdered samples available were extracted layer by layer and the sample of shallow depth was supposed to contain more sulfates from external environment.

Titration experiment was recommended in ASTM C114 standard (C114-13 (2013)) and employed in this study as the most applicable quantification method.

As for the titration experiments, powdered samples were firstly decomposed in hydrochloric acid to eliminate interruptions of carbonate and sulfite. The reactions are listed below:

$$CO_3^{2-} + 2H^+ \rightarrow CO_2(\uparrow) + H_2O \tag{5.1}$$

$$SO_3^{2-} + 2H^+ \rightarrow SO_2(\uparrow) + H_2O \tag{5.2}$$

The main reaction of sulfate titration experiment, where

$$BaCl_2 \cdot 2H_2O + SO_4^{2-} \rightarrow BaSO_4(\downarrow) + 2Cl^- + 2H_2O \tag{5.3}$$
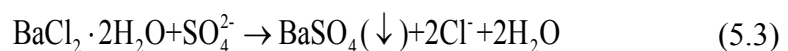
Sulfate was completely precipitated by barium chloride solution $(BaCl_2 \cdot 2H_2O)$ under stirring. The precipitate barium sulfate $BaSO_4$ was dried and then weighed while the equivalent sulfate (SO_4^{2-}) content was calculated.

Barium sulfate precipitated in the solution that was filtrated to completely obtain the barium sulfate. The content of sulfate inside cement-based composites varied by layers according to the diffusion of sulfate ingress. The deeper sample extracted, the less sulfate content it might contain. Powdered samples were sorted by layers and reacted by barium chloride solution and the barium sulfate precipitate was well formed and weighed to get the sulfate concentration by layers.

5.3.2 POSSIBLE SULFATE SOURCES

The possible sulfate compositions after exposure are from either external environment or inherent gypsum if the Portland cement was not completely hydrated. The initial SO_3 content was provided by the cement supplier and listed in Table 5.3. Thus the sulfate results obtained in this work was attributed to both external solution and inherent gypsum.

Table 5.3. SO_3 content in the three binders

	Type GU	Type HS	Blend IC
By mass (%)	2.7138	2.2185	1.8997
Content (mol/m3)	192.2441	157.1519	134.5709

5.4 TRIAL EXPERIMENT

5.4.1 MODIFICATIONS

Considering the low sulfate concentration inside the sample tested in this study, 3 grams instead of 1 gram of cement mortar powder was grinded for decomposition. 20 mL distilled water and 5 mL 37% chloride acid solution were mixed for decomposition. To determine the most efficient decomposition conditions, 6 cases were firstly applied in this work: 10 min, 35

min and 60 min of stirring while heating; 15 min, 30 min and 60 min of stirring at indoor temperature. However, heating temperature was not determined in the pretest. A suggested temperature of 80 ℃ would be used in the formal experiments. Two schemes of filtration were planned for the trial. One was to use syringe and syringe filter to separate solution and insoluble impurities and the other was to use centrifugation for separation.

Adequate volume of 10% barium chloride solution was added to each set of sample until the barium sulfate precipitate was well formed. Air pump filtration was used to obtain the wet precipitate of barium sulfate. Gooch crucible, filter paper and barium sulfate precipitate were oven dried and reweighed. The temperature of oven drying was 105 ℃ and oven drying lasted for 3 hours. After oven drying, all the samples cooled down to indoor temperature in desiccator for 30 min.

5.4.2 PREPARATIONS

20 grams powdered sample was smashed from cylinder surface as shown in Figure 5.1 and then grinded. The specimen selected was cast by Type GU cement and exposed to sulfate attack for 12 weeks. Fragments were grinded to fine cement powder and sorted to six samples (each of 3 grams). Besides, 20ml distilled water and 5ml 37% Chloride Acid solution were mixed for decomposition at indoor temperature.

Figure 5.1. Smashed cylindrical specimen and surface fragments

5.4.3 PROCEDURES

Drying & Weighing. As shown in Figure 5.2, six sets of Gooch crucibles with 24mm Microfiber Filters were oven dried and weighed prior to experiment as well as the powdered samples. All the sets and samples were dried at temperature of 105℃ for 3 hours and cooled down to indoor temperature in desiccator for 30 minutes.
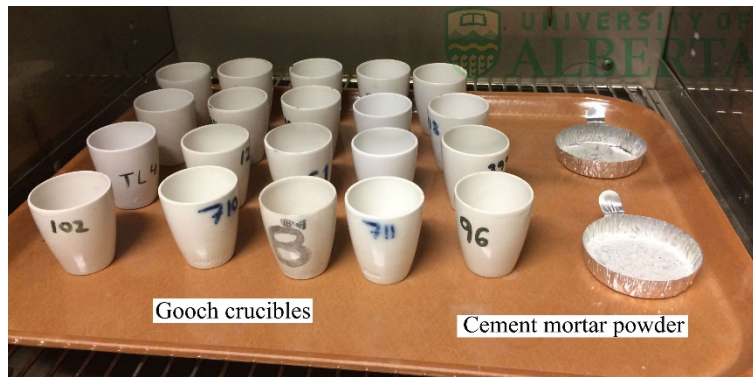
Figure 5.2. Oven drying of Gooch crucibles and cement mortar powder

Decomposition. Two kinds of decomposition conditions were applied in trial, stirring at indoor temperature and heated stirring. Heating temperature was firstly set around 60℃. Moreover, the fineness of powdered sample would affect the degree of decomposition so powder should be sieved during the formal experiment as shown in Figure 5.3, Figure 5.4.
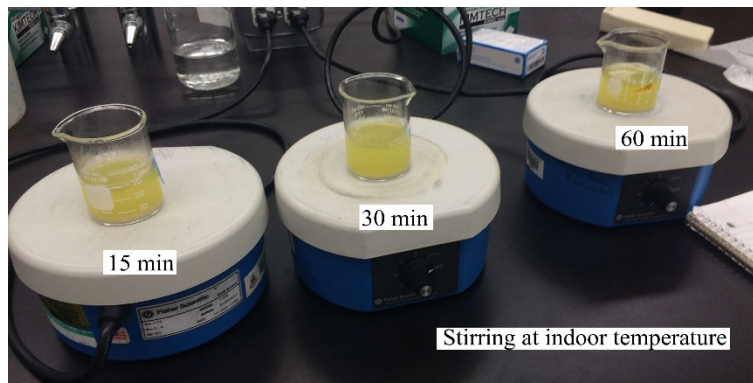
Figure 5.3. Stirring at indoor temperature for 15, 30 and 60 min
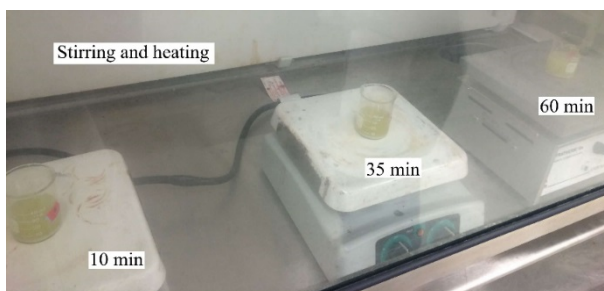
Figure 5.4. Stirring and heating for 10, 35 and 60 min

Filtration-1. After the decomposition, syringes and syringe filter units were introduced for solid-liquid separation. Because of the operating limit, only 5 mL solution was filtrated out of 25 mL mixture solution, so all the precipitate obtained later were 20% of the assumed initial weight.

Titration. After the filtration, 5ml (out of 25ml) solution reacted with sufficient 10% of Barium Chloride $BaCl_2$ solution and precipitation was witnessed as shown in Figure 5.5. The volume of Barium Chloride solution was 15 mL in the trial experiment.
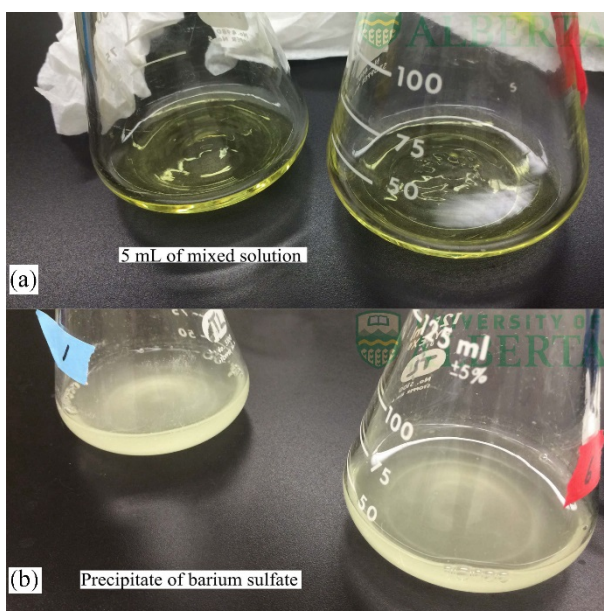
Figure 5.5. Mixed solution before (a) and after (b) titration

Filtration-2. This was to separate the barium sulfate precipitation and the reacted solution. Air pump filter was employed. After the filtration, wet barium sulfate precipitates remained on the filter paper. The weight of barium sulfate was weighed after completely dried.

Drying and Weighing. The Gooch crucible, filter paper and barium sulfate precipitate would be reweighed after 3 hours of oven drying and 30 min of cooling down. The weight change was equal to the weight of barium sulfate precipitate.

5.4.4 CALCULATIONS AND RESULTS

Table 5.4. Weight change calculations of six sets of samples

Set No.	Cond.	Duration (min)	Weight 1 (g)	Weight 2 (g)	Change (g)	Change *(g)
1	S.	15	22.9199	22.9408	0.0209	0.0209
2	S.	30	24.0742	24.0956	0.0214	0.0214
3	S.	60	24.1662	24.1875	0.0213	0.0213
4	S.& H.	60	27.2748	27.2942	0.0194	0.0388
5	S.& H.	35	25.0197	25.0567	0.037	0.0370
6	S.& H.	10	23.1241	23.1554	0.0313	0.0313

S.--Stirring; S.&H.--Stirring & Heating; *--Equivalent quality of 5ML solution

The weight change of set-4 showed that there was 0.0388g of barium sulfate precipitate produced by 0.6 g of cement mortar powder. The amount is significant that means this kind of experiment is effective to determine the sulfate concentration.

It is shown in Figure 5.6 that the weights of barium sulfate precipitate change few at indoor temperature. The decomposition at indoor temperature is slower than heating. It is suggested in this study to apply stirring and heating for at least 60 min in order to fully decompose the cement mortar powder.
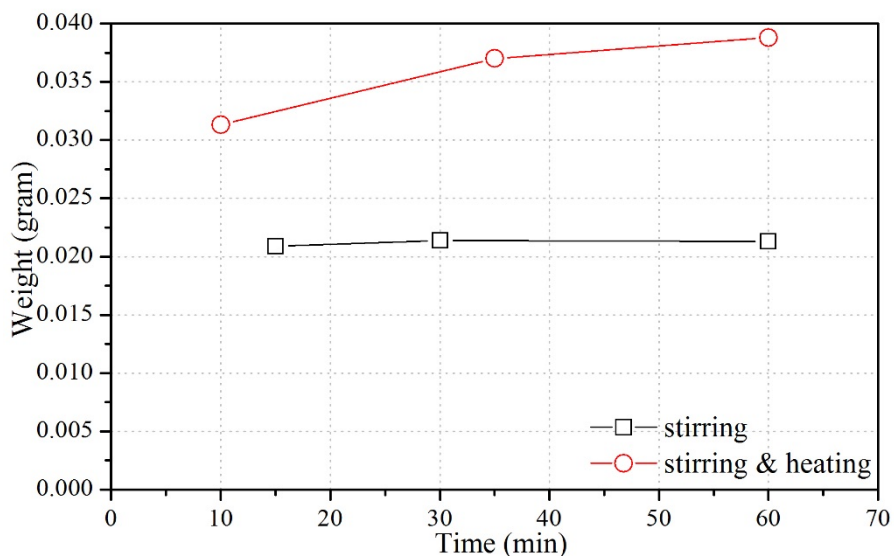
Figure 5.6. Weight of precipitate obtained in two experiment conditions

5.5 FORMAL PROCEDURES

5.5.1 GENERAL CONDITIONS

In accordance with the titration trial and related content in ASTM C114 standard, the methodology was improved and finalized in this study. Experiment was operated at indoor temperature except drying, cooling and decomposition. Procedures containing reactions (decomposition and titration) were finalized in fume hood for security purpose. Tools including flasks, pipettes, beakers and funnels were cleaned and dried prior to formal experiment.

5.5.2 THE FIRST WEIGHING

To weigh completely dried reactants, powdered samples were oven dried with aluminum dishes at $105℃$ for 3 hours. Besides, Gooch crucibles and filter paper were oven dried with same setups as well. Figure 5.7 presents the completely dried powders obtained through sample extraction method.

Figure 5.7. Labelled powdered samples after oven-drying
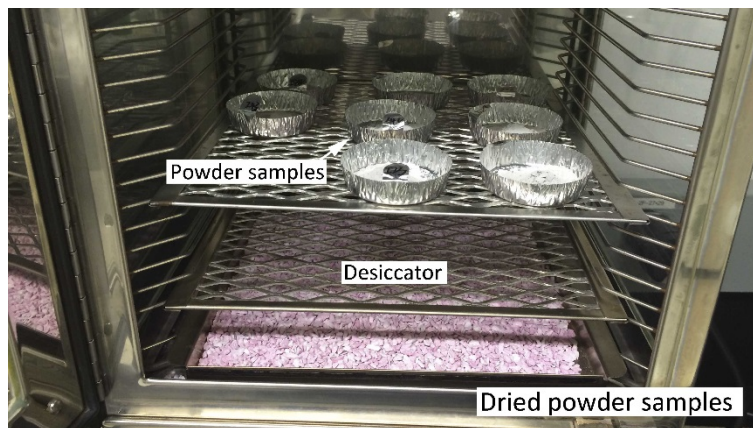
Figure 5.8. Drying powdered samples to indoor temperature in desiccator

All the powdered samples and crucibles were required to be cooled down to indoor temperature in the desiccator for 30 minutes (see Figure 5.8) and then weighed. The sample temperature was then recorded.

Figure 5.9 presents that powdered sample was being weighed in 250 mL flask that had been tarred beforehand. The weights of powdered samples were named 'Weight-P-#' and the weights of crucible units were named 'Weight-1-#' according to the sticks on Gooch crucibles.

Figure 5.9. Weighing for initial weights of powdered samples and crucibles

5.5.3 DECOMPOSITION

As mentioned in ASTM C114 standard, it is suggested to heat the solution until it is evident that decomposition of the cement is complete. However, higher temperature may cause evaporation of hydrochloric acid. Appropriate temperature of 60 centigrade was chosen when decomposing. Standard flask of 250 mL capacity was used for each sample in order to mitigate evaporation (see Figure 5.10). It was recommended to have 60 minutes vigorously stirring at the same temperature for complete decomposition.
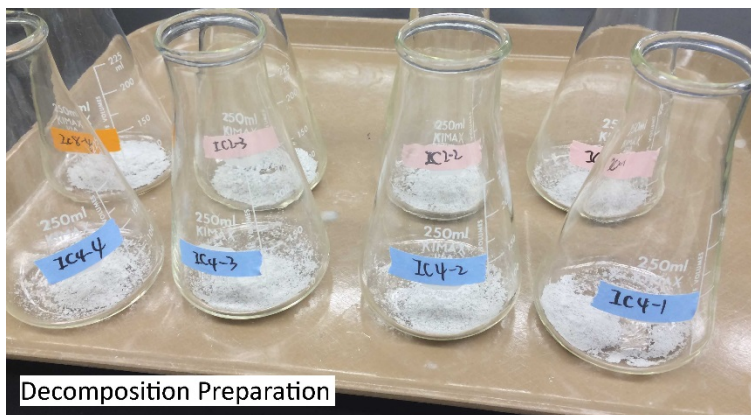
Figure 5.10. Samples in standard flasks before decomposition

To maintain the temperature while stirring, detailed procedures were developed and listed below. The volumes of distilled water and hydrochloric acid of each sample were determined after the trial experiment.

■ 20 mL of hot distilled water under boiling at 0 min (under boiling means cooling down for 10 min after boiling that was decided in this program).

■ 5 mL of Hydrochloric acid with indoor temperature at 0 min.

■ 20 mL more hot distilled water just under boiling at 30 min during decomposition in order to keep the solution temperature just under boiling.

■ After stirring for 60 minutes, mixed solutions placed with another 30 minutes for preliminary sedimentation.
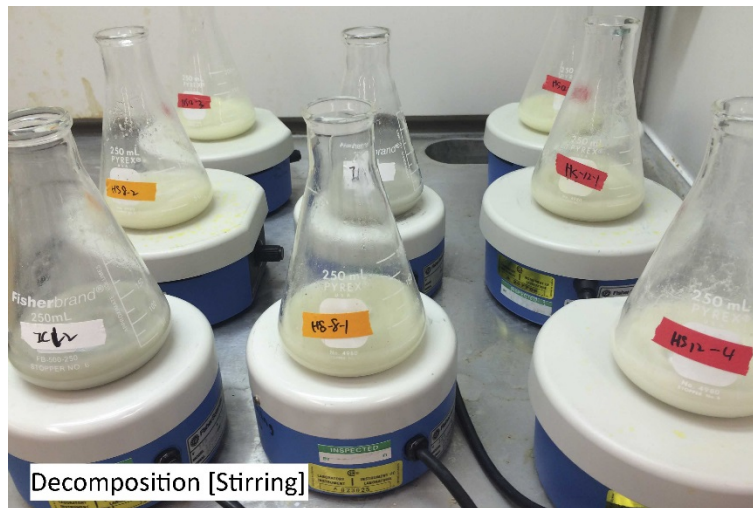
Figure 5.11. Decomposition of cement samples

5.5.4 CENTRIFUGATION

According to trial experiment, samples with fine aggregates were hardly to get fully filtrated. Besides, filtrated solution may not be very clear and stable that affected the final result.

Centrifugation employed in this study improved the filtration with higher efficiency and quality. Therefore it was recommended to go through centrifugation prior to filtration. In particular, 40-45 mL of placed solution was stored in centrifuge tube preparing for centrifugation as shown in Figure 5.12.
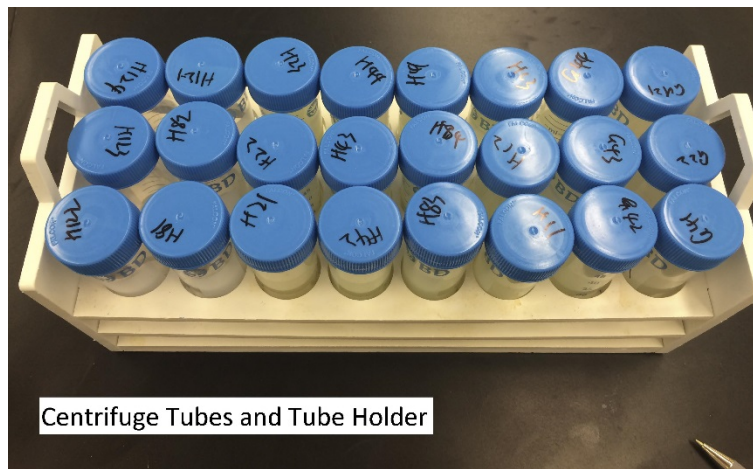
Figure 5.12. 40-45 mL mixed samples stored in 50 mL centrifuge tubes

Figure 5.13. Symmetric centrifuge setup (8,000 xg at 20 centigrade)

Eight sample tubes with extra two balance weight tubes were centrifuged once with symmetric installation as shown in Figure 5.13. All centrifuged solutions were required to have 60 minutes standing after centrifugation for later filtration. Only the upper clear solution (around 30 mL) was pipetted for filtration. Table 5.5 lists the setting parameters employed during the centrifugation.

Table 5.5. Setting parameters of the centrifugation

CENTRIFUGE MODEL	Thermo Scientific LYNX-4000
G-FORCE	8,000 xg
TEMPERATURE	20 centigrade
DURATION	07 minutes

5.5.5 FILTRATION

Clear solutions were filtrated after the centrifugation that accelerated the speed of filtration. Standard funnels and medium size filter papers (Diameter of 11 cm), as shown in Figure 5.15, were set to filter for the reactants. The average filtration duration was short and recorded around 2 min because of the preprocessing of centrifugation. This step, to a large extent, clarified the solutions for titration.
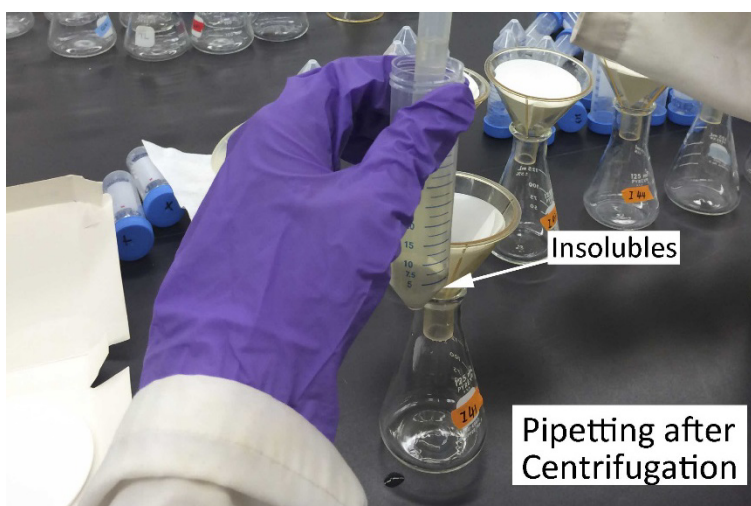
Figure 5.14. Filtration for clear reactant solutions

Figure 5.14 presents the pipetting process after the centrifugation. After pipetting the centrifuged solution from tubes, filter through a medium-textured paper with standard funnel. 30 mL of solution was re-pipetted for titration experiment.
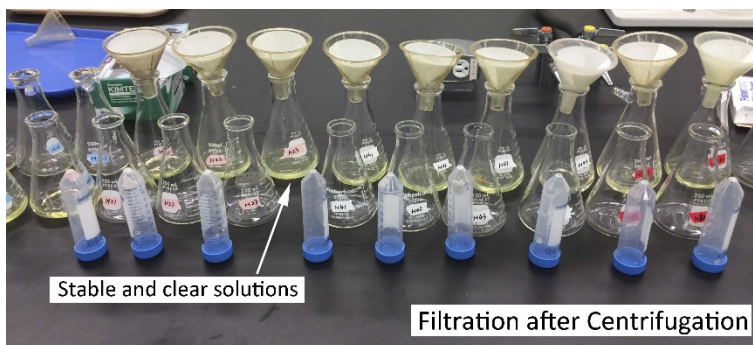
Figure 5.15. Filtration experiment after centrifugation

Figure 5.16 presents the 30 mL standard pipettes used for pipetting. Clear solutions were stored in standard flasks for 30 minutes and ready for the titration.
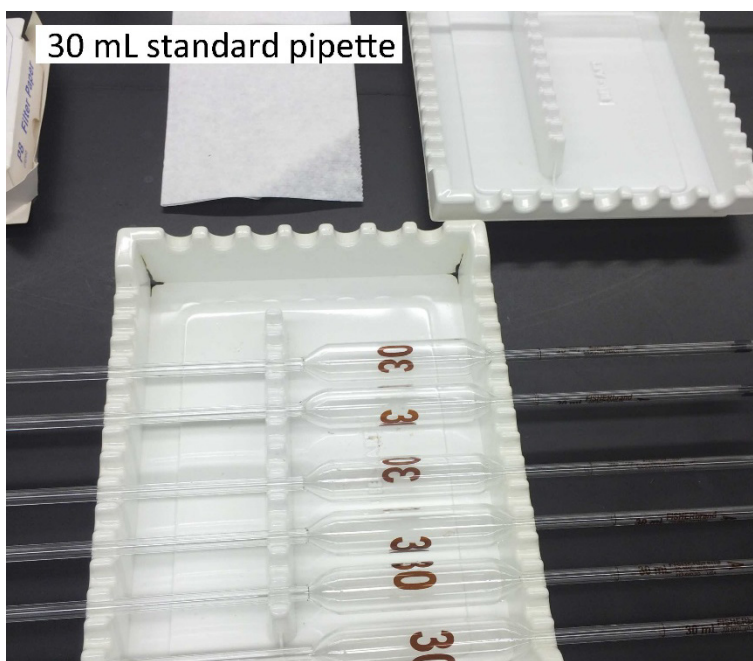
Figure 5.16. 30 mL standard pipette for titration

5.5.6 TITRATION

Based on the reaction equation of Eq. (5.3), 10% of $BaCl_2$ solution was used to fully precipitate the sulfate. It was suggested by the trial to add excess $BaCl_2$ solution. All the chemicals were commercial sourced from Fisher Scientific.

As expected, the barium sulfate precipitate was perceptible and clear as soon as the titration experiment began as shown in Figure 5.17.
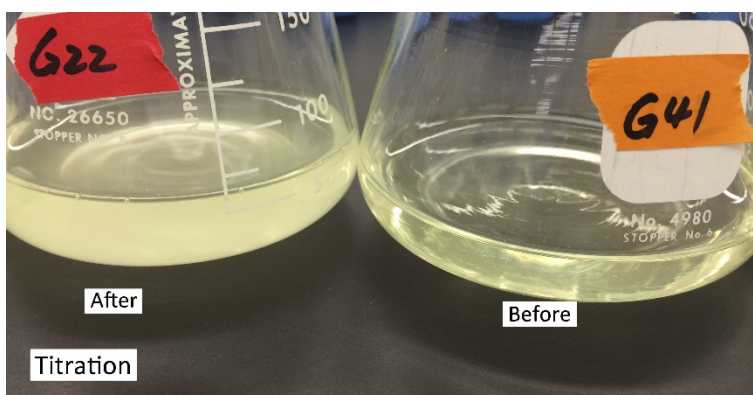
Figure 5.17. Sample solutions right before and after titration
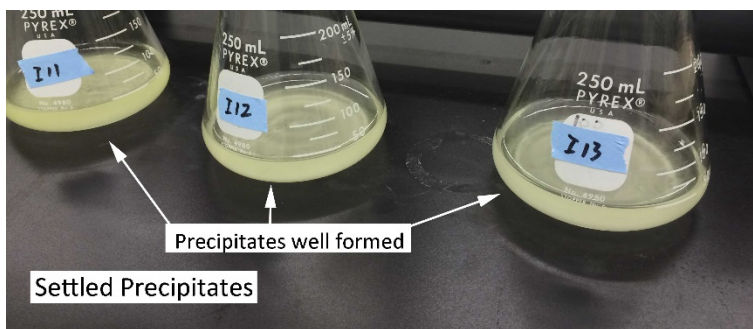
Figure 5.18. Well-formed barium sulfate precipitates after titration

Add slowly, dropwise, 10 mL of hot $BaCl_2$ solution and keep shocking until the precipitate was well formed. Digesting the solution for 2 hours to make sure the reaction was complete. Figure 5.18 presents that precipitate $BaSO_4$ was well formed after digestion.

5.5.7 Air-Pump Filtration

To obtain the completely dried barium sulfate precipitate, air pump filtration is employed in this study. Figure 5.19 and Figure 5.20 show the installation of air pump filtration. The Gooch crucible units are pre-weighed in the first weighing procedure that makes it easy to calculate the weight of precipitates.
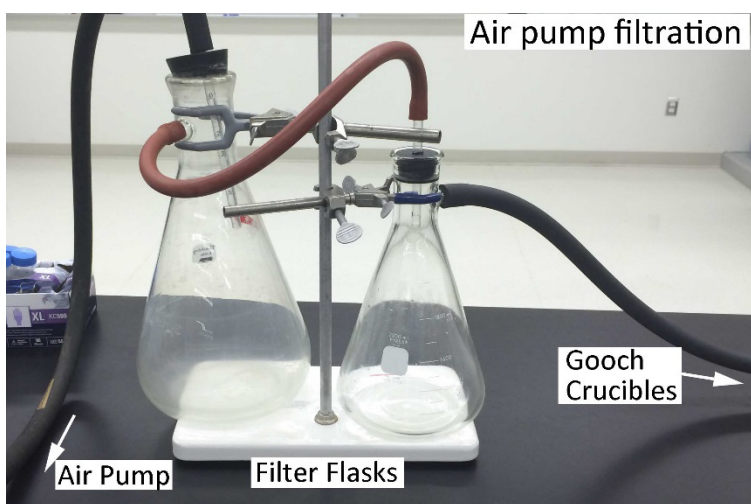
Figure 5.19. Air pump filtration (filter flasks)
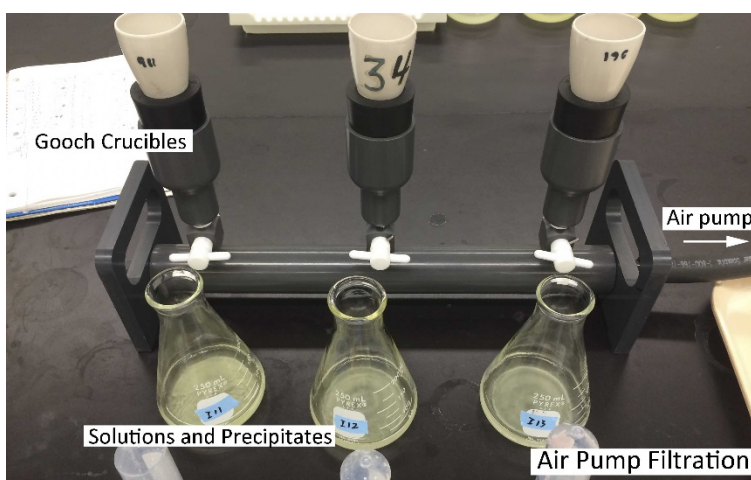
Figure 5.20. Air pump filtration setups with three Gooch crucibles

5.5.8 THE FINAL WEIGHING

After the air pump filtration, place Gooch crucibles with wet precipitates in a salver. Then oven dry all the samples at temperature of 105 centigrade for 12 hours. Cool down the Gooch crucible in the desiccator for over 30 minutes, and then weigh.

The final weights were named 'Weight-2-#' according to the labels on each Gooch crucible. The weight increments (Weight 2 – Weight 1) were determined as the weight of dry barium sulfate precipitate. The weighing was operated using the same balance as the first weighing for consistency purpose.

5.6 CALCULATION FOR SULFATE CONCENTRATION

With the calculated density of tested samples, the sulfate concentrations were calculated by Eq. (5.6). The mass of barium sulfate precipitate and cement sample were calculated by Eq. (5.4) and Eq. (5.5).

$$m_{BaSO_4} = Weight_2 - Weight_1 \qquad (5.4)$$

$$m_{c.m.} = Weight_P \qquad (5.5)$$

Where:

$Weight_1$ = the weight of Gooch crucible unit

$Weight_2$ = the weight of Gooch crucible unit with $BaSO_4$ precipitate

$Weight_P$ = the weight of extracted sample of each layer

To fit the sulfate profiles in numerical modeling, the unit of sulfate concentration is converted to molar per cubic meter with the molar mass of barium sulfate. According to the

titration reactions presented, the sulfate concentrations in tested samples are accessible and can be calculated as below:

$$C_s = \frac{n_{SO_4^{2-}}}{V_{c.m.}} = \frac{n_{BaSO_4}}{V_{c.m.}} = \frac{m_{BaSO_4}}{M_{BaSO_4}} \bigg/ \frac{m_{c.m.}}{\rho_{c.m.}} = \frac{m_{BaSO_4} \cdot \rho_{c.m.}}{M_{BaSO_4} \cdot m_{c.m.}}$$ (5.6)

Where:

C_s = sulfate molar concentration in titrated sample (mol / m^3)

$n_{SO_4^{2-}} / n_{BaSO_4}$ = amount-of-substance of precipitated sulfate (mol)

$V_{c.m.}$ = volume of powdered sample per layer (mm^3)

m_{BaSO_4} = mass of barium sulfate precipitate obtained per layer (g)

$m_{c.m.}$ = weight of powdered sample per layer (g)

$\rho_{c.m.}$ = density of cement mortar sample (g/mm^3)

M_{BaSO_4} = molar mass of barium sulfate (g/mol)

5.7 ANALYSIS ON RESULTS

5.7.1 SULFATE CONCENTRATIONS
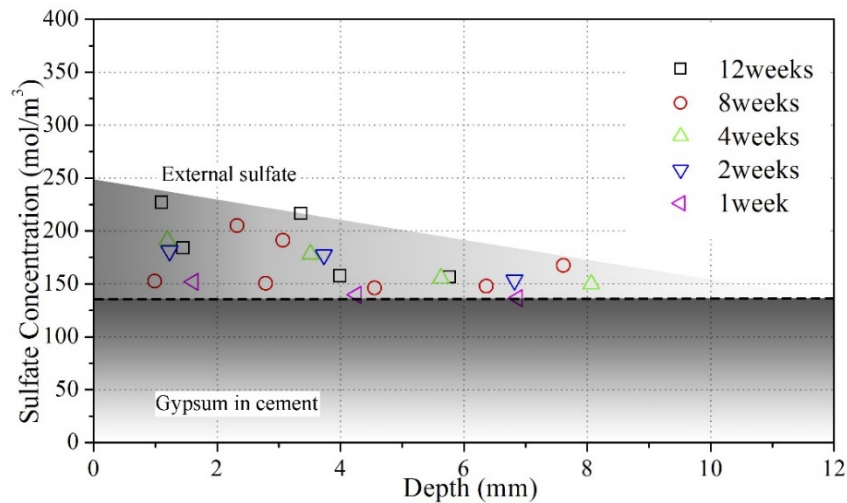
Figure 5.21. Absolute sulfate concentration as affected by exposure duration (Type GU)
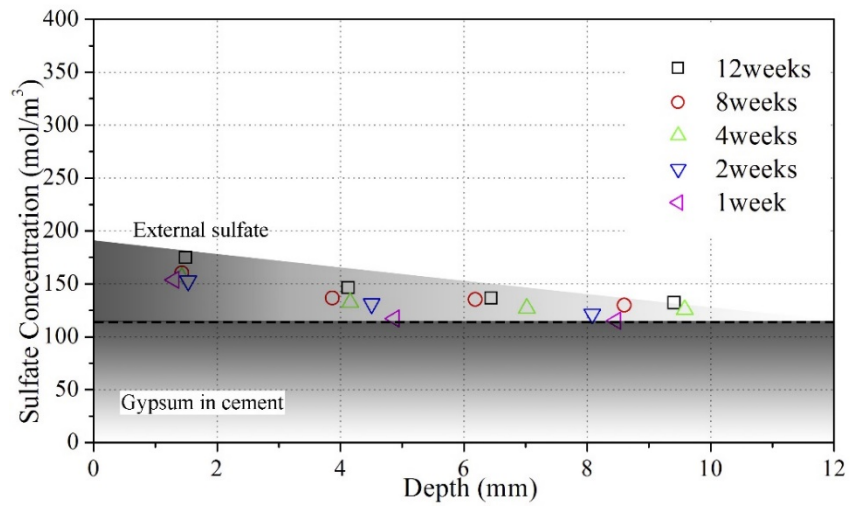
Figure 5.22. Absolute sulfate concentration as affected by exposure duration (Type HS)
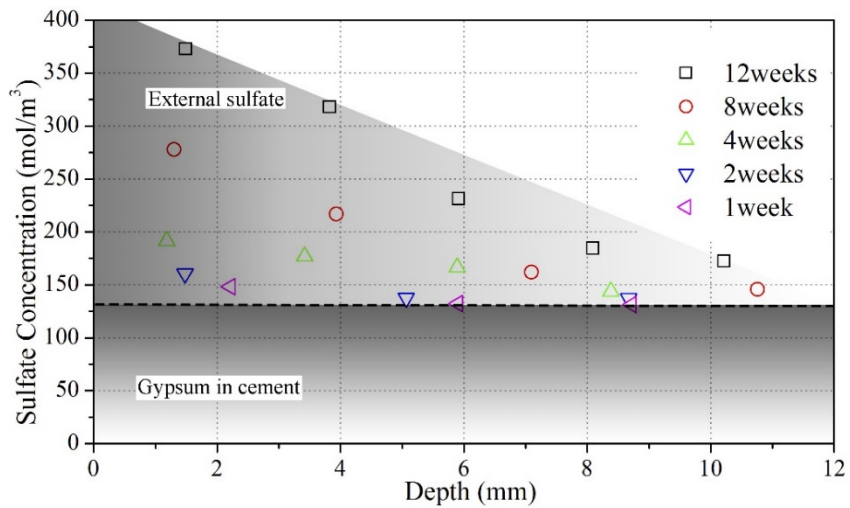
Figure 5.23. Absolute sulfate concentration as affected by exposure duration (Blend IC)

Calculated sulfate concentrations are plotted as affected by the extraction depth and exposure duration in Figure 5.21, Figure 5.22 and Figure 5.23. It is to be noted that the sulfate concentration obtained decreased with extraction depth for each type binder. As expected, sulfate concentration increased with sulfate exposure duration.

5.7.2 CURRENT FINDINGS

Sulfate Exposure. Three type of cement samples are examined for sulfate content as affected by exposure durations and extracted depths. As expected, the sulfate contents tested decrease with extraction depths from the specimen surface.

Sulfate contents increase with the increase of exposure duration along the depth from the surface. This property also corroborates the development of sulfate attack proposed by diffusion theory in relevant literatures.

Binder Types. From the sulfate concentrations plotted, HS type samples contain lowest concentrations among three tested type samples within 12 weeks exposure.

The maximum sulfate concentration in HS type cement is tested of only 170 molars per cubic meter at depth closest to the surface. Moreover, the sulfate contents detected do not increase with exposure time, which means HS type cement has excellent and stable resistance to the external sulfate attack.

It is a remarkable fact that the InterCem blend is examined to have highest sulfate content in comparison with GU and HS cements. After 12 weeks exposure, the sulfate concentration in InterCem sample at depth of 1.5 mm is tested of 370 molars per cubic meter that is twice as much as the sulfate concentration at the same depth in HS type sample.

From the content results calculated, the sulfate concentration in InterCem sample exceeds the other two (Type GU and HS) after 1 week's exposure. What can be concluded is that the fly ash replacement in InterCem blend does not improve the diffusion resistance of cement sample, at least within 12 weeks' exposure in this study. The mechanism of diffusion resistance in cement based material is explained in numerical modeling chapter.

Sulfate Baseline Revision. It is witnessed that the sulfate content is not close to zero for all type samples at depth over 10 mm after 1 week exposure (see Figure 5.21, Figure 5.22 and Figure 5.23). Nevertheless, external sulfates are not supposed to infiltrate over 10 mm after only 1 week of sulfate exposure based on diffusion theory. The sulfate composition detected over 10 mm is identified as inherent gypsum in the cement blends.

All the cement mortar samples are exposed to sulfate environment with 4 weeks curing after de-molding thus it is reasonably proposed that there still has unconsumed gypsum in the sample within 12 weeks exposure. The lowest sulfate concentration obtained by 1 week exposure is set as the baseline of external sulfate simulation for each type cement. Limited by the laboratory availability, the sulfate concentrations were examined only in the specimens exposed to sulfate environment. In comparison with these results, sulfate concentrations inside specimens submerged in water are supposed to be examined in the future work.

Surface concentration revision. In addition, the tested sulfate concentration at the depth close to sample surface reaches the external sulfate concentration only in InterCem sample. While GU type and HS type samples have lower sulfate concentration near the sample surface. This should be taken into consideration when fitting experimental data to the numerical modeling.

A reasonable inference is proposed that considering the short-term exposure (12 weeks) employed, the surface concentration of sample/structure is lower than the external sulfate concentration, particularly under higher sulfate environment. External sulfate is more likely to infiltrate deeper along the micro pores and cracks, prior to surface concentration accumulation. The relationship between exposure durations and surface concentrations is explained in numerical modeling portion.

5.8 SUGGESTIONS AND FUTURE RESEARCH

5.8.1 LABORATORY CONDITIONS

Compared to other chemical analysis methods, titration experiment has its advantage in research of sulfate attack. The determination of available sulfate in cement based material is direct and exclusive. This method eliminates the influence of other chemical compositions that may affect the concentration results. Since titration is also suggested in related ASTM standard, it is improved in this study for specific research purpose. However, the concentration results are sensitively affected by the laboratory environments and instrument requirements. All the procedures included require plenty of tools and chemicals that may lead to several operation errors. Besides, it is necessary to maintain consistency during the whole titration experiments. In this study, 59 titration experiments are finalized within one week so that the results are reliable. Concentration precision is greatly depended on the thickness of the samples extracted.

Theoretically, it is better to extract sample in thinner layer for more precise equivalent depth. But thinner layer contains less sample that lowers the titration precision in contrast. Titrating precision interacts with extraction thickness so that around 2 grams is preferred in this study.

5.8.2 FUTURE RESEARCH

The concentration results from titration experiment are calculated for the determination of diffusion coefficient D and the weighted average stoichiometric coefficient λ with known tricalcium aluminate content and external sulfate concentration. However, the titration experiment has few potential in further engineering application because of several limits and conditions. Cement based materials with various mineral admixtures and water-binder ratios perform different diffusion capacities that can be determined by the values of coefficient D. Cement types containing featured tricalcium aluminate contents also affect

the sulfate attack resistance. Each kind of cement based material requires sample extraction and titration experiments with for coefficients determination.

Besides, titration experiment is time consuming and limited in the laboratory environment in order to obtain sulfate concentration profiles. The experimental results obtained will be used to fit the numerical modeling of the materials examined. After the quick visual assessment method is fully verified, it is unnecessary to employ titration experiment with the image analysis. The diffusion coefficient D and concentration profile can be easily determined for variety of cement based materials. Numerical modeling with quick visual assessment is supposed to be the preferred solution for sulfate attack research of cement based materials.

6 NUMERICAL MODELING ON SULFATE DIFFUSION

6.1 DIFFUSION THEORIES AND BASIC MODELING

6.1.1 OBJECTIVES

In order to study the diffusion-reaction behavior of cement-based composites subjected to adverse sulfate attack, numerical modeling is highly preferred and widely used (Tixier and Mobasher 2003; Tixier and Mobasher 2003). The fundamental diffusion mechanism of sulfate attack conformed to the Fick's Second Law that explains the mechanism of ion diffusion in homogeneous matrix. However, the sulfate attack inside cement-based composites consists of complicated reactions with inherent compounds and it is hardly to evaluate the precision of selected approximation methods involved with these reactions. The scheme of this study is to firstly investigate the accuracy of various finite methods through non-reaction diffusion and further develop the diffusion-reaction process upon several selected approximation approaches.

The main task of this chapter is to discuss and compare existing finite difference methods by simulating the external sulfate diffusion without internal chemical reactions. Non-reaction diffusion model, widely employed by researchers (Chalee et al. 2009; Song et al. 2009) to simulate the chloride penetration to cement-based materials, was preliminarily applied in this chapter to compare the errors caused by finite difference methods.

Since the non-reaction diffusion was mathematically solved by Error Function Solution, the simulating precisions of examined methods could be discussed in comparison with the exact solution. In this manner, only the external sulfate concentration and diffusion coefficient were taken under consideration as the parameters in the present modeling. The errors caused by approximate methods were investigated for further development of sulfate attack modeling.

The diffusion model involved with complicated reactions was demonstrated in detail in the next chapter of data fitting through the favorable finite difference methods decided in this study.

6.1.2 BASIC POSTULATIONS

Considering the simplicity of simulation, some basic postulations should be drawn,

■ The numerical modeling programs developed in this study were one dimensional limited to exposure conditions.

■ Portland cement-based composites was assumed as a homogeneous system and the variance of the internal geometric microstructures is ignored.

■ Diffusion was regard as the main transport mechanism for sulfate ingress into Portland cement-based composites, and the model was proposed by Assuming Fick's law of diffusion and the absence of convection.

■ All available gypsum added to the clinker is consumed for primary ettringite formation (assuming sufficient calcium aluminates are present for this reaction to take place), and the primary ettringite formed has been entirely converted to monosulfate at the time the sulfate attack begins, and the penetrating sulfates react with the available Portlandite in the microstructure of the C-S-H to form gypsum.

■ In order to compare with the result of close form solution of the Fick's second law, the initial concentration of CA C_0 and the rate constant k of the chemical reaction between reacting calcium aluminates and sulfate ingress were assumed as 0 in this study. The

diffusion-reaction model was simplified into a non-reaction diffusion model, in which the behavior of sulfate attack in the composites was regarded as a process of diffusion of the sulfate ions.

6.1.3 DIFFUSION MODEL FORMATION

In this study the experimental data were used to generate a model for predicting the sulfate diffusion profile without chemical reactions of cement-based composites in adverse sulfate environment by applying Fick's second law (Crank 1979) as shown in Eq. (6.1)

$$\frac{\partial C}{\partial t} = \frac{\partial}{\partial x}\left(D\frac{\partial C}{\partial x}\right)$$
(6.1)

If the diffusion coefficient D does not change with the concentration C, Eq. (6.1) can be presented:

$$\frac{\partial C}{\partial t} = D\frac{\partial^2 C}{\partial x^2}$$
(6.2)

Fick's Second Law explains that, when applying non-steady diffusion inside homogeneous matrix, at the distance of x, the rate of concentration variation to time equals to the negative rate of diffusion flux to the distance.

The diffusion coefficient D in Eq. (6.1, 6.2) is a quantified parameter that represents the matrix resistance to the external ion diffusion. In previous study, experimental data obtained from titration were introduced to determine the diffusion coefficient D of each examined composite.

6.1.4 Finite Difference Method

The principle of finite difference methods is close to the numerical schemes used to solve ordinary differential equations. As shown in Figure 6.1, the FDM is aimed to approximate the values of the continuous function *f(x)* on a set of discrete points in the plane.
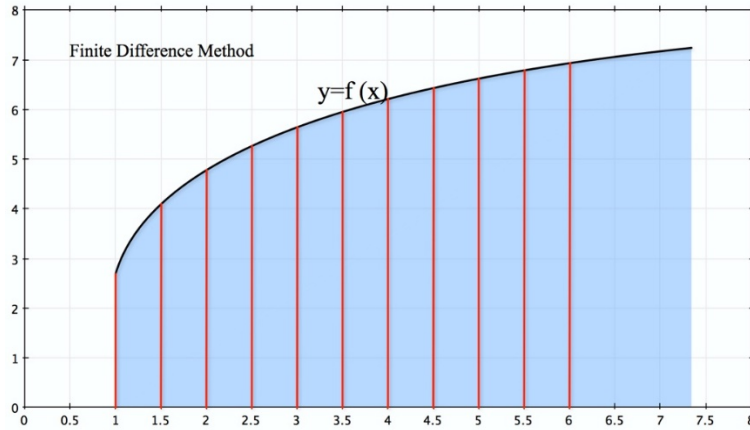
Figure 6.1. Sample interpretation of finite difference method (FDM)

It consists in approximating the differential operator by replacing the derivatives in the equation using differential quotients. The domain is partitioned in space and in time and approximations of the solution are computed at the space or time points. The error between the numerical solution and the exact solution is determined by the error that is committed by going from a differential operator to a difference operator.

This error is called the discretization error/truncation error. The term truncation error reflects the fact that a finite part of a Taylor series is used in the approximation. The truncation error of finite difference method was discussed in this study.

6.2 ERROR DISCUSSION OF APPROXIMATIONS

6.2.1 TAYLOR'S SERIES AND DEVIATION

The finite difference methods depend on the Taylor's theorem that develops an approximate simulation. However, errors caused by this kind of methods are supposed to be discussed through the basic formulation of the theory.

Assuming the function whose derivatives are to be approximated is properly-behaved, by Taylor's theorem, Taylor Series expansion is created.

$$f(x_0 + h) = f(x_0) + \frac{f'(x_0)}{1!}h + \frac{f^{(2)}(x_0)}{2!}h^2 + \cdots + \frac{f^{(n)}(x_0)}{n!}h^n + R_n(x) \qquad (6.3)$$

Where $n!$ denotes the factorial of n, and $Rn(x)$ is a remainder term, denoting the difference between the Taylor polynomial of degree n and the original function.

An approximation for the second order of the function "f" is derived. For the treatment of problems, it is convenient to retain only the first two terms of the previous expression:

$$f(x_0 + h) = f(x_0) + f'(x_0)h + \frac{h^2}{2}f''(x_0 + h) \qquad (6.4)$$

Setting, $x_0 = a$ we have,

$$f(a + h) = f(a) + f'(a)h + R_1(x) \qquad (6.5)$$

Dividing across by h gives:

$$\frac{f(a + h)}{h} = \frac{f(a)}{h} + f'(a) + \frac{R_1(x)}{h} \qquad (6.6)$$

Solving for $f'(a)$:

$$f'(a) = \frac{f(a+h) - f(a)}{h} - O(h^2) \qquad\qquad (6.7)$$

Assuming that $O(h^2)$ is sufficiently small, the approximation of the first derivative of f is:

$$f'(a) \approx \frac{f(a+h) - f(a)}{h} \qquad\qquad (6.8)$$

6.2.2 ERRORS AFFECTED BY FINITE INCREMENTS

The error in a method's solution is defined as the difference between its approximation and the exact analytical solution. The two sources of error in finite difference methods are round-off error, the loss of precision due to computer rounding of decimal quantities, and truncation error or discretization error, the difference between the exact solution of the finite difference equation and the exact quantity assuming perfect arithmetic (that is, assuming no round-off).

The finite difference method relies on discretizing a function on a grid.

In this study, the discretization error was caused by two calculation steps, time step and space step. This is usually done by dividing the domain into a uniform grid as shown in Figure 6.1. Note that this means that finite-difference methods produce sets of discrete numerical approximations to the derivative, often in a "time-stepping" manner.(Hoffman and Frankel 2001)

6.3 NON-REACTION DIFFUSION MODEL

6.3.1 INTRODUCTION

In accordance with the diffusion theory employed at the outset, non-reaction diffusion numerical model was preliminarily developed by means of several finite difference methods in comparison with exact solution of Error Function Solution (EFS).

In particular, this physical diffusion model, considering only the properties of permeability and external ion concentration, was widely introduced to simulate the chloride corrosion to cement-based systems. Note that in the present instance, the non-reaction diffusion was considered as one dimensional model that simulated the ion diffusion from the boundary.

6.3.2 THE NON-REACTION DIFFUSION TASK

The process of sulfate ion diffusion in Portland cement-based composites can be described by Fick's second law as following,

$$\frac{\partial C}{\partial t} = D \frac{\partial^2 C}{\partial x^2}$$

(6.9)

where C is the concentration of sulfate ion in the matrix, t is the exposure time, D is the diffusion coefficient of matrix, x is the position. In this case, D was chosen to $1.5 \times 10^{-12} \, \text{m}^2/\text{s}$ for approximation evaluation based on the diffusion model in related literatures.

The following set of initial and boundary conditions is prescribed:

$$C(x,0) = 0, C(0,t) = C_s, C(\infty,t) = 0$$

(6.10)

Where C_s is the surface concentration of sulfate ion in external environment, $C_s = 30$ mol/m^3 in this case. The accuracy of finite difference method was discussed by applying these parameters.

6.4 THE ERROR FUNCTION SOLUTION

6.4.1 INTRODUCTION

The error function solution is widely used approach to simulate the chloride corrosions to cement-based structures (Vu and Stewart 2000).

In terms of the non-reaction diffusion case, some mathematicians had concluded the exact solution to get the concentration distribution. This error function solution only explains the physical diffusion processing of ions. It was introduced in this study to evaluate the errors caused by approximation method such finite difference methods.

The reason why it was necessary to find approximate solutions is that if the chemical reactions are taken under consideration, there was no exact solution for the diffusion-reaction behavior.

6.4.2 THE EQUATION OF EXACT SOLUTION

For the one-dimensional chloride diffusion, the error function solution to Fick's second law is fitted to the sulfate concentration profiles. With the initial condition and the boundary conditions determined by Eq. (6.10), we obtain the error function-based solution for two-dimensional diffusion problems:

$$C(x,y,t) = C_0 + (C_s - C_0)\left[1 - \mathrm{erf}\left(\frac{x}{2\sqrt{Dt}}\right) \cdot \mathrm{erf}\left(\frac{y}{2\sqrt{Dt}}\right)\right] \qquad (6.11)$$

Where *erf (x)* is an error function defined as:

$$\text{erf}(x) = \frac{2}{\sqrt{\pi}} \int_0^x e^{-z^2} dz \tag{6.12}$$

So we can get the solution equation for one-dimensional diffusion:

$$C(x,t) = C_0 + (C_s - C_0)\left[1 - \text{erf}\left(\frac{x}{2\sqrt{Dt}}\right)\right] \tag{6.13}$$

Where *erf (x)* is an error function defined as following:

$$\text{erf}(x) = \frac{2}{\sqrt{\pi}} \int_0^x e^{-z^2} dz \tag{6.14}$$

In this problem, we set T=7300 days, X=100 mm

$$C_s = 30, \quad C_0 = 0 \tag{6.15}$$

6.4.3 EFS VISUALIZATION IN SOFTWARE

The exact solution of on dimensional error function was solved by mathematical software and the sulfate profiles were plotted as shown in Figure 6.2. Note that in this case, the maximum exposure duration was defined to 10 years considering the service life of cement-based structures.
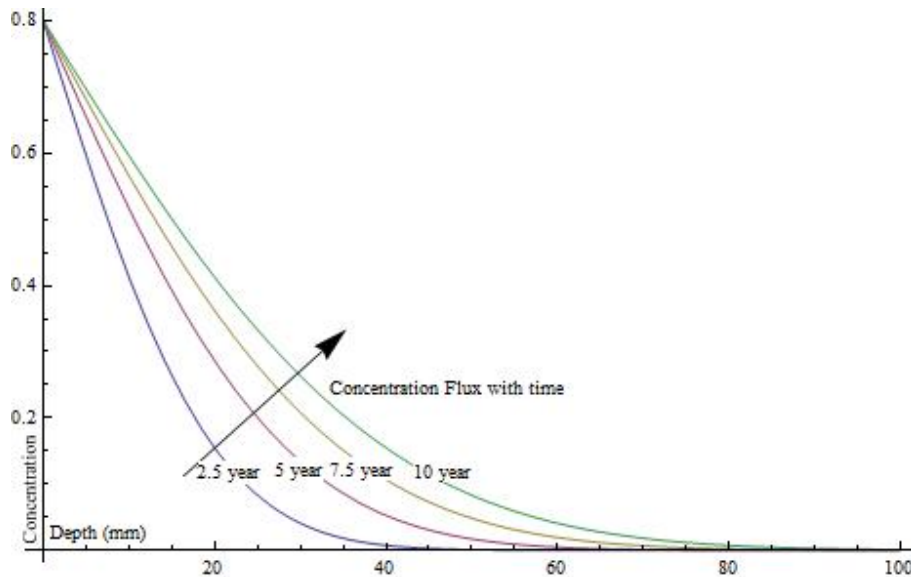
Figure 6.2. Exact concentration profiles for physical diffusion by error function theory

As shown in Figure 6.2, the exact concentration profiles are retrieved by error function solution. As expected, the concentration profiles have a consistent drop with depth whereas it evolved with exposure duration.

Considering the finite and discontinued concentration scatters in the approximation approaches, the error function solution was divided by space step that was employed in the approximation within space domain. The concentration results at the same distance obtained by exact solution and approximation approaches were compared in this work.

6.5   FINITE DIFFERENCE METHODS

6.5.1 BASIC SETUP AND INCREMENTS

Modeling Graphic Sketching. A slab of thickness *L* made by cement-based composites can be modeled by Finite Difference Method as shown in Figure 6.3, and it is exposed to a sulfate environment transversally from both ends (blue boundaries in the figure). That is, the matrix is subjected to one dimensional ion diffusion.

The space increment is represented as i and the space domain is divided into $2n$ sub-domain, while the increment of time is represented as a subscript j and the time domain is divided into m subdomain. The following set of initial and boundary conditions is prescribed:

$$\text{For } t=0, \ 0<x<L: \qquad\qquad U = 0 \text{ and } C = C_0 \qquad (6.16)$$

$$\text{For } x=0, \text{ and } x=L: \qquad\qquad U = U_0 \text{ and } C = 0 \qquad (6.17)$$
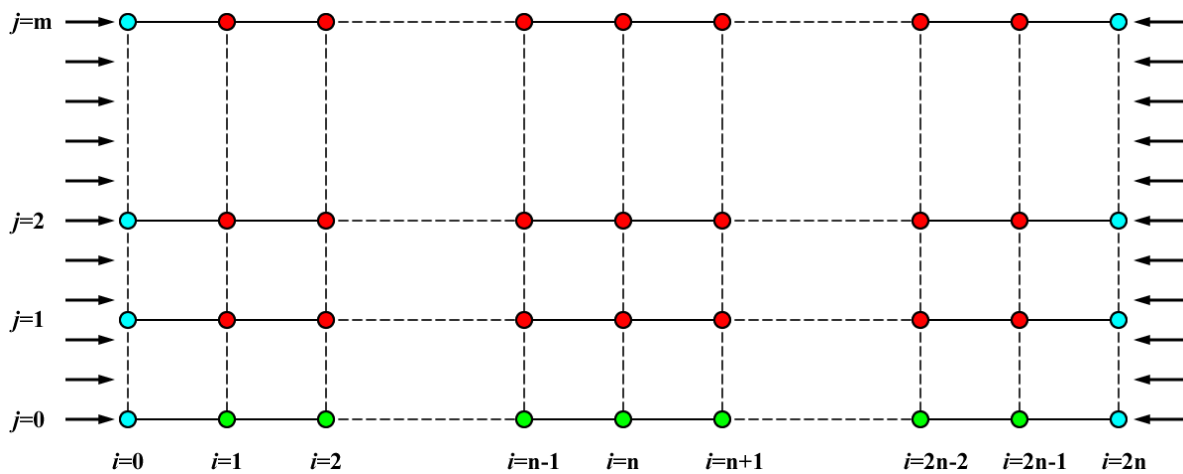
Figure 6.3. Domain setups for Finite Difference Method (FDM)

The space domain was set symmetrically due to the difficulty determining the far end of ion diffusion. Theoretically, the diffusion evolves with exposure duration thus the boundary condition of the far end remains a concern. Symmetric system was introduced in this model allowing for the increase of exposure duration. One additional boundary condition was employed that the sulfate concentrations at $i=n-1$ and $i=n+1$ are identical at any exposure duration.

6.5.2 EXPLICIT METHOD

Finite forward difference equation. Finite Forward Difference (Explicit) method is a widely used finite difference method for the resolution of Partial Differential Equations (PDEs). By means of applying the forward difference equation, we have to be very careful of the convergence conditions. This method is limited by these conditions.

In addition, errors caused by dividing domain to finite steps were analyzed and discussed.

Rule of Iteration.
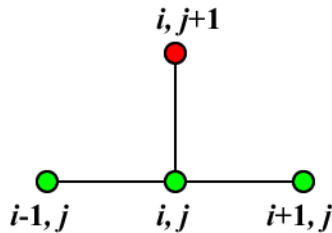
Figure 6.4. Rule of iteration for explicit finite difference method

The stencil for the most common explicit method for the heat equation.

$$\frac{u_i^{n+1} - u_i^n}{\Delta t} = F_i^n \left(u, x, t, \frac{\partial u}{\partial x}, \frac{\partial^2 u}{\partial x^2} \right) \qquad (6.18)$$

(Forward Euler)

That means the value of u at distance of i and time step $j+1$ was dependent on the current value at distance i and time j, and the nearby values of i-$1, j$ and $i+1, j$.

Using a forward difference at time t_n and a second-order central difference for the space derivative at position x_j (FTCS) we get the recurrence equation:

$$\frac{u_j^{n+1} - u_j^n}{\Delta t} = D \cdot \frac{u_{j+1}^n - 2u_j^n + u_{j-1}^n}{(\Delta x)^2} \tag{6.19}$$

This is an explicit method for solving the one-dimensional heat equation.

We can obtain u_j^{n+1} from the other values this way:

$$u_j^{n+1} = (1 - 2r) \cdot u_j^n + r \cdot u_{j-1}^n + r \cdot u_{j+1}^n \tag{6.20}$$

$$\text{Where } r = D \cdot \frac{\Delta t}{(\Delta x)^2} \tag{6.21}$$

So, with this recurrence relation, and knowing the values at time n, one can obtain the corresponding values at time $n + 1$. The u_0^n and u_J^n must be replaced by the boundary conditions, in this example they are both 0.

This explicit method is known to be numerically stable and convergent whenever $r \leq 0.5$. The numerical errors are proportional to the time step and the square of the space step:

$$\Delta u = O(k) + O(h^2) \tag{6.22}$$

Formula Derivation.

In the program, the sulfate concentration u_j^n in Euler equation was converted to $U_{i,j}$ as following:

$$\frac{\partial U}{\partial t} = \frac{U_{i,j+1} - U_{i,j}}{\Delta t} \tag{6.23}$$

The recurrence equation of the PDE (6.23) can be obtained:

$$\frac{U_{i,j+1} - U_{i,j}}{\Delta t} = D \frac{U_{i+1,j} - 2U_{i,j} + U_{i-1,j}}{(\Delta x)^2} \qquad (6.24)$$

$U_{i,j+1}$ can be obtain from the other values this way:

$$U_{i,j+1} = r \cdot U_{i+1,j} + [1 - 2r] U_{i,j} + r \cdot U_{i-1,j} \qquad (6.25)$$

With the boundary condition and initial condition employed for diffusion without reactions, where:

$$U_{n,0} = 0 \text{ (initial)}, \ U_{0,j} = U_{2n,j} = 0 \text{ (boundary)} \qquad (6.26)$$

According to the symmetry of the model,

$$U_{n-1,j} = U_{n+1,j} \qquad (6.27)$$

The concentration U can be solved by Explicit Method as following,

$$U_{1,1} = r \cdot U_{2,0} + [1 - 2r] U_{1,0} + r \cdot U_{0,0} = r \cdot U_0 \qquad (6.28)$$

$$U_{i,1} = r \cdot U_{i+1,0} + [1 - 2r] U_{i,0} + r \cdot U_{i-1,0} = 0 \qquad \text{(for } i>1) \qquad (6.29)$$

$$U_{1,j+1} = r \cdot U_{2,j} + \left[1 - 2r\right] U_{1,j} + r \cdot U_{0,j} = r \cdot U_{2,j} + \left[1 - 2r\right] U_{1,j} + r \cdot U_0 \qquad (6.30)$$

$$U_{i,j+1} = r \cdot U_{i+1,j} + \left[1 - 2r\right] U_{i,j} + r \cdot U_{i-1,j} \qquad \text{(for } n > i > 1\text{)} \qquad (6.31)$$

$$U_{n,j+1} = r \cdot U_{n+1,j} + \left[1 - 2r\right] U_{n,j} + r \cdot U_{n-1,j} = \left[1 - 2r\right] U_{n,j} + 2r \cdot U_{n-1,j} \qquad (6.32)$$

Convergence Conditions. Owing to the rule of iteration of explicit finite difference method, one of the limits of this method is the convergence condition. The iteration coefficient of r, affected by the time step, space step and diffusion coefficient D, determines the convergence in explicit method.

$$U_{i,j+1} = r \cdot U_{i+1,j} + \left[1 - 2r\right] U_{i,j} + r \cdot U_{i-1,j} \qquad (6.33)$$

$$\text{Where } r = D \frac{\Delta t}{\left(\Delta x\right)^2} \qquad (6.34)$$
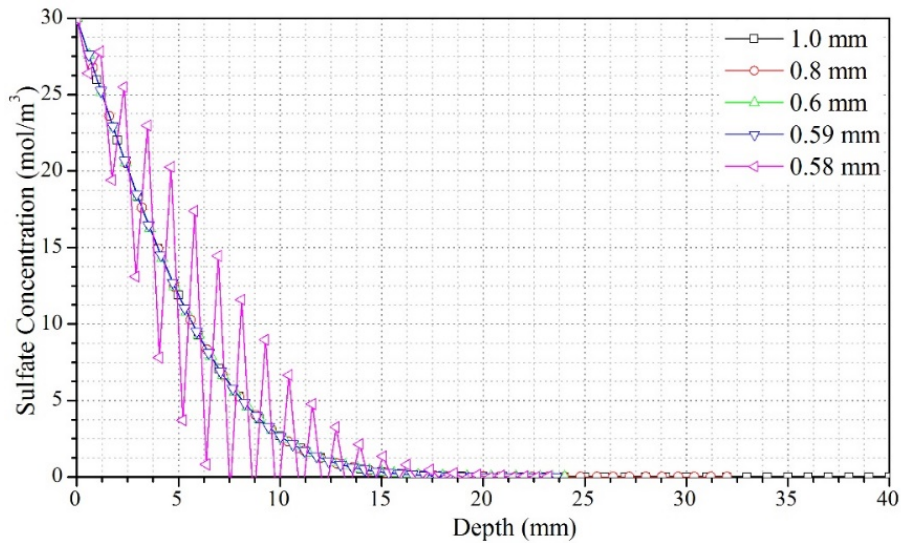
Figure 6.5. Sulfate concentration profiles as affected by space increment after 50 days exposure

Referring to the iteration rule of explicit method, the coefficient r in this model was limited not exceeding 0.5 in order to obtain convergent results. Varied time and space steps were chosen upon explicit method to investigate the convergence. As presented in Figure 6.5, when reducing the space increment from 1 mm to 0.58 mm with diffusion coefficient (1.5 $\times 10^{-12}$ m^2/s) and time step (1day) unaltered, the value of r exceed 0.5 (r = 0.5136 when space step = 0.58 mm). The sulfate concentration profile waved within space domain of 20 mm and was not converged.
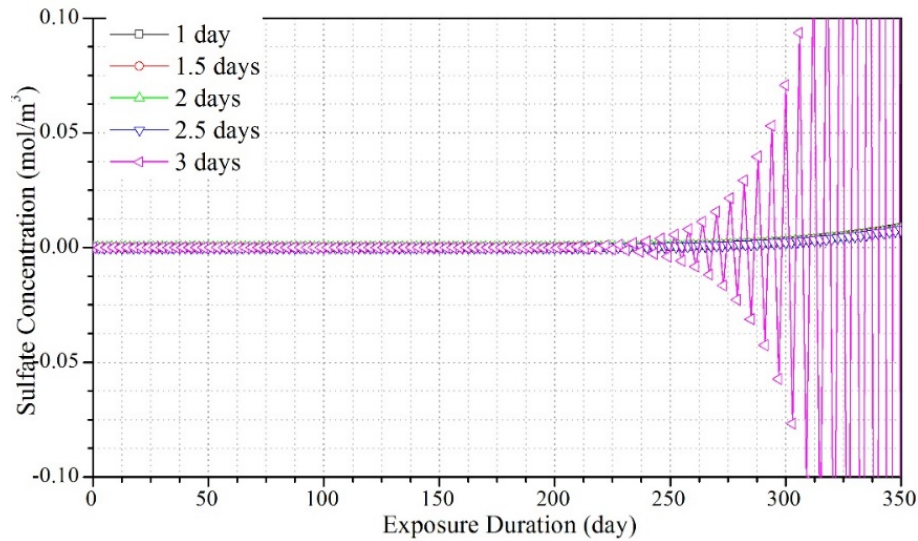
Figure 6.6. Sulfate concentration profiles as affected by time increment at the depth of 40 mm

Likewise, when increasing the time step from 1-day to 3-day with diffusion coefficient and space step unaltered, the value of r exceed 0.5 (r = 0.5184 when time step = 3 days). The attendant sulfate concentration profile had dramatic waving and was not converged as seen in Figure 6.6. The sulfate concentration in Figure 6.6 was at the distance of 40 mm from the boundary and the model was unreliable with the coefficient r over 0.5.

Based on the definition of r as expressed in Eq. (6.34), the effect caused by space step was remarkably critical to the value of r than that by the time step because the space step was

quadratic in the expression. It is suggested to give priority to the adjustment of time step when improving the explicit model due to the less effect to the convergence.

Error Discussion. Varied time steps were introduced to the explicit model within the convergence condition that $r < 0.5$, and the sulfate concentration profiles and relative errors upon time steps were presented as following, note that all the error discussions were retrieved after 50-day of exposure duration.
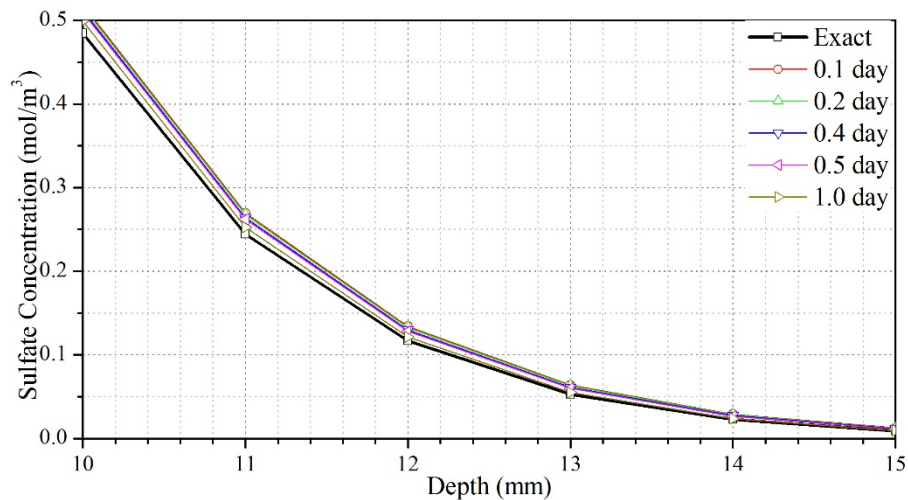
Figure 6.7. Sulfate profiles as affected by varied time step through Explicit Method
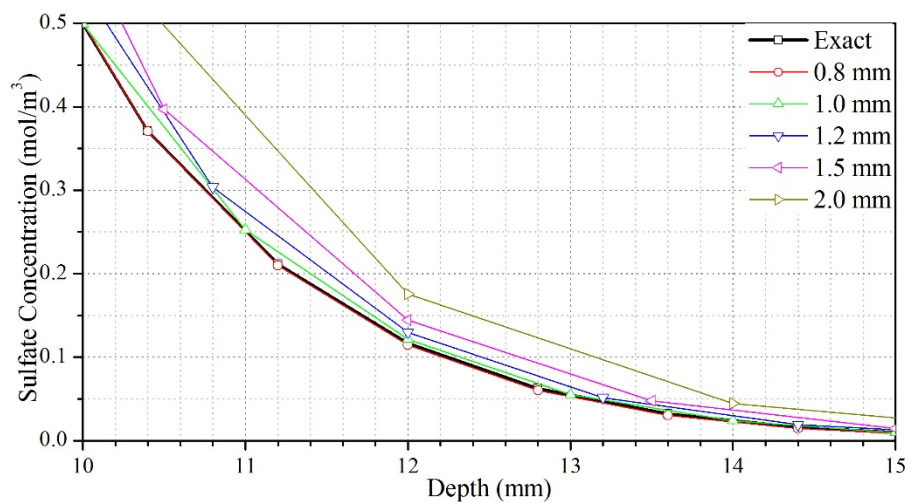
Figure 6.8. Sulfate profiles as affected by varied space step through Explicit Method

Figure 6.7 and Figure 6.8 present the sulfate profiles as affected by variations of time and space steps. As expected, one can see that the variation of space step had greater deviation from the exact solution than that of time step. However, errors caused by both variations were very small and decreased with diffusion depth.
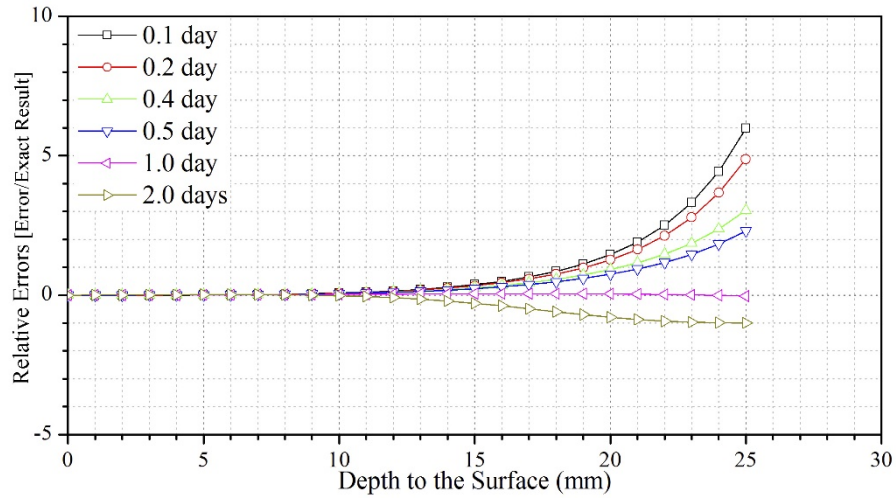
Figure 6.9. Simulation errors as affected by varied time step through Explicit Method
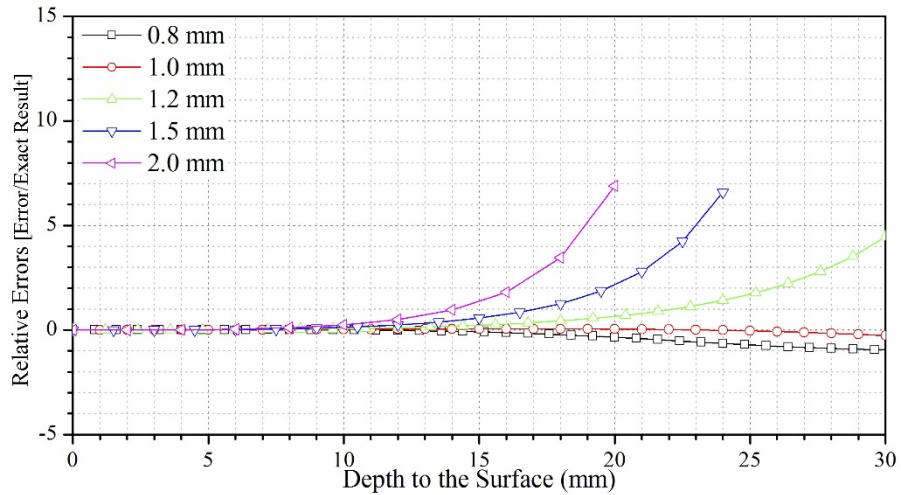
Figure 6.10. Simulation errors as affected by varied space step through Explicit Method

According to the comparison between the solution from explicit method and exact solution, the absolute errors were decreasing with diffusion depth. This was contributed to the widely varied concentrations at the depth of 100mm and 10mm where $C_{(x = 10 \text{ mm})}$ =0.4843 mol/m^3 whereas $C_{(x = 20 \text{ mm})}$ =0.000045 mol/m^3. Thus the error was even negligible as for the order of magnitude at depth of 10mm. Relative errors were introduced to evaluate the accuracy upon varied steps compared with the exact solution.

As shown in Figure 6.9 and Figure 6.10, it is recognized that the relative errors caused by space step were more pronounced than that by time steps similar to the trend concluded from Figure 6.7 and Figure 6.8. However, the relative error showed rapid increment in performance with increasing diffusion depth caused by either time step or space step.

Note that in this case, the relative errors within 10 mm of depth were acceptable upon all the space and time steps employed. The maximum relative error at the distance of 10 mm was calculated to 24.71% by choosing space step of 2 mm, and the maximum error was7.042% by choosing time space of 0.1 day. When applying huge amount of iterations, the error accumulated so that lager space steps and smaller time steps were not acceptable for approximation. As a result, the optimum time step was chosen to 1 day and space step to 1 mm in this study.

Sulfate Concentration Profiles. The sulfate profiles plotted in Figure 6.11 shows that, without chemical consumption, the sulfate concentrations decreased with depth. Time-dependent model also indicated that sulfate concentration accumulated with exposure durations at defined depth under diffusion.
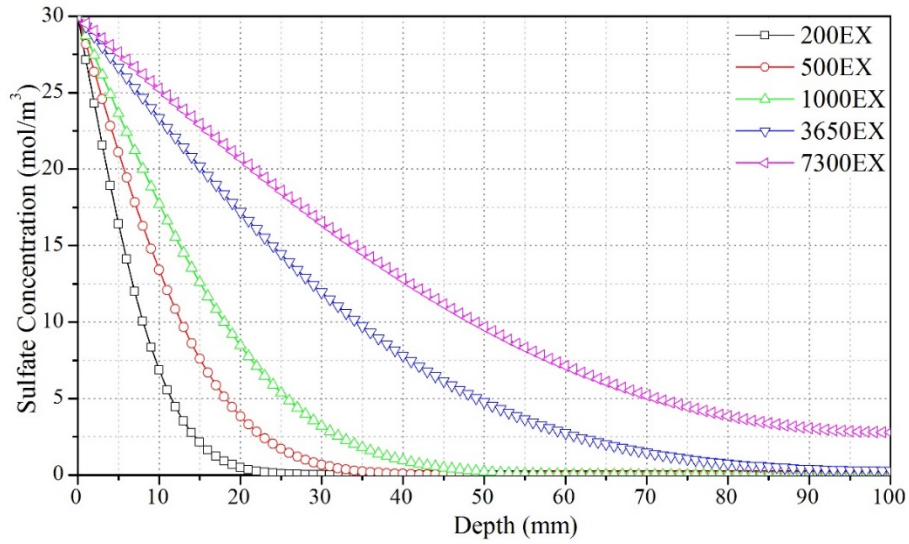
Figure 6.11. Sulfate concentration simulated by Explict method as affected by depth

6.5.3 IMPLICIT METHOD

Introduction. Different from the explicit method, implicit finite difference method find a solution by solving an equation involving both the current state of the system and the later one. This method was unconditionally converged compared with explicit method because of the rule of iteration presents as following,

Rule of iteration.
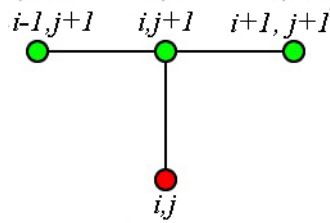
Figure 6.12. Rule of iteration of implicit method

The implicit method stencil.

$$\frac{u_i^{n+1} - u_i^n}{\Delta t} = F_i^{n+1}\left(u, x, t, \frac{\partial u}{\partial x}, \frac{\partial^2 u}{\partial x^2}\right) \qquad (6.35)$$

(Backward Euler)

Eq. (6.35) shows the Partial Differential Equation of implicit method and the iteration in modeling can be explained. That is, the value of u at distance of i and time step j was dependent on the latter value at distance i and time $j+1$, and the nearby values of $i-1, j+1$ and $i+1, j+1$.

If we use the backward difference at time t_{n+1} and a second-order central difference for the space derivative at position x_j (The Backward Time, Centered Space Method "BTCS") we get the recurrence equation:

$$\frac{u_j^{n+1} - u_j^n}{\Delta t} = D \cdot \frac{u_{j+1}^{n+1} - 2u_j^{n+1} + u_{j-1}^{n+1}}{(\Delta x)^2} \qquad (6.36)$$

This is an implicit method for solving the one-dimensional heat equation.

We can obtain u_j^{n+1} from solving a system of linear equations:

$$(1 + 2r) \cdot u_j^{n+1} - r \cdot u_{j-1}^{n+1} - r \cdot u_{j+1}^{n+1} = u_j^n \qquad (6.37)$$

Where the r is also defined as,

$$r = D \cdot \frac{\Delta t}{(\Delta x)^2} \qquad (6.38)$$

The scheme is always numerically stable and convergent but usually more numerically intensive than the explicit method as it requires solving a system of numerical equations on each time step. The errors are linear over the time step and quadratic over the space step:

$$\Delta u = O(k) + O(h^2) \tag{6.39}$$

Rearrangement of Linear Formula. Again, convert the sulfate concentration u_j^n in Euler equation to $U_{i,j}$ as following:

$$\frac{U_{i,j+1} - U_{i,j}}{\Delta t} = D \cdot \frac{U_{i-1,j+1} - 2U_{i,j+1} + U_{i+1,j+1}}{(\Delta x)^2} \tag{6.1}$$

Rearrange the formula,

$$[1 + 2r] \cdot U_{i,j+1} - r \cdot U_{i-1,j+1} - r \cdot U_{i+1,j+1} = U_{i,j} \tag{6.2}$$

$$U_{1,0} = -r \cdot U_{0,1} + [1 + 2r] \cdot U_{1,1} - r \cdot U_{2,1} \tag{6.3}$$

$$U_{2,0} = \qquad -r \cdot U_{1,1} + [1 + 2r] \cdot U_{2,1} - r \cdot U_{3,1} \tag{6.4}$$

With the same boundary and initial conditions, the Implicit Method was solved by matrix iteration.

Original Matrix of Iteration.

$$[A_U]\{U_{,j+1}\} = \{U_{,j}\} \tag{6.5}$$

$$\{U_{,j+1}\} = \begin{bmatrix} U_{0,j+1} & U_{1,j+1} & U_{2,j+1} & \cdots & U_{n,j+1} & U_{n+1,j+1} \end{bmatrix}^{\mathrm{T}} \tag{6.6}$$

$$\{U_{,j}\} = \begin{bmatrix} U_{1,j} & U_{2,j} & U_{3,j} & \cdots & U_{n-1,j} & U_{n,j} \end{bmatrix}^{\mathrm{T}} \tag{6.7}$$

$$\begin{vmatrix} -r & 1+2r & -r & 0 & \cdots & & \cdots & 0 \\ 0 & -r & 1+2r & -r & \ddots & & \ddots & \vdots \\ \vdots & \ddots & \cdots & \cdots & \cdots & & \ddots & \vdots \\ \vdots & \ddots & \ddots & -r & 1+2r & & -r & 0 \\ 0 & \cdots & & \cdots & 0 & -r & 1+2r & -r \end{vmatrix} = \begin{bmatrix} A_U \end{bmatrix} \tag{6.8}$$

where, $\{U_{,j+1}\}$ is (n+2)×1 order vector and $\{U_{,j}\}$ is n×1 order vectors, and the initial matrix of A_U is (n+2)×n order matrix.

Modified Matrix of Iteration. Considering the convenience when programming these iterations into MATLAB, the original matrix was improved to n×n matrix with following adjustments.

$$\begin{bmatrix} A_U' \end{bmatrix}\{U_{j+1}'\} = \{U_j'\} + \{U_{IM}\} \tag{6.9}$$

$$\{U_{j+1}'\} = \begin{bmatrix} U_{1,j+1}' & U_{2,j+1}' & U_{3,j+1}' & \cdots & U_{n-1,j+1}' & U_{n,j+1}' \end{bmatrix}^{\mathrm{T}} \tag{6.10}$$

$$\{U_j'\} = \begin{bmatrix} U_{1,j}' & U_{2,j}' & U_{3,j}' & \cdots & U_{n-1,j}' & U_{n,j}' \end{bmatrix}^{\mathrm{T}} \tag{6.11}$$

where, $\{U_{,j+1}'\}$ and $\{U_{,j}'\}$ are n×1 order vectors, and indicate the corresponding values at time $j+1$ and at time j respectively. $\{U_{IM}\}$ is n×1 order vector,

$$\{U_{IM}\} = \begin{bmatrix} -2r \cdot U_0 & 0 & \cdots & 0 \end{bmatrix}^{\mathrm{T}} \tag{6.12}$$

$$
\begin{vmatrix}
1+2r & -r & 0 & \cdots & & 0 \\
-r & 1+2r & -r & \ddots & & \vdots \\
0 & \cdots & \cdots & \cdots & & 0 \\
\vdots & \ddots & -r & 1+2r & -r \\
0 & \cdots & 0 & -2r & 1+2r
\end{vmatrix} = \left[A_U' \right]
\qquad (6.13)
$$

The modified matrix of A_U' is n×n matrix and employed in the MATLAB programming.

Error Discussion. The Implicit Method was absolutely converged so that there was no limits for the variation of time and space steps. However, the same variations of time and space steps employed in explicit method were chosen in comparison of accuracy between these two approaches.
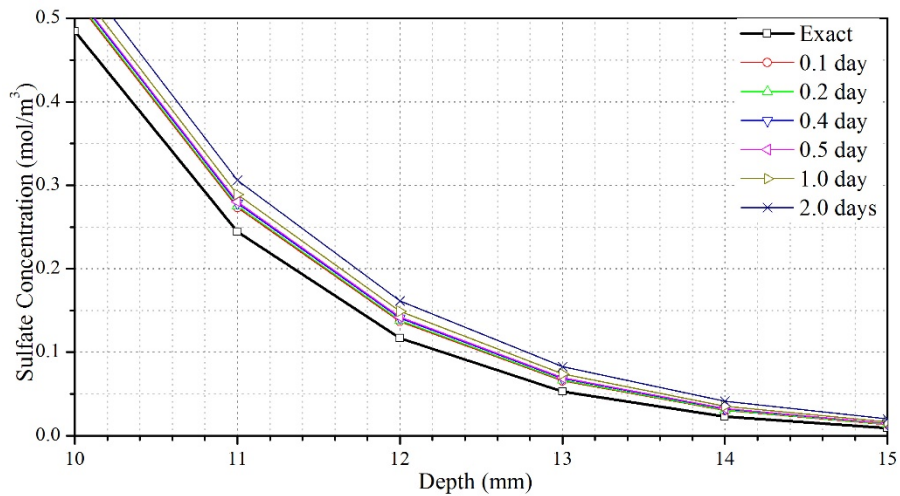
Figure 6.13. Sulfate profiles as affected by varied time step through Implicit Method
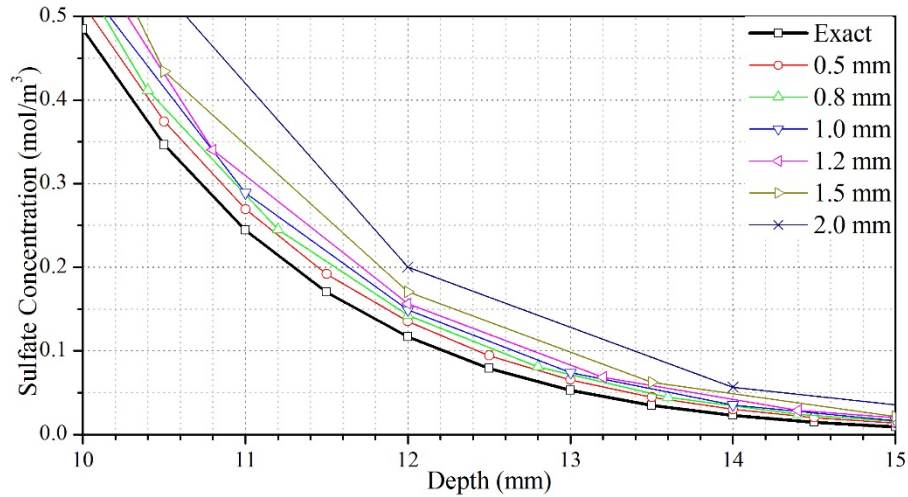
Figure 6.14. Sulfate profiles as affected by varied space step through Implicit Method

Figure 6.13 and Figure 6.14 present the sulfate profiles as affected by variations of time and space steps. Also, the variation of space step had greater deviation from the exact solution than that of time step. Comparing the sulfate concentration results obtained by explicit method and implicit method, it was noted that the accuracy of approximation upon implicit method was lower than that upon explicit method although the implicit method has no convergence limits. Again, relative errors were introduced to evaluate the accuracy upon varied steps compared with the exact solution.
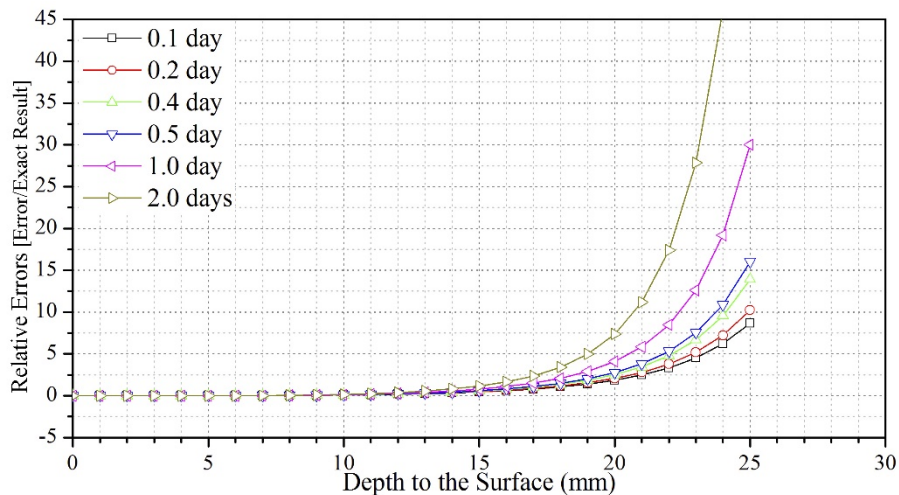
Figure 6.15. Simulation errors as affected by varied time step through Implicit Method
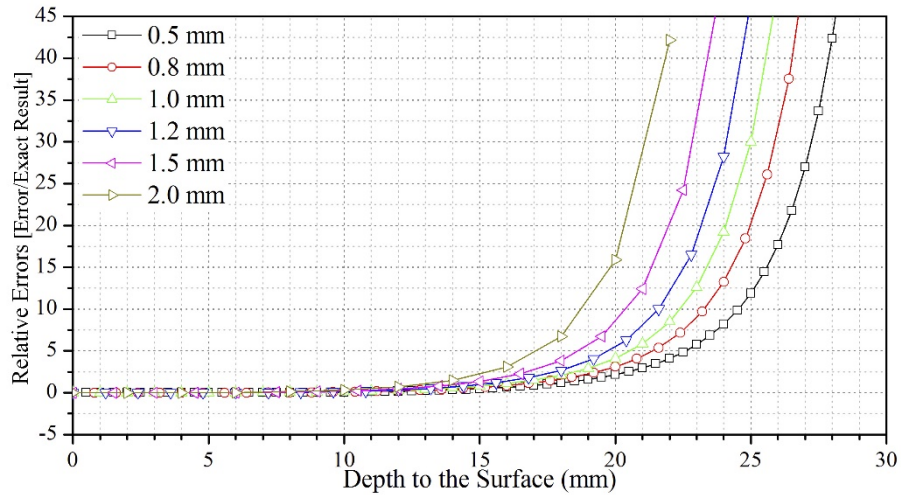
Figure 6.16. Simulation errors as affected by varied space step through Implicit Method

As shown in Figure 6.15 and Figure 6.16, it is recognized that all the relative errors obtained through implicit method were significantly larger than those upon explicit method, which was corroborated with the sulfate profiles as shown in Figure 6.13 and Figure 6.14. The error/exact ratio exceeded 10 at diffusion depth of 25 mm caused by variations of time step whereas the ratio exceeded 10 at diffusion depth of 20 mm caused by variations of space step. The maximum relative error at the distance of 10 mm was calculated to 32.09% by choosing space step of 2 mm, and the maximum error was 15.74% by choosing time space of 2 day.

It is likely that the direction of time iteration through implicit method was opposite to the real situation of time-dependent diffusion, which resulted in the lower accuracy than explicit method in approximation. Still, when applying huge amount of iterations, the error accumulated so that lager space steps and smaller time steps were not acceptable for approximation. As a result, the optimum time step was still chosen to 1 day and space step to 1 mm in this study.

Sulfate Concentration Profiles. Similar sulfate profiles were witnessed through implicit method in Figure 6.17 that, without chemical consumption, the sulfate concentrations decreased with depth. Time-dependent model also indicated that sulfate concentration accumulated with exposure durations at defined depth under diffusion.
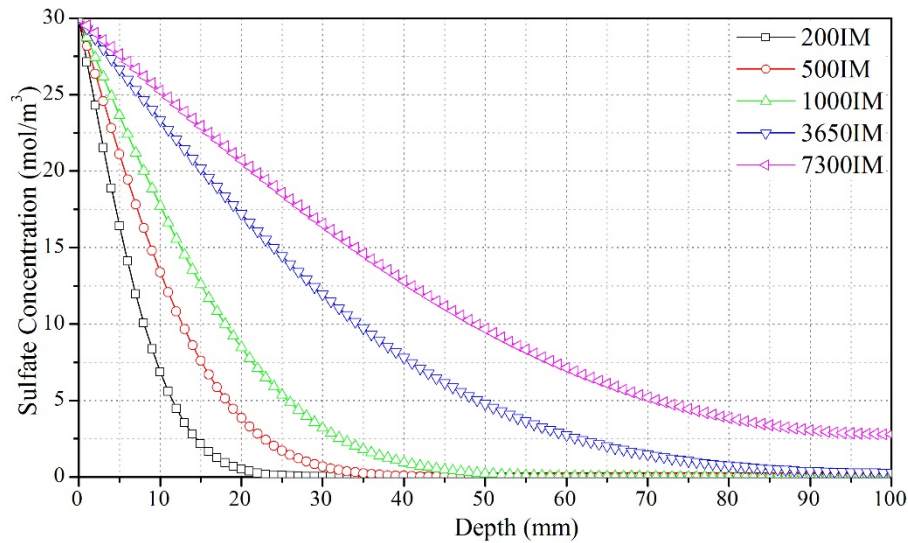
Figure 6.17. Sulfate profiles as affected by exposure duration through Implicit Method

6.5.4 Crank–Nicolson Method

Introduction. In numerical analysis, the Crank–Nicolson method is a finite difference method used for numerically solving the heat equation and similar partial differential equations. It is a second-order method in time, it is implicit in time and can be written as an implicit Runge–Kutta method, and it is numerically stable. The method was developed by John Crank and Phyllis Nicolson in the mid-20th century.

For diffusion equations (and many other equations), it can be shown the Crank–Nicolson method is unconditionally stable. However, the approximate solutions can still contain (decaying) spurious oscillations if the ratio of time step Δt times the thermal diffusivity to the square of space step, Δx^2, is large (typically larger than 1/2 per Von Neumann stability analysis). For this reason, whenever large time steps or high spatial resolution is necessary,

the less accurate backward Euler method is often used, which is both stable and immune to oscillations.

Rule of Iteration. This formula is known as the Crank–Nicolson method.
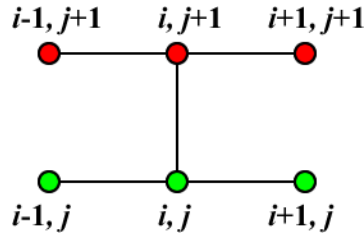
Figure 6.18. Rule of iteration of Crank-Nicolson Method

The Crank–Nicolson stencil.

$$\frac{u_i^{n+1} - u_i^n}{\Delta t} = \frac{1}{2}\left[F_i^{n+1}\left(u,x,t,\frac{\partial u}{\partial x},\frac{\partial^2 u}{\partial x^2} \right) + F_i^n\left(u,x,t,\frac{\partial u}{\partial x},\frac{\partial^2 u}{\partial x^2} \right) \right] \qquad (6.14)$$

(Crank-Nicolson Iteration)

Finally if we use the central difference at time $t_{n+1}/2$ and a second-order central difference for the space derivative at position x_j ("CTCS") we get the recurrence equation:

$$\frac{u_j^{n+1} - u_j^n}{k} = D \cdot \frac{1}{2}\cdot\left(\frac{u_{j+1}^{n+1} - 2u_j^{n+1} + u_{j-1}^{n+1}}{h^2} + \frac{u_{j+1}^n - 2u_j^n + u_{j-1}^n}{h^2} \right) \qquad (6.15)$$

We can obtain u_j^{n+1} from solving a system of linear equations:

$$(2+2r)u_j^{n+1} - ru_{j-1}^{n+1} - ru_{j+1}^{n+1} = (2-2r)u_j^n + ru_{j-1}^n + ru_{j+1}^n \qquad (6.16)$$

Also,

$$r = D \cdot \frac{\Delta t}{(\Delta x)^2} \qquad (6.17)$$

The scheme is always numerically stable and convergent but usually more numerically intensive as it requires solving a system of numerical equations on each time step. The errors are quadratic over both the time step and the space step:

$$\Delta u = O(k) + O(h^2) \qquad (6.18)$$

Formula Derivation. Again, convert the sulfate concentration u_j^n in Euler equation to $U_{i,j}$ as following:

$$\frac{U_{i,j+1} - U_{i,j}}{\Delta t} = \frac{D}{2}\left[\frac{U_{i+1,j+1} - 2U_{i,j+1} + U_{i-1,j+1}}{(\Delta x)^2} + \frac{U_{i+1,j} - 2U_{i,j} + U_{i-1,j}}{(\Delta x)^2} \right] \qquad (6.19)$$

$U_{i,j+1}$ can be obtain from the other values this way:

$$-\frac{r}{2}U_{i+1,j+1} + (1+r)U_{i,j+1} - \frac{r}{2}U_{i-1,j+1} = \frac{r}{2}U_{i+1,j} + (1-r)U_{i,j} + \frac{r}{2}U_{i-1,j} \qquad (6.20)$$

Where,

$$r = \frac{D\Delta t}{(\Delta x)^2} \qquad (6.21)$$

According to the boundary condition and initial condition,

$$U_{n,0} = 0 \text{ (initial)}, \quad U_{0,j} = U_{2n,j} = 0 \text{ (boundary)} \tag{6.22}$$

And the symmetry of the model,

$$U_{n-1,j} = U_{n+1,j} \tag{6.23}$$

Several expressions can be derived as following,

For $i=1$ and $j=0$

$$-\frac{r}{2}U_{2,1} + (1+r)U_{1,1} - \frac{r}{2}U_{0,1} = \frac{r}{2}U_{2,0} + (1-r)U_{1,0} + \frac{r}{2}U_{0,0} \tag{6.24}$$

$$-\frac{r}{2}U_{2,1} + (1+r)U_{1,1} = rU_0 \tag{6.25}$$

For $i>1$ and $j=0$

$$-\frac{r}{2}U_{i+1,1} + (1+r)U_{i,1} - \frac{r}{2}U_{i-1,1} = \frac{r}{2}U_{i+1,0} + (1-r)U_{i,0} + \frac{r}{2}U_{i-1,0} \tag{6.26}$$

$$-\frac{r}{2}U_{i+1,1} + (1+r)U_{i,1} - \frac{r}{2}U_{i-1,1} = 0 \tag{6.27}$$

For $i=1$ and $j>0$

$$-\frac{r}{2}U_{2,j+1} + (1+r)U_{1,j+1} - \frac{r}{2}U_{0,j+1} = \frac{r}{2}U_{2,j} + (1-r)U_{1,j} + \frac{r}{2}U_{0,j} \tag{6.28}$$

$$-\frac{r}{2}U_{2,j+1} + (1+r)U_{1,j+1} = \frac{r}{2}U_{2,j} + (1-r)U_{1,j} + rU_0 \tag{6.29}$$

For $n>i>1$ and $j>0$

$$-\frac{r}{2}U_{i+1,j+1} + (1+r)U_{i,j+1} - \frac{r}{2}U_{i-1,j+1} = \frac{r}{2}U_{i+1,j} + (1-r)U_{i,j} + \frac{r}{2}U_{i-1,j} \tag{6.30}$$

For $i=n$ and $j>0$

$$-\frac{r}{2}U_{n+1,j+1}+(1+r)U_{n,j+1}-\frac{r}{2}U_{n-1,j+1}=\frac{r}{2}U_{n+1,j}+(1-r)U_{n,j}+\frac{r}{2}U_{n-1,j} \qquad (6.31)$$

$$(1+r)U_{n,j+1}-r\cdot U_{n-1,j+1}=(1-r)U_{n,j}+r\cdot U_{n-1,j} \qquad (6.32)$$

Expressing linear equation sets in matrix form

$$[A_U]\{U_{,j+1}\}=[B_U]\{U_{,j}\}+\{U_{CN}\} \qquad (6.33)$$

where, $\{U_{,j+1}\}$ and $\{U_{,j}\}$ are $n\times1$ order vectors, and indicate the corresponding values at

time $j+1$ and at time j respectively. $\{U_{CN}\}$ is $n\times1$ order vector,

$$\{U_{CN}\}=\begin{bmatrix}-2\cdot r\cdot U_0 & 0 & \cdots & 0\end{bmatrix}^T \qquad (6.34)$$

A_U and B_U are $n\times n$ order tri-diagonal matrixes,

$$\begin{vmatrix} 2(1+r) & -r & 0 & \cdots & & 0 \\ -r & 2(1+r) & -r & \ddots & & \vdots \\ 0 & \cdots & \cdots & \cdots & & 0 \\ \vdots & & \ddots & -r & 2(1+r) & -r \\ 0 & & \cdots & 0 & -2r & 2(1+r) \end{vmatrix}=[A_U] \qquad (6.35)$$

$$\begin{vmatrix} -2(1-r) & r & 0 & \cdots & & 0 \\ r & -2(1-r) & r & \ddots & & \vdots \\ 0 & \cdots & \cdots & \cdots & & 0 \\ \vdots & & \ddots & r & -2(1-r) & r \\ 0 & & \cdots & 0 & 2r & -2(1-r) \end{vmatrix}=[B_U] \qquad (6.36)$$

Error Discussion. Same as the Implicit Method, Crank-Nicolson method was converged with varied time and space steps. To compare the errors by applying Crank-Nicolson method, the same variations of time and space steps employed were chosen.
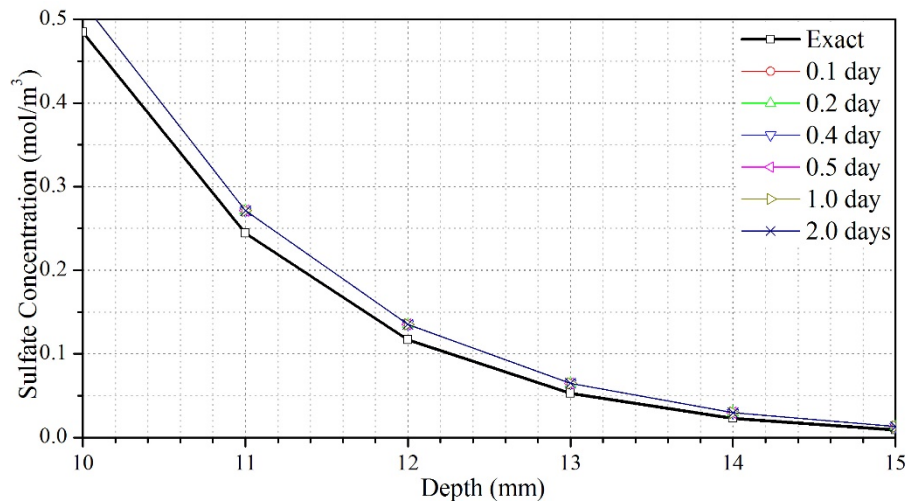
Figure 6.19. Sulfate profiles as affected by varied time step through Crank-Nicolson Method
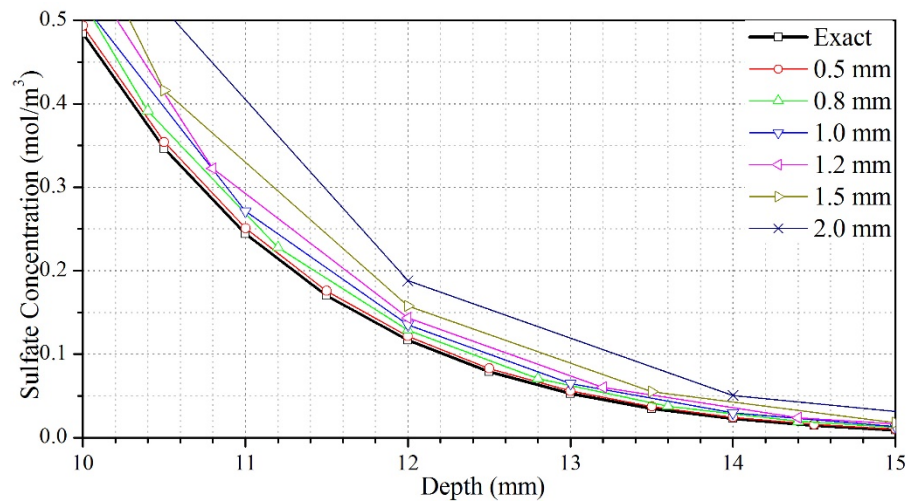
Figure 6.20. Sulfate profiles as affected by varied space step through Crank-Nicolson Method

Figure 6.19 and Figure 6.20 present the sulfate profiles as affected by variations of time and space steps using Crank-Nicolson approach. One can see that there was no perceptible

deviations by choosing varied time steps. In contrast, the error caused by variation of space steps was more pronounced in comparison with other two approaches.

Comparing the sulfate concentration results obtained by explicit method and implicit method, it was noted that the accuracy of approximation through Crank-Nicolson method was not as good as that through explicit method. Again, relative errors were introduced to evaluate the accuracy upon varied steps compared with the exact solution.
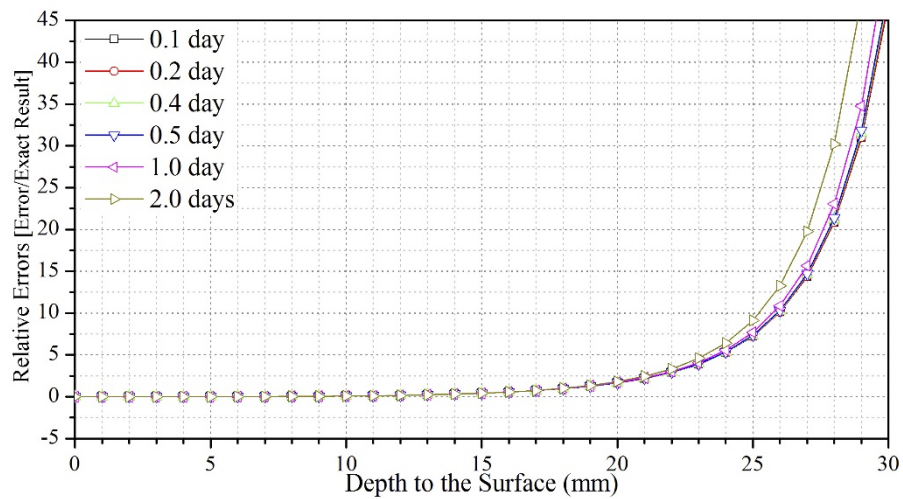
Figure 6.21. Simulation errors as affected by varied time step through Crank-Nicolson Method
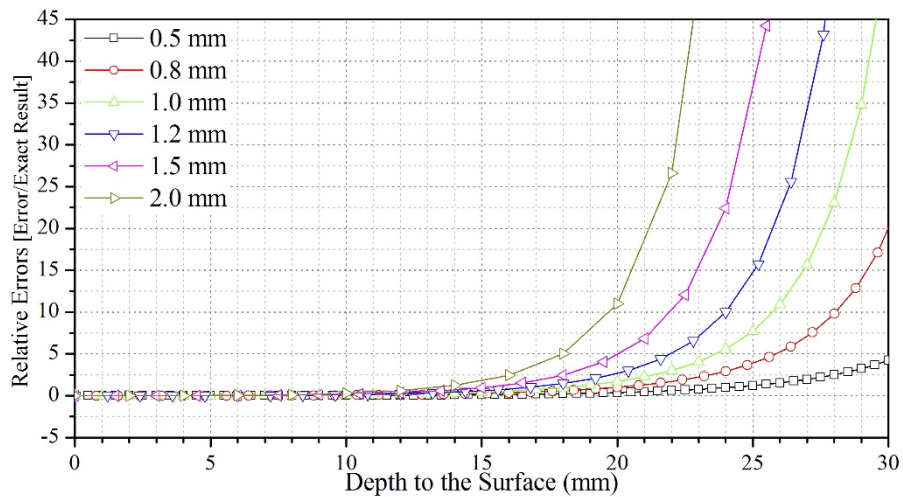
Figure 6.22. Simulation errors as affected by varied space step through Crank-Nicolson Method

As shown in Figure 6.21 and Figure 6.22, it is recognized although the error caused by variation of time step increased after diffusion depth over 20 mm, the deviation of these errors was very limited. Nevertheless, the errors caused by variation of space step were widely varied as shown in Figure 6.22.

The error/exact ratio exceeded 10 at diffusion depth of 25 mm caused by variations of time step, however, the ratio exceeded 10 at diffusion depth of 20 mm only choosing the space step of 2.0 mm. The maximum relative error at the distance of 10 mm was calculated to 28.46% by choosing space step of 2 mm, and the maximum error was 7.48% by choosing time space of 0.1 day.

As demonstrated in the introduction, the Crank-Nicolson method was a combined approach averaged by explicit and implicit methods, which was verified through the errors retrieved. This approach had the advantage of implicit method that no convergence conditions were required and the advantage of explicit method that of higher approximation accuracy.

Sulfate Concentration Profiles. As shown in Figure 6.23, the Crank-Nicolson method showed acceptable performance in sulfate concentration approximation.
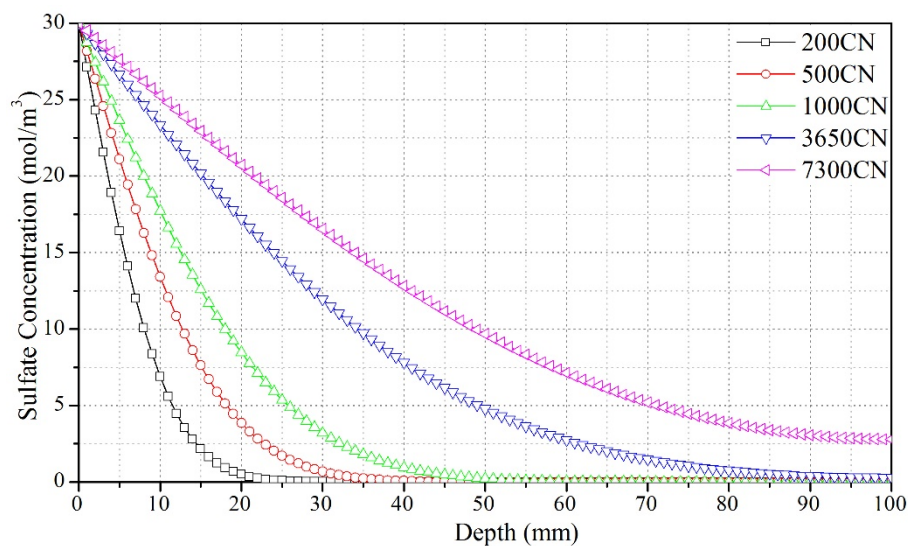
Figure 6.23. Sulfate profiles as affected by exposure duration through Crank-Nicolson Method

6.6 RESULTS COMPARISON AND DISCUSSION

As discussed above, the time step was chosen to 1 day and the space step to 1 mm with acceptable error variations through examined finite difference methods.

Hence sulfate profiles were plotted through three tested finite difference methods in comparison with the exact solution. As presented in Figure 6.24, all these approximation methods showed high accuracy in sulfate concentration simulation.
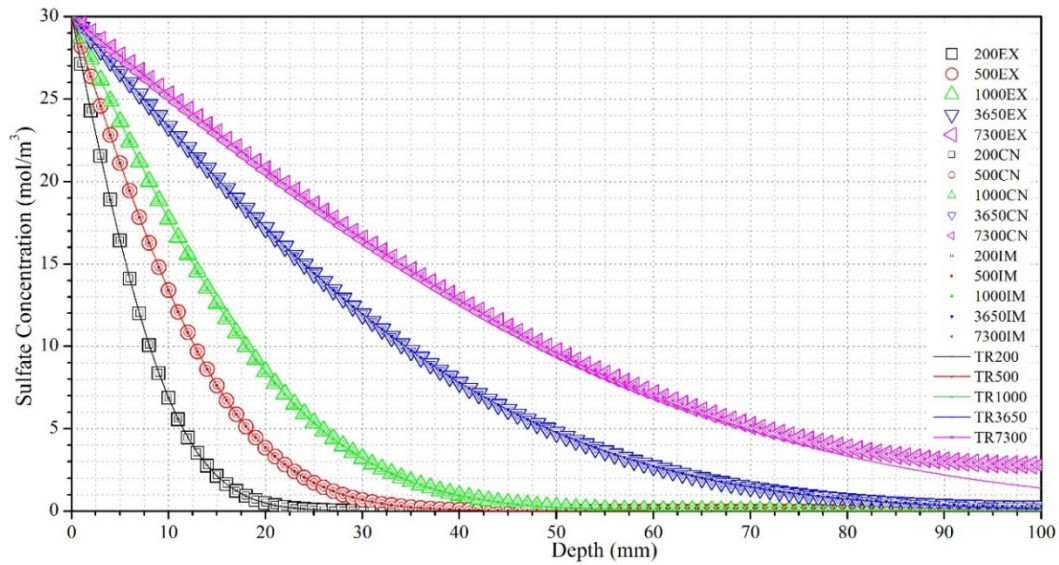
Figure 6.24. Sulfate profiles as affected by finite difference methods within 10-year exposure
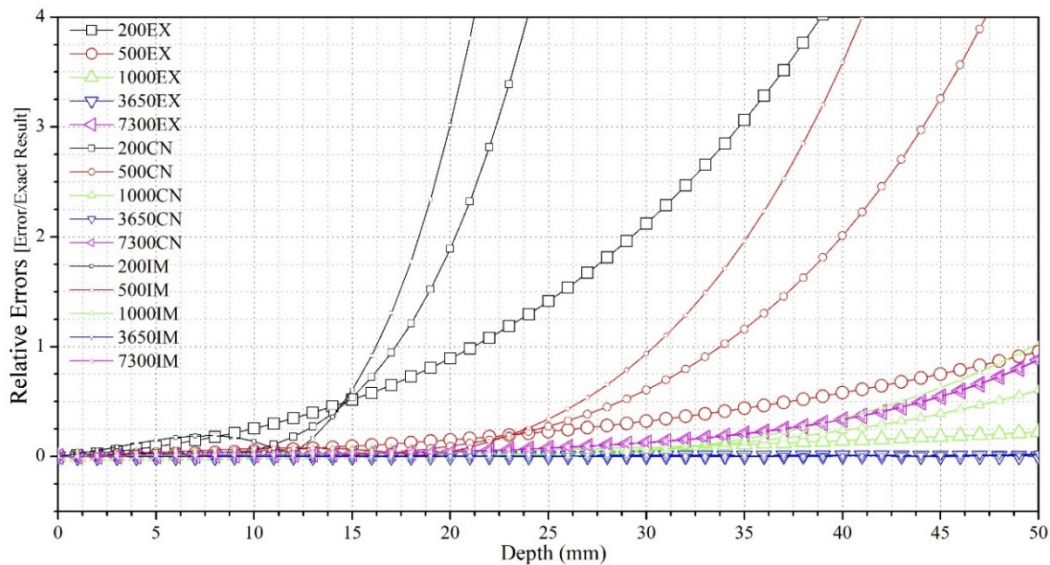
Figure 6.25. Relative errors caused by finite difference approximation within 10-year exposure

It is worth noting that, from the relative errors presented in Figure 6.25, explicit finite difference method registered the highest accuracy in all exposure durations whereas the implicit method was seen to be the approximation of the lowest accuracy. Besides, with the optimum time and space steps selected, all these finite difference methods upon 1000-day of exposure had very limited errors within 50 mm. Long-term exposure resulted in higher accuracy in simulation than exposure under 1000 days.

Usually the Crank–Nicolson scheme is the most accurate scheme for small time increment. The explicit scheme is the least accurate and can be unstable, but is also the easiest to implement and the least numerically intensive. The implicit scheme works the best for large time increment. In this manner, the explicit method and Crank-Nicolson method were preferred for further modeling development.

6.7 CONCLUSIONS AND SUGGESTIONS

6.7.1 CURRENT FINDINGS AND METHOD PREFERENCE

■ Based on the non-reaction diffusion theory, three finite difference methods were employed to simulate the sulfate ion diffusion inside cement-based composites. The errors were discussed in detail and these finite difference methods including explicit, implicit and Crank-Nicolson method, showed reasonable and acceptable errors in comparison with error function solution.

■ The error remarkably decreased with exposure duration through all three finite difference methods employed. These methods had high simulating accuracy within 1-year of exposure and the steps were supposed to be improved to smaller when predicting the concentration within 1-year exposure to sulfate environment.

- Explicit method was investigated of the minimum error in simulation although it had convergence limit when choosing the time step and space step. This was because the rule of iteration of explicit was the same as the diffusion direction. However, stable finite difference methods such as implicit method and Crank-Nicolson method were examined of larger errors in comparison with explicit method. Crank-Nicolson method presented better performance in simulation.

- As a result, the explicit method was chosen for further diffusion-reaction modeling involved with chemical reactions under sulfate attack. The optimum time step and space step was chosen to 1 day and 1 mm by this study.

6.7.2 Future Work on Numerical Modeling

For the Numerical Modeling currently developed, the research focused on the simple one dimensional diffusion of external sulfate attack. When applying the explicit method, the converged conditions are supposed to be determined firstly. There are defined ranges for time step and space step by using explicit Method. In terms of the implicit method, the difficulty is to set up the iteration matrix and apply the method to programming languages. The errors are discussed for Explicit Method and Implicit Method compared with exact solution.

7 DIFFUSION-REACTION NUMERICAL MODELING AND DATA FITTING

7.1 MODELING INVOLVED CHEMICAL REACTIONS

7.1.1 BACKGROUND AND INTRODUCTION

This chapter describes the specific numerical model involved with chemical reactions, which is extended from the physical diffusion model as demonstrated in the last chapter. Two finite element methods, explicit method and Crank-Nicolson method, were chosen for their high simulating precision and convergence.

Sulfate ingress from external environment, after consumed by the internal compositions, was obtained through improved model in order to fit the experimental results from titration experiments.

7.1.2 MECHANISM OF EXTERNAL SULFATE ATTACK

The mechanism of adverse sulfate attack to cement-based composites has been studied in detail by civil and material researchers. Expansion caused by ettringite formation is the most widely recognized mechanism of sulfate attack in literature.(Wang 1994) The chemical reactions inside Portland cement prior to hardening are listed:

$$C_3A + 3C\bar{S}H_2 + 26H = C_6A\bar{S}_3H_{32} \tag{7.37}$$

However, if all the gypsum is consumed before the entire C3A has reacted, then ettringite transforms to another form of calcium aluminate sulfate:

$$2C_3A + C_6A\bar{S}_3H_{32} + 4H = 3C_4A\bar{S}H_{12} \tag{7.38}$$

The formation of monosulfate occurs because in most cements, there is not sufficient gypsum provided to consume all the C3A into ettringite. The monosulfate, however, remains

a potential risk of ettringite re-formation in the presence of further sulfate ions, for example, the external sulfate attack.

$$C_4A\bar{S}H_{12} + 2C\bar{S}H + 16H = C_6A\bar{S}_3H_{32} \tag{7.39}$$

The transformation from monosulfate to ettringite is a highly expansive reaction as explained in the numerical modeling. Besides, some researchers mentioned that the formation of gypsum during sulfate attack also leads to expansion. (Tian and Cohen 2000) The reaction of gypsum formation is listed below.

$$Na_2SO_{4\ (external)} + Ca(OH)_2 \leftrightarrow CaSO_{4\ (gypsum)} + NaOH \tag{7.40}$$

7.1.3 REACTIONS INVOLVED IN SULFATE ATTACK PROCESS

In order to apply the series of chemical reactions into numerical modeling, two reactants, C_3A and SO_3 (represented of gypsum in cement-based composites), were chosen and the reactions were rearranged by Tixier R, Mobasher B (Tixier and Mobasher 2003). ThesThree main components in several forms of calcium aluminate phases in a hydrated cement paste were considered: C_4AH_{13}, $C_4A\bar{S}H_{12}$ and residual anhydrous C_3A. The relative proportions of the components are evaluated from the C_3A, gypsum content of the cement, the cement dosage, and the degree of hydration.

The three compounds may react with sulfate ingress according to one of the following reactions(Tixier and Mobasher 2003; Tixier and Mobasher 2003):

$$C_4AH_{13} + 3C\bar{S}H_2 + 14H \rightarrow C_6A\bar{S}_3H_{32} + CH \tag{7.41}$$

$$C_4A\bar{S}H_{12} + 2C\bar{S}H_2 + 16H \rightarrow C_6A\bar{S}_3H_{32} \tag{7.42}$$

$$C_3A+3C\overline{S}H_2+26H \rightarrow C_6A\overline{S}_3H_{32} \qquad (7.43)$$

These reactions are lumped in a global sulfate phase-aluminate phase reaction as

$$CA+\lambda C\overline{S}H_2+nH \rightarrow C_6A\overline{S}_3H_{32} \qquad (7.44)$$

Where CA signifies an equivalent grouping of the reacting calcium aluminates, and λ and n represent the weighted average stoichiometric coefficient of the lumped reaction for $C\overline{S}H_2$ and H respectively, obtained from the coefficients of the individual reaction. The value of λ represents the degree of initial hydration and C_3A consumption during external sulfate exposure.

7.1.4 MODEL BASED ON THE DIFFUSION-REACTION

The process of sulfate diffusion in Portland cement-based composites can be described by Fick's second law as following,

$$\frac{\partial C}{\partial t} = D\frac{\partial^2 C}{\partial x^2} \qquad (7.45)$$

In Eq. (7.9) C is the concentration of substances in matrix, t is the exposure duration, D is the diffusion coefficient of sulfate while x is the position.

Fick's second law simply describes the diffusion of substances in matrix. However, the substances in matrix are converted and consumed by chemical reactions while diffusion. The change rates of concentration of SO_4^{2-} and CA can be expressed as following (Tixier and Mobasher 2003),

$$\frac{\partial C_{\mathrm{SO_4^{2-}}}}{\partial t} = -kC_{\mathrm{SO_4^{2-}}}C_{\mathrm{CA}} \qquad (7.46)$$

$$\frac{\partial C_{\mathrm{CA}}}{\partial t} = -\frac{kC_{\mathrm{SO_4^{2-}}}C_{\mathrm{CA}}}{\lambda} \qquad (7.47)$$

with k representing the rate constant. Assuming Fick's law of diffusion, the following equations are obtained by substituting the variables (Sun et al. 2013): U and C, with $U = C_{\mathrm{SO_4^{2-}}}$, $C = C_{\mathrm{CA}}$:

$$\frac{\partial U}{\partial t} = D\frac{\partial^2 U}{\partial x^2} - kUC \qquad (7.48)$$

$$\frac{\partial C}{\partial t} = -\frac{kUC}{\lambda} \qquad (7.49)$$

Because the calcium aluminates are immobile and the content is evenly distributed in the cement-based composites, no diffusion term was used for "CA" in Eq. (7.13). U_0 can be defined as the sulfate concentration of the aggressive solution, which was imposed from both boundaries, and C_0, the initial concentration of CA, assumed to be homogeneously distributed throughout the domain.

Moreover, Ω is the internal domain of material in which Eq. (7.10) applies; Γ denotes the boundary of modeling. The following set of initial and boundary conditions is prescribed:

$$U(\Omega, 0) = 0, \quad C(\Omega, 0) = C_0 \qquad (7.50)$$

$$U(\Gamma, t) = U_0, \quad C(\Gamma, t) = 0 \tag{7.51}$$

Substituting Eq. (7.13) to Eq. (7.12), the following equation is obtained

$$\frac{\partial(U - \lambda C)}{\partial t} = D \frac{\partial^2 U}{\partial x^2} \tag{7.52}$$

Because C is the concentration of CA, which only depends on *t*, but doesn't depends on *x*, Eq. (7.16) can leads to:

$$\frac{\partial(U - \lambda C)}{\partial t} = D \frac{\partial^2(U - \lambda C)}{\partial x^2} \tag{7.53}$$

By defining *Z=U- λC*, the following equation is obtained:

$$\frac{\partial Z}{\partial t} = D \frac{\partial^2 Z}{\partial x^2} \tag{7.54}$$

Substituting $C = \dfrac{U - Z}{\lambda}$ to Eq. (7.12), the following equation is obtained (Tixier and Mobasher 2003; Tixier and Mobasher 2003):

$$\frac{\partial U}{\partial t} = D \frac{\partial^2 U}{\partial x^2} - \frac{kU^2}{\lambda} + \frac{kUZ}{\lambda} \tag{7.55}$$

with the initial condition,

$$U(\Omega, 0) = 0, \quad Z(\Omega, 0) = -\lambda C_0 \tag{7.56}$$

and the boundary conditions,

$$U(\Gamma, t) = U_0, \qquad Z(\Gamma, t) = U_0 \tag{7.57}$$

Eq. (7.19) can be solved for U using a numerical method with the value of Z obtained from the closed-form solution from Eq. (7.18) computed at each time and space increment.

7.1.5 DIFFUSION-REACTION MODELING BY EXPLICIT METHOD
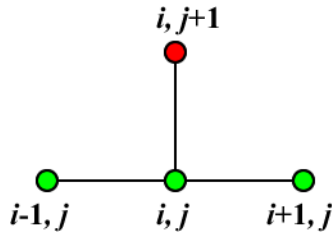
Figure 7.1. Rule of iteration upon explicit method

Using a forward difference at time t_j and a second-order central difference for the space derivative at position x_i, as shown in Figure 1, the explicit method (where i represents position and j time) transforms each component of the PDE (7.18) into the following:

$$\frac{\partial Z}{\partial t} = \frac{Z_{i,j+1} - Z_{i,j}}{\Delta t} \tag{7.58}$$

$$\frac{\partial^2 Z}{\partial x^2} = \frac{Z_{i+1,j} - 2Z_{i,j} + Z_{i-1,j}}{(\Delta x)^2} \tag{7.59}$$

The recurrence equation of the PDE (7.18) can be obtained:

$$\frac{Z_{i,j+1} - Z_{i,j}}{\Delta t} = D \frac{Z_{i+1,j} - 2Z_{i,j} + Z_{i-1,j}}{(\Delta x)^2} \tag{7.60}$$

$Z_{i,j+1}$ can be obtain from the other values this way:

$$Z_{i,j+1} = \frac{D\Delta t}{(\Delta x)^2} Z_{i+1,j} + \left[1 - \frac{2D\Delta t}{(\Delta x)^2}\right] Z_{i,j} + \frac{D\Delta t}{(\Delta x)^2} Z_{i-1,j} \qquad (7.61)$$

The explicit method transforms each component of the PDE (7.19) into the following:

$$\frac{\partial U}{\partial t} = \frac{U_{i,j+1} - U_{i,j}}{\Delta t} \qquad (7.62)$$

$$\frac{\partial^2 U}{\partial x^2} = \frac{U_{i+1,j} - 2U_{i,j} + U_{i-1,j}}{(\Delta x)^2} \qquad (7.63)$$

$$U = U_{i,j}; \qquad\qquad Z = Z_{i,j} \qquad (7.64)$$

The recurrence equation of the PDE (7.19) can be obtained:

$$\frac{U_{i,j+1} - U_{i,j}}{\Delta t} = D\frac{U_{i+1,j} - 2U_{i,j} + U_{i-1,j}}{(\Delta x)^2} - \frac{k}{\lambda} U_{i,j}^2 + \frac{k}{\lambda} U_{i,j} Z_{i,j} \qquad (7.65)$$

$U_{i,j+1}$ can be obtain from the other values this way:

$$U_{i,j+1} = \frac{D\Delta t}{(\Delta x)^2} U_{i+1,j} + \left[1 - \frac{2D\Delta t}{(\Delta x)^2} - \frac{k\Delta t}{\lambda} U_{i,j} + \frac{k\Delta t}{\lambda} Z_{i,j}\right] U_{i,j} + \frac{D\Delta t}{(\Delta x)^2} U_{i-1,j} \quad (7.66)$$

According to the initial condition, when $j=0$,

$$U_{i,0} = 0, \quad Z_{i,0} = -\lambda C_0 \qquad (7.67)$$

According to the boundary condition, when $i=0$ and $i=2n$

$$U_{0,j} = U_0, \; U_{2n,j} = U_0, \; Z_{0,j} = U_0, \; Z_{2n,j} = U_0 \tag{7.68}$$

According to the symmetry of the model:

$$U_{n-1,j} = U_{n+1,j}, \qquad Z_{n-1,j} = Z_{n+1,j} \tag{7.69}$$

According to Eq. (7.31), (7.32) and (7.33), Eq. (7.25) can be list as following,

$$Z_{1,1} = \frac{D\Delta t}{(\Delta x)^2} Z_{2,0} + \left[1 - \frac{2D\Delta t}{(\Delta x)^2} \right] Z_{1,0} + \frac{D\Delta t}{(\Delta x)^2} Z_{0,0} = \left[\frac{D\Delta t}{(\Delta x)^2} - 1 \right] \lambda C_0 + \frac{D\Delta t}{(\Delta x)^2} U_0 \tag{7.70}$$

$$Z_{i,1} = \frac{D\Delta t}{(\Delta x)^2} Z_{i+1,0} + \left[1 - \frac{2D\Delta t}{(\Delta x)^2} \right] Z_{i,0} + \frac{D\Delta t}{(\Delta x)^2} Z_{i-1,0} = -\lambda C_0 \qquad \text{(for } i>1\text{)} \tag{7.71}$$

$$Z_{1,j+1} = \frac{D\Delta t}{(\Delta x)^2} Z_{2,j} + \left[1 - \frac{2D\Delta t}{(\Delta x)^2} \right] Z_{1,j} + \frac{D\Delta t}{(\Delta x)^2} Z_{0,j} = \frac{D\Delta t}{(\Delta x)^2} Z_{2,j} + \left[1 - \frac{2D\Delta t}{(\Delta x)^2} \right] Z_{1,j} + \frac{D\Delta t}{(\Delta x)^2} U_0 \tag{7.72}$$

$$Z_{i,j+1} = \frac{D\Delta t}{(\Delta x)^2} Z_{i+1,j} + \left[1 - \frac{2D\Delta t}{(\Delta x)^2} \right] Z_{i,j} + \frac{D\Delta t}{(\Delta x)^2} Z_{i-1,j} \qquad \text{(for } n>i>1\text{)} \tag{7.73}$$

$$Z_{n,j+1} = \frac{D\Delta t}{(\Delta x)^2} Z_{n+1,j} + \left[1 - \frac{2D\Delta t}{(\Delta x)^2} \right] Z_{n,j} + \frac{D\Delta t}{(\Delta x)^2} Z_{n-1,j} = \left[1 - \frac{2D\Delta t}{(\Delta x)^2} \right] Z_{n,j} + \frac{2D\Delta t}{(\Delta x)^2} Z_{n-1,j} \tag{7.74}$$

According to Eq. (31), (32) and (33), Eq. (30) can be list as following:

$$U_{1,1} = \frac{D\Delta t}{(\Delta x)^2} U_{2,0} + \left[1 - \frac{2D\Delta t}{(\Delta x)^2} - \frac{k\Delta t}{\lambda} U_{1,0} + \frac{k\Delta t}{\lambda} Z_{1,0} \right] U_{1,0} + \frac{D\Delta t}{(\Delta x)^2} U_{0,0} = \frac{D\Delta t}{(\Delta x)^2} U_0 \tag{7.75}$$

$$U_{i,1} = \frac{D\Delta t}{(\Delta x)^2} U_{i+1,0} + \left[1 - \frac{2D\Delta t}{(\Delta x)^2} - \frac{k\Delta t}{\lambda} U_{i,0} + \frac{k\Delta t}{\lambda} Z_{i,0} \right] U_{i,0} + \frac{D\Delta t}{(\Delta x)^2} U_{i-1,0} = 0 \qquad \text{(for } i>1\text{)}$$

(7.76)

$$U_{1,j+1} = \frac{D\Delta t}{(\Delta x)^2} U_{2,j} + \left[1 - \frac{2D\Delta t}{(\Delta x)^2} - \frac{k\Delta t}{\lambda} U_{1,j} + \frac{k\Delta t}{\lambda} Z_{1,j} \right] U_{1,j} + \frac{D\Delta t}{(\Delta x)^2} U_{0,j}$$

$$= \frac{D\Delta t}{(\Delta x)^2} U_{2,j} + \left[1 - \frac{2D\Delta t}{(\Delta x)^2} - \frac{k\Delta t}{\lambda} U_{1,j} + \frac{k\Delta t}{\lambda} Z_{1,j} \right] U_{1,j} + \frac{D\Delta t}{(\Delta x)^2} U_0$$

(7.77)

$$U_{i,j+1} = \frac{D\Delta t}{(\Delta x)^2} U_{i+1,j} + \left[1 - \frac{2D\Delta t}{(\Delta x)^2} - \frac{k\Delta t}{\lambda} U_{i,j} + \frac{k\Delta t}{\lambda} Z_{i,j} \right] U_{i,j} + \frac{D\Delta t}{(\Delta x)^2} U_{i-1,j} \qquad \text{(for } i>1\text{)} \quad (7.78)$$

$$U_{n,j+1} = \frac{D\Delta t}{(\Delta x)^2} U_{n+1,j} + \left[1 - \frac{2D\Delta t}{(\Delta x)^2} - \frac{k\Delta t}{\lambda} U_{n,j} + \frac{k\Delta t}{\lambda} Z_{n,j} \right] U_{n,j} + \frac{D\Delta t}{(\Delta x)^2} U_{n-1,j}$$

$$= \left[1 - \frac{2D\Delta t}{(\Delta x)^2} - \frac{k\Delta t}{\lambda} U_{n,j} + \frac{k\Delta t}{\lambda} Z_{n,j} \right] U_{n,j} + \frac{2D\Delta t}{(\Delta x)^2} U_{n-1,j}$$

(7.79)

So, with this recurrence relation, and knowing the values at time j, one can obtain the corresponding values at time $j+1$. So Z and sulfate concentration U in field can be computed by Eq. (7.34) to (7.38) and Eq. (7.39) to (7.43) respectively. Then, according to $C = \frac{U - Z}{\lambda}$, calcium aluminate concentration C is obtained from normalization constants.

However, this explicit method is known to be numerically stable when the convergence condition is satisfied and the numerical errors are proportional to the time step Δt and the square of the space step $(\Delta x)^2$.
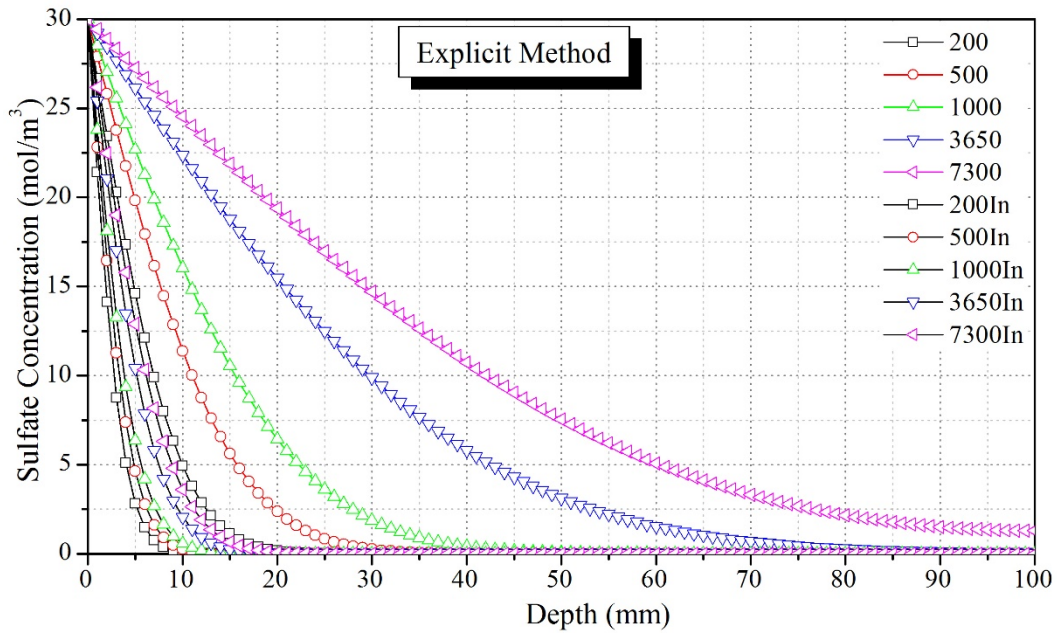
Figure 7.2. Sulfate concentration with or without chemical reactions through explicit method

Referring to the example settings in the non-reaction diffusion of C=30 mol/m^3, D=1.5×10^{-12} m^2/s , and the defined C$_3$A content of C$_0$=100 mol/m^3 in the initial cement, the profiles of sulfate concentration after chemical consumption were plotted in comparison with non-reaction diffusion profiles as shown in Figure 7.2.

Note that with high C$_3$A content and preliminarily defined λ value of 2.8, the residual sulfate concentration after 12-week exposure was even lower than the concentration after 1-week exposure upon physical diffusion. It is concluded presently that the chemical consumption of sulfate ingress from external was significant with high C$_3$A content.

7.2 RESULTS OF DIFFUSION-REACTION BEHAVIOR

7.2.1 MODELING PROCEDURE

The present sulfate modeling work was fulfilled using the MATLAB based on the finite difference method. The cement-based composites were exposed to external sulfate ion from two opposite surfaces and defined as one dimensional diffusion. To fully understand the sulfate attack behavior in the Portland cement-based composites, the following different cases have been studied:

In accordance with the result comparison and error discussion studied in the last chapter, the space increment was chosen of 1 mm while the time interment of 1day in the diffusion-reaction model. The distributions of sulfate concentration and production of ettringite were calculated by explicit method and Crank–Nicolson method based on finite difference theory.

- **Case 1.** The sulfate concentration in environment U_0 in the different model ranged from 30 mol/m^3 to 300 mol/m^3 for analyzing the effects of the conditions of the environment on the distribution of sulfate concentration of material.

- **Case 2.** The diffusion coefficient of sulfate in material D in the different model ranged from 1.0×10^{-12} m^2/s to 16.0×10^{-12} for analyzing the effects of the compactness of cement-based material on the sulfate resistance of material.

- **Case 3.** The initial concentration of CA C_0 in the different model ranged from 30 mol/m^3 to 150 mol/m^3 for analyzing the effects of the content of calcium aluminates CA on the sulfate resistance of material.

- **Case 4.** The rate constant k of the chemical reaction between reacting calcium aluminates and sulfate ingress in the different model ranged from 1.0×10^{-11} mol/m^3·s

$(8.64 \times 10^{-7}$ mol/m^3·d) to 1.0×10^{-7} mol/m^3·s $(8.64 \times 10^{-3}$ mol/m^3·d) for analyzing the effects of the rate constant of the chemical reaction on the sulfate resistance of material.

■ **Case 5.** The weighted average stoichiometric coefficient of the lumped reaction for C$\bar{S}$H$_2$ λ in the different model ranged from 2 to 3 for analyzing the effects of the content of calcium aluminate monosulfate C$_4$A$\bar{S}$H$_{12}$ in material on the distribution of sulfate concentration of material.

With the development of diffusion-reaction modeling, the sulfate concentration profiles involved with chemical reactions were retrieved as well as the ettringite production. Several featured parameters in the numerical modeling were separately analyzed in order to decide which one governed the sulfate attack process.

7.2.2 SULFATE CONCENTRATION AND ETTRINGITE PRODUCTION

Sulfate concentration and ettringite production, defined as featured compounds in the sulfate attack processing, were chosen as indicators as affected by the above parameters.

The production of ettringite was studied as the main reason that resulted in volumetric expansion and attendant cracking. Moreover, the production of ettringite and C$_3$A residual content were two governing compounds when calculating the strain change in the next stage of numerical modeling.

7.2.3 EXTERNAL SULFATE CONCENTRATION U_0
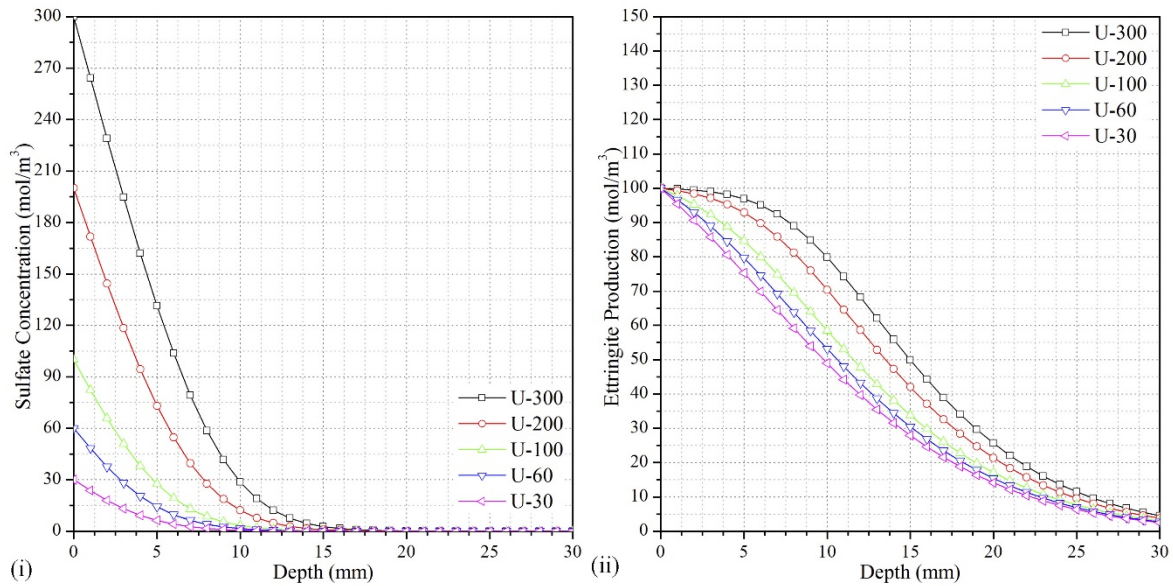
Figure 7.3. Sulfate concentration (i) and Ettringite production (ii) as affected by U_0 after 500-day exposure
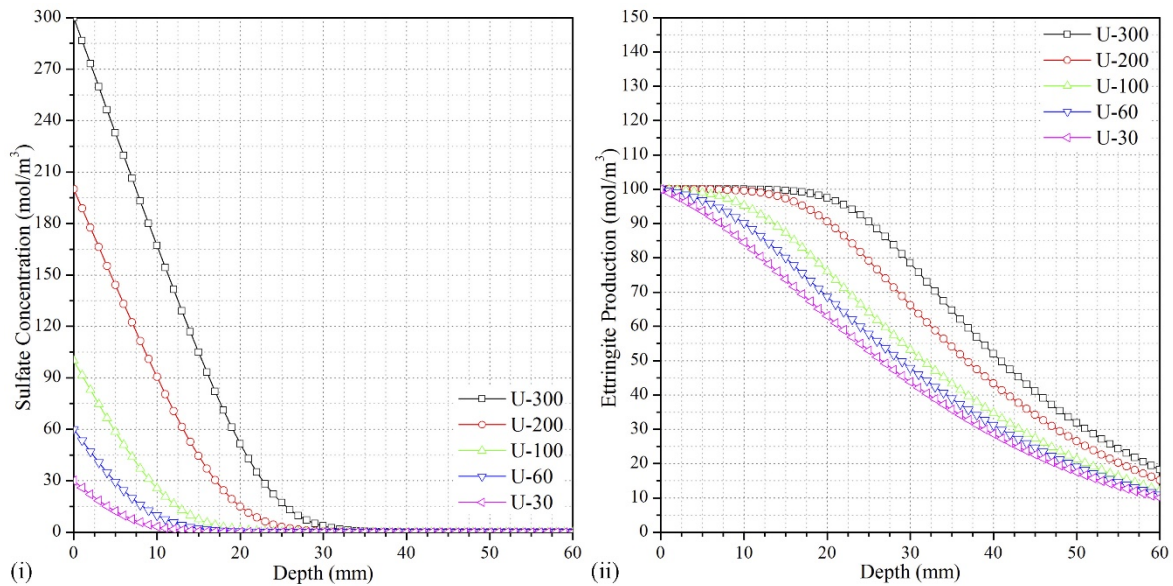
Figure 7.4. Sulfate concentration (i) and Ettringite production (ii) as affected by U_0 after 10-year exposure

As presented in Figure 7.3 and Figure 7.4, it is to be noted that the variation of external sulfate concentration had pronounced effect to the sulfate diffusion inside cement-based composite whereas had limited effect to the ettringite production within 10-year of sulfate exposure.

7.2.4 INHERENT C$_3$A CONTENT C_0
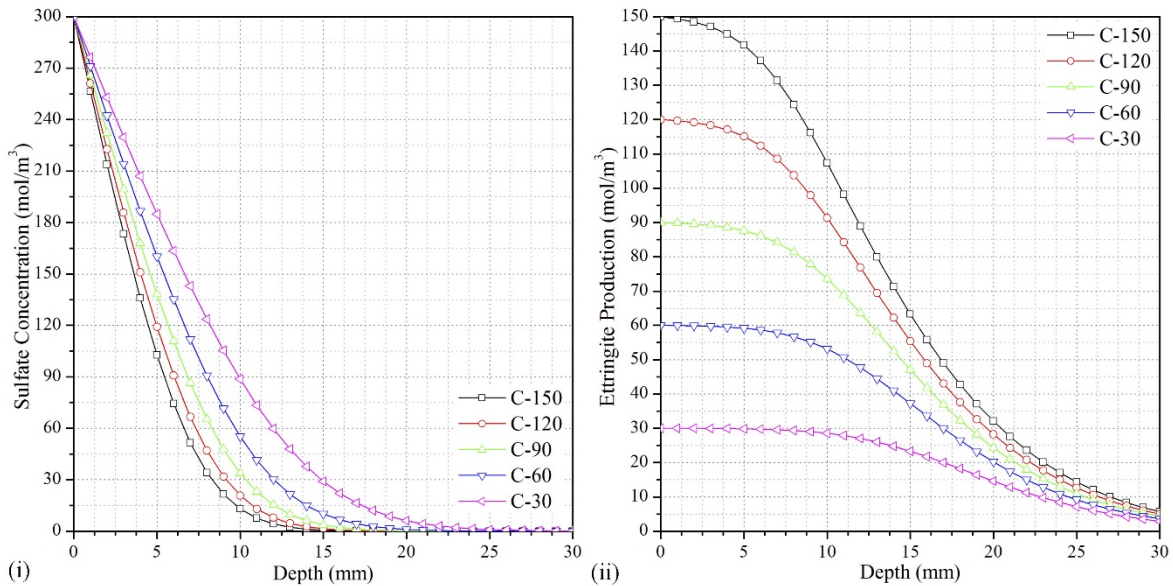
Figure 7.5. Sulfate concentration (i) and Ettringite production (ii) as affected by C_0 after 500-day exposure
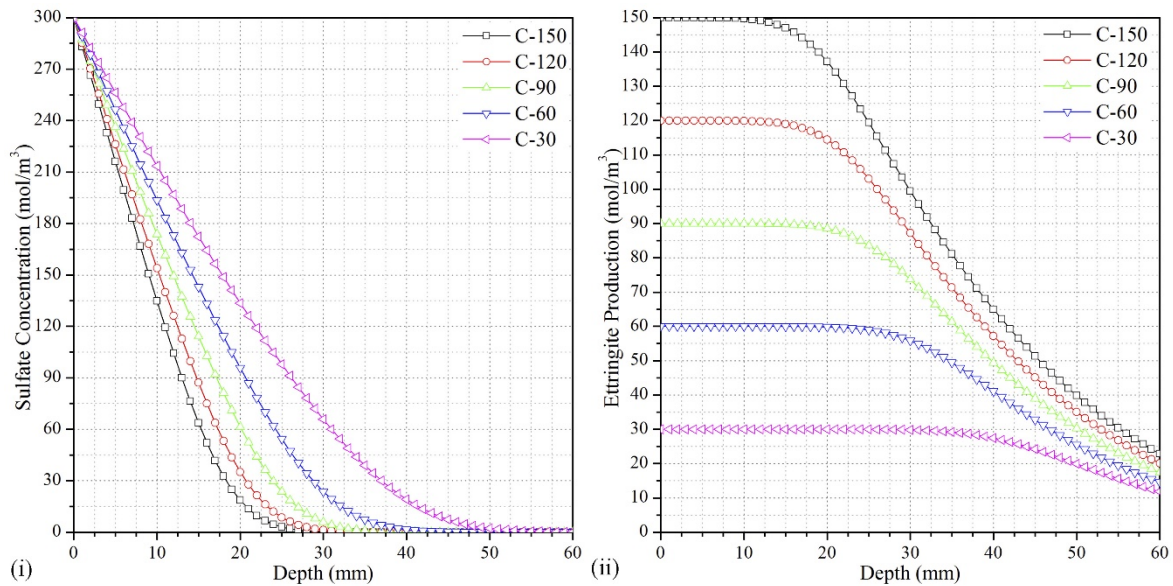
Figure 7.6. Sulfate concentration (i) and Ettringite production (ii) as affected by C_0 after 10-year exposure

One can see that, in Figure 7.5 and Figure 7.6, the variation of C$_3$A content in initial cement had enormous influence to the ettringite production in comparison with the effect to sulfate concentration inside the material. That is, the initial content of C$_3$A governed the potential ettringite production that resulted in attendant expansion in volume.

7.2.5 DIFFUSION COEFFICIENT D
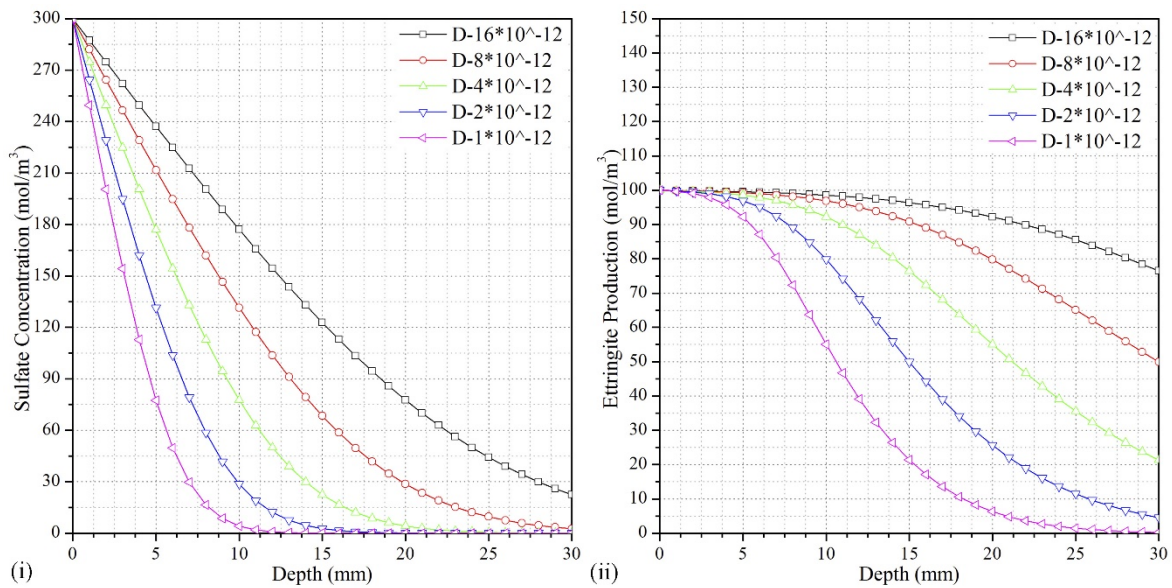
Figure 7.7. Sulfate concentration (i) and Ettringite production (ii) as affected by *D* after 500-day exposure
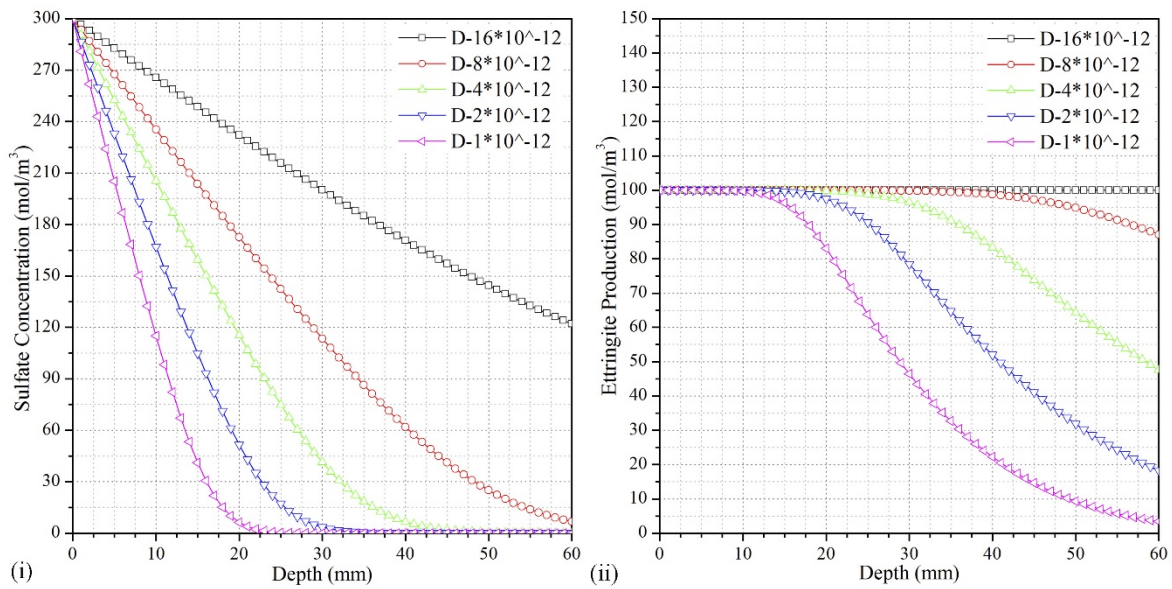
Figure 7.8. Sulfate concentration (i) and Ettringite production (ii) as affected by *D* after 10-year exposure

Diffusion coefficient of *D*, defined as the parameter that represented the capacity of physical diffusion, showed great influence to sulfate concentration as shown in Figure 7.7 and Figure 7.8. In addition, the increase of *D* did not change the maximum ettringite production but resulted in much deeper ettringite production.

7.2.6 Reaction Constant K
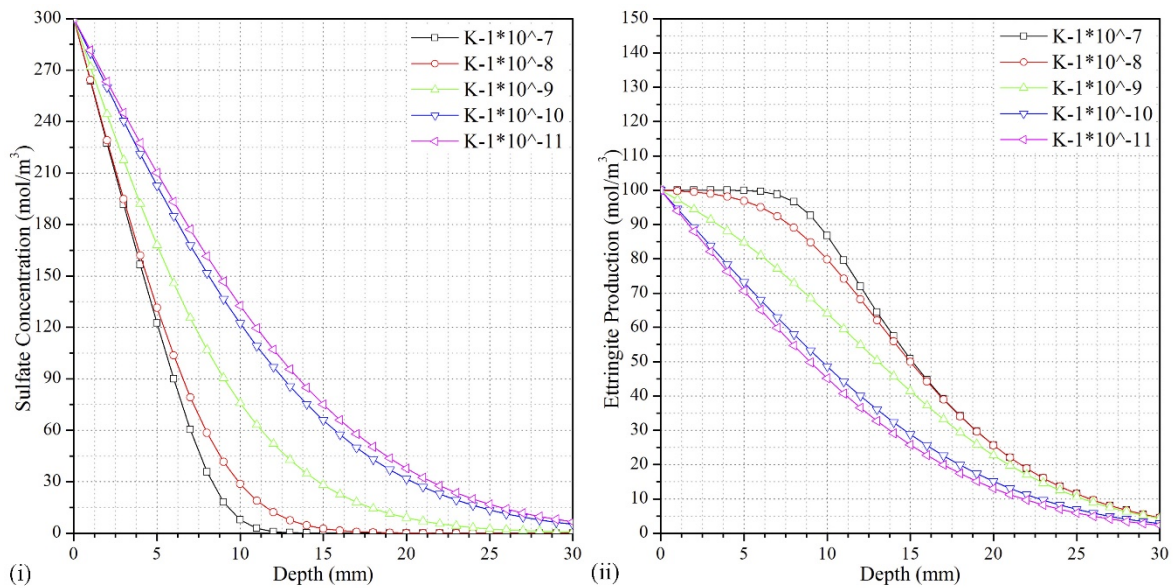
Figure 7.9. Sulfate concentration (i) and Ettringite production (ii) as affected by K after 500-day exposure
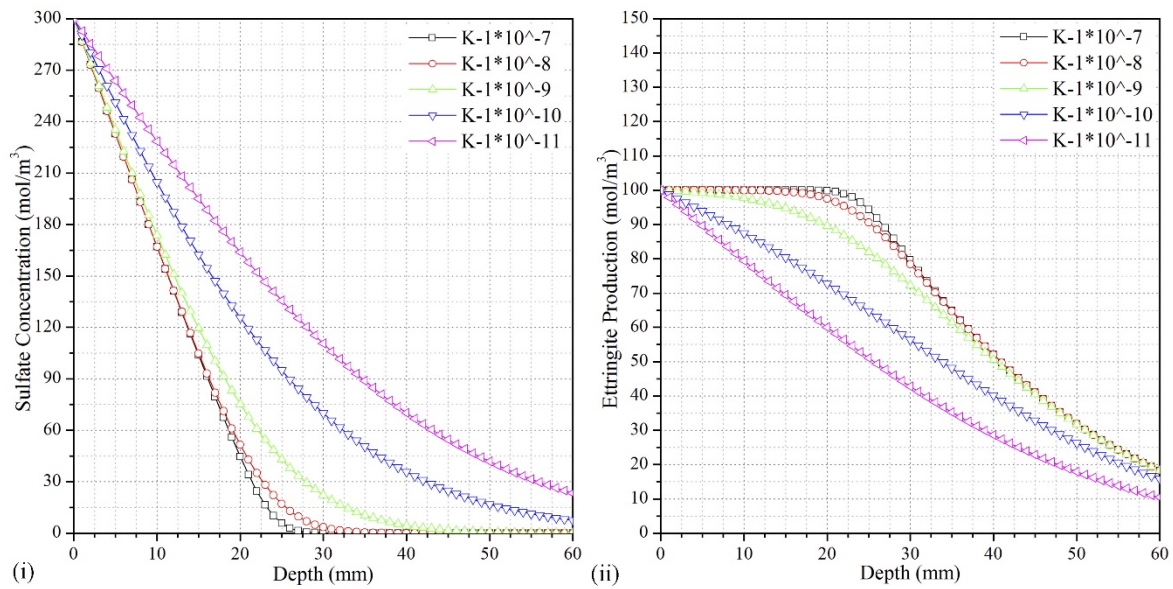
Figure 7.10. Sulfate concentration (i) and Ettringite production (ii) as affected by K after 10-year exposure

The value of reaction rate k was constant during reactions in this study. However, the effect caused by variation of k was investigated and presented in Figure 7.9 and Figure 7.10. The influence witnessed was not as significant as that caused by D, U_0 and C_0.

7.2.7 REACTION PROPORTIONAL COEFFICIENT λ
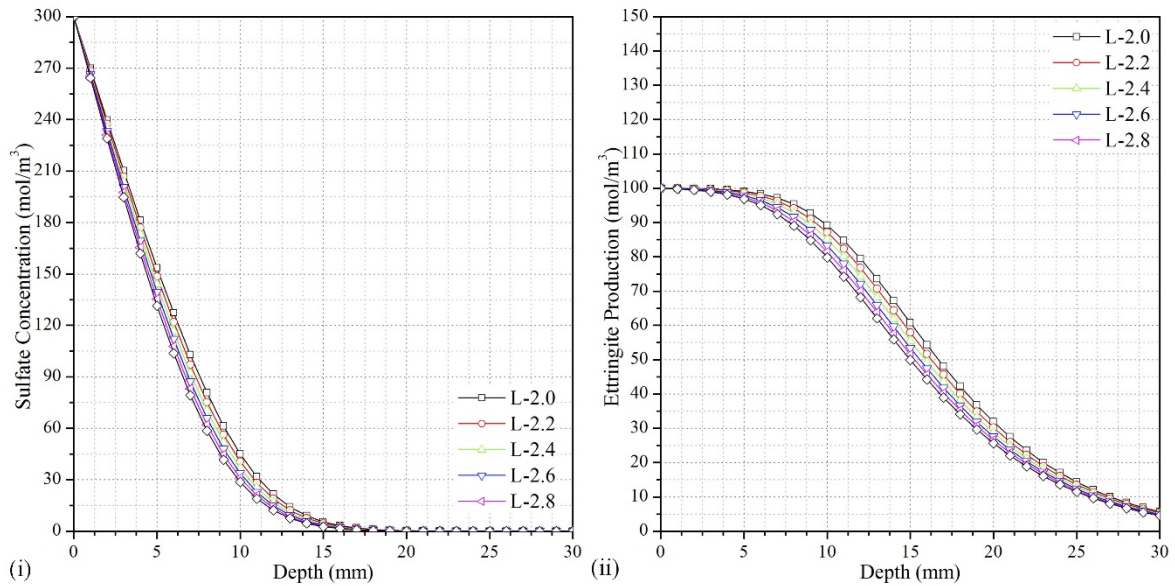
Figure 7.11. Sulfate concentration (i) and Ettringite production (ii) as affected by λ after 500-day exposure
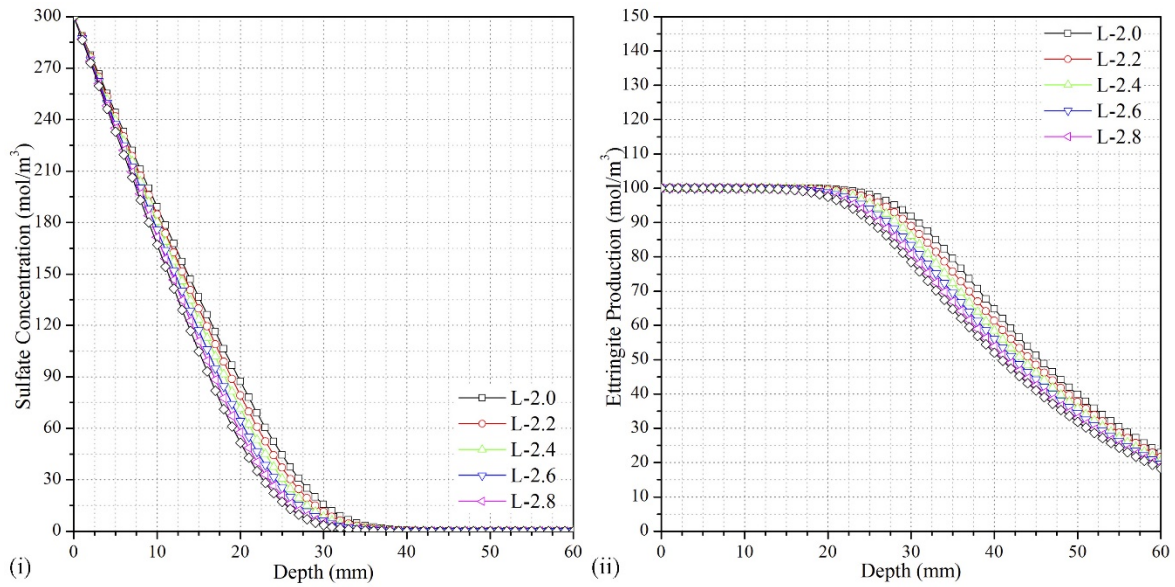
Figure 7.12. Sulfate concentration (i) and Ettringite production (ii) as affected by λ after 10-year exposure

The reaction proportional coefficient λ was introduced in the numerical modeling that determine the ratio of three possible reactions as listed in Eq. (7.5, 7.6, and 7.7).

It is to be noted that, the reaction proportional coefficient that represents the degree of three sulfate attack reactions, had little effect on the sulfate concentration and ettringite production as shown in Figure 7.11 and Figure 7.12. There was no significant difference between λ value between 2.0 to 3.0 after 500-day exposure and 10-year exposure to sulfate attack.

It was investigated that the value of λ *did not* govern the amount, nor the depth of Ettringite production during sulfate attack. It is likely that each reaction listed in Eq. (5, 6 and 7) was expansive due to the productions. Detailed study in the coefficient k was investigated in the collaboration research of strain-stress response and service life production.

In conclusion, the diffusion coefficient D and the inherent C_3A content, were examined to show greater effects to the ettringite production in cement-based composites in comparison with the variation of external sulfate concentration *U,* reaction rate *k* and the reaction proportional coefficient λ. Particularly, the diffusion coefficient *D* affected the ettringite production in depth whereas the C_3A content affected the ettringite production in amount.

7.3   DATA FITTING OF EXPERIMENTAL RESULTS

7.3.1 COMPOSITIONS OF EXAMINED CEMENTS AND ENVIRONMENT

In this research program aimed to simulating sulfate diffusion, three types of binder were investigated for their sulfate concentrations inside specimen after 1, 2, 4, 8 and 12 weeks of sulfate exposure. Besides, the compositions in the initial binders were provided by the material supplier.

External Sulfate Concentration. In according with the numerical model studied by Tixier R, Mobasher B (Tixier and Mobasher 2003) for sulfate attack simulation, theoritically, the sulfate concentration on the exposure surface was equal to the sulfate concentration in external environment. However, in the numerical simulation of chloride diffusion studied by Chalee W (Chalee et al. 2009), it was recognized that the boundary concetraiton in diffusion process was lower than the constant concentration in the environment. In this manner, when fitting experimental sulfate results to the numerical simulation, the boundary concentration was supposed to be adjustable below external sulfate concentration considering the short-term sulfate expouse employed in this study.

Tricalcium aluminate (C_3A) Content. As analyzed above, the content of tricalcium aluminate (C_3A) governed the maximum ettringite production during sulfate exposure. However, same amount of ettringite formation might not lead to same volumetric expansion affected by the initial gypsum content, which was studied in the collaboration research program. According to the mill test certificates for CSA Portland cement type GU and HS, C_3A contents in commercial sourced cements were available. As for the blend IC with 30% fly ash replacement of Type GU cement, C_3A content was calculated of 70% from the Type GU cement.

Inherent Gypsum Content. The initial gypsum in the binder was provided by the material supplier. Based on the collaborated program with Dr. Chen Zheng, with the same C_3A content in binder, the initial gypsum content affected the proportion of reactions listed in Eq. (7.5, 7.6 and 7.7) and was manifested as the variation of λ in the model. In addition, it was recognized by Tian B, Cohen MD that the formation of gupsum under sulfate attack may cause expanison in volume (Tian and Cohen 2000). However, above findings were not

considered in this numerical model. Moreover, it was witnessed from the titrating results that the initial gypsum might not be consumed during hydration.

7.3.2 THE PARAMETERS IN THE NUMERICAL MODEL

The Diffusion Coefficient D. Based on the Fick's second law that explains the diffusion process, the diffusion coefficient was introduced to represent the resistance to ion diffusion of cement-based material. The diffusion coefficient was affected by complicated factors including density, porosity, and air-void network. It is hardly quantify the value of D and there is no existing literatures explaining the relationship between cement-based compositions and diffusion coefficient.

The main purpose of data fitting between modeling profiles and experimental results was to determine the diffusion coefficient D upon varied cement-based composites. For the same material used, the diffusion coefficient was unaltered as affected by external sulfate and exposure duration.

The Reaction Proportional Coefficient λ. As discussed above, the variation of reaction proportional coefficient λ from 2.0 to 3.0 had very little effect to the sulfate concentration as well as the ettringite production. Preliminarily, the λ was chosen of 2.5 for all examined binders and revision on coefficient λ was required after data fitting.

7.3.3 DETERMINATION OF PARAMETERS IN NUMERICAL MODELING
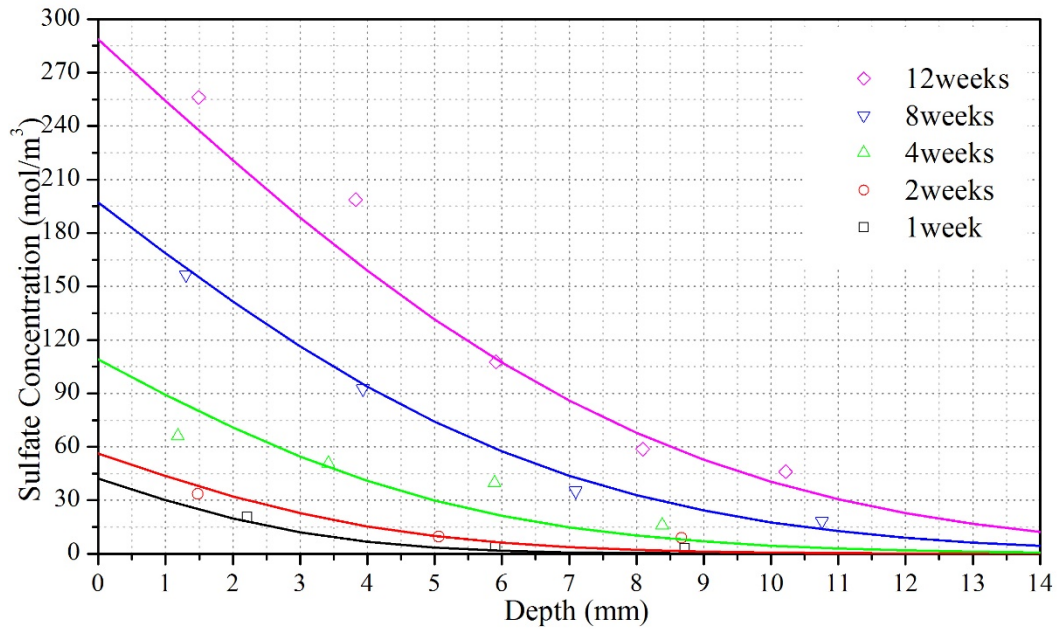
Figure 7.13. Data fitting of experimental results to the modeling (IC blend)
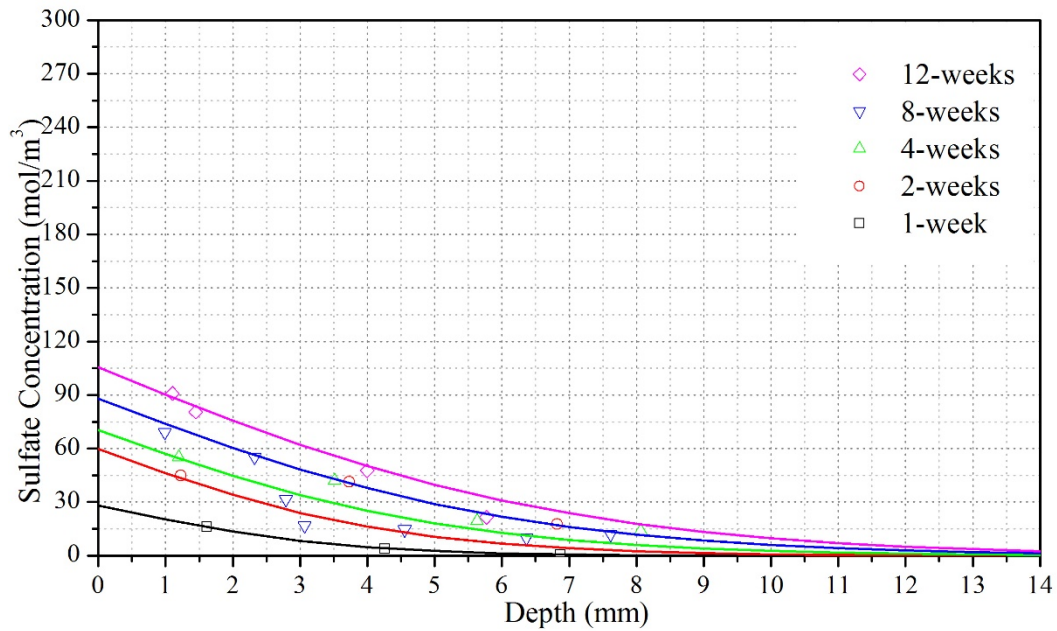
Figure 7.14. Data fitting of experimental results to the modeling (Type GU)
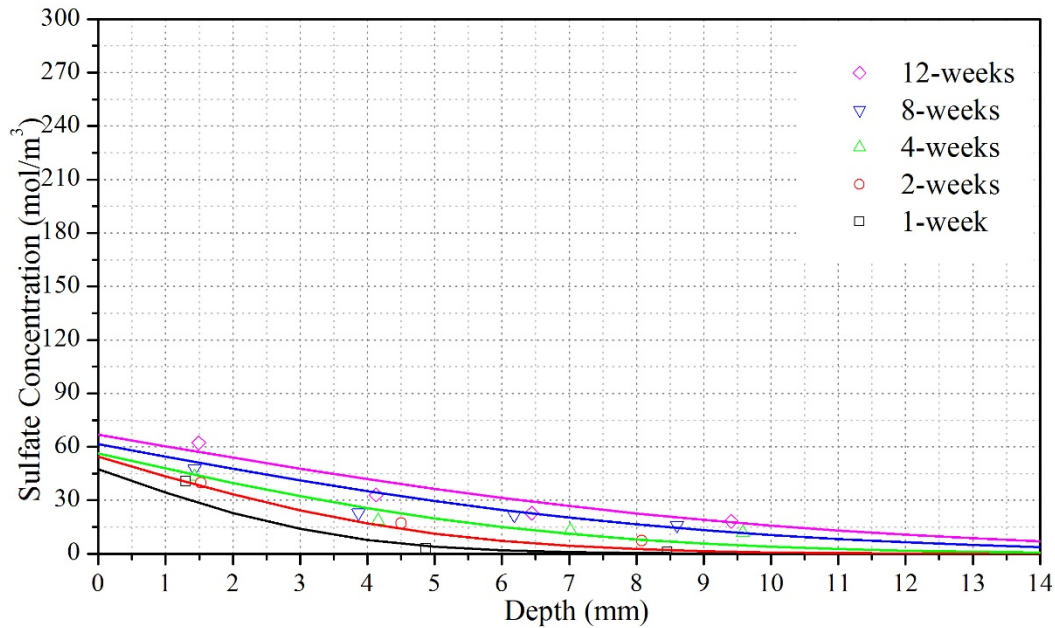
Figure 7.15. Data fitting of the experimental results to the modeling (Type HS)

Table 7.1. Initial chemical compositions and parameters after data fitting

	C_3A	SO_3	D	K	λ
	% by mass	% by mass	m^2/s	m^2/s	N/A
Type GU	6.177	2.714	9.00E-12	1.00E-08	2.5
Blend IC	4.324	2.218	8.50E-12	1.00E-08	2.5
Type HS	0.808	1.9	7.00E-12	1.00E-08	3

Table 7.2. Boundary concentrations determined after data fitting (mol/m^3)

	1-week	**2-week**	**4-week**	**8-week**	**12-week**
Type GU	28.16901	59.85915	70.42254	88.02817	105.6338
Blend IC	42.25352	56.33803	109.1549	197.1831	288.7324
Type HS	49.29577	52.11268	54.57746	58.4507	66.90141

Based on the sulfate concentrations obtained from titration experiment, numerical model was fitted to determine the parameters for each type binder examined as shown from Figure 7.13 to Figure 7.15. As listed in Table 7.1, the reaction rate k was constant for all type binders because same kinds of chemical reactions took place under sulfate attack. λ for Type GU and

blend IC was the same since the SO_3/C_3A ratios were the same of both binders. Type HS cement of the lowest C_3A content was mostly subjected to external sulfate attack as per Eq. (7) so that the value of λ was chosen of 3.0. It was recognized by the author that, the matched diffusion coefficients D for three binders were close as shown in Table 7.1. One can see that, in Table 7.2, the resistance of cement-based composites to sulfate diffusion was manifested as the variation of boundary concentration after varying exposure durations.

7.3.4 ETTRINGITE PRODUCTION AND C_3A CONCENTRATION

After the experimental data had been fitted to the numerical modeling, all the parameters were determined corresponding to three examined cement binders. Therefore, the C_3A concentration and ettringite production were calculated with these parameters. Note that the threshold of ettringite production was dependent on the initial C_3A content in the binder, which was presented in following figures.
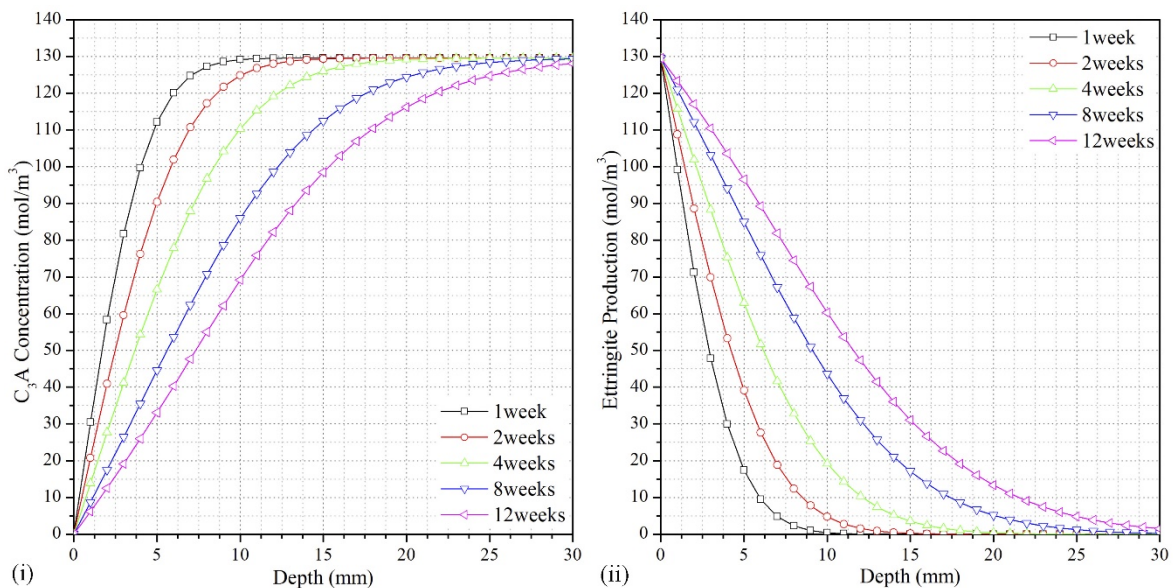
Figure 7.16. Ettringite production (i) and C3A residual (ii) after 12-week exposure (Type GU)

Type GU cement, containing the maximum C_3A content among the three tested binders, was investigated to have the maximum potential ettringite production as shown in Figure 7.16. It was corroborated with the diffusion-reaction behavior demonstrated at the outset.
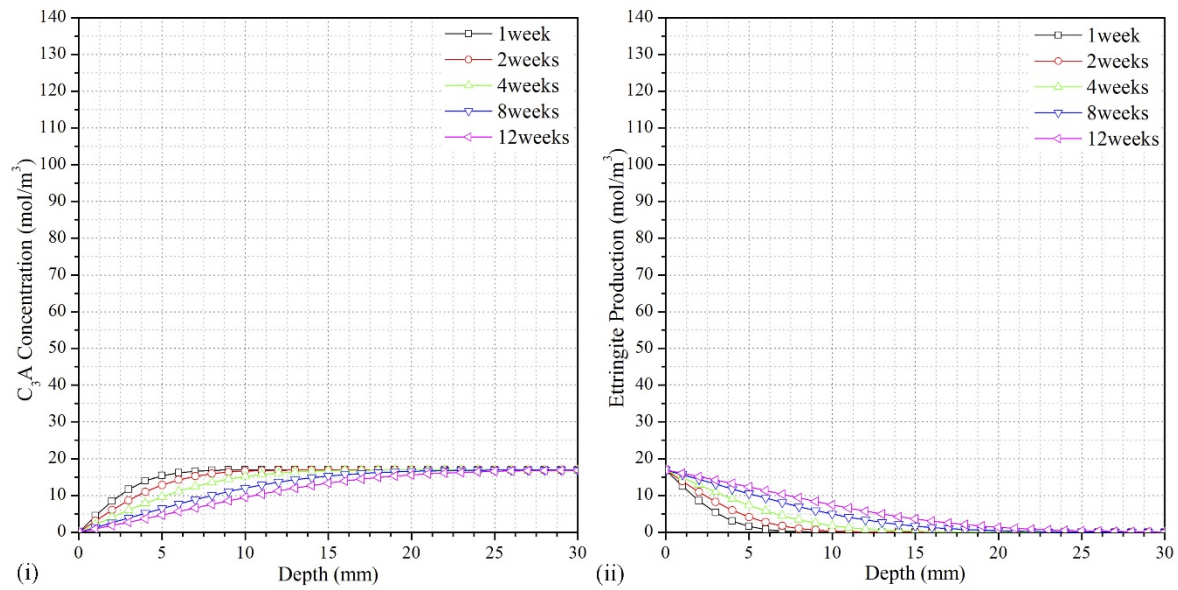
Figure 7.17. Ettringite production (i) and C3A residual (ii) after 12-week exposure (Type HS)
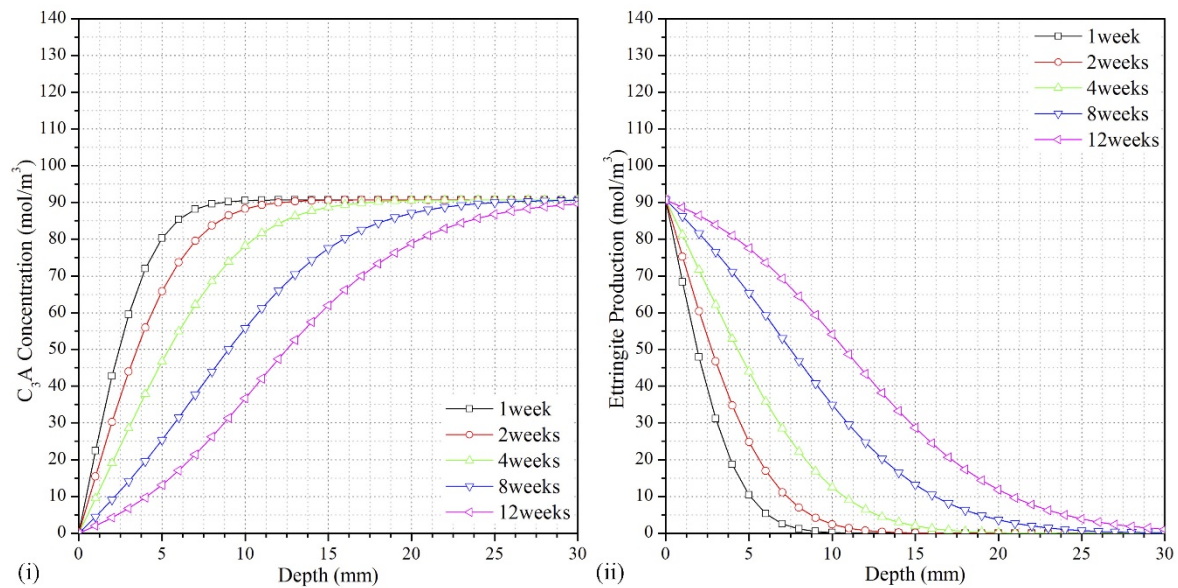
Figure 7.18. Ettringite production (i) and C3A residual (ii) after 12-week exposure (Blend IC)

It was seen in Figure 7.17 and Figure 7.18 that, the maximum ettringite production depended on the inherent C_3A content in the binder. Type HS cement containing extreme low C_3A content presented very limited ettringite production, which made this cement of excellent resistance to external sulfate attack. Blend IC had the potential to produce 70% of the ettringite of Type GU cement theoretically, while it might not be the governing factor that resulted in the worse resistance of blend IC binder.

7.4   REVISIONS ON BASIC POSTULATION

According to the experimental results of sulfate concentration obtained in the titration experiment, several settings in current modeling were supposed to be revised. In reality, the sulfate diffusion inside specimen was not as same as the sulfate profiles theoretically simulated by finite difference methods (FDM).

7.4.1 REVISION ON BOUNDARY CONCENTRATION

Firstly, it was recognized by the author that the sulfate concentration at the specimen edge was supposed to be revised in order to fit experimental sulfate concentration.

From the experimental results retrieved, the boundary concentration was markedly lower than the concentration in the external environment. It was likely that, because of the short-term exposure or better resistance of matrix, the boundary concentration might not reach the concentration in environment. With the increase of exposure duration, the boundary concentration got closer to the external sulfate concentration whereas the rate of increment varied by cement-based composites. In this study, the maximum boundary concentration upon IC blend matrix after 12-week exposure was simulated to 288 mol/m^3 that was still lower than the external sulfate concentration of 352 mol/m^3. The boundary concentrations of Type GU and HS matrixes were significantly lower than the external sulfate concentration.

It had been studied by researchers (Chalee et al. 2009) that the boundary/surface concentration of ion diffusion was dependent on the exposure duration and water-to-cement ratio whereas it was not related to the effect caused by mineral admixtures such as fly ash. Accordingly, the concentration adjustment in literature was not applicable to fit the boundary concentrations simulated in this study. A new ratio of U-Boundary/U_0 was introduced to describe the variations of boundary concentration upon varied cement-based composites.
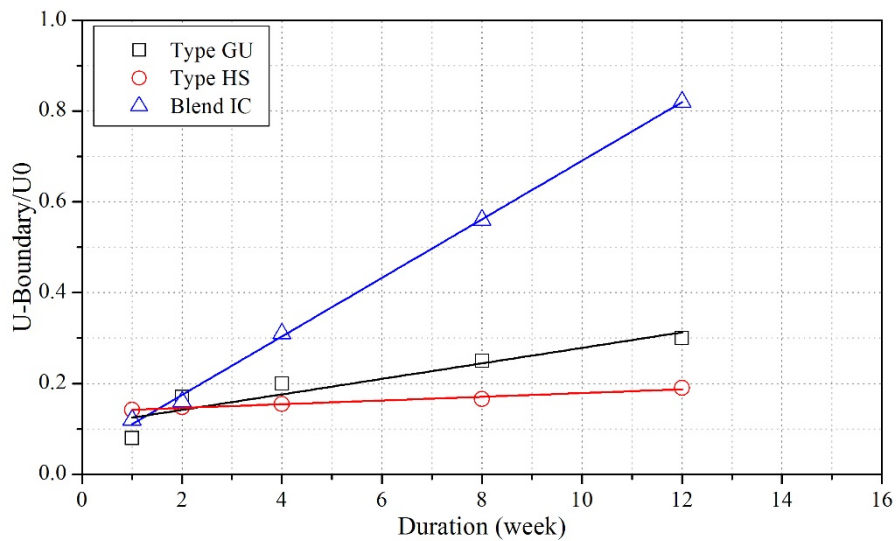
Figure 7.19. U-Boundary/U_0 ratio as affected by exposure duration

As shown in Figure 7.19, it was recognized that within relatively short-term sulfate exposure of 12 week, all three examined binders were investigated not reaching the external sulfate concentration at surface. Considering further numerical modeling aimed to predict service life of cement-based composites, it was suggested in this study that the concentration at the surface were likely to approach the external concentration after 1 year sulfate exposure compared with the short-term (0.23 year) employed in this work.

7.4.2 REVISION ON INHERENT GYPSUM CONTENT

In accordance with the sulfate concentrations retrieved from titration experiments, it was worth noting that the minimum sulfate concentration detected in cement-based composites was not close to 0 at the maximum depth over 10 mm after only 1 week of sulfate exposure. However, it was simulated through model that external sulfate was not able to infiltrate to 10 mm after 1-week exposure. It is likely that the inherent gypsum in cement was not consumed when specimen started to be exposed to sulfate environment.

Revision on the baseline of experimental results was that the deepest sulfate concentration after the shortest exposure duration was regarded as zero, hence the model was employed to fit the experimental results upon this revision.

7.5 CURRENT FINDINGS

7.5.1 MODEL-BASED FINDINGS

The diffusion coefficient D and the inherent C_3A content, were examined to show greater effects to the ettringite production in cement-based composites in comparison with the variation of external sulfate concentration U, reaction rate k and the reaction proportional coefficient λ. Particularly, the diffusion coefficient D affected the ettringite production in depth whereas the C_3A content affected the ettringite production in amount.

From the numerical model fitted, it was concluded that, when subjected to external sulfate attack, Type GU cement was likely to form the maximum ettringite production whereas Type HS produced the minimum ettringite due to the lowest C_3A content in the cement. However, Blend IC specimen was detected of the maximum sulfate concentration in comparison with other two cement specimens, which means that the Blend IC specimen is the most permeable to sulfate diffusion when subjected to external sulfate attack.

In addition, theoretical numerical model was supposed to be revised upon boundary concentration and other parameters in the model. It was proposed in this study that external sulfate was more likely to diffuse in depth rather than concentration accumulation near the specimen surface.

7.5.2 EXPERIMENT-BASED FINDINGS

In accordance with the expansion results and air-void networks retrieved in chapter 2, the Blend IC prismatic specimens were measured to have the maximum expansion under adverse external sulfate attack. The effect of replacing ordinary Portland cement by fly ash admixture was also not pronounced from the results of sulfate concentration.

The reason why blend IC performed the highest sulfate concentration inside specimen was more related to air-void networks rather than the amount of ettringite production. The lower ettringite formation in Blend IC specimen, compared to Type GU specimen, still led to larger expansion since the air-void networks were more compact in Blend IC specimen owing to the "filling effect" of fly ash admixture. It is proposed in this program that the Blend IC specimen cracks at the beginning of sulfate exposure and more external sulfates diffuse into specimen for long-term exposure.

8 VISUAL ASSESSMENT ON SULFATE DIFFUSION BY IMAGE ANALYSIS

8.1 BACKGROUND AND INTRODUCTION

8.1.1 PROBLEMS ENCOUNTERED

Investigation on resistance to sulfate attack of cement-based composites has been studied for the recent decades. Previous researchers focused on the effect of sulfate ingress to the microstructure inside cement-based systems. Diffusion modeling was recently introduced to simulate the sulfate attack process considering chemical reactions in related literatures.

In addition, evaluation on the sulfate concentration inside specimen was developed by the author by means of titration experiment as demonstrated in previous chapters. The titration experiment developed has high precision in sulfate content determination but is time-consuming. Laboratory environment is also limited to evaluate sulfate ingress from the external. Novel and convenient assessment on sulfate diffusion in cement-based composites is needed in this case.

8.1.2 INSPIRATION

It was recognized by the author that the cross sections inside the cylindrical specimen showed similar color variations after exposure to external sulfate attack. The peripheral area of round cross section was witnessed of lighter color than that in the central area. A hypothesis is proposed that the lighter color near the edge was attributed to sulfate attack conforming to the sulfate diffusion direction from edge to center. It was inspired by similar analysis method that the sulfate ingress was perceptible and can be investigated through color analysis on captured images. Preliminarily, the objective of this image analysis method is to evaluate the resistance to sulfate attack through the measurement of lighter area within the cross section.

8.1.3 REVIEW OF THE EXPOSURE CONDITIONS AND CEMENT COMPOSITES

In this research program on resistance of cement-based composites to sulfate attack, three binders, CSA Type GU, HS cement and a blend of 30:70 of fly ash to Type GU cement, were examined for their resistance to adverse sulfate attack. Note that the available specimens for image analysis were cylinders of Φ 50 mm * 100 mm. All the cylindrical specimens were exposed to 5% Na_2SO_4 solution and taken out for image analysis after 1, 2, 4, 8 and 12 weeks exposure in comparison with the same cylinders submerged in water environment. The external sulfates infiltrated into the specimen from two directions, end side and broadside, and each cylinder was sliced to 5 pieces after exposure. Cross sections at the cutting surfaces were chosen for color variation analysis in this work.

8.1.4 OVERVIEW OF THE VISUAL ASSESSMENT METHOD

Because of the sensitivity of this visual assessment method, a brief chapter including the introduction and results is presented in this thesis. Detailed procedures and mechanisms is reported separately.

Visual assessment on sulfate diffusion was originally developed with the images captured of cross section. Two evaluation methods were introduced in order to identify the sulfate diffusion from external environment. The principle of these two methods depended on the color variation and contrast inside cement-based composites caused by diffused sodium sulfate when subjected to external sulfate attack.

Method-1. Area Ratio Method was designed to calculate the amount of pixels within two areas: one was the whole area of cross section; the other was the undiffused area that was identified by the color variation. The diffusion depth was then obtained with the size of cross section. Tools in existing image analysis software were required in Area Ratio Method.

Mehod-2. Grayscale Variation Method was designed to normalize the color variation inside the capture image. RGB colors were converted to grayscales system in order to quantify the color variation after exposure. In addition, a synthetic evaluation system was established based on fuzzy mathematics.

8.2 RESULTS AND DISCUSSION

8.2.1 RESULTS OF AREA RATIO METHOD

Coordinate System of Prismatic Cross Section. It is defined to set the geometric center of the cylinder section as the origin of coordinates. Therefore, the locations of analyzed sections are decided and presented in Figure 8.1. The size of longitudinal rectangular section is 100 mm $\times$ 50 mm and all the calculated profiles of sulfate diffusion are within the rectangular section.
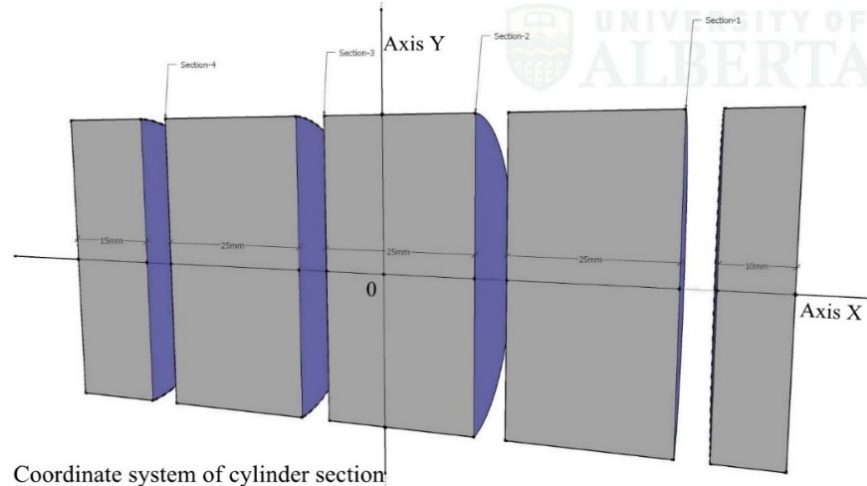
Figure 8.1. Coordinate system of analyzed cross section of area ratio method

Results as Affected by Exposure Duration.
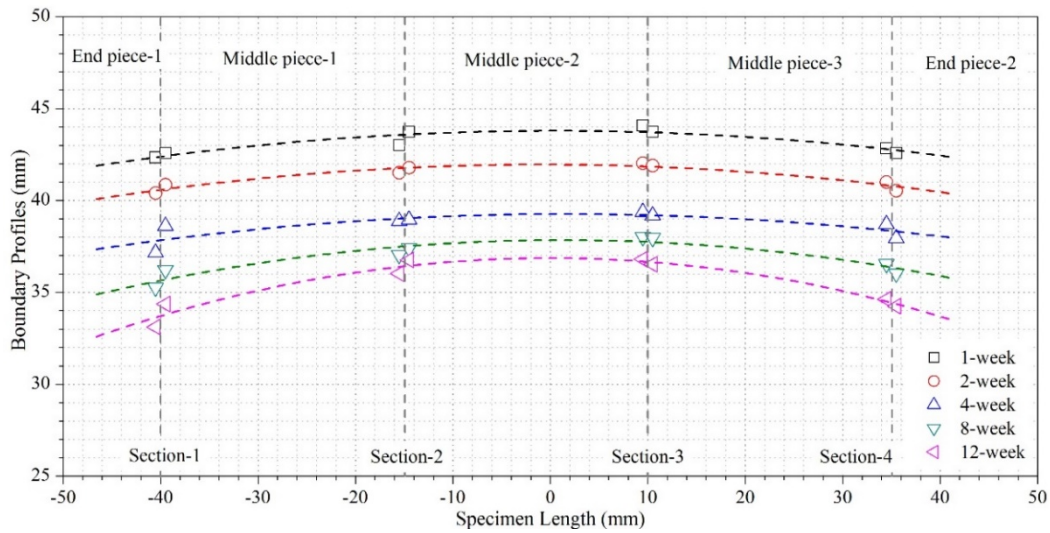
Figure 8.2. Boundaries of sulfate ingress in prismatic section as affected by exposure duration (Type GU)
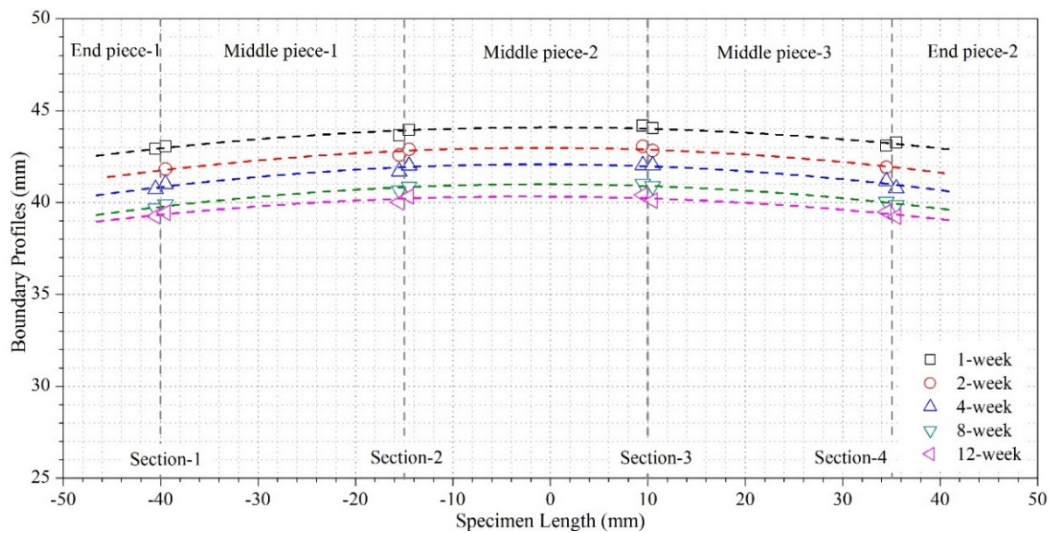
Figure 8.3. Boundaries of sulfate ingress in prismatic section as affected by exposure duration (Type HS)
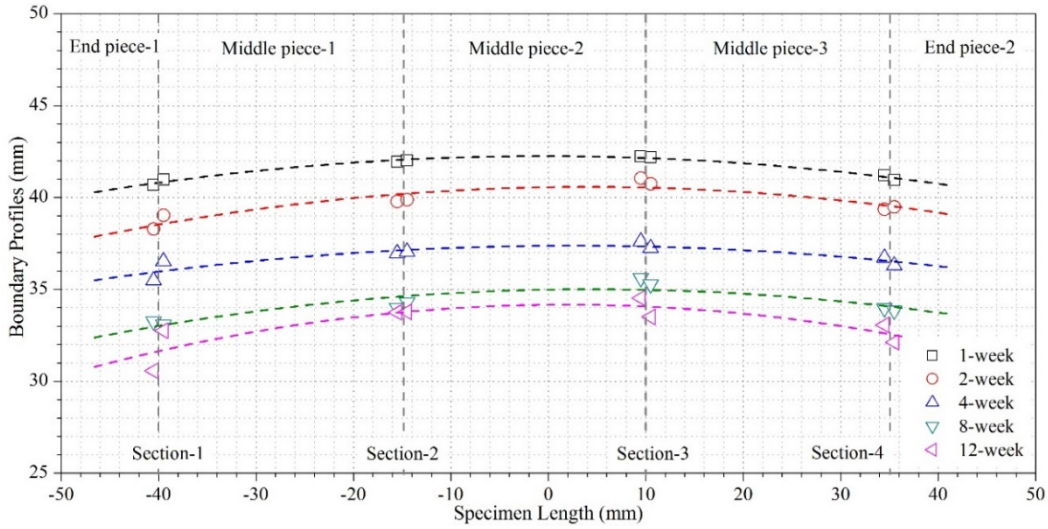
Figure 8.4. Boundaries of sulfate ingress in prismatic section as affected by exposure duration (Blend IC)

Figure 8.2 to Figure 8.4 present the calculated Boundaries of sulfate diffusion. The profile were similar to parabola that was corroborated with the result retrieve by numerical simulation (Tixier and Mobasher 2003). It was witnessed that sulfate diffusion at both end pieces were deeper than that at middle ones, owing to the two dimensional sulfate attack to end pieces.

Additionally, sulfate boundaries inside blend IC specimen were closer to the center, which meant that blend IC was more susceptible to the external sulfate attack.
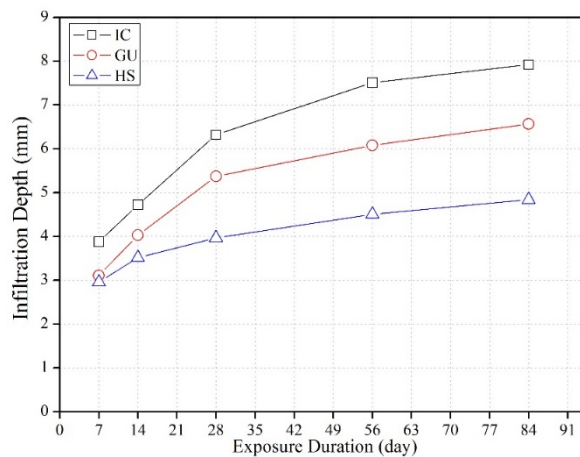
Figure 8.5. One-dimensional diffusion depths as affected by exposure duration

The diffusion depths in the middle piece were chosen and regarded as the invasion depth under one dimensional sulfate attack. As shown in Figure 8.5, Type GU and blend IC performed very close trend of depth increment that was higher than the depth increment of Type HS specimen.

Results as Affected by Cement Type.
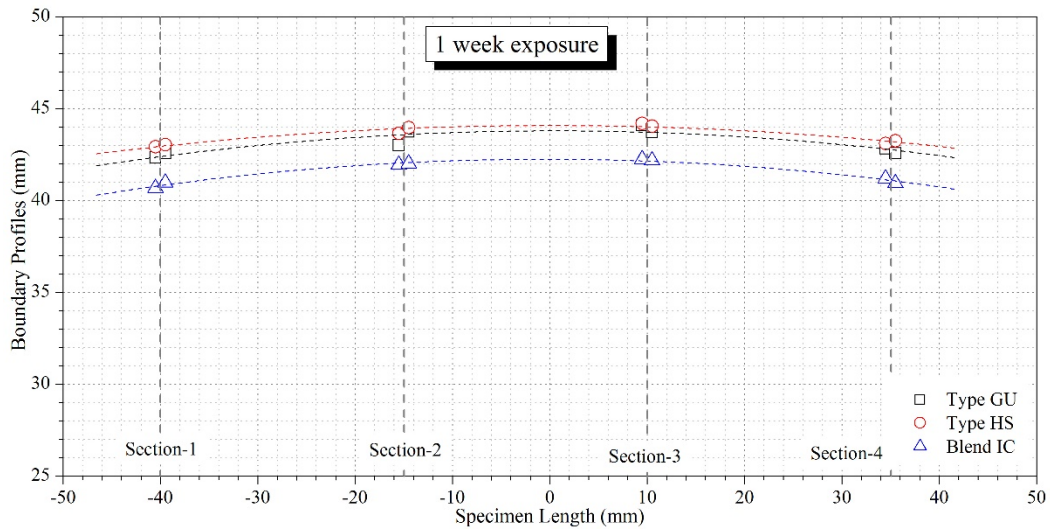
Figure 8.6. Boundaries of sulfate ingress in prismatic section as affected by binders (1-week)
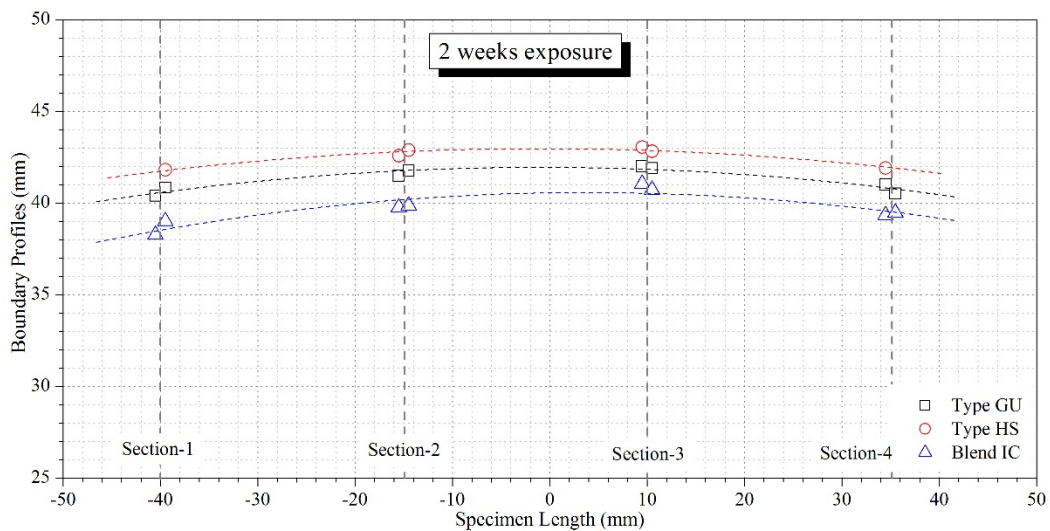
Figure 8.7. Boundaries of sulfate ingress in prismatic section as affected by binders (2-week)
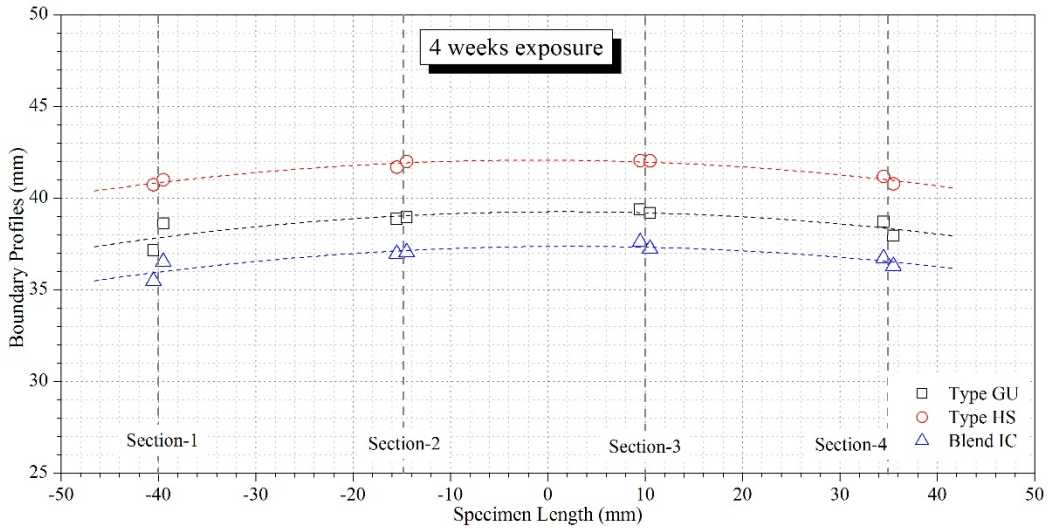
Figure 8.8. Boundaries of sulfate ingress in prismatic section as affected by binders (4-week)

As shown from Figure 8.6 to Figure 8.8, it was recognized by the author that the diffusion depth at the first week of exposure varied very little by cement binders. The variation increased with exposure duration and it was noted that Blend IC specimen had the maximum diffusion depth at varying durations of sulfate exposure.
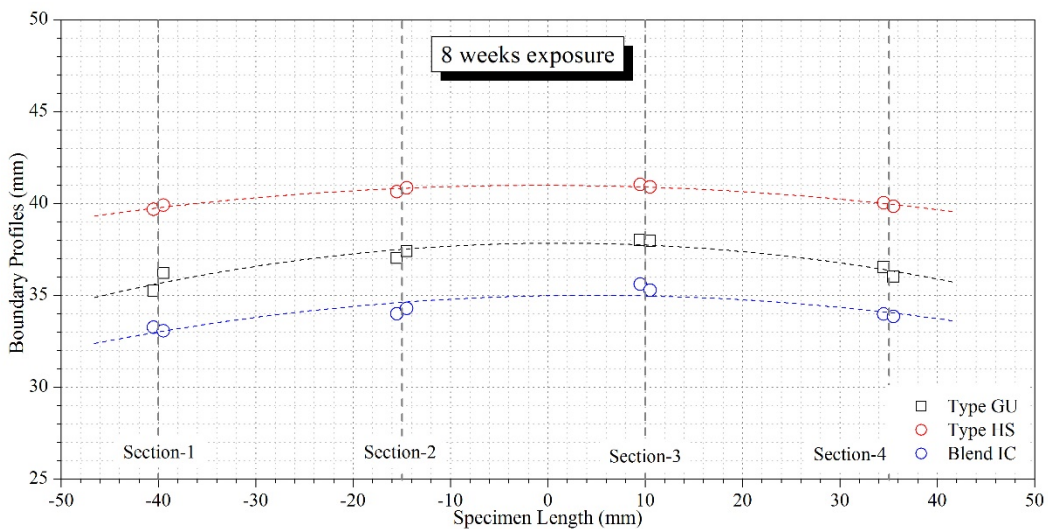
Figure 8.9. Boundaries of sulfate ingress in prismatic section as affected by binders (8-week)
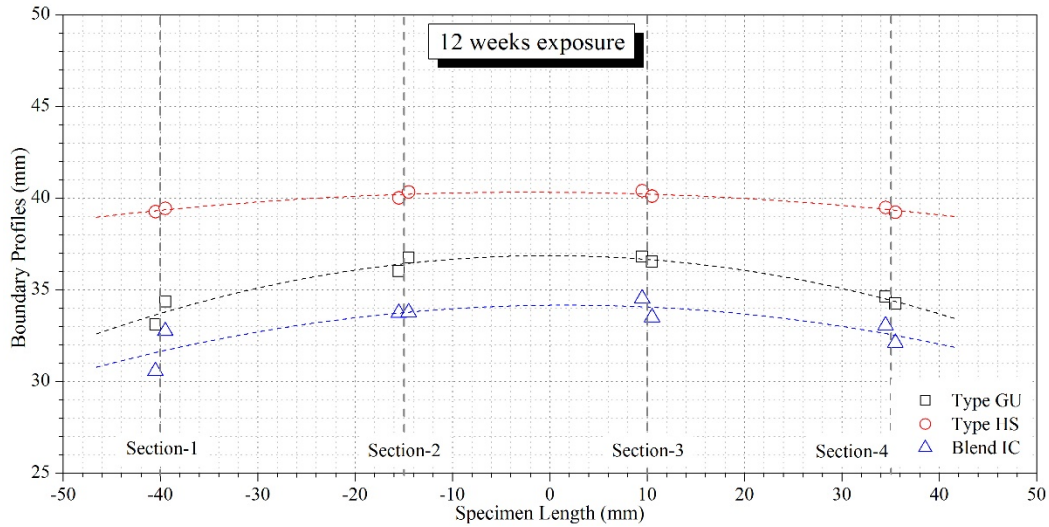
Figure 8.10. Boundaries of sulfate ingress in prismatic section as affected by binders (12-week)

As shown in Figure 8.9 and Figure 8.10, the diffusion depth increased with exposure durations for each type binder. As expected, Type HS cement performed the minimum diffusion depth after 8 weeks and 12 weeks of sulfate exposure. Blend IC was witnessed to have the maximum diffusion depth, around 8 mm from the surface, after 12 weeks of sulfate exposure.

8.2.2 RESULTS OF GRAYSCALE VARIATION METHOD

Normalization of Grayscale Statistic. As stated in photographing setups, ambient light condition and camera setting were unaltered in order to maintain similar gray scale. However, images captured at different time comprised grayscale of varied gradations as shown in: (i) absolute grayscale statistics. Normalization on grayscale, calibrating varied grayscales to defined scope, was required allowing for comparison.

For the grayscale statistic of each image, the minimum *three* grayscales was chosen and averaged as the lower limit. The average of the maximum *three* grayscale was also obtained as the upper limit. In this manner, the lower boundary was normalized to relative scale of 1 while the upper boundary to relative scale of 2 as shown in: (ii) normalized scale statistics.

The reason why choosing the averaged scale of the maximum/minimum three grayscales is to avoid the unreasonable grayscale caused by fine aggregate.

Results as Affected by Exposure Duration. After the normalization of absolute grayscales, variations were plotted as affected by the sulfate exposure duration up to 12 weeks.
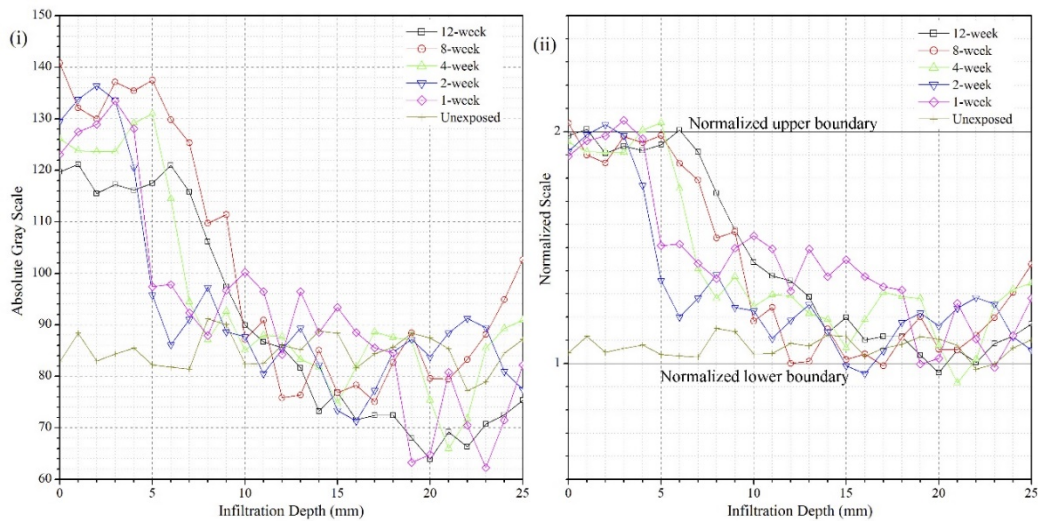
Figure 8.11. Grayscale statistic of InterCem blend within 12 weeks: (i) absolute grayscale; (ii) normalized scale
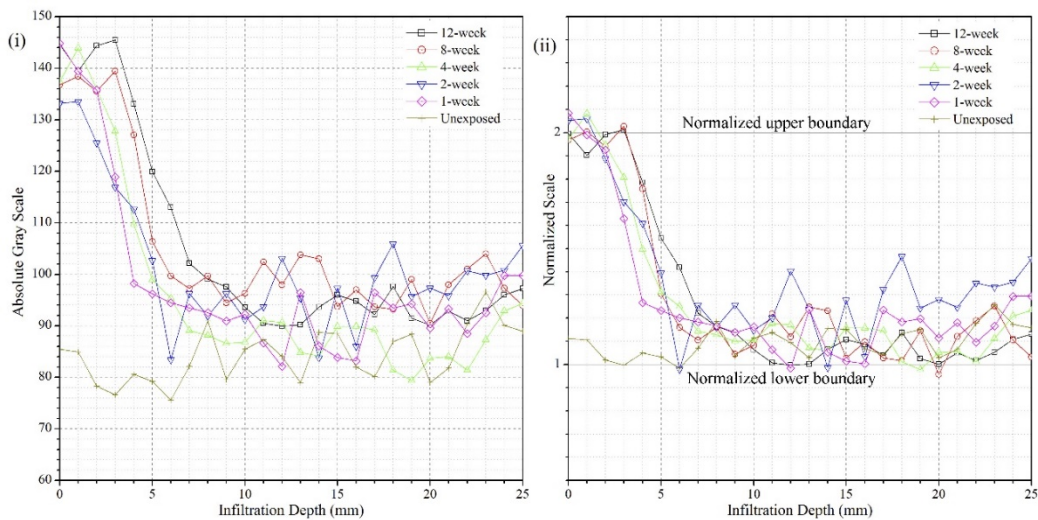
Figure 8.12. Grayscale statistic of Type HS within 12 weeks: (i) absolute grayscale; (ii) normalized scale
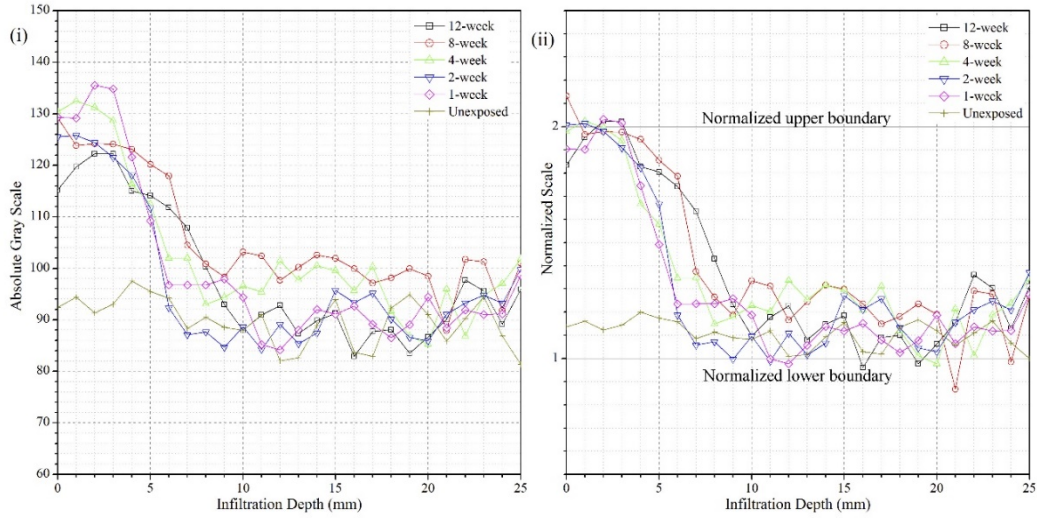
Figure 8.13. Grayscale statistic of Type GU within 12 weeks: (i) absolute grayscale; (ii) normalized scale

As presented from Figure 8.11 to Figure 8.13, one can see that, the normalization limited most absolute grayscales within the range from 1.0 to 2.0. It was very convenient to compare the grayscale variations as affected by exposure duration within normalized region.

In comparison with the unexposed cases, exposed sections showed significant grayscale increase near the edge, which was corroborated with the hypothesis mentioned at the outset. Additionally, the defined diffusion depth evolved with the exposure duration for all tested binder types. All the diffusion depths obtained located in the range form 3.0 mm to 10.0 mm.

Results as Affected by Cement Type.
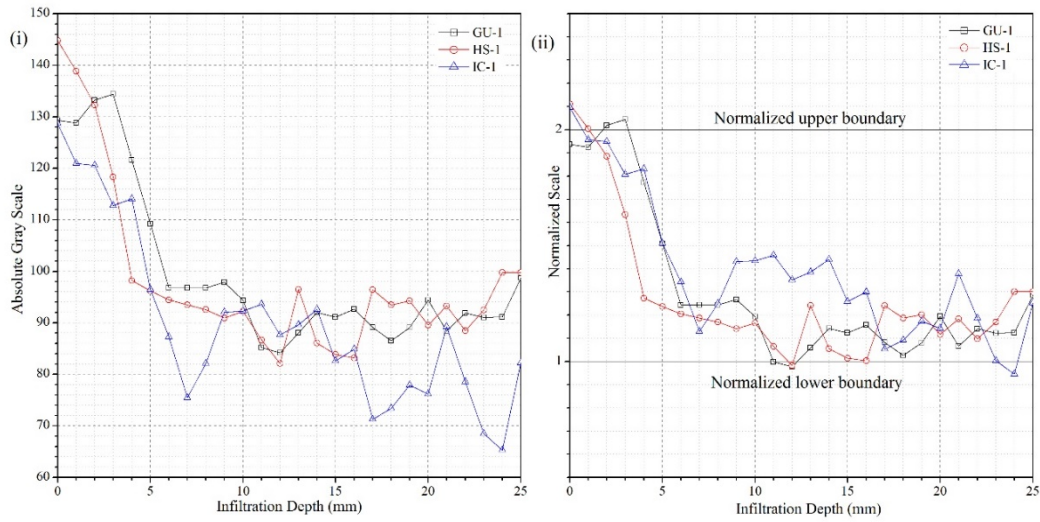
Figure 8.14. Grayscale statistic at 1-week exposure: (i) absolute grayscale; (ii) normalized scale
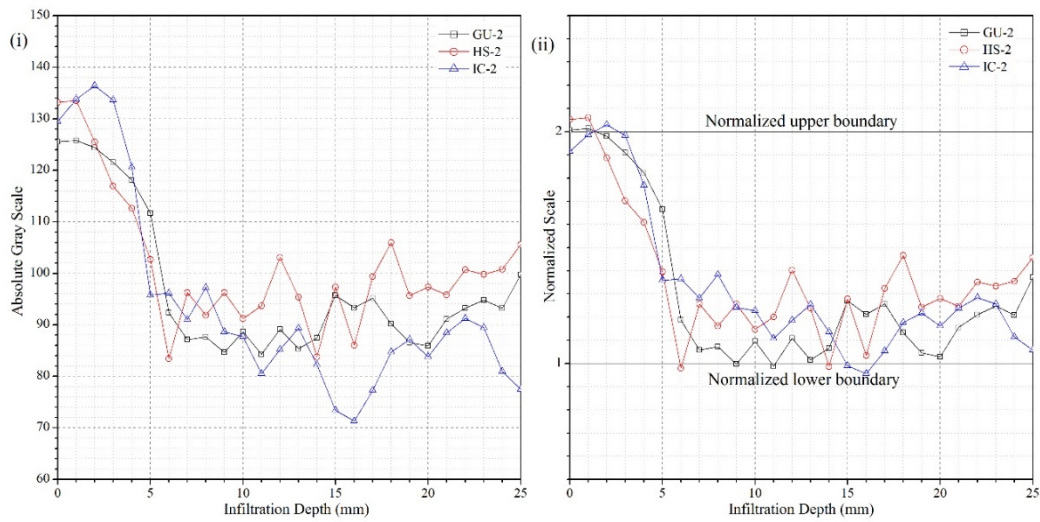
Figure 8.15. Grayscale statistic at 2-week exposure: (i) absolute grayscale; (ii) normalized scale
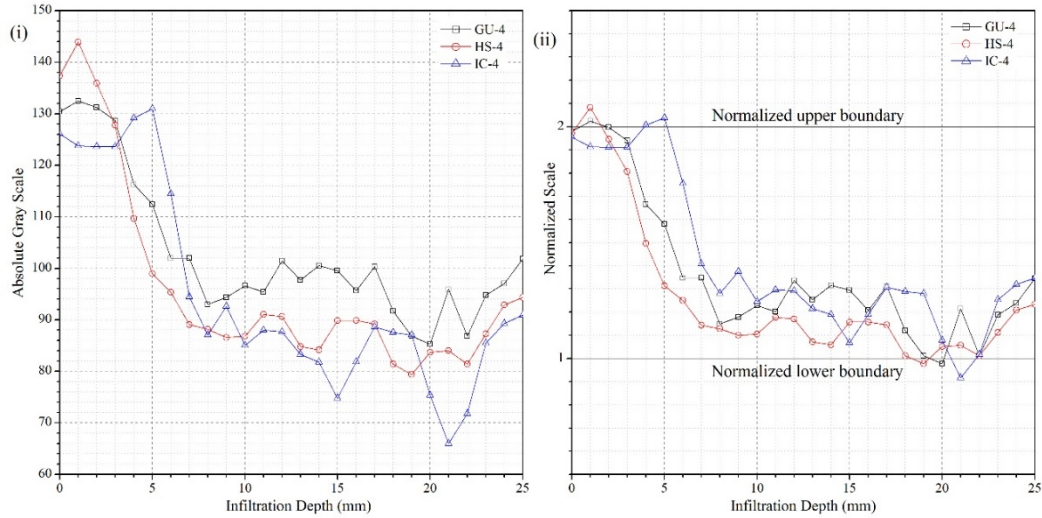
Figure 8.16. Grayscale statistic at 4-week exposure: (i) absolute grayscale; (ii) normalized scale
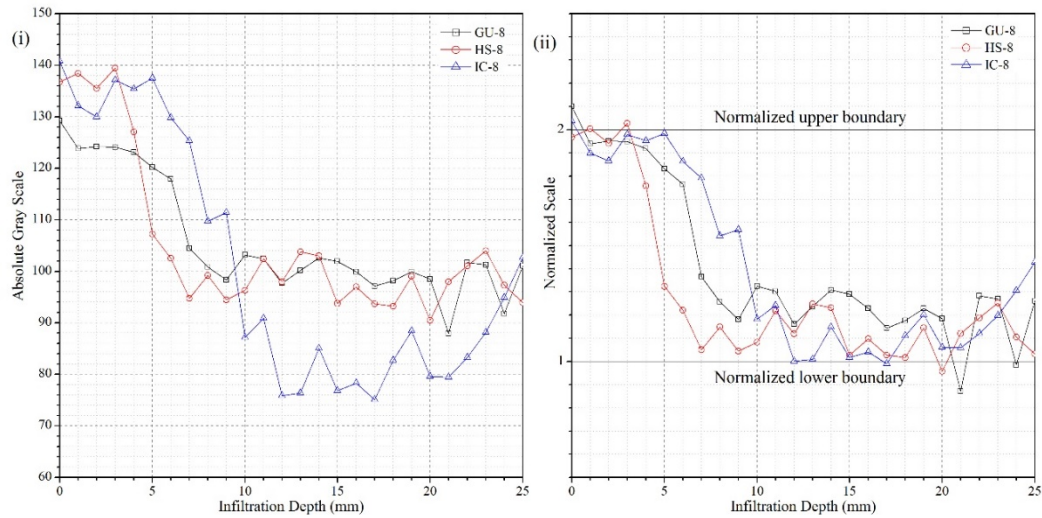
Figure 8.17. Grayscale statistic at 8-week exposure: (i) absolute grayscale; (ii) normalized scale

As presented from Figure 8.14 to Figure 8.18, cement-based composite blend IC was more susceptible to external sulfate attack than other two cement types after varying exposure durations, as evident from the maximum diffusion depth obtained through normalized scale analysis. It is to be noted that after very short-term exposure such as 1 week or 2 weeks, the

grayscale variations of three type binders were very close whereas the deviation between these grayscale profiles increased with exposure durations.
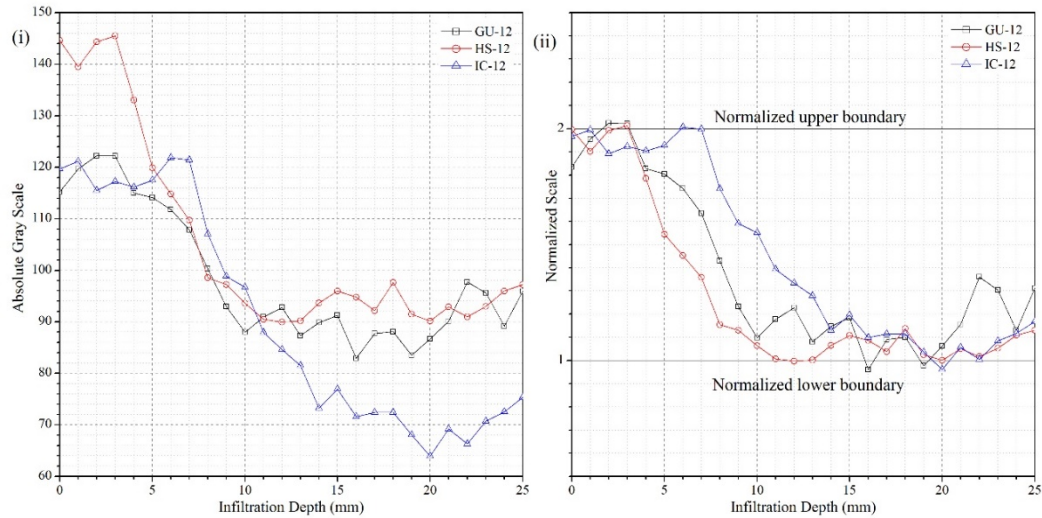
Figure 8.18. Grayscale statistic at 12-week exposure: (i) absolute grayscale; (ii) normalized scale

8.2.3 RESULTS COMPARISON OF AREA RATIO METHOD AND GRAYSCALE VARIATION METHOD

The one dimensional diffusion depths of sulfate attack after varying exposure durations were retrieved by either Area Ratio Method or Grayscale Variation Method. Figure 8.19 presents the diffusion depths obtained through two approaches developed in this work.
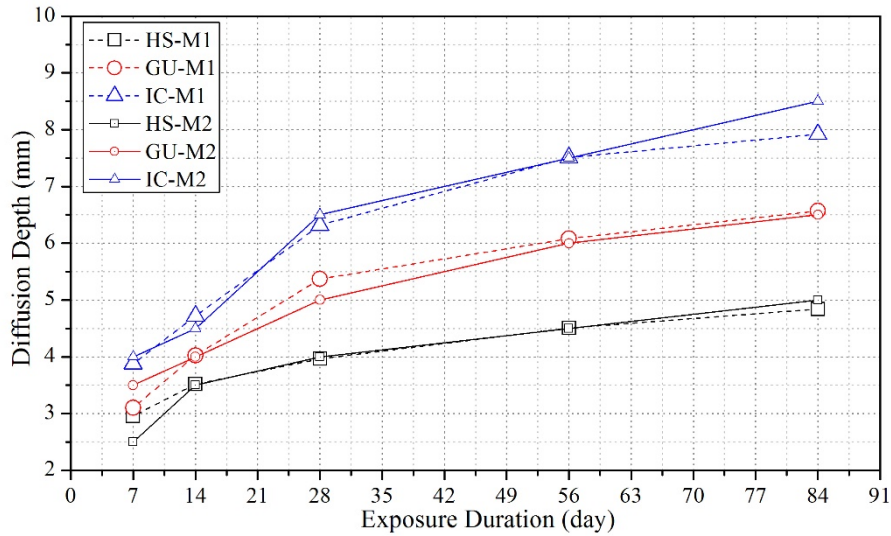
Figure 8.19. Comparison of diffusion depths by Area Ratio Method (M1) and Grayscale Statistics (M2)

It was recognized that, when subjected to one dimensional sulfate diffusion from external, blended binder IC with fly ash was more susceptible to sulfate attack, manifested as the maximum diffusion depths witnessed at any time during exposure. Whereas Type HS cement has the minimum diffusion depth and the minimum depth increment within 12 weeks of exposure as well. This was corroborated with the results concluded through titration experiment on sulfate concentration determination.

Besides, the two image analyzing methods developed in this work showed very close results of diffusion depth, which means that these two approaches are both reliable.

8.3 CURRENT FINDINGS AND POTENTIALS

8.3.1 CURRENT FINDINGS

Method Development. It has been verified through chemical reaction that the external sulfate ingress to cement-based composites contributes to the color variation within the cross section. Deeper sulfate diffusion may lead to higher possibility of volumetric expansion and deteriorate the cement-based system. Two approaches were developed to identify the sulfate diffusion by capturing image cross section.

The Area Ratio Method developed in this work is convenient and simple to identify the sulfate diffusion inside cement-based composites by capturing the image of cross section. It is also applicable to determine the diffusion depth even under asymmetrical exposure environment.

Grayscale Variation Method is an originally developed image analyzing approach with detailed mechanism explained in this study. The color variation caused by sulfate diffusion was transformed to grayscale statistic that quantitatively assesses the diffused area or depth of external sulfate attack.

Conclusions upon Examined Cement-based Composites. Based on the results retrieved through Area Ratio Method and Grayscale Statistics, the following conclusions may be drawn that the diffused area caused by external sulfate attack inside cement-based composites increases with exposure durations in all three examined binders.

At any duration of sulfate exposure, Blend IC binder was evaluated to perform the worst resistance to external sulfate diffusion. As expected, Type HS cement was highly preferred for its excellent performance in resistance to sulfate diffusion from external environment.

Potentials in Engineering Application. The analysis combined with area ratio method and grayscale statistic has potentials in the area of practical engineering application. According to the marked results, image analysis by visual assessment is intended for two cases of real-world application: one case is concrete structure subjected to one dimensional sulfate attack such as seawalls; the other one is concrete structure subjected to two dimensional sulfate attack such as columns in marine environment.

Concrete seawall along the coastline, as simulated in Figure 8.20, is recognized to subject to one dimensional sulfate diffusion from the marine environment. Standard cylindrical specimen is suggested for visual assessment bored from the seawall. Note that the length of specimen is supposed to be over 200 mm in order that color gradation is perceptible in the specimen.
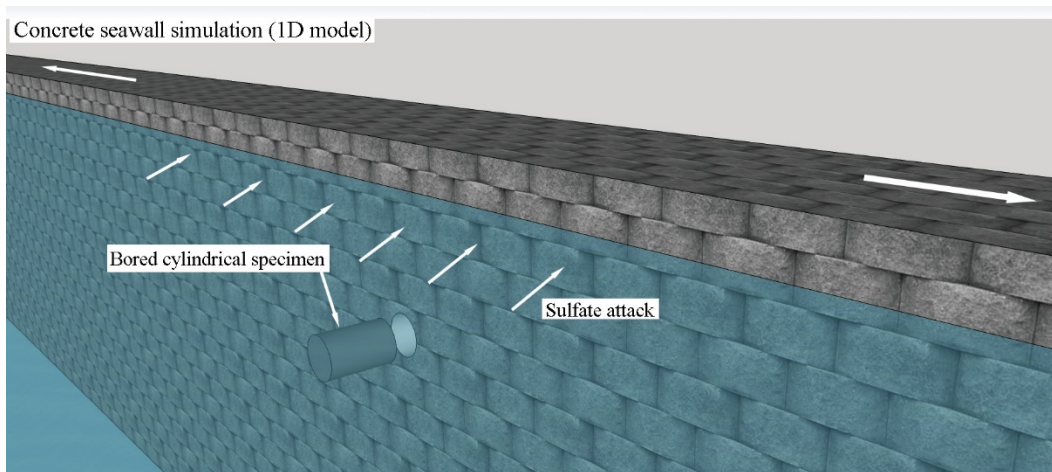
Figure 8.20. Simulated concrete seawall subjected to one dimensional sulfate attack

Rectangular concrete columns in marine environment, as simulated in Figure 8.21, is subjected to two dimensional sulfate attack mostly at the corners. It was corroborated by experimental results obtained from specimens immersed in the sulfate solution, whereas the dimensions of column may affect the sulfate ingress.
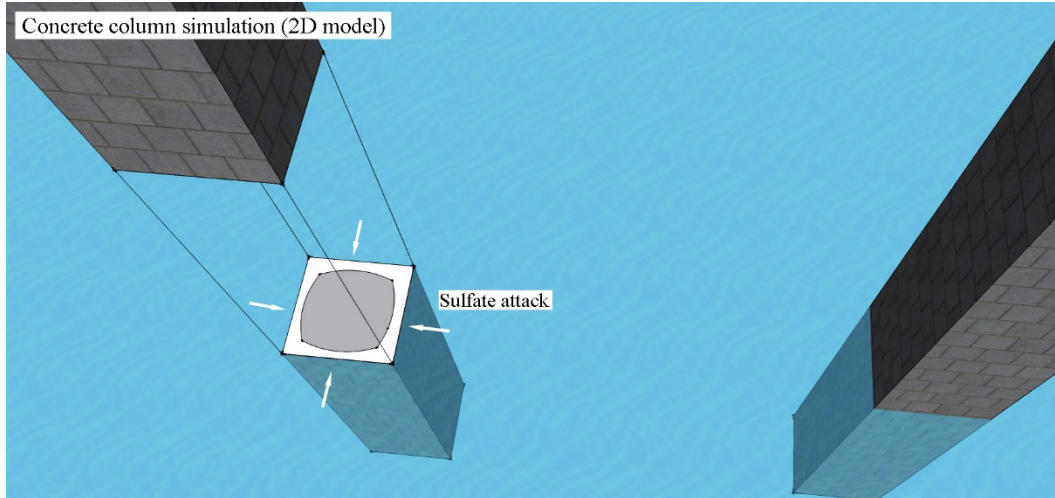
Figure 8.21. Simulated concrete column subjected to two dimensional sulfate attack

To sum up, it is available to quickly evaluate the sulfate attack resistance of concrete or cement instead of complicated chemical analysis methods.

However, the grayscale gradation and boundary are affected by exposure duration and sulfate concentration in the real engineering environment. Low-sulfate condition perhaps leads to unrecognizable boundary so that, in this case, barium chloride is required to participate the sulfates in concrete structure. More experiments are needed in real engineering conditions to investigate the effect of visual assessment developed.

The present study is a detailed experimental investigation on the resistance to sulfate attack by visual assessment. As mentioned in the limit points, this preliminary scheme of analysis requires manual area measurement or grayscale extraction that are time-consuming. Thus the future work is supposed to focus on the following directions:

8.3.2 POSSIBLE OBSTACLES

External Sulfate-rich Environment. The image analysis may meet problems for engineering application considering the lower sulfate concentration in the real work condition than laboratory environment. The transition zone would not be distinguishable as the cylinders tested in the university laboratory. Moreover, exposed time in the real work condition maybe limited and shorter than 12 weeks. It is advised that some extended procedures should have priority during analysis. Dry cutting samples are suggested since water will dilute the sulfate concentration on the section. Spraying high concentration barium chloride solution is also required in order to identify the sulfate attack region.

Color Variation by Various Cement Composites. It has been recognized that the color of Type HS cement (matrix in the image) is slightly darker than other two binders. If varied cement types or admixtures are applied in the future, it is required to recheck the color variation and contrast upon different cement compositions.

Other Kinds of Sulfate Attack. In this study, the sodium sulfate attack was investigated for its effect to color variations by visual assessment. The influence caused by other kind of sulfate attack remains a concern. Crystallization of diffused sodium sulfate was regarded as the governing mechanism of visual assessment.

8.3.3 FURTHER DEVELOPMENT

Photographing/Image Capture. Images captured by more advanced camera or lens are preferred for analysis containing much more pixels in defined area. It is to be noted that same batch of images are captured with unaltered camera settings considering the analysis precision. In the present instance, the image of cement or concrete is captured perpendicular to the direction of external sulfate ingress. The color gradations along the sulfate diffusion

should be perceptible within images no matter what kind of specimens or structures are analyzed.

Software Potentials. A more specific software or mode is required with automatic post processing including color revision, grayscale extraction and numerical statistic. Based on various image processing applications, the gradation of grayscale can be identified as affected by infiltration depth. Note that this study employed Adobe© Photoshop© CS6 to process the image analysis.

Mobile Potentials. With the development of smart phones, high-definition (HD) camera and high-resolution screen are equipped with enormous potentiality on image analysis. Hence smart-phone-based applications are adequate to mobilize the image analysis out of laboratory environment. Qualitative visual assessment on sulfate attack resistance is easily achieved with images captured by smart phone camera. On the other hand, more exact evaluation by calculating the infiltration depth would be available transforming the above statistics from software to smart-phone-based application. Programmed codes in mobile software are introduced to compute grayscale variation within captured images.

9 CONCLUSIONS AND FUTURE RESEARCH

9.1 CURRENT ACHIEVEMENTS

9.1.1 CONVENTIONAL EVALUATION ON SULFATE RESISTANCE

The resistance of cement-based composites to sulfate attack was evaluated by expansion measurement in this study. The results revealed that the binder with fly ash replacement showed the maximum length change, which was corroborated to the findings obtained through titration experiment that accessed the sulfate content inside specimen.

Three different binders were examined for sulfate resistance through mechanical and chemical analysis. Based on the results noted, the following conclusions may be drawn:

The effect of sulfate exposure on compressive and tensile response of cement based systems is not as reflective of damage as evident from the length change measurements. As expected the mix with Type HS cement showed minimum change in length upon exposure, whereas the fly ash blended IC binder exhibited the largest change in length.

9.1.2 SULFATE CONCENTRATION AND NUMERICAL MODEL

The numerical modeling developed in this study consists of two stages. The first stage is to establish the diffusion modeling that involved with chemical reaction of sulfate ingress broadly based on the simulation of chloride diffusion; the second stage is to calculate the volumetric expansion caused by external sulfate attack based on the diffusion modeling developed in the first stage, with the strain-stress response of the examined composites, it is possible to predict the crack initiation and service life with defined thickness of cement-based composites.

In particular, with the input of several featured properties such as external sulfate concentration, diffusion coefficient and inherent C_3A content, the sulfate profile after exposure to sulfate environment can be retrieved for defined type of binder. Furthermore, the strain expansion can be calculated considering the volumetric change caused by the

production of ettringite during the sulfate exposure. With the strain-stress response, modulus of elasticity and porosity obtained through conventional tests, the cement-based materials are likely to crack when the strain expansion exceeds the maximum tensile strain. Whereby the crack initiation and service life prediction can be developed through the numerical modeling.

Sulfate concentration measured as a function of sampling depth indicates that the fly ash blended system allowed maximum sulfate ingress, while those in the Type GU and Type HS cement mixes were comparable and much lower.

The air-void network as quantified using Mercury Intrusion Porosimetry illustrates that although the total porosity was identical, the median pore size with the IC binder is 5-6 times smaller than that with the Types GU and HS cement. Therefore, the formation of ettringite in the former results in expansion and allows deeper sulfate ingress. However, it is likely that continued exposure to sulfate results in a healing that manifests in higher strength at 12 weeks exposure.

9.1.3 VISUAL ASSESSMENT BY IMAGE ANALYSIS

A visual evaluation on sulfate diffusion has been developed in this study. By means of photographing on the cross section and post-processing on image, the affected depth of external sulfate diffusion can be identified by two approaches studied in this work. Image analysis is a quick and convenient method in order to retrieve the diffusion depth after exposure to external sulfate attack. Therefore, it is suggested to employ this visual assessment on sulfate diffusion instead of complicated titration experiment.

Besides, there is potential relationship between the diffusion depth retrieved by visual assessment and the numerical model. Further study is required to combine these two evaluation approaches.

9.1.4 THE LINK BETWEEN CURRENT ACHIEVEMENTS

Compared with the conventional evaluation on sulfate attack to cement-based composites, the sulfate concentration obtained through titration experiment is aimed to assess the resistance to sulfate with higher accuracy, also as the fundamental property to the numerical model.

9.2 LIMITATIONS OF CURRENT FINDINGS

9.2.1 LIMITATIONS OF EXPERIMENTAL PROGRAM

The sample extraction and titration experiment developed in this study are limited for plain cement mortar specimens subjected to sulfate attack. The powdered samples are supposed to be extracted layer by layer from the surface exposed to sulfate environment, and the samples extracted are defined under one dimensional sulfate diffusion. Prepared specimens are preferred for sample extraction, while cement-based structures, such as columns, beams, and seawalls, are also applicable to extract samples.

The titration experiment is limited in laboratory environment with extracted samples. Further, to obtain accurate sulfate concentration in powdered sample, several procedures like filtration, centrifugation, and drying were employed before titration, which makes the experiment time-consuming.

9.2.2 LIMITATIONS OF NUMERICAL MODELLING

Both the diffusion model developed in Chapter 6 and diffusion-reaction model developed in Chapter 7 are simulated for the process of one dimensional sulfate attack. The limitation of these one dimensional numerical model is that only cement paste or cement mortar structure is applicable since they are regarded as homogeneous matrix for sulfate diffusion. Whereas cement-based composition containing undiffused compounds, such as coarse aggregate, cannot be simulated through one dimensional numerical model under sulfate attack. In this

case, two dimensional diffusion model is required to simulated the sulfate attack progress in concrete structures containing coarse aggregates.

9.2.3 LIMITATIONS OF VISUAL ASSESSMENT

Preliminarily, the visual assessment on sulfate diffusion was developed for cement mortar matrix or cement paste matrix without fine aggregates. Considering the effect caused by coarse aggregates in concrete and reinforcement bars in real concrete structures, the visual assessment is supposed to be improved when extracting grayscales inside the cross section.

9.3 FUTURE RESEARCH

9.3.1 DEVELOPMENT UPON CEMENT-BASED COMPOSITES

- **C$_3$A and SO$_3$ content.** Cement-based composites with varying C$_3$A and SO$_3$ contents are recommended for future numerical simulation after the basic model developed in this program. As studied in this study, inherent C$_3$A content has significant effect to the potential ettringite production and volumetric expansion.

- **Mineral Admixtures.** Based on the conclusion that the fly ash replacement does not facilitate the resistance of cement-based composites to sulfate attack, the effect of other mineral admixtures to the sulfate resistance, such as slag and silica fume, are supposed to be examined with specifically developed numerical model.

- **Fibers.** Numerical model upon cement-based composites containing fiber admixtures such as steel fibers and ploy fibers are also suggested to be improved in accordance with the numerical model developed in this work.

- **Course Aggregates.** The present numerical model is intended for the diffusion reaction process of sulfate attack in cement mortar materials. Further development on numerical model is required for the simulation of concrete composites consisting of course aggregates that are impermeable to sulfate diffusion.

- **Curing Prior to Sulfate Exposure.** The deterioration of Blend IC when exposed to sulfate environment may be attributed to the short-term curing of 28 days, in which the effect of fly ash replacement is not completely reinforced. Longer curing duration prior to exposure, more than 28 days experienced in this work, is highly suggested in comparison with the short-term curing.

9.3.2 DEVELOPMENT ON NUMERICAL MODEL SIMULATION

- **Two dimensional sulfate attack.** Current numerical model is based on one dimensional sulfate diffusion that sulfates diffuses from symmetric directions. This model has limited applications in the real world, for instance, the coastal concrete seawalls is studied under one dimensional sulfate diffusion. In most real conditions of sulfate exposure, the cement-based system is subjected to two dimensional sulfate diffusion from external environment. It is necessary to develop two dimensional diffusion reaction model upon the simulation of structures such as concrete beams and columns. In addition, the convection in the real environment is supposed to be taken under consideration inside the numerical model.

- **Hybrid Attack conditions.** In the program already studied, sodium sulfate attack is the only durability issue considered in the numerical model. However, other kinds of sulfate attack are supposed to be included in the simulation as well as corrosion caused

by chloride diffusion. Hybrid attack conditions containing physical and physicochemical diffusions are more complicated and future research on hybrid attack conditions are required.

9.3.3 DEVELOPMENT ON PRACTICAL APPLICATION

■ **Computer-based simulation applications.** Currently, the numerical model is achieved based on the MATLAB programing. In accordance with the collaboration research with Dr. Chen Zhen for the cracking development simulation and service life prediction under sulfate attack, an integrated programing software is realizable. By means of transforming numerical theories for MATLAB language to C++ or other programming languages, the well-developed research program can be commercialized to mutual applications.

■ **Mobile and smartphone-based applications.** Mobile and smartphone-based potentials are proposed based on the current findings of visual assessment. Considering the results obtained through image analysis, evaluation on sulfate diffusion can be achieved by smartphones equipped with portable cameras. With the fast development of mobile smartphones, high resolution image is available for sulfate attack assessment. Further, the numerical model program can be transformed from MATLAB language to smartphone-based language so that mobile application combined with image analysis and numerical model is preferred for engineering attack conditions.

REFERENCES

Al-Dulaijan, S., Maslehuddin, M., Al-Zahrani, M., Sharif, A., Shameem, M., and Ibrahim, M. (2003). "Sulfate resistance of plain and blended cements exposed to varying concentrations of sodium sulfate." *Cement and Concrete Composites*, 25(4), 429-437.

C114-13, A. ((2013)). ""Standard Test Methods for Chemical Analysis of Hydraulic Cement"."ASTM International, West Conshohocken, PA. , 32. DOI: 10.1520/C0114-1513.

Chalee, W., Jaturapitakkul, C., and Chindaprasirt, P. (2009). "Predicting the chloride penetration of fly ash concrete in seawater." *Marine structures*, 22(3), 341-353.

Crank, J. (1979). *The mathematics of diffusion*, Oxford university press.

Irassar, E., Di Maio, A., and Batic, O. (1996). "Sulfate attack on concrete with mineral admixtures." *Cement and Concrete Research*, 26(1), 113-123.

Mamun, M., and Bindiganavile, V. (2011). "Sulphate resistance of fibre reinforced cement-based foams." *Construction and Building Materials*, 25(8), 3427-3442.

Sahmaran, M., Kasap, O., Duru, K., and Yaman, I. (2007). "Effects of mix composition and water–cement ratio on the sulfate resistance of blended cements." *Cement and Concrete composites*, 29(3), 159-167.

Santhanam, M., Cohen, M. D., and Olek, J. (2002). "Mechanism of sulfate attack: a fresh look: part 1: summary of experimental results." *Cement and concrete research*, 32(6), 915-921.

Santhanam, M., Cohen, M. D., and Olek, J. (2003). "Effects of gypsum formation on the performance of cement mortars during external sulfate attack." *Cement and concrete research*, 33(3), 325-332.

Song, H.-W., Shim, H.-B., Petcherdchoo, A., and Park, S.-K. (2009). "Service life prediction of repaired concrete structures under chloride environment using finite difference method." *Cement and Concrete Composites*, 31(2), 120-127.

Sun, C., Chen, J., Zhu, J., Zhang, M., and Ye, J. (2013). "A new diffusion model of sulfate ions in concrete." *Construction and Building Materials*, 39, 39-45.

Tian, B., and Cohen, M. D. (2000). "Does gypsum formation during sulfate attack on concrete lead to expansion?" *Cement and Concrete Research*, 30(1), 117-123.

Tixier, R., and Mobasher, B. (2003). "Modeling of damage in cement-based materials subjected to external sulfate attack. I: formulation." *Journal of materials in civil engineering*, 15(4), 305-313.

Tixier, R., and Mobasher, B. (2003). "Modeling of damage in cement-based materials subjected to external sulfate attack. II: Comparison with experiments." *Journal of materials in civil engineering*, 15(4), 314-322.

Torii, K., and Kawamura, M. (1994). "Effects of fly ash and silica fume on the resistance of mortar to sulfuric acid and sulfate attack." *Cement and Concrete Research*, 24(2),

361-370.

Torii, K., Taniguchi, K., and Kawamura, M. (1995). "Sulfate resistance of high fly ash content concrete." *Cement and Concrete Research*, 25(4), 759-768.

Wang, J. G. (1994). "Sulfate attack on hardened cement paste." *Cement and Concrete Research*, 24(4), 735-742.

Al-Dulaijan, S., Maslehuddin, M., Al-Zahrani, M., Sharif, A., Shameem, M., and Ibrahim, M. (2003). "Sulfate resistance of plain and blended cements exposed to varying concentrations of sodium sulfate." *Cement and Concrete Composites*, 25(4), 429-437.

C39/39M-14a, A. ((2014)). ""Standard Test Method for Compressive Strength of Cylindrical Concrete Specimens"."ASTM International, West Conshohocken, PA. , 7. DOI: 10.1520/C0039_C0039M-1514A.

C490/490M-11, A. ((2011)). ""Standard Practice for Use of Apparatus for the Determination of Length Change of Hardened Cement Paste, Mortar, and Concrete"."ASTM International, West Conshohocken, PA. , 5. DOI: 10.1520/C0490_C0490M-1511E1501.

C496/C496M-11, A. ((2011)). ""Standard Test Method for Splitting Tensile Strength of Cylindrical Concrete Specimens"."ASTM International, West Conshohocken, PA. , 5. DOI: 10.1520/C0496_C0496M-1511.

C1012/1012M-13, A. ((2013)). ""Standard Test Method for Length Change of Hydraulic-Cement Mortars Exposed to a Sulfate Solution"."ASTM International, West Conshohocken, PA. , 8. DOI: 10.1520/C1012_C1012M-1513.

Mamun, M., and Bindiganavile, V. (2011). "Sulphate resistance of fibre reinforced cement-based foams." *Construction and Building Materials*, 25(8), 3427-3442.

Sahmaran, M., Kasap, O., Duru, K., and Yaman, I. (2007). "Effects of mix composition and water–cement ratio on the sulfate resistance of blended cements." *Cement and Concrete composites*, 29(3), 159-167.

Santhanam, M., Cohen, M. D., and Olek, J. (2002). "Mechanism of sulfate attack: a fresh look: part 1: summary of experimental results." *Cement and concrete research*, 32(6), 915-921.

Santhanam, M., Cohen, M. D., and Olek, J. (2003). "Effects of gypsum formation on the performance of cement mortars during external sulfate attack." *Cement and concrete research*, 33(3), 325-332.

C114-13, A. ((2013)). ""Standard Test Methods for Chemical Analysis of Hydraulic Cement"."ASTM International, West Conshohocken, PA. , 32. DOI: 10.1520/C0114-1513.

Sun, C., Chen, J., Zhu, J., Zhang, M., and Ye, J. (2013). "A new diffusion model of sulfate

ions in concrete." *Construction and Building Materials*, 39, 39-45.

C114-13, A. ((2013)). ""Standard Test Methods for Chemical Analysis of Hydraulic Cement"."ASTM International, West Conshohocken, PA. , 32. DOI: 10.1520/C0114-1513.

C265-08, A. ((2008)). ""Standard Test Method for Water-Extractable Sulfate in Hydrated Hydraulic Cement Mortar"."ASTM International, West Conshohocken, PA. , 3. DOI: 10.1520/C0265-1508.

Sun, C., Chen, J., Zhu, J., Zhang, M., and Ye, J. (2013). "A new diffusion model of sulfate ions in concrete." *Construction and Building Materials*, 39, 39-45.

Chalee, W., Jaturapitakkul, C., and Chindaprasirt, P. (2009). "Predicting the chloride penetration of fly ash concrete in seawater." *Marine structures*, 22(3), 341-353.

Crank, J. (1979). *The mathematics of diffusion*, Oxford university press.

Hoffman, J. D., and Frankel, S. (2001). *Numerical methods for engineers and scientists*, CRC press.

Song, H.-W., Shim, H.-B., Petcherdchoo, A., and Park, S.-K. (2009). "Service life prediction of repaired concrete structures under chloride environment using finite difference method." *Cement and Concrete Composites*, 31(2), 120-127.

Tixier, R., and Mobasher, B. (2003). "Modeling of damage in cement-based materials subjected to external sulfate attack. I: formulation." *Journal of materials in civil engineering*, 15(4), 305-313.

Tixier, R., and Mobasher, B. (2003). "Modeling of damage in cement-based materials subjected to external sulfate attack. II: Comparison with experiments." *Journal of materials in civil engineering*, 15(4), 314-322.

Vu, K. A. T., and Stewart, M. G. (2000). "Structural reliability of concrete bridges including improved chloride-induced corrosion models." *Structural safety*, 22(4), 313-333.

Information from Internet: https://en.wikipedia.org/wiki/Finite_difference_method

Chalee, W., Jaturapitakkul, C., and Chindaprasirt, P. (2009). "Predicting the chloride penetration of fly ash concrete in seawater." *Marine structures*, 22(3), 341-353.

Sun, C., Chen, J., Zhu, J., Zhang, M., and Ye, J. (2013). "A new diffusion model of sulfate ions in concrete." *Construction and Building Materials*, 39, 39-45.

Tian, B., and Cohen, M. D. (2000). "Does gypsum formation during sulfate attack on concrete lead to expansion?" *Cement and Concrete Research*, 30(1), 117-123.

Tixier, R., and Mobasher, B. (2003). "Modeling of damage in cement-based materials subjected to external sulfate attack. I: formulation." *Journal of materials in civil engineering*, 15(4), 305-313.

Tixier, R., and Mobasher, B. (2003). "Modeling of damage in cement-based materials

subjected to external sulfate attack. II: Comparison with experiments." *Journal of materials in civil engineering*, 15(4), 314-322.

Wang, J. G. (1994). "Sulfate attack on hardened cement paste." *Cement and Concrete Research*, 24(4), 735-742.

Tixier, R., and Mobasher, B. (2003). "Modeling of damage in cement-based materials subjected to external sulfate attack. I: formulation." *Journal of materials in civil engineering*, 15(4), 305-313.

Information from website: www.photoshopessentials.com

APPENDIX A-TABLES AND FIGURES

Chapter 3: Physical Properties

Table 1. Sulfate required in the liquid environment

Length Test				
# of Bars	Min Sulph (g)	Max Sulph (g)	Min vol. of soln per Cyl. (L)	0.625
45	1406.25	1800	Max vol. of soln per Cyl. (L)	0.8
36	1125	1440	Sulfate (g) per (L) of soln	50
27	843.75	1080		
18	562.5	720		
9	281.25	360		
Sum	4218.75	5400		
Compression Test				
# of Cyls	Min Sulph (g)	Max Sulph (g)	Min vol. of soln per Cyl. (L)	2.3
45	5175	6750	Max vol. of soln per Cyl. (L)	3
36	4140	5400	Sulfate (g) per (L) of soln	50
27	3105	4050		
18	2070	2700		
9	1035	1350		
Sum	15525	20250		
Split Tensile Test				
# of Cyls	Min Sulph (g)	Max Sulph (g)	Min vol. of soln per Cyl. (L)	0.685
45	1541.25	1991.25	Max vol. of soln per Cyl. (L)	0.885
36	1233	1593	Sulfate (g) per (L) of soln	50
27	924.75	1194.75		
18	616.5	796.5		
9	308.25	398.25		
Sum	4623.75	5973.75		
CATSCAN Test				
# of Cyls	Min Sulph (g)	Max Sulph (g)	Min vol. of soln per Cyl. (L)	0.685
15	513.75	663.75	Max vol. of soln per Cyl. (L)	0.885
12	411	531	Sulfate (g) per (L) of soln	50
9	308.25	398.25		
6	205.5	265.5		
3	102.75	132.75		

Sum	1541.25	1991.25			
Total Sulfate required	25.90875	to	33.615		
Total distilled water required	518.175	to	672.3	L	

Table 2. Mill Test Certificate for CSA Portland cement Type GU (provided by Lehigh)

LEHIGH
HEIDELBERGCEMENT Group

Lehigh Cement
12640 Inland Way
Edmonton, AB T5V 1K2
Phone 780-420-2500
Fax 780-420-2665
www.LehighHansonCanada.com

MILL TEST CERTIFICATE FOR CSA PORTLAND CEMENT TYPE GU

Production for Week Ending 2016:		05-Apr	12-Apr	19-Apr	26-Apr	03-May	10-May	17-May	24-May	31-May	07-Jun	14-Jun	21-Jun	28-Jun
CHEMICAL ANALYSIS														
SiO_2	%	20.2	20.4	20.1	20.3	19.9	20.0	20.1	20.3	20.3	20.3	20.3	20.3	20.1
Al_2O_3	%	4.4	4.6	4.7	4.6	4.5	4.5	4.4	4.4	4.4	4.4	4.5	4.6	4.5
Fe_2O_3	%	3.4	3.4	3.4	3.4	3.4	3.2	3.3	3.4	3.5	3.4	3.4	3.4	3.5
CaO	%	62.9	62.7	62.8	62.7	62.8	62.6	62.8	62.8	62.6	63.0	62.9	62.8	62.8
MgO	%	2.80	2.81	2.81	2.93	2.90	2.89	2.82	2.71	2.59	2.79	2.81	2.69	2.70
SO_3	%	2.83	2.74	2.61	2.71	2.73	2.67	2.69	2.72	2.73	2.72	2.70	2.69	2.74
Loss on Ignition	%	2.12	2.15	2.35	2.06	2.16	2.35	2.50	2.47	2.34	2.34	2.52	2.27	1.81
Na_2O	%	0.23	0.24	0.25	0.24	0.24	0.25	0.24	0.23	0.24	0.24	0.24	0.24	0.24
K_2O	%	0.45	0.48	0.45	0.45	0.46	0.48	0.45	0.46	0.47	0.44	0.44	0.45	0.44
Insoluble Residue	%	0.48	0.55	0.36	0.44	0.39	0.36	0.43	0.42	0.36	0.37	0.32	0.49	0.33
T. Alk.	%	0.52	0.56	0.55	0.54	0.54	0.56	0.53	0.53	0.55	0.53	0.53	0.53	0.52
C_3S	%	60	57	59	57	61	61	61	59	58	60	59	58	60
C_2S	%	12	15	13	15	11	12	11	13	14	13	13	15	12
C_3A	%	5.8	6.3	6.6	6.5	6.2	6.5	6.1	6.0	5.7	5.9	6.1	6.5	6.1
C_4AF	%	10.4	10.3	10.3	10.4	10.2	9.9	10.0	10.2	10.6	10.3	10.4	10.4	10.6
PHYSICAL PROPERTIES														
Blaine	m²/kg	425	420	412	419	423	426	423	425	422	423	430	425	427
Retained on 45μ sieve	%	7.25	4.13	4.41	4.30	4.23	4.00	3.75	4.35	4.33	4.51	4.16	4.80	5.11
Autoclave Expansion	%	0.087	0.087	0.107	0.104	0.096	0.102	0.152	0.079	0.078	0.075	0.087	0.092	0.065
Vicat Initial Set	min	64	64	73	68	77	73	85	78	69	73	79	71	65
False Set	%	77	77	63	74	82	84	74	67	87	67	74	86	78
Air Content	%	8.50	8.50	8.50	8.50	8.50	8.50	8.50	10.35	10.35	10.35	10.35	10.35	8.80
3 Day	MPa	20.2	21.3	22.7	22.2	23.1	22.8	22.6	22.0	20.7	24.4	24.7	21.6	22.4
7 Day	MPa	25.6	27.9	30.0	29.0	30.1	29.5	30.6	29.1	29.0	32.4	32.8	29.5	30.4
28 Day	MPa	39.4	40.3	41.9	41.1	42.6	42.3	43.2	42.6	41.7	44.6	45.0	42.5	

Manufactured cement conforms to CSA Standard A3001-13.

No adjustment has been made for possible use of limestone or inorganic processing addition.

Date: July 16, 2015

Jeff Matchett

Table 3. Mill Test Certificate for CSA Portland cement Type HS (provided by Lehigh)

LEHIGH
HEIDELBERGCEMENT Group

Lehigh Cement
12640 Inland Way
Edmonton, AB T5V 1K2
Phone 780-420-2500
Fax 780-420-2665
www.LehighHansonCanada.com

MILL TEST CERTIFICATE FOR CSA PORTLAND CEMENT TYPE HS

Production for Week Ending 2015:		05-Apr	12-Apr	19-Apr	26-Apr	03-May	10-May	17-May	24-May	31-May	07-Jun	14-Jun	21-Jun	28-Jun
CHEMICAL ANALYSIS														
SiO_2	%	21.2	20.8	20.8	21.3	21.1	20.5	20.6	20.8	20.8	21.1	21.0	20.9	20.6
Al_2O_3	%	3.4	3.2	3.2	3.3	3.2	3.3	3.3	3.4	3.3	3.4	3.3	3.3	3.3
Fe_2O_3	%	4.7	4.7	4.7	4.8	4.6	4.6	4.7	4.7	4.7	4.6	4.7	4.7	4.8
CaO	%	61.8	62.0	61.9	61.8	61.8	62.1	62.3	62.1	62.2	62.1	62.3	62.1	62.0
MgO	%	2.77	2.71	2.74	2.83	2.79	2.71	2.75	2.70	2.54	2.61	2.64	2.59	2.65
SO_3	%	2.14	2.27	2.18	2.27	2.26	2.21	2.27	2.16	2.19	2.22	2.24	2.24	2.19
Loss on ignition	%	1.92	2.10	2.01	1.36	1.48	1.92	1.54	1.79	2.02	2.26	2.34	1.71	2.50
Na_2O	%	0.33	0.30	0.29	0.31	0.31	0.30	0.31	0.31	0.29	0.29	0.29	0.29	0.30
K_2O	%	0.48	0.48	0.51	0.49	0.49	0.47	0.49	0.48	0.46	0.45	0.46	0.47	0.45
Insoluble Residue	%	0.35	0.58	0.42	0.36	0.45	0.35	0.32	0.41	0.34	0.32	0.41	0.50	0.45
T. Alk.	%	0.64	0.62	0.63	0.63	0.64	0.60	0.63	0.63	0.59	0.59	0.59	0.60	0.59
C_3S	%	56	60	60	55	56	62	62	60	60	56	59	59	61
C_2S	%	19	15	15	20	18	12	12	15	15	18	16	16	13
C_3A	%	1.0	0.5	0.6	0.6	0.7	0.9	0.9	0.9	0.8	1.1	1.0	0.9	0.6
C_4AF	%	14.2	14.3	14.2	14.5	14.0	14.0	14.1	14.4	14.3	14.1	14.2	14.3	14.5
PHYSICAL PROPERTIES														
Blaine	m^2/kg	453	430	420	426	426	440	441	439	444	440	445	440	446
Retained on 45μ sieve	%	2.88	3.28	3.13	2.80	3.00	2.17	1.82	2.35	2.61	2.73	3.19	3.14	4.07
Autoclave Expansion	%	0.024	0.024	0.043	0.043	0.029	0.029	0.025	0.025	0.029	0.032	0.034	0.035	0.024
Sulphate Expansion	%	0.025	0.025	0.026	0.026	0.024	0.022	0.022	0.022	0.023	0.025	0.027	0.025	0.025
Vicat Initial Set	min	89	89	90	90	107	107	98	98	95	92	99	103	97
False Set	%	72	72	75	75	50	50	61	61	57	52	75	87	66
Air Content	%	8.50	8.50	8.60	8.60	8.60	8.60	9.10	9.10	9.50	9.90	9.63	9.50	8.70
3 Day	MPa	21.4	19.1	19.8	20.8	20.4	21.9	21.5	21.4	20.5	22.0	21.6	20.4	20.6
7 Day	MPa	27.2	26.2	24.8	25.8	26.5	27.7	27.9	28.4	28.5	28.8	28.8	27.0	27.0
28 Day	MPa	40.6	37.1	38.2	40.3	39.1	42.8	41.7	42.6	41.2	42.8	44.2		

Manufactured cement conforms to CSA Standard A3001-13.

No adjustment has been made for possible use of limestone or inorganic processing addition.

Date: July 16, 2015

Table 4. Mill Test Certificate for InterCem (CSA Blended Portland cement Type HSb-30F)

LEHIGH
HEIDELBERGCEMENT Group

Lehigh Cement
12640 Inland Way
Edmonton, AB T5V 1K2
Phone 780-420-2500
Fax 780-420-2665
www.LehighHansonCanada.com

MILL TEST CERTIFICATE FOR INTERCEM (CSA BLENDED PORTLAND CEMENT TYPE HSb-30F)

Production for Week Ending 2015:		05-Apr	12-Apr	19-Apr	26-Apr	03-May	10-May	17-May	24-May	31-May	07-Jun	14-Jun	21-Jun	28-Jun
CHEMICAL ANALYSIS														
SO_3	%	2.75	2.76	2.74	2.68	2.79	2.71	2.65	2.72	2.74	2.70	2.71	2.68	2.70
Loss on Ignition	%	1.45	1.22	1.45	1.36	1.39	1.37	1.27	1.54	1.19	1.43	1.48	1.55	1.52
Alkalis from Clinker (As Na2O)	%	0.37	0.39	0.38	0.38	0.38	0.40	0.37	0.37	0.38	0.37	0.37	0.37	0.37
PHYSICAL PROPERTIES														
Blaine	m^2/kg	550	538	541	538	540	536	534	543	544	541	549	555	553
Retained on 45µ sieve	%	5.22	5.06	5.09	4.63	4.65	4.82	5.20	5.50	5.40	4.99	4.54	4.66	5.22
Autoclave Expansion	%	-0.026	0.004	0.004	0.023	0.023	0.047	0.047	0.006	0.006	0.022	0.027	0.013	0.013
Sulphate Expansion	%													
Vicat Initial Set	min	90	80	80	97	97	87	87	81	81	76	74	72	72
False Set	%	85	73	73	90	90	80	80	93	93	75	69	76	76
Air Content	%	6.90			7.90	7.90			6.80	6.80	6.80		6.60	6.60
1 Day	MPa	10.7	11.8	9.4	10.9	11.8	10.8	11.7	10.6	11.4	11.3	10.4	10.8	10.8
3 Day	MPa	18.3	19.2	16.4	18.0	17.9	17.7	17.2	17.2	16.2	18.1	18.3	17.2	18.5
7 Day	MPa	22.4	23.4	21.6	22.0	22.6	22.6	22.6	21.5	21.5	23.1	23.2	21.6	23.1
28 Day	MPa	35.7	35.0	33.4	35.9	35.9	36.6	37.8	35.8	36.0	36.7	36.3	35.4	

Manufactured cement conforms to CSA Standard A3001-13.

No adjustment has been made for possible use of limestone or inorganic processing addition.

Date: July 16, 2015

Jeff Matchett
Jeff Matchett
Plant Chemist

Table 5. Length Change Measurement (Type GU-Sulfate Exposure)

Sulfate	0W	Reading	Sulfate	1W		Sulfate	2W	
Specimen	Length	Li	Specimen	Length	ΔL (%)	Specimen	Length	ΔL (%)
Ref 1	652		Ref 1	652		Ref 1	652	
1	1718	1066	0	1721	0.003048	1	1723	0.00508
2	2043	1391	0	2046	0.003048	2	2049	0.006096
3	1871	1219	0	1873	0.002032	3	1875	0.004064

4	1011	359	0	1015	0.004064	4	1017	0.006096
5	1727	1075	0	1729	0.002032	5	1739	0.012192
6	603	-49	0	603	0	6	605	0.002032
Ref 2	651		Ref 2	652		Ref 2	652	
pH=7.79			pH=7.71			pH=7.78		
AVE					0.0023707			0.0059267
Sulfate	4W		Sulfate	8W		Sulfate	12W	
Specimen	Length	ΔL (%)	Specimen	Length	ΔL (%)	Specimen	Length	ΔL (%)
Ref 1	649		Ref 1	649		Ref 1	649	
1	1715	0	1	1727	0.012192	1	1730	0.01524
2	2046	0.006096	2	2052	0.012192	2	2055	0.01524
3	1875	0.007112	3	1877	0.009144	3	1881	0.013208
4	1013	0.00508	4	1015	0.007112	4	1016	0.008128
5	1727	0.003048	5	1731	0.007112	5	1733	0.009144
6	612	0.012192	6	615	0.01524	6	616	0.016256
Ref 2	650		Ref 2	649		Ref 2	649	
pH=7.73			pH=7.7			pH=7.7		
AVE		0.005588			0.0104987			0.0128693

Table 6. Length Change Measurement (Type GU-Water Immersion)

Water	0W		Water	1W		Water	2W	
Specimen	Length	Li	Specimen	Length	ΔL (%)	Specimen	Length	ΔL (%)
Ref 1	652		Ref 1	652		Ref 1	652	
1	37	-615	1	32	-0.00508	1	35	-0.002032
2	2066	1414	2	2066	0	2	2068	0.002032
3	2134	1482	3	2137	0.003048	3	2135	0.001016
4	1997	1345	4	1996	-0.001016	4	1996	-0.001016
5	2414	1762	5	2412	-0.002032	5	2413	-0.001016
6	2210	1558	6	2202	-0.008128	6	2205	-0.00508
7	24	-628	7	24	0	7	24	0
8	1922	1270	8	1923	0.001016	8	1925	0.003048
Ref 2	653		Ref 2	652	0	Ref 2	652	
Water	4W		Water	8W		Water	12W	
Specimen	Length	ΔL (%)	Specimen	Length	ΔL (%)	Specimen	Length	ΔL (%)
Ref 1	649		Ref 1	649		Ref 1	646	
1	39	0.00508	1	36	0.002032	1	40	0.009144

2	2069	0.006096	2	2070	0.007112	2	2067	0.007112
3	2133	0.002032	3	2135	0.004064	3	2133	0.00508
4	1996	0.002032	4	1998	0.004064	4	1996	0.00508
5	2410	-0.001016	5	2411	0	5	2410	0.002032
6	2209	0.002032	6	2211	0.004064	6	2209	0.00508
7	24	0.003048	7	27	0.006096	7	26	0.008128
8	1927	0.008128	8	1929	0.01016	8	1924	0.008128
Ref 2	649		Ref 2	649		Ref 2	646	

Table 7. Length Change Measurement (Type HS-Water Immersion)

Water	0W		Water	1W		Water	2W	
Specimen	Length	Li	Specimen	Length	ΔL (%)	Specimen	Length	ΔL (%)
Ref 1	652		Ref 1	649		Ref 1	649	
1	1064	412	1	1060	-0.001016	1	1066	0.00508
2	1406	754	2	1399	-0.004064	2	1404	0.001016
3	2002	1350	3	1998	-0.001016	3	2000	0.001016
4	1458	806	4	1454	-0.001016	4	1459	0.004064
5	2285	1633	5	2282	0	5	2284	0.002032
6	2193	1541	6	2193	0.003048	6	2195	0.00508
Ref 2	652		Ref 2	649		Ref 2	650	
Ave		0			-0.000677			0.003048
Water	4W		Water	8W		Water	12W	
Specimen	Length	ΔL (%)	Specimen	Length	ΔL (%)	Specimen	Length	ΔL (%)
Ref 1	649		Ref 1	649		Ref 1	647	
1	1069	0.008128	1	1069	0.008128	1	1064	0.00508
2	1404	0.001016	2	1405	0.002032	2	1404	0.003048
3	1997	-0.002032	3	2005	0.006096	3	2010	0.013208
4	1457	0.002032	4	1462	0.007112	4	1468	0.01524
5	2280	-0.002032	5	2288	0.006096	5	2294	0.014224
6	2190	0	6	2200	0.01016	6	2198	0.01016
Ref 2	652		Ref 2	649		Ref 2		
		0.0011853			0.006604			0.01016

Table 8. Length Change Measurement (Type HS-Sulfate Exposure)

Sulfate	0W		Sulfate	1W		Sulfate	2W	
Specimen	Length	Li	Specimen	Length	ΔL (%)	Specimen	Length	ΔL (%)
Ref 1	652		Ref 1	650		Ref 1	649	
1	2400	1748	1	2401	0.003048	1	2404	0.007112
2	2179	1527	2	2179	0.002032	2	2174	-0.002032
3	1514	862	3	1515	0.003048	3	1516	0.00508
4	2210	1558	4	2210	0.002032	4	2208	0.001016
5	1956	1304	5	1952	-0.002032	5	1955	0.002032
6	1504	852	6	1503	0.001016	6	1501	0
Ref 2	652		Ref 2	650		Ref 2	650	
pH=7.77			pH=7.51			pH=7.60		
Sulfate	4W		Sulfate	8W		Sulfate	12W	
Specimen	Length	ΔL (%)	Specimen	Length	ΔL (%)	Specimen	Length	ΔL (%)
Ref 1	645		Ref 1	649		Ref 1	647	
1	2394	0.001016	1	2406	0.009144	1	2407	0.012192
2	2171	-0.001016	2	2185	0.009144	2	2186	0.012192
3	1512	0.00508	3	1520	0.009144	3	1520	0.011176
4	2202	-0.001016	4	2214	0.007112	4	2213	0.008128
5	1950	0.001016	5	1958	0.00508	5	1959	0.008128
6	1496	-0.001016	6	1508	0.007112	6	1515	0.016256
Ref 2	645		Ref 2	650		Ref 2	647	
pH=7.54			pH=7.62			pH=7.58		

Table 9. Length Change Measurement (Blend IC-Water Immersion)

Water	0W		Water	1W		Water	2W	
Specimen	Length	Li	Specimen	Length	ΔL (%)	Specimen	Length	ΔL (%)
Ref 1	650		Ref 1	650		Ref 1	649	
1	2190	1540	1	2195	0.00508	1	2198	0.009144
2	167	-483	2	169	0.002032	2	171	0.00508
3	2171	1521	3	2172	0.001016	3	2174	0.004064
4	1271	621	4	1269	-0.002032	4	1272	0.002032
5	1885	1235	5	1886	0.001016	5	1884	0
6	1758	1108	6	1764	0.006096	6	1761	0.004064
Ref 2	651		Ref 2	650		Ref 2	650	
Water	4W		Water	8W		Water	12W	
Specimen	Length	ΔL (%)	Specimen	Length	ΔL (%)	Specimen	Length	ΔL (%)

Ref 1	649		Ref 1	649		Ref 1	647	
1	2195	0.006096	1	2194	0.00508	1	2200	0.013208
2	170	0.004064	2	170	0.004064	2	172	0.008128
3	2174	0.004064	3	2174	0.004064	3	2177	0.009144
4	1270	0	4	1271	0.001016	4	1275	0.007112
5	1883	-0.001016	5	1886	0.002032	5	1889	0.007112
6	1764	0.007112	6	1766	0.009144	6	1764	0.009144
Ref 2	650		Ref 2	649		Ref 2	647	

Table 10. Length Change Measurement (Blend IC-Sulfate Exposure)

Sulfate	0W		Sulfate	1W		Sulfate	2W	
Specimen	Length	Li	Specimen	Length	ΔL (%)	Specimen	Length	ΔL (%)
Ref 1	652		Ref 1	650		Ref 1	649	
1	2155	1503	1	2156	0.003048	1	2156	0.004064
2	1310	658	2	1318	0.01016	2	1318	0.011176
3	1933	1281	3	1937	0.006096	3	1936	0.006096
4	1085	433	4	1090	0.007112	4	1090	0.008128
5	78	-574	5	80	0.004064	5	79	0.004064
6	1957	1305	6	1961	0.006096	6	1962	0.008128
Ref 2	651		Ref 2	650		Ref 2	649	
pH=7.72			pH=7.55			pH=7.56		
Sulfate	4W		Sulfate	8W		Sulfate	12W	
Specimen	Length	ΔL (%)	Specimen	Length	ΔL (%)	Specimen	Length	ΔL (%)
Ref 1	651		Ref 1	650		Ref 1	647	
1	2159	0.00508	1	2161	0.008128	1	2167	0.017272
2	1315	0.006096	2	1324	0.016256	2	1325	0.02032
3	1936	0.004064	3	1941	0.01016	3	1945	0.017272
4	1090	0.006096	4	1097	0.014224	4	1103	0.023368
5	80	0.003048	5	85	0.009144	5	89	0.016256
6	1961	0.00508	6	1968	0.013208	6	1971	0.019304
Ref 2	651		Ref 2	650		Ref 2	647	
pH=	7.53		pH=	7.7		pH=		

Table 11. Sample Calculation for Compressive Strength (Type GU)

Water	0W		Water	1W		Water	2W	

Specimen	Strength(MPa)	Force(kN)	Specimen	Strength(MPa)	Force(kN)	Specimen	Strength(MPa)	Force(kN)
1	41.599289	183.78	1	42.916667	189.6	1	44.673172	197.36
2	42.074632	185.88	2	44.120869	194.92	2	48.285778	213.32
3	44.071071	194.7	3	47.258132	208.78	3	48.53024	214.4
AVE	42.581664			44.765223			47.163063	
	0W		Sulfate	1W		Sulfate	2W	
Specimen	Strength(MPa)	Force(kN)	Specimen	Strength(MPa)	Force(kN)	Specimen	Strength(MPa)	Force(kN)
1	41.599289	183.78	1	45.972443	203.1	1	47.457323	209.66
2	42.074632	185.88	2	48.168074	212.8	2	52.944138	233.9
3	44.071071	194.7	3	49.173085	217.24	3	53.894823	238.1
AVE	42.581664			47.7712			51.432095	
Water	4W		Water	8W		Water	12W	
Specimen	Strength(MPa)	Force(kN)	Specimen	Strength(MPa)	Force(kN)	Specimen	Strength(MPa)	Force(kN)
1	49.105178	216.94	1	47.402998	209.42	1	51.088037	225.7
2	50.218839	221.86	2	56.022548	247.5	2	55.144296	243.62
3	50.327489	222.34	3	56.633704	250.2	3	58.521494	258.54
	49.883835			53.353083			54.917942	
Sulfate	4W		Sulfate	8W		Sulfate	12W	
Specimen	Strength(MPa)	Force(kN)	Specimen	Strength(MPa)	Force(kN)	Specimen	Strength(MPa)	Force(kN)
1	51.576961	227.86	1	47.294349	208.94	1	58.091422	256.64
2	51.631286	228.1	2	52.260549	230.88	2	59.173392	261.42
3	55.41592	244.82	3	59.829818	264.32	3	59.621573	263.4
	52.874723			53.128239			58.962129	

Table 12. Sample Calculation for Splitting Tensile Strength (Type GU)

	0W		Water	1W		Water	2W	
Specimen	Strength(MPa)	Force(kN)	Specimen	Strength(MPa)	Force(kN)	Specimen	Strength(MPa)	Force(kN)
1	3.9725088	31.2	1	3.9190327	30.78	1	4.2118779	33.08
2	4.015799	31.54	2	4.1915061	32.92	2	4.5021766	35.36
3	4.2093314	33.06	3	4.329016	34	3	4.6091288	36.2
AVE	4.0658797			4.1465183			4.4410611	
	0W		Sulfate	1W		Sulfate	2W	
Specimen	Strength(MPa)	Force(kN)	Specimen	Strength(MPa)	Force(kN)	Specimen	Strength(MPa)	Force(kN)
1	3.9725088	31.2	1	4.3519343	34.18	1	4.13803	32.5
2	4.015799	31.54	2	4.7721035	37.48	2	4.4741654	35.14
3	4.2093314	33.06	3	4.8204866	37.86	3	4.7542782	37.34
AVE	4.0658797			4.6481748			4.4554912	

Water	4W		Water	8W		Water	12W	
Specimen	Strength(MPa)	Force(kN)	Specimen	Strength(MPa)	Force(kN)	Specimen	Strength(MPa)	Force(kN)
1	4.5123626	35.44	1	4.6804302	36.76	1	4.9681825	39.02
2	4.7924754	37.64	2	4.716081	37.04	2	5.3807122	42.26
3	5.1184248	40.2	3	4.7313598	37.16	3	5.6633715	44.48
	4.8077542			4.7092903			5.3374221	
Sulfate	4W		Sulfate	8W		Sulfate	12W	
Specimen	Strength(MPa)	Force(kN)	Specimen	Strength(MPa)	Force(kN)	Specimen	Strength(MPa)	Force(kN)
1	4.5862105	36.02	1	4.5352809	35.62	1	4.710988	37
2	4.769557	37.46	2	4.5403738	35.66	2	4.8994275	38.48
3	4.9045205	38.52	3	4.9961938	39.24	3	5.4087235	42.48
	4.7534293			4.6906162			5.0063797	

Table 13. Sample Calculation for Compressive Strength (Type HS)

Water	0W		Water	1W		Water	2W	
Specimen	Strength(MPa)	Force(kN)	Specimen	Strength(MPa)	Force(kN)	Specimen	Strength(MPa)	Force(kN)
1	42.038415	185.72	1	36.184907	159.86	1	39.666228	175.24
2	43.736068	193.22	2	39.946906	176.48	2	40.458466	178.74
3	47.194753	208.5	3	40.277383	177.94	3	40.942863	180.88
AVE	44.323079			38.803066			40.355852	
Sulfate	0W		Sulfate	1W		Sulfate	2W	
Specimen	Strength(MPa)	Force(kN)	Specimen	Strength(MPa)	Force(kN)	Specimen	Strength(MPa)	Force(kN)
1	42.038415	185.72	1	23.359705	103.2	1	37.796546	166.98
2	43.736068	193.22	2	36.279976	160.28	2	39.208993	173.22
3	47.194753	208.5	3	44.849728	198.14	3	40.979079	181.04
AVE	44.323079			40.564852			39.328206	
Water	4W		Water	8W		Water	12W	
Specimen	Strength(MPa)	Force(kN)	Specimen	Strength(MPa)	Force(kN)	Specimen	Strength(MPa)	Force(kN)
1	39.72508	175.5	1	49.331532	217.94	1	40.290964	178
2	44.473981	196.48	2	53.283668	235.4	2	45.008176	198.84
3	45.637439	201.62	3	54.533141	240.92	3	55.017538	243.06
	43.278833			52.38278			46.772226	206.63333
Sulfate	4W		Sulfate	8W		Sulfate	12W	
Specimen	Strength(MPa)	Force(kN)	Specimen	Strength(MPa)	Force(kN)	Specimen	Strength(MPa)	Force(kN)
1	40.847794	180.46	1	51.232904	226.34	1	44.795403	197.9
2	46.244067	204.3	2	57.249386	252.92	2	45.157569	199.5
3	47.697258	210.72	3	58.503385	258.46	3	48.367265	213.68

44.929707			55.661892			46.106746	203.69333

Table 14. Sample Calculation for Splitting Tensile Strength (Type HS)

	0W		Water	1W		Water	2W	
Specimen	Strength(MPa)	Force(kN)	Specimen	Strength(MPa)	Force(kN)	Specimen	Strength(MPa)	Force(kN)
1	4.0539962	31.84	1	3.9776018	31.24	1	4.0234384	31.6
2	4.1049258	32.24	2	4.206785	33.04	2	4.1736807	32.78
3	5.087867	39.96	3	4.3010047	33.78	3	4.7924754	37.64
AVE	4.4155963		AVE	4.1617971		AVE	4.3298648	
	0W		Sulfate	1W		Sulfate	2W	
Specimen	Strength(MPa)	Force(kN)	Specimen	Strength(MPa)	Force(kN)	Specimen	Strength(MPa)	Force(kN)
1	4.0539962	31.84	1	3.687303	28.96	1	3.7535115	29.48
2	4.1049258	32.24	2	3.8731961	30.42	2	3.9012074	30.64
3	5.087867	39.96	3	3.9750553	31.22	3	4.201692	33
AVE	4.4155963		AVE	3.8451848		AVE	3.952137	
Water	4W		Water	8W		Water	12W	
Specimen	Strength(MPa)	Force(kN)	Specimen	Strength(MPa)	Force(kN)	Specimen	Strength(MPa)	Force(kN)
1	3.9801482	31.26	1	4.6600584	36.6	1	3.7713369	29.62
2	4.3392019	34.08	2	4.8281261	37.92	2	4.3111906	33.86
3	4.4155963	34.68	3	4.9427177	38.82	3	4.7721035	37.48
AVE	4.2449822		AVE	4.8103007		AVE	4.284877	
Sulfate	4W		Sulfate	8W		Sulfate	12W	
Specimen	Strength(MPa)	Force(kN)	Specimen	Strength(MPa)	Force(kN)	Specimen	Strength(MPa)	Force(kN)
1	4.2857258	33.66	1	4.0896469	32.12	1	4.0387173	31.72
2	4.5276414	35.56	2	4.2729934	33.56	2	4.3060977	33.82
3	4.8153937	37.82	3	4.6931626	36.86	3	4.6040358	36.16
AVE	4.5429203		AVE	4.3519343		AVE	4.3162836	

Table 15. Sample Calculation for Compressive Strength (Blend IC)

	0W		Water	1W		Water	2W	
Specimen	Strength(MPa)	Force(kN)	Specimen	Strength(MPa)	Force(kN)	Specimen	Strength(MPa)	Force(kN)
1	40.503737	178.94	1	36.47464	161.14	1	39.086762	172.68

	0W							
2	41.010769	181.18	2	36.796063	162.56	2	40.236639	177.76
3	41.472531	183.22	3	37.429853	165.36	3	42.699368	188.64
AVE	40.995679			36.900185			40.674256	
	0W		Sulfate	1W		Sulfate	2W	
Specimen	Strength(MPa)	Force(kN)	Specimen	Strength(MPa)	Force(kN)	Specimen	Strength(MPa)	Force(kN)
1	40.503737	178.94	1	40.766307	180.1	1	40.87043	180.56
2	41.010769	181.18	2	40.793469	180.22	2	41.31861	182.54
3	41.472531	183.22	3	42.210444	186.48	3	42.916667	189.6
AVE	40.995679			41.25674			41.701902	
Water	4W		Water	8W		Water	12W	
Specimen	Strength(MPa)	Force(kN)	Specimen	Strength(MPa)	Force(kN)	Specimen	Strength(MPa)	Force(kN)
1	37.656207	166.36	1	49.843092	220.2	1	47.742529	210.92
2	38.231145	168.9	2	50.626276	223.66	2	50.6806	223.9
3	40.73009	179.94	3	51.477366	227.42	3	53.491914	236.32
AVE	38.872481			50.648911			50.638348	
Sulfate	4W		Sulfate	8W		Sulfate	12W	
Specimen	Strength(MPa)	Force(kN)	Specimen	Strength(MPa)	Force(kN)	Specimen	Strength(MPa)	Force(kN)
1	42.862343	189.36	1	49.317951	217.88	1	46.760154	206.58
2	46.470421	205.3	2	52.387308	231.44	2	55.216729	243.94
3	49.322478	217.9	3	52.713257	232.88	3	N/A	
AVE	46.218414			51.472838			50.988441	

Table 16. Sample Calculation for Splitting Tensile Strength (Blend IC)

	0W		Water	1W		Water	2W	
Specimen	Strength(MPa)	Force(kN)	Specimen	Strength(MPa)	Force(kN)	Specimen	Strength(MPa)	Force(kN)
1	3.8655566	30.36	1	3.947044	31	1	3.8681031	30.38
2	3.9444975	30.98	2	4.1456694	32.56	2	4.2322498	33.24
3	4.010706	31.5	3	4.7415458	37.24	3	4.3111906	33.86
AVE	3.9402534			4.2780864			4.1371812	
	0W		Sulfate	1W		Sulfate	2W	
Specimen	Strength(MPa)	Force(kN)	Specimen	Strength(MPa)	Force(kN)	Specimen	Strength(MPa)	Force(kN)
1	3.8655566	30.36	1	4.1227511	32.38	1	4.13803	32.5
2	3.9444975	30.98	2	4.2449822	33.34	2	4.2908188	33.7
3	4.010706	31.5	3	4.588757	36.04	3	4.323923	33.96
AVE	3.9402534			4.3188301			4.2509239	
Water	4W		Water	8W		Water	12W	

Specimen	Strength(MPa)	Force(kN)	Specimen	Strength(MPa)	Force(kN)	Specimen	Strength(MPa)	Force(kN)
1	4.074368	32	1	4.206785	33.04	1	4.3162836	33.9
2	4.2220638	33.16	2	4.4079569	34.62	2	4.4792583	35.18
3	4.4996302	35.34	3	4.4436076	34.9	3	4.8179402	37.84
AVE	4.265354			4.3527831			4.5378274	
Sulfate	4W		Sulfate	8W		Sulfate	12W	
Specimen	Strength(MPa)	Force(kN)	Specimen	Strength(MPa)	Force(kN)	Specimen	Strength(MPa)	Force(kN)
1	4.3646667	34.28	1	4.5276414	35.56	1	5.1540755	40.48
2	4.3646667	34.28	2	4.9147064	38.6	2	5.533501	43.46
3	5.0267515	39.48	3	5.2330164	41.1	3	5.6735574	44.56
AVE	4.5853617			4.8917881			5.4537113	

Chapter 4: Sample Extraction

Table 1. Extraction Measurements and Equivalent Depths Calculation (Blend IC-12 weeks)

ICS-12		A_i (mm)	B_{i1}(mm)	B_{i2}(mm)	h(mm)	H(mm)	V_i/A(mm)	x_i(mm)
Layer-1	Hole-1	4.20	2.76	2.97	2.8650	1.3350	3.3100	1.6700
	Hole-2	3.58	2.05	2.06	2.0550	1.5250	2.5633	1.3069
	Hole-3	3.53	2.67	2.63	2.6500	0.8800	2.9433	1.4790
	Hole-4	3.80	2.56	2.59	2.5750	1.2250	2.9833	1.5056

	AVE	3.78	2.51	2.56	2.54	1.24	2.9500	1.4904
Layer-2	Hole-1	5.89	4.36	4.31	4.3350	1.5550	4.8533	2.4405
	Hole-2	5.65	4.23	4.37	4.3000	1.3500	4.7500	2.3857
	Hole-3	5.44	4.10	4.04	4.0700	1.3700	4.5267	2.2749
	Hole-4	5.46	4.16	4.34	4.2500	1.2100	4.6533	2.3354
	AVE	5.61	4.21	4.27	4.24	1.37	4.6958	2.3591
Layer-3	Hole-1	8.02	6.32	6.62	6.4700	1.5500	6.9867	3.5029
	Hole-2	7.85	6.27	6.58	6.4250	1.4250	6.9000	3.4582
	Hole-3	8.06	6.65	6.72	6.6850	1.3750	7.1433	3.5790
	Hole-4	8.16	6.40	7.96	7.1800	0.9800	7.5067	3.7569
	AVE	8.02	6.41	6.97	6.69	1.33	7.1342	3.5742
Layer-4	Hole-1	9.89	8.39	8.28	8.3350	1.5550	8.8533	4.4343
	Hole-2	9.30	8.64	8.50	8.5700	0.7300	8.8133	4.4083
	Hole-3	9.95	9.06	9.10	9.0800	0.8700	9.3700	4.6872
	Hole-4	9.73	9.05	9.02	9.0350	0.6950	9.2667	4.6348
	AVE	9.72	8.79	8.73	8.76	0.96	9.0758	4.5412
Layer-5	Hole-1	12.31	10.84	10.35	10.5950	1.7150	11.1667	5.5906
	Hole-2	11.92	10.97	11.15	11.0600	0.8600	11.3467	5.6751
	Hole-3	12.27	11.17	11.51	11.3400	0.9300	11.6500	5.8271
	Hole-4	12.11	11.02	10.54	10.7800	1.3300	11.2233	5.6160
	AVE	12.15	11.00	10.89	10.94	1.21	11.3467	5.6772

Table 2. Extraction Measurements and Equivalent Depths Calculation (Blend IC-8 weeks)

ICS-8		A_i(mm)	B_{i1}(mm)	B_{i2}(mm)	h(mm)	H(mm)	V_i/A(mm)	x_i(mm)
Layer-1	Hole-1	3.35	2.25	1.85	2.0500	1.3000	2.4833	1.2606
	Hole-2	3.12	1.95	1.92	1.9350	1.1850	2.3300	1.1817
	Hole-3	3.67	2.43	2.35	2.3900	1.2800	2.8167	1.4245
	Hole-4	3.62	2.57	2.22	2.3950	1.2250	2.8033	1.4165
	Hole-5	3.02	1.90	2.38	2.1400	0.8800	2.4333	1.2255
	AVE	3.36	2.22	2.14	2.18	1.17	2.5733	1.3018

Layer-2	Hole-1	6.26	4.95	5.04	4.9950	1.2650	5.4167	2.7165
	Hole-2	5.97	4.62	4.58	4.6000	1.3700	5.0567	2.5386
	Hole-3	6.38	5.03	4.77	4.9000	1.4800	5.3933	2.7079
	Hole-4	6.05	4.91	4.86	4.8850	1.1650	5.2733	2.6438
	AVE	6.17	4.88	4.81	4.85	1.32	5.2850	2.6517
Layer-3	Hole-1	9.46	8.69	8.87	8.7800	0.6800	9.0067	4.5048
	Hole-2	9.24	8.39	8.30	8.3450	0.8950	8.6433	4.3242
	Hole-3	9.99	8.98	8.98	8.9800	1.0100	9.3167	4.6614
	Hole-4	9.23	8.19	8.71	8.4500	0.7800	8.7100	4.3569
	AVE	9.48	8.56	8.72	8.64	0.84	8.9192	4.4618
Layer-4	Hole-1	13.28	12.25	12.25	12.2500	1.0300	12.5933	6.2990
	Hole-2	damaged						
	Hole-3							
	Hole-4							
	AVE						12.5933	6.2990

Table 3. Extraction Measurements and Equivalent Depths Calculation (Blend IC-4 weeks)

ICS-4		A_i(mm)	B_{i1}(mm)	B_{i2}(mm)	h(mm)	H(mm)	V_i/A(mm)	x_i(mm)
Layer-1	Hole-1	3.07	1.75	2.01	1.8800	1.1900	2.2767	1.1556
	Hole-2	3.14	1.71	2.12	1.9150	1.2250	2.3233	1.1796
	Hole-3	2.67	1.65	1.86	1.7550	0.9150	2.0600	1.0413
	Hole-4	3.63	1.79	2.59	2.1900	1.4400	2.6700	1.3566
	AVE	3.13	1.73	2.15	1.94	1.19	2.3325	1.1833
Layer-2	Hole-1	5.34	4.27	4.42	4.3450	0.9950	4.6767	2.3442
	Hole-2	5.29	4.21	4.27	4.2400	1.0500	4.5900	2.3017
	Hole-3	5.30	4.08	4.59	4.3350	0.9650	4.6567	2.3339
	Hole-4	4.95	3.25	4.17	3.7100	1.2400	4.1233	2.0720
	AVE	5.22	3.95	4.36	4.16	1.06	4.5117	2.2629
Layer-3	Hole-1	7.77	6.89	7.26	7.0750	0.6950	7.3067	3.6552
	Hole-2	8.27	7.41	7.65	7.5300	0.7400	7.7767	3.8903
	Hole-3	7.71	6.51	6.97	6.7400	0.9700	7.0633	3.5354
	Hole-4	7.65	6.54	6.66	6.6000	1.0500	6.9500	3.4794
	AVE	7.85	6.84	7.14	6.99	0.86	7.2742	3.6401
Layer-4	Hole-1	10.22	9.29	10.02	9.6550	0.5650	9.8433	4.9226
	Hole-2	10.06	8.47	8.88	8.6750	1.3850	9.1367	4.5742
	Hole-3	10.39	8.84	9.16	9.0000	1.3900	9.4633	4.7373
	Hole-4	10.08	8.95	9.42	9.1850	0.8950	9.4833	4.7440

| AVE | | 10.19 | 8.89 | 9.37 | 9.13 | 1.06 | 9.4817 | 4.7445 |

Table 4. Extraction Measurements and Equivalent Depths Calculation (Blend IC-2 weeks)

ICS-2		A_i(mm)	B_{i1}(mm)	B_{i2}(mm)	h(mm)	H(mm)	V_i/A(mm)	x_i(mm)
Layer-1	Hole-1	3.70	2.31	2.47	2.3900	1.3100	2.8267	1.4302
	Hole-2	3.52	1.88	2.43	2.1550	1.3650	2.6100	1.3248
	Hole-3	3.44	1.97	2.76	2.3650	1.0750	2.7233	1.3735
	Hole-4	4.15	3.22	3.33	3.2750	0.8750	3.5667	1.7893
	AVE	3.70	2.35	2.75	2.55	1.16	2.9317	1.4794
Layer-2	Hole-1	7.40	6.32	6.43	6.3750	1.0250	6.7167	3.3627
	Hole-2	7.68	6.21	7.29	6.7500	0.9300	7.0600	3.5334
	Hole-3	8.40	7.55	7.99	7.7700	0.6300	7.9800	3.9914
	Hole-4	7.62	6.77	6.83	6.8000	0.8200	7.0733	3.5393
	AVE	7.78	6.71	7.14	6.92	0.85	7.2075	3.6067
Layer-3	Hole-1	Damaged						
	Hole-2							
	Hole-3	10.44	9.49	10.35	9.9200	0.5200	10.0933	5.0474
	Hole-4	10.65	9.88	10.04	9.9600	0.6900	10.1900	5.0963
	AVE	10.55	9.69	10.20	9.94	0.61	10.1417	5.0719

Table 5. Extraction Measurements and Equivalent Depths Calculation (Blend IC-1 week)

ICS-1		A_i(mm)	B_{i1}(mm)	B_{i2}(mm)	h(mm)	H(mm)	V_i/A(mm)	x_i(mm)
Layer-1	Hole-1	5.27	3.63	3.76	3.6950	1.5750	4.2200	2.1263
	Hole-2	4.96	3.56	3.37	3.4650	1.4950	3.9633	1.9973
	Hole-3	5.23	4.08	4.16	4.1200	1.1100	4.4900	2.2526
	Hole-4	5.75	4.21	4.86	4.5350	1.2150	4.9400	2.4783
	AVE	5.30	3.87	4.04	3.95	1.35	4.4033	2.2136
Layer-2	Hole-1	8.17	7.17	6.90	7.0350	1.1350	7.4133	3.7115
	Hole-2	8.44	6.82	7.07	6.9450	1.4950	7.4433	3.7300
	Hole-3	8.36	6.87	6.83	6.8500	1.5100	7.3533	3.6853
	Hole-4	8.24	7.03	6.99	7.0100	1.2300	7.4200	3.7157
	AVE	8.30	6.97	6.95	6.96	1.34	7.4075	3.7106
Layer-3	Hole-1	10.47	10.03	10.17	10.1000	0.3700	10.2233	5.1120
	Hole-2	10.51	9.53	9.80	9.6650	0.8450	9.9467	4.9753
	Hole-3	11.18	9.41	9.99	9.7000	1.4800	10.1933	5.1026
	Hole-4	10.49	9.46	9.58	9.5200	0.9700	9.8433	4.9243

		A_i(mm)	B_{i1}(mm)	B_{i2}(mm)	h(mm)	H(mm)	V_i/A(mm)	x_i(mm)
	AVE	10.66	9.61	9.89	9.75	0.92	10.0517	5.0286

Table 6. Extraction Measurements and Equivalent Depths Calculation (Type HS-12 weeks)

HSS-12		A_i(mm)	B_{i1}(mm)	B_{i2}(mm)	h(mm)	H(mm)	V_i/A(mm)	x_i(mm)
Layer-1	Hole-1	3.51	2.83	2.61	2.7200	0.7900	2.9833	1.4975
	Hole-2	3.88	2.55	2.34	2.4450	1.4350	2.9233	1.4812
	Hole-3	3.74	2.57	2.48	2.5250	1.2150	2.9300	1.4790
	Hole-4	3.69	2.44	2.88	2.6600	1.0300	3.0033	1.5115
	AVE	3.71	2.60	2.58	2.59	1.12	2.9600	1.4923
Layer-2	Hole-1	6.03	4.47	5.16	4.8150	1.2150	5.2200	2.6179
	Hole-2	6.13	4.77	5.13	4.9500	1.1800	5.3433	2.6789
	Hole-3	5.70	4.97	4.49	4.7300	0.9700	5.0533	2.5318
	Hole-4	6.29	5.50	4.92	5.2100	1.0800	5.5700	2.7908
	AVE	6.04	4.93	4.93	4.93	1.11	5.2967	2.6549
Layer-3	Hole-1	8.13	6.74	6.87	6.8050	1.3250	7.2467	3.6301
	Hole-2	7.97	6.55	7.44	6.9950	0.9750	7.3200	3.6636
	Hole-3	8.44	7.17	7.11	7.1400	1.3000	7.5733	3.7929
	Hole-4	8.70	7.92	8.00	7.9600	0.7400	8.2067	4.1052
	AVE	8.31	7.10	7.36	7.23	1.09	7.5867	3.7979
Layer-4	Hole-1	12.30	11.14	11.30	11.2200	1.0800	11.5800	5.7928
	Hole-2	11.82	10.59	10.99	10.7900	1.0300	11.1333	5.5693
	Hole-3	11.63	10.17	10.65	10.4100	1.2200	10.8167	5.4122
	Hole-4	12.08	10.92	11.21	11.0650	1.0150	11.4033	5.7042
	AVE	11.96	10.71	11.04	10.87	1.09	11.2333	5.6196

Table 7. Extraction Measurements and Equivalent Depths Calculation (Type HS-8 weeks)

HSS-8		A_i(mm)	B_{i1}(mm)	B_{i2}(mm)	h(mm)	H(mm)	V_i/A(mm)	x_i(mm)
Layer-1	Hole-1	3.69	2.14	2.62	2.3800	1.3100	2.8167	1.4253
	Hole-2	3.46	1.79	2.17	1.9800	1.4800	2.4733	1.2613
	Hole-3	3.81	2.05	2.10	2.0750	1.7350	2.6533	1.3582
	Hole-4	3.90	2.96	3.20	3.0800	0.8200	3.3533	1.6822
	AVE	3.72	2.24	2.52	2.38	1.34	2.8242	1.4317
Layer-2	Hole-1	6.18	4.81	4.79	4.8000	1.3800	5.2600	2.6401
	Hole-2	5.50	3.99	4.04	4.0150	1.4850	4.5100	2.2686
	Hole-3	5.86	4.14	4.60	4.3700	1.4900	4.8667	2.4460
	Hole-4	5.98	4.35	4.66	4.5050	1.4750	4.9967	2.5104

	AVE	5.88	4.32	4.52	4.42	1.46	4.9083	2.4663
Layer-3	Hole-1	8.44	6.96	7.10	7.0300	1.4100	7.5000	3.7574
	Hole-2	9.01	7.37	7.35	7.3600	1.6500	7.9100	3.9646
	Hole-3	7.76	6.21	6.32	6.2650	1.4950	6.7633	3.3908
	Hole-4	8.25	7.35	7.45	7.4000	0.8500	7.6833	3.8443
	AVE	8.37	6.97	7.06	7.01	1.35	7.4642	3.7393
Layer-4	Hole-1	10.51	9.43	9.75	9.5900	0.9200	9.8967	4.9507
	Hole-2	10.78	9.60	9.87	9.7350	1.0450	10.0833	5.0447
	Hole-3	10.45	9.07	9.03	9.0500	1.4000	9.5167	4.7641
	Hole-4	10.20	9.38	9.00	9.1900	1.0100	9.5267	4.7663
	AVE	10.49	9.37	9.41	9.39	1.09	9.7558	4.8814

Table 8. Extraction Measurements and Equivalent Depths Calculation (Type HS-4 weeks)

HSS-4		A_i(mm)	B_{i1}(mm)	B_{i2}(mm)	h(mm)	H(mm)	V_i/A(mm)	x_i(mm)
Layer-1	Hole-1	3.82	2.55	3.45	3.0000	0.8200	3.2733	1.6424
	Hole-2	3.86	2.03	2.73	2.3800	1.4800	2.8733	1.4578
	Hole-3	3.56	1.96	2.47	2.2150	1.3450	2.6633	1.3505
	Hole-4	3.27	1.69	2.50	2.0950	1.1750	2.4867	1.2588
	AVE	3.63	2.06	2.79	2.42	1.21	2.8242	1.4274
Layer-2	Hole-1	6.65	4.87	5.84	5.3550	1.2950	5.7867	2.9014
	Hole-2	6.33	4.36	5.04	4.7000	1.6300	5.2433	2.6357
	Hole-3	6.19	4.88	5.16	5.0200	1.1700	5.4100	2.7120
	Hole-4	6.37	4.58	5.56	5.0700	1.3000	5.5033	2.7602
	AVE	6.39	4.67	5.40	5.04	1.35	5.4858	2.7523
Layer-3	Hole-1	9.11	7.74	8.71	8.2250	0.8850	8.5200	4.2626
	Hole-2	9.17	8.03	8.56	8.2950	0.8750	8.5867	4.2958
	Hole-3	9.25	7.96	8.86	8.4100	0.8400	8.6900	4.3473
	Hole-4	9.02	7.83	8.65	8.2400	0.7800	8.5000	4.2520
	AVE	9.14	7.89	8.70	8.29	0.84	8.5742	4.2894
Layer-4	Hole-1	11.42	10.21	10.85	10.5300	0.8900	10.8267	5.4154
	Hole-2	10.66	8.99	10.28	9.6350	1.0250	9.9767	4.9913
	Hole-3				N/A			
	Hole-4	11.73	10.11	10.94	10.5250	1.2050	10.9267	5.4670
	AVE	11.27	9.77	10.69	10.23	1.04	10.5767	5.2912

Table 9. Extraction Measurements and Equivalent Depths Calculation (Type HS-2 weeks)

HSS-2		A_i(mm)	B_{i1}(mm)	B_{i2}(mm)	h(mm)	H(mm)	V_i/A(mm)	x_i(mm)
Layer-1	Hole-1	3.64	2.71	2.53	2.6200	1.0200	2.9600	1.4898
	Hole-2	3.49	2.29	2.03	2.1600	1.3300	2.6033	1.3205
	Hole-3	3.97	3.10	3.04	3.0700	0.9000	3.3700	1.6917
	Hole-4	3.95	2.95	2.74	2.8450	1.1050	3.2133	1.6172
	AVE	3.76	2.76	2.59	2.67	1.09	3.0367	1.5298
Layer-2	Hole-1	7.32	5.62	5.69	5.6550	1.6650	6.2100	3.1174
	Hole-2	6.61	5.13	5.04	5.0850	1.5250	5.5933	2.8082
	Hole-3	6.99	5.54	5.78	5.6600	1.3300	6.1033	3.0597
	Hole-4	6.85	5.28	5.60	5.4400	1.4100	5.9100	2.9643
	AVE	6.94	5.39	5.53	5.46	1.48	5.9542	2.9874
Layer-3	Hole-1	10.92	10.04	10.16	10.1000	0.8200	10.3733	5.1885
	Hole-2	11.43	10.39	10.66	10.5250	0.9050	10.8267	5.4154
	Hole-3	10.37	9.09	9.54	9.3150	1.0550	9.6667	4.8365
	Hole-4	10.68	9.95	9.49	9.7200	0.9600	10.0400	5.0225
	AVE	10.85	9.87	9.96	9.92	0.94	10.2267	5.1157

Table 10. Extraction Measurements and Equivalent Depths Calculation (Type HS-1 week)

HSS-1		A_i(mm)	B_{i1}(mm)	B_{i2}(mm)	h(mm)	H(mm)	V_i/A(mm)	x_i(mm)
Layer-1	Hole-1	3.86	2.75	2.65	2.7000	1.1600	3.0867	1.5554
	Hole-2	3.15	2.10	2.26	2.1800	0.9700	2.5033	1.2621
	Hole-3	2.90	1.71	1.77	1.7400	1.1600	2.1267	1.0809
	Hole-4	3.27	2.44	2.15	2.2950	0.9750	2.6200	1.3201
	AVE	3.30	2.25	2.21	2.23	1.07	2.5842	1.3046
Layer-2	Hole-1	7.97	6.87	7.23	7.0500	0.9200	7.3567	3.6815
	Hole-2	7.85	7.12	7.00	7.0600	0.7900	7.3233	3.6640
	Hole-3	8.00	7.17	7.12	7.1450	0.8550	7.4300	3.7177
	Hole-4	7.31	6.12	6.23	6.1750	1.1350	6.5533	3.2821
	AVE	7.78	6.82	6.90	6.86	0.92	7.1658	3.5864
Layer-3	Hole-1	10.45	9.41	9.72	9.5650	0.8850	9.8600	4.9322
	Hole-2	10.17	9.60	9.28	9.4400	0.7300	9.6833	4.8432
	Hole-3	10.59	9.73	9.66	9.6950	0.8950	9.9933	4.9989
	Hole-4	10.11	9.12	9.27	9.1950	0.9150	9.5000	4.7524
	AVE	10.33	9.47	9.48	9.47	0.86	9.7592	4.8817

Table 11. Extraction Measurements and Equivalent Depths Calculation (Type GU-12 weeks)

GUS-12		A_i(mm)	B_{i1}(mm)	B_{i2}(mm)	h(mm)	H(mm)	V_i/A(mm)	x_i(mm)
Layer-1	Hole-1	2.85	1.75	1.72	1.7350	1.1150	2.1067	1.0697
	Hole-2	2.56	1.20	1.30	1.2500	1.3100	1.6867	0.8716
	Hole-3	2.74	1.74	1.77	1.7550	0.9850	2.0833	1.0546
	Hole-4	3.10	1.96	1.60	1.7800	1.3200	2.2200	1.1318
	Hole-5	3.36	2.51	2.37	2.4400	0.9200	2.7467	1.3819
	AVE	2.92	1.83	1.75	1.7920	1.1300	2.1687	1.1007
Layer-2	Hole-1	5.98	4.99	4.68	4.8350	1.1450	5.2167	2.6153
	Hole-2	5.37	4.28	4.18	4.2300	1.1400	4.6100	2.3128
	Hole-3	4.79	3.49	3.16	3.3250	1.4650	3.8133	1.9223
	AVE	5.38	4.25	4.01	4.1300	1.2500	4.5467	2.2829
Layer-3	Hole-1	7.09	5.93	6.17	6.0500	1.0400	6.3967	3.2030
	Hole-2	8.38	7.15	7.28	7.2150	1.1650	7.6033	3.8066
	AVE	7.74	6.54	6.73	6.6325	1.1025	7.0000	3.5048
Layer-4	Hole-1	4.04	2.17	2.29	2.2300	1.8100	2.8333	1.4488
Layer-5	Hole-1	6.38	4.51	4.57	4.5400	1.8400	5.1533	2.5949

Table 12. Extraction Measurements and Equivalent Depths Calculation (Type GU-8 weeks)

GUS-8		A_i(mm)	B_{i1}(mm)	B_{i2}(mm)	h(mm)	H(mm)	V_i/A(mm)	x_i(mm)
Layer-1	Hole-1	6.96	5.93	5.47	5.7000	1.2600	6.1200	3.0672
Layer-2	Hole-1	5.19	4.62	4.10	4.3600	0.8300	4.6367	2.3225
Layer-3	Hole-1	11.45	10.08	10.22	10.1500	1.3000	10.5833	5.2961
							0.0000	#DIV/0!
Layer-4	Hole-1	3.08	2.03	1.44	1.7350	1.3450	2.1833	1.1147
	Hole-2	2.97	1.24	1.83	1.5350	1.4350	2.0133	1.0351
	Hole-3	2.68	1.46	1.19	1.3250	1.3550	1.7767	0.9170
	Hole-4	2.63	1.29	1.25	1.2700	1.3600	1.7233	0.8915
	AVE	2.84	1.51	1.43	1.47	1.37	1.9242	0.9896
Layer-5	Hole-1	4.62	3.99	3.60	3.7950	0.8250	4.0700	2.0396
	Hole-2	4.29	3.11	3.00	3.0550	1.2350	3.4667	1.7456
	Hole-3	4.27	2.96	3.26	3.1100	1.1600	3.4967	1.7590
	Hole-4	4.33	3.20	3.54	3.3700	0.9600	3.6900	1.8519
	AVE	4.3775	3.3150	3.3500	3.3325	1.0450	3.6808	1.8490
Layer-6	Hole-1	6.72	5.55	5.87	5.7100	1.0100	6.0467	3.0280
	Hole-2	6.06	4.47	4.56	4.5150	1.5450	5.0300	2.5282
	Hole-3	5.87	4.64	4.53	4.5850	1.2850	5.0133	2.5158

	Hole-4	6.11	5.28	5.34	5.3100	0.8000	5.5767	2.7915
	AVE	6.19	4.99	5.08	5.03	1.16	5.4167	2.7159
Layer-7	Hole-1	8.45	7.62	7.47	7.5450	0.9050	7.8467	3.9262
	Hole-2	7.66	6.25	6.20	6.2250	1.4350	6.7033	3.3602
	Hole-3	8.20	7.03	6.85	6.9400	1.2600	7.3600	3.6860
	Hole-4	8.08	7.00	6.91	6.9550	1.1250	7.3300	3.6698
	AVE	8.10	6.98	6.86	6.92	1.18	7.3100	3.6606

Table 13. Extraction Measurements and Equivalent Depths Calculation (Type GU-4 weeks)

GUS-4		A_i(mm)	B_{i1}(mm)	B_{i2}(mm)	h(mm)	H(mm)	V_i/A(mm)	x_i(mm)
Layer-1	Hole-1	3.00	2.45	2.05	2.2500	0.7500	2.5000	1.2563
	Hole-2	3.34	2.63	2.43	2.5300	0.8100	2.8000	1.4065
	Hole-3	2.65	1.84	1.89	1.8650	0.7850	2.1267	1.0714
	Hole-4	2.77	1.75	1.66	1.7050	1.0650	2.0600	1.0453
	AVE	2.94	2.17	2.01	2.09	0.85	2.3717	1.1949
Layer-2	Hole-1	6.31	5.18	4.99	5.0850	1.2250	5.4933	2.7543
	Hole-2	5.69	4.66	4.52	4.5900	1.1000	4.9567	2.4851
	Hole-3	4.76	3.66	3.18	3.4200	1.3400	3.8667	1.9462
	Hole-4	5.12	3.90	3.64	3.7700	1.3500	4.2200	2.1220
	AVE	5.47	4.35	4.08	4.22	1.25	4.6342	2.3269
Layer-3	Hole-1	7.67	7.25	7.00	7.1250	0.5450	7.3067	3.6545
	Hole-2	7.22	6.05	6.16	6.1050	1.1150	6.4767	3.2437
	Hole-3	7.44	6.27	6.06	6.1650	1.2750	6.5900	3.3019
	Hole-4	6.95	5.92	5.64	5.7800	1.1700	6.1700	3.0912
	AVE	7.32	6.37	6.22	6.29	1.03	6.6358	3.3228
Layer-4	Hole-1	10.63	9.97	9.58	9.7750	0.8550	10.0600	5.0320
	Hole-2	10.14	8.98	8.75	8.8650	1.2750	9.2900	4.6499
	Hole-3	10.27	9.30	9.09	9.1950	1.0750	9.5533	4.7800
	Hole-4	9.83	8.62	8.74	8.6800	1.1500	9.0633	4.5357
	AVE	10.22	9.22	9.04	9.13	1.09	9.4917	4.7494

Table 14. Extraction Measurements and Equivalent Depths Calculation (Type GU-2 weeks)

GUS-2		A_i(mm)	B_{i1}(mm)	B_{i2}(mm)	h(mm)	H(mm)	V_i/A(mm)	x_i(mm)
Layer-1	Hole-1	3.33	1.98	2.16	2.0700	1.2600	2.4900	1.2627
	Hole-2	3.44	2.23	2.22	2.2250	1.2150	2.6300	1.3306
	Hole-3	3.05	2.21	2.03	2.1200	0.9300	2.4300	1.2249

	Hole-4	2.83	1.82	1.86	1.8400	0.9900	2.1700	1.0975
	AVE	3.16	2.06	2.07	2.06	1.10	2.4300	1.2289
Layer-2	Hole-1	5.70	5.04	4.77	4.9050	0.7950	5.1700	2.5884
	Hole-2	5.57	4.56	4.30	4.4300	1.1400	4.8100	2.4125
	Hole-3	5.60	4.22	4.59	4.4050	1.1950	4.8033	2.4099
	Hole-4	6.12	5.13	4.77	4.9500	1.1700	5.3400	2.6771
	AVE	5.75	4.74	4.61	4.67	1.08	5.0308	2.5220
Layer-3	Hole-1	9.29	8.60	8.65	8.6250	0.6650	8.8467	4.4247
	Hole-2	9.67	8.67	8.29	8.4800	1.1900	8.8767	4.4428
	Hole-3	9.01	8.21	8.06	8.1350	0.8750	8.4267	4.2159
	Hole-4	9.07	7.97	7.86	7.9150	1.1550	8.3000	4.1545
	AVE	9.26	8.36	8.22	8.29	0.97	8.6125	4.3095

Table15. Extraction Measurements and Equivalent Depths Calculation (Type GU-1 week)

GUS-1		A_i(mm)	B_{i1}(mm)	B_{i2}(mm)	h(mm)	H(mm)	V_i/A(mm)	x_i(mm)
Layer-1	Hole-1	4.10	3.14	2.90	3.0200	1.0800	3.3800	1.6996
	Hole-2	4.14	3.07	2.86	2.9650	1.1750	3.3567	1.6898
	Hole-3	3.04	1.71	2.04	1.8750	1.1650	2.2633	1.1483
	Hole-4	4.47	3.63	3.49	3.5600	0.9100	3.8633	1.9376
		3.94	2.89	2.82	2.86	1.08	3.2158	1.6188
Layer-2	Hole-1	6.16	5.09	5.02	5.0550	1.1050	5.4233	2.7179
	Hole-2	6.44	5.28	5.22	5.2500	1.1900	5.6467	2.8303
	Hole-3	5.47	4.61	4.41	4.5100	0.9600	4.8300	2.4203
	Hole-4	6.19	4.94	4.80	4.8700	1.3200	5.3100	2.6641
		6.07	4.98	4.86	4.92	1.14	5.3025	2.6582
Layer-3	Hole-1	9.15	8.33	7.70	8.0150	1.1350	8.3933	4.2009
	Hole-2	9.04	7.82	7.95	7.8850	1.1550	8.2700	4.1395
	Hole-3	9.30	7.79	7.90	7.8450	1.4550	8.3300	4.1721
	Hole-4	9.48	8.48	8.32	8.4000	1.0800	8.7600	4.3837
		9.24	8.11	7.97	8.04	1.21	8.4383	4.2240

Chapter 5: Titration Experiment

Table 1. Calculation of Sulfate Concentration by layers (Type GU)

Label	Crucible No.	Weight.P(g)	Weight 1(g)	Weight 2(g)	m-BaSO$_4$ (g)	n-SO$_3$ (mmol)	C (mol/m^3)

GUS121	#102	1.8085	25.9099	25.9503	0.0404	0.17339	226.841
GUS122	#96	1.7402	25.7266	25.7637	0.0371	0.15923	216.488
GUS123	#710	1.7201	27.3818	27.4083	0.0265	0.11373	156.441
GUS124	#184	0.5804	21.03	21.0405	0.0105	0.04506	183.705
GUS125	#16	0.6703	28.2471	28.2575	0.0104	0.04464	157.552
GUS81	#68	1.6464	26.356	26.387	0.031	0.13305	191.199
GUS82	#62	1.0602	26.2484	26.2698	0.0214	0.09185	204.967
GUS83	#142	1.1693	27.5304	27.5497	0.0193	0.08283	167.606
GUS84	#421	1.3968	25.245	25.266	0.021	0.09013	152.667
GUS85	#TL18	1.4975	30.9698	30.992	0.0222	0.09528	150.538
GUS86	#640	1.2383	27.3793	27.3971	0.0178	0.07639	145.966
GUS87	#TL4	1.1598	32.3304	32.3473	0.0169	0.07253	147.966
GUS41	#181	1.3184	28.359	28.3838	0.0248	0.10644	191.013
GUS42	#4040	1.5915	22.643	22.6709	0.0279	0.11974	178.015
GUS43	#907	1.3989	22.9443	22.9657	0.0214	0.09185	155.341
GUS44	#706	1.8036	26.8282	26.8548	0.0266	0.11416	149.762
GUS21	#188	1.4985	21.9393	21.966	0.0267	0.11459	180.931
GUS22	#3	1.9527	23.4046	23.4387	0.0341	0.14635	177.328
GUS23	#399	2.5129	23.3608	23.3988	0.038	0.16309	153.556
GUS11	#TL21	1.9916	30.3227	30.3525	0.0298	0.12790	151.940
GUS12	#123	1.4681	27.4987	27.5189	0.0202	0.08670	139.719
GUS13	#711	2.0827	27.0176	27.0456	0.028	0.12017	136.518

Table 2. Calculation of Sulfate Concentration by layers (Type HS)

Label	Crucible No.	Weight.P(g)	Weight 1(g)	Weight 2(g)	m-BaSO4 (g)	n-SO3 (mmol)	C (mol/m3)
HSS121	#167	2.0034	24.7725	24.8076	0.0351	0.15064	174.601
HSS122	#TL6	1.772	30.1414	30.1674	0.026	0.11159	146.223
HSS123	#24	1.6218	27.1533	27.1755	0.0222	0.09528	136.415
HSS124	#405	2.3037	25.877	25.9075	0.0305	0.13090	131.941
HSS81	#412	1.8198	25.4641	25.4934	0.0293	0.12575	160.454
HSS82	#158	1.6793	28.2909	28.3139	0.023	0.09871	136.492
HSS83	#90	1.8067	27.8329	27.8574	0.0245	0.10515	135.141
HSS84	#79	1.4279	23.3447	23.3633	0.0186	0.07983	129.814
HSS41	#784	1.8824	27.2327	27.2622	0.0295	0.12661	156.177
HSS42	#151	2.0184	23.426	23.4528	0.0268	0.11502	132.323
HSS43	#178	2.0277	23.3155	23.3413	0.0258	0.11073	126.801
HSS44	#29	1.7597	27.2555	27.2777	0.0222	0.09528	125.725

HSS21	#21	1.9435	25.8582	25.888	0.0298	0.12790	152.805
HSS22	#134	2.0153	25.5515	25.578	0.0265	0.11373	131.043
HSS23	#5	2.5909	24.7442	24.7758	0.0316	0.13562	121.547
HSS11	#35	1.4584	26.4145	26.437	0.0225	0.09657	153.749
HSS12	#81	2.6509	25.29	25.3212	0.0312	0.13391	117.292
HSS13	#427	1.7995	25.8309	25.8517	0.0208	0.08927	115.191

Table 3. Calculation of Sulfate Concentration by layers (Blend IC)

Label	Crucible No.	Weight.P(g)	Weight 1(g)	Weight 2(g)	m-BaSO4 (g)	n-SO3 (mmol)	C (mol/m3)
ICS121	#9001	1.6196	24.3662	24.4277	0.0615	0.26395	372.879
ICS122	#TL11	1.2906	31.1757	31.2175	0.0418	0.17940	318.042
ICS123	#189	1.6391	21.3791	21.4177	0.0386	0.16567	231.250
ICS124	#114	1.6392	23.5854	23.6162	0.0308	0.13219	184.510
ICS125	#91	1.4986	26.1238	26.1501	0.0263	0.11288	172.334
ICS81	#192	1.8057	21.3617	21.4128	0.0511	0.21931	277.892
ICS82	#107	1.9797	23.4917	23.5354	0.0437	0.18755	216.762
ICS83	#183	2.3027	21.1114	21.1494	0.038	0.16309	162.049
ICS84	#53	2.6468	27.2506	27.2899	0.0393	0.16867	145.805
ICS41	#94	1.339	23.2528	23.2789	0.0261	0.11202	191.408
ICS42	#190	1.8044	21.2989	21.3314	0.0325	0.13948	176.869
ICS43	#154	2.1301	28.1171	28.1532	0.0361	0.15494	166.421
ICS44	#144	1.333	24.8256	24.8451	0.0195	0.08369	143.650
ICS21	#398	1.964	22.5797	22.6118	0.0321	0.13777	160.496
ICS22	#44	3.2616	21.9132	21.9589	0.0457	0.19614	137.590
ICS23	#169	2.3452	24.5147	24.5474	0.0327	0.14034	136.920
ICS11	#911	2.7302	26.634	26.6752	0.0412	0.17682	148.185
ICS12	#34	1.9455	23.6246	23.6508	0.0262	0.11245	132.242
ICS13	#196	1.7963	22.1661	22.1901	0.024	0.10300	131.200

Chapter 6: Numerical Modeling

Table 1. Relative Errors to Exact Solution as Affected by Time Increment (Explicit Method)

Depth (mm)	0.1 day	0.2 day	0.4 day	0.5 day	1.0 day	2.0 days
0	0	0	0	0	0	0
1	-0.00036	-0.00019	0.00015	0.000319	0.001163	0.002826

2	-0.00064	-0.00026	0.00049	0.000865	0.002733	0.006434
3	-0.00049	8.73E-05	0.00125	0.001832	0.004737	0.010537
4	0.000544	0.001278	0.002749	0.003486	0.007185	0.014653
5	0.003094	0.00386	0.005399	0.006173	0.01008	0.018085
6	0.007915	0.00851	0.00971	0.010317	0.013407	0.019897
7	0.01591	0.016032	0.016286	0.016419	0.01714	0.018894
8	0.028134	0.027367	0.025833	0.025066	0.021235	0.013627
9	0.045821	0.043611	0.039167	0.036932	0.025629	0.002401
10	0.07042	0.066046	0.057231	0.05279	0.030238	-0.01666
11	0.103663	0.096191	0.081127	0.073535	0.034952	-0.04553
12	0.147661	0.135878	0.11215	0.100205	0.039636	-0.0861
13	0.20504	0.18736	0.151854	0.134026	0.044117	-0.1399
14	0.279138	0.253465	0.202126	0.17646	0.048189	-0.20786
15	0.374284	0.337811	0.265306	0.229282	0.051602	-0.28981
16	0.496195	0.445101	0.344332	0.294675	0.054064	-0.3842
17	0.652544	0.581561	0.442952	0.375359	0.05523	-0.48773
18	0.853789	0.755543	0.566013	0.474773	0.054708	-0.59529
19	1.114401	0.978419	0.719863	0.597309	0.052054	-0.70035
20	1.454693	1.265887	0.912916	0.748641	0.046773	-0.7957
21	1.903614	1.639919	1.156453	0.93618	0.038329	-0.87485
22	2.50305	2.13171	1.465787	1.1697	0.026151	-0.93359
23	3.314577	2.786204	1.86194	1.462229	0.00965	-0.97121
24	4.430232	3.669141	2.374134	1.831309	-0.01176	-0.99087
25	5.989971	4.878226	3.043493	2.300809	-0.03863	-0.99839

Table 2. Relative Errors to Exact Solution as Affected by Space Increment (Explicit Method)

Depth	0.8mm	Depth	1mm	Depth	1.2mm	Depth	1.5mm	Depth	2mm
0	0	0	0	0	0	0	0	0	0
0.8	0.001047	1	0.001163	1.2	0.001163	1.5	0.00089	2	-0.00037
1.6	0.002354	2	0.002733	2.4	0.002991	3	0.003398	4	0.007161
2.4	0.003882	3	0.004737	3.6	0.005835	4.5	0.009649	6	0.036587
3.2	0.005559	4	0.007185	4.8	0.010168	6	0.022657	8	0.107242
4	0.007285	5	0.01008	6	0.016592	7.5	0.046313	10	0.247128
4.8	0.008928	6	0.013407	7.2	0.025836	9	0.08551	12	0.503074
5.6	0.010319	7	0.01714	8.4	0.038758	10.5	0.146527	14	0.963745
6.4	0.011259	8	0.021235	9.6	0.056352	12	0.237787	16	1.81258
7.2	0.011508	9	0.025629	10.8	0.079768	13.5	0.371181	18	3.458881

8	0.010795	10	0.030238	12	0.11034	15	0.564287	20	6.889086
8.8	0.008811	11	0.034952	13.2	0.149631	16.5	0.844108	22	14.68794
9.6	0.005215	12	0.039636	14.4	0.199507	18	1.253507	24	34.27449
10.4	-0.00036	13	0.044117	15.6	0.262223	19.5	1.862624	26	89.1475
11.2	-0.00832	14	0.048189	16.8	0.340546	21	2.789748	28	262.008
12	-0.01906	15	0.051602	18	0.437924	22.5	4.240651	30	878.4025
12.8	-0.03301	16	0.054064	19.2	0.5587	24	6.585129	32	3392.422
13.6	-0.05056	17	0.05523	20.4	0.708395	25.5	10.51087	34	12857.82
14.4	-0.07211	18	0.054708	21.6	0.894091	27	17.34348		
15.2	-0.09799	19	0.052054	22.8	1.124933	28.5	29.73615		
16	-0.12847	20	0.046773	24	1.4128	30	53.21248		
16.8	-0.16371	21	0.038329	25.2	1.773198	31.5	99.64597		
17.6	-0.20377	22	0.026151	26.4	2.226449	33	200.9214		
18.4	-0.24855	23	0.00965	27.6	2.799269	34.5	383.1061		
19.2	-0.29778	24	-0.01176	28.8	3.526924				
20	-0.351	25	-0.03863	30	4.45606				
20.8	-0.40753	26	-0.07144	31.2	5.646447				
21.6	-0.46652	27	-0.11056	32.4	7.232896				
22.4	-0.52694	28	-0.15618	33.6	8.648343				
23.2	-0.58759	29	-0.20828	34.8	5.517964				
24	-0.64719	30	-0.26649						
24.8	-0.70446	31	-0.3307						
25.6	-0.75814	32	-0.39638						
26.4	-0.80714	33	-0.45789						
27.2	-0.85058	34	-0.60809						
28	-0.88791								
28.8	-0.91887								
29.6	-0.9436								
30.4	-0.96252								
31.2	-0.97634								

Table 3. Relative Errors to Exact Solution as Affected by Time Increment (Implicit Method)

Depth (mm)	0.1day	0.2 day	0.4 day	0.5 day	1 day	2 days
0	0	0	0	0	0	0
1	-0.000704	-0.000875	-0.001220	-0.001392	-0.002260	-0.004022
2	-0.001392	-0.001770	-0.002527	-0.002906	-0.004809	-0.008647

3	-0.001658	-0.002239	-0.003403	-0.003985	-0.006895	-0.012713
4	-0.000921	-0.001652	-0.003110	-0.003838	-0.007460	-0.014618
5	0.001570	0.000812	-0.000696	-0.001446	-0.005158	-0.012388
6	0.006738	0.006155	0.005000	0.004429	0.001626	-0.003714
7	0.015676	0.015565	0.015351	0.015249	0.014786	0.014068
8	0.029667	0.030433	0.031964	0.032729	0.036544	0.044102
9	0.050213	0.052397	0.056738	0.058896	0.069556	0.090236
10	0.079101	0.083409	0.091959	0.096203	0.117106	0.157414
11	0.118493	0.125850	0.140453	0.147699	0.183396	0.252271
12	0.171074	0.182703	0.205813	0.217294	0.273990	0.384049
13	0.240257	0.257795	0.292733	0.310134	0.396476	0.566010
14	0.330484	0.356157	0.407502	0.433172	0.561477	0.817680
15	0.447655	0.484546	0.558723	0.596002	0.784191	1.168459
16	0.599756	0.652205	0.758402	0.812133	1.086814	1.663605
17	0.797784	0.872010	1.023599	1.100931	1.502417	2.374375
18	1.057138	1.162198	1.378987	1.490676	2.081264	3.415599
19	1.399718	1.549030	1.860893	2.023417	2.901351	4.976934
20	1.857192	2.070970	2.523779	2.762875	4.086357	7.379818
21	2.476109	2.785351	3.450864	3.807523	5.836902	11.184032
22	3.326096	3.779192	4.771861	5.312716	8.486272	17.392568
23	4.513191	5.187112	6.693202	7.528900	12.602172	27.856775
24	6.201961	7.221564	9.550646	10.869062	19.177227	46.101416
25	8.65291	10.22489	13.90290	16.03053	29.99506	79.05669
26	12.28701	14.76089	20.70207	24.22017	48.35298	140.81047
27	17.79931	21.77937	31.61128	37.58114	80.52900	261.00504
28	26.36350	32.91880	49.61177	60.02248	138.84800	504.27059
29	40.00753	51.07500	80.19103	98.87285	248.27907	1016.76020
30	62.32861	81.50773	133.74915	168.29163	461.13786	2141.88389

Table 3. Relative Errors to Exact Solution as Affected by Space Increment (Implicit Method)

Depth	0.5 mm	Depth	0.8 mm	Depth	1.0 mm	Depth	1.2 mm	Depth	1.5 mm	Depth	2.0 mm
0	0.0000	0	0.0000	0	0.0000	0	0.0000	0	0.0000	0	0.0000
0.5	-0.0009	0.8	-0.0016	1	-0.0023	1.2	-0.0031	1.5	-0.0046	2	-0.0080
1	-0.0018	1.6	-0.0035	2	-0.0048	2.4	-0.0062	3	-0.0081	4	-0.0065
1.5	-0.0029	2.4	-0.0053	3	-0.0069	3.6	-0.0077	4.5	-0.0051	6	0.0267
2	-0.0040	3.2	-0.0068	4	-0.0075	4.8	-0.0050	6	0.0117	8	0.1206

2.5	-0.0051	4	-0.0075	5	-0.0052	6	0.0051	7.5	0.0517	10	0.3209
3	-0.0061	4.8	-0.0066	6	0.0016	7.2	0.0264	9	0.1267	12	0.7136
3.5	-0.0069	5.6	-0.0037	7	0.0148	8.4	0.0636	10.5	0.2540	14	1.4870
4	-0.0074	6.4	0.0022	8	0.0365	9.6	0.1225	12	0.4610	16	3.0934
4.5	-0.0076	7.2	0.0118	9	0.0696	10.8	0.2110	13.5	0.7941	18	6.7288
5	-0.0071	8	0.0262	10	0.1171	12	0.3405	15	1.3365	20	15.9024
5.5	-0.0061	8.8	0.0466	11	0.1834	13.2	0.5277	16.5	2.2453	22	42.1672
6	-0.0042	9.6	0.0743	12	0.2740	14.4	0.7981	18	3.8315	24	128.6499
6.5	-0.0013	10.4	0.1108	13	0.3965	15.6	1.1926	19.5	6.7448		
7	0.0027	11.2	0.1582	14	0.5615	16.8	1.7775	21	12.4208		
7.5	0.0081	12	0.2189	15	0.7842	18	2.6649	22.5	24.2326		
8	0.0150	12.8	0.2959	16	1.0868	19.2	4.0492	24	50.6392		
8.5	0.0237	13.6	0.3932	17	1.5024	20.4	6.2797	25.5	114.3730		
9	0.0344	14.4	0.5159	18	2.0813	21.6	10.0059				
9.5	0.0475	15.2	0.6709	19	2.9014	22.8	16.4824				
10	0.0630	16	0.8671	20	4.0864	24	28.2284				
10.5	0.0816	16.8	1.1170	21	5.8369	25.2	50.5175				
11	0.1034	17.6	1.4375	22	8.4863	26.4	94.8764				
11.5	0.1289	18.4	1.8520	23	12.6022						
12	0.1586	19.2	2.3938	24	19.1772						
12.5	0.1930	20	3.1099	25	29.9951						
13	0.2328	20.8	4.0686	26	48.3530						
13.5	0.2787	21.6	5.3699	27	80.5290						
14	0.3315	22.4	7.1629								
14.5	0.3922	23.2	9.6727								
15	0.4621	24	13.2451								
15.5	0.5425	24.8	18.4203								
16	0.6350	25.6	26.0564								
16.5	0.7416	26.4	37.5411								
17	0.8648	27.2	55.1595								
17.5	1.0072	28	82.7463								
18	1.1725										
18.5	1.3649										
19	1.5893										

Table 5. Relative Errors to Exact Solution as Affected by Time Increment (Crank-Nicolson Method)

Depth (mm)	0.1day	0.2 day	0.4 day	0.5 day	1 day	2 days

0	0	0	0	0	0	0
1	-0.000532	-0.000532	-0.000530	-0.000529	-0.0005184	-0.000476
2	-0.001014	-0.001013	-0.001010	-0.001007	-0.0009857	-0.000899
3	-0.001076	-0.001074	-0.001070	-0.001066	-0.00103706	-0.000920
4	-0.000189	-0.000188	-0.000183	-0.000180	-0.00015147	-0.000038
5	0.002331	0.002332	0.002334	0.002336	0.002350161	0.002408
6	0.007324	0.007324	0.007322	0.007320	0.007305373	0.007248
7	0.015791	0.015788	0.015779	0.015772	0.015714655	0.015485
8	0.028899	0.028895	0.028877	0.028864	0.028755882	0.028321
9	0.048019	0.048013	0.047988	0.047970	0.047814808	0.047194
10	0.074769	0.074762	0.074734	0.074713	0.074538234	0.073838
11	0.111095	0.111090	0.111069	0.111052	0.11091782	0.110380
12	0.159393	0.159394	0.159397	0.159399	0.159415212	0.159486
13	0.222677	0.222691	0.222747	0.222790	0.223143835	0.224568
14	0.304824	0.304863	0.305022	0.305140	0.306130525	0.310101
15	0.410928	0.411011	0.411347	0.411598	0.413692571	0.422075
16	0.547802	0.547959	0.548587	0.549059	0.552985543	0.568674
17	0.724716	0.724991	0.726094	0.726921	0.733808979	0.761294
18	0.954483	0.954948	0.956807	0.958200	0.969808338	1.016097
19	1.255093	1.255857	1.258914	1.261206	1.280296125	1.356425
20	1.652193	1.653432	1.658387	1.662103	1.693056397	1.816620
21	2.182933	2.184927	2.192903	2.198885	2.248737136	2.448171
22	2.902012	2.905216	2.918035	2.927651	3.007850695	3.329835
23	3.891343	3.896507	3.917169	3.932673	4.062134684	4.584591
24	5.275803	5.284178	5.317702	5.342867	5.553339106	6.408724
25	7.24933	7.26305	7.31796	7.35921	7.704906213	9.12276
26	10.11904	10.14177	10.23284	10.30129	10.87649064	13.26288
27	14.38116	14.41939	14.57262	14.68788	15.65975807	19.74879
28	20.85473	20.92008	21.18222	21.37961	23.05060852	30.20030
29	30.92092	31.03469	31.49147	31.83584	34.7650291	47.54878
30	46.96833	47.17041	47.98254	48.59569	53.84032714	77.26210

Table 6. Relative Errors to Exact Solution as Affected by Space Increment (Crank-Nicolson Method)

Depth	0.5 mm	Depth	0.8 mm	Depth	1.0 mm	Depth	1.2 mm	Depth	1.5 mm	Depth	2.0 mm
0	0.0000	0	0.0000	0	0.0000	0	0.0000	0	0.0000	0	0.0000
0.5	-0.0001	0.8	-0.0003	1	-0.0005	1.2	-0.0009	1.5	-0.0018	2	-0.0041

1	-0.0001	1.6	-0.0005	2	-0.0010	2.4	-0.0016	3	-0.0023	4	0.0003
1.5	-0.0002	2.4	-0.0007	3	-0.0010	3.6	-0.0009	4.5	0.0022	6	0.0315
2	-0.0002	3.2	-0.0006	4	-0.0002	4.8	0.0025	6	0.0170	8	0.1139
2.5	-0.0002	4	-0.0001	5	0.0024	6	0.0107	7.5	0.0488	10	0.2846
3	-0.0002	4.8	0.0011	6	0.0073	7.2	0.0259	9	0.1063	12	0.6101
3.5	-0.0002	5.6	0.0031	7	0.0157	8.4	0.0512	10.5	0.2014	14	1.2270
4	0.0000	6.4	0.0065	8	0.0288	9.6	0.0900	12	0.3516	16	2.4437
4.5	0.0002	7.2	0.0114	9	0.0478	10.8	0.1469	13.5	0.5848	18	5.0209
5	0.0006	8	0.0184	10	0.0745	12	0.2279	15	0.9476	20	11.0173
5.5	0.0011	8.8	0.0278	11	0.1109	13.2	0.3412	16.5	1.5217	22	26.6096
6	0.0018	9.6	0.0403	12	0.1594	14.4	0.4987	18	2.4562	24	72.5423
6.5	0.0027	10.4	0.0565	13	0.2231	15.6	0.7176	19.5	4.0365		
7	0.0038	11.2	0.0770	14	0.3061	16.8	1.0239	21	6.8350		
7.5	0.0053	12	0.1027	15	0.4137	18	1.4577	22.5	12.0592		
8	0.0071	12.8	0.1345	16	0.5530	19.2	2.0829	24	22.4009		
8.5	0.0093	13.6	0.1737	17	0.7338	20.4	3.0032	25.5	44.2202		
9	0.0119	14.4	0.2215	18	0.9698	21.6	4.3921				
9.5	0.0150	15.2	0.2798	19	1.2803	22.8	6.5486				
10	0.0187	16	0.3505	20	1.6931	24	10.0036				
10.5	0.0230	16.8	0.4363	21	2.2487	25.2	15.7310				
11	0.0280	17.6	0.5404	22	3.0079	26.4	25.5796				
11.5	0.0338	18.4	0.6671	23	4.0621						
12	0.0404	19.2	0.8217	24	5.5533						
12.5	0.0480	20	1.0110	25	7.7049						
13	0.0567	20.8	1.2443	26	10.8765						
13.5	0.0665	21.6	1.5333	27	15.6598						
14	0.0776	22.4	1.8942								
14.5	0.0902	23.2	2.3485								
15	0.1043	24	2.9255								
15.5	0.1202	24.8	3.6657								
16	0.1380	25.6	4.6255								
16.5	0.1578	26.4	5.8844								
17	0.1801	27.2	7.5558								
17.5	0.2049	28	9.8041								
18	0.2326										
18.5	0.2634										
19	0.2978										

Table 7. Sulfate Concentrations and Errors by MATLAB and MS-EXCEL (Explicit Method)

| Depth (mm) | Sulfate Concentration (mol/m^3) | | | | | | Error (%) | | | |
| | Error Function | | MATLAB | | MS-EXCEL | | MATLAB | | MS-EXCEL | |
	200-day	500-day	200-day	500-day	200-day	500-day	200-day	500-day	200-day	500-day
0	30.0000	30.0000	30.0000	30.0000	30.0000	30.0000	0.0000	0.0000	0.0000	0.0000
1	27.1278	28.1808	27.1243	28.1799	27.1314	28.1818	-0.0130	-0.0032	0.0134	0.0033
2	24.2968	26.3722	24.2899	26.3704	24.3039	26.3740	-0.0283	-0.0067	0.0292	0.0069
3	21.5465	24.5843	21.5365	24.5817	21.5567	24.5870	-0.0463	-0.0106	0.0476	0.0110
4	18.9128	22.8272	18.9002	22.8238	18.9258	22.8307	-0.0670	-0.0150	0.0686	0.0155
5	16.4271	21.1103	16.4122	21.1061	16.4422	21.1146	-0.0905	-0.0198	0.0923	0.0204
6	14.1146	19.4423	14.0981	19.4375	14.1314	19.4473	-0.1170	-0.0250	0.1188	0.0257
7	11.9942	17.8312	11.9766	17.8258	12.0119	17.8368	-0.1467	-0.0306	0.1480	0.0314
8	10.0777	16.2841	10.0596	16.2781	10.0958	16.2902	-0.1797	-0.0368	0.1799	0.0376
9	8.3705	14.8069	8.3524	14.8005	8.3885	14.8134	-0.2161	-0.0434	0.2146	0.0442
10	6.8715	13.4046	6.8539	13.3979	6.8888	13.4115	-0.2561	-0.0505	0.2520	0.0512
11	5.5741	12.0812	5.5574	12.0742	5.5904	12.0883	-0.2999	-0.0581	0.2921	0.0587
12	4.4674	10.8393	4.4519	10.8321	4.4824	10.8465	-0.3476	-0.0663	0.3347	0.0666
13	3.5369	9.6807	3.5228	9.6735	3.5504	9.6880	-0.3994	-0.0750	0.3798	0.0750
14	2.7658	8.6061	2.7532	8.5988	2.7776	8.6133	-0.4554	-0.0842	0.4273	0.0838
15	2.1359	7.6150	2.1249	7.6078	2.1461	7.6221	-0.5158	-0.0940	0.4771	0.0930
16	1.6288	6.7063	1.6193	6.6993	1.6374	6.7132	-0.5810	-0.1045	0.5289	0.1027
17	1.2263	5.8779	1.2183	5.8711	1.2334	5.8845	-0.6509	-0.1155	0.5827	0.1128
18	0.9115	5.1271	0.9049	5.1206	0.9173	5.1334	-0.7260	-0.1271	0.6382	0.1232
19	0.6688	4.4505	0.6634	4.4443	0.6734	4.4565	-0.8063	-0.1394	0.6954	0.1341
20	0.4843	3.8444	0.4800	3.8385	0.4880	3.8500	-0.8922	-0.1523	0.7538	0.1454
21	0.3462	3.3045	0.3428	3.2990	0.3490	3.3097	-0.9839	-0.1659	0.8134	0.1571
22	0.2442	2.8263	0.2416	2.8212	0.2463	2.8311	-1.0816	-0.1802	0.8737	0.1692
23	0.1700	2.4053	0.1680	2.4006	0.1716	2.4096	-1.1858	-0.1952	0.9347	0.1816
24	0.1168	2.0367	0.1153	2.0324	0.1179	2.0406	-1.2966	-0.2110	0.9959	0.1943
25	0.0791	1.7159	0.0780	1.7120	0.0800	1.7194	-1.4144	-0.2274	1.0570	0.2074
26	0.0529	1.4382	0.0521	1.4347	0.0535	1.4414	-1.5395	-0.2447	1.1177	0.2208
27	0.0349	1.1994	0.0343	1.1962	0.0353	1.2022	-1.6724	-0.2627	1.1775	0.2346
28	0.0227	0.9951	0.0223	0.9923	0.0230	0.9975	-1.8133	-0.2816	1.2362	0.2486
29	0.0146	0.8213	0.0143	0.8188	0.0148	0.8235	-1.9627	-0.3013	1.2932	0.2628
30	0.0092	0.6744	0.0090	0.6722	0.0094	0.6762	-2.1210	-0.3218	1.3481	0.2773
31	0.0058	0.5508	0.0056	0.5489	0.0059	0.5524	-2.2886	-0.3433	1.4005	0.2921
32	0.0036	0.4476	0.0035	0.4460	0.0036	0.4490	-2.4660	-0.3656	1.4497	0.3070

33	0.0022	0.3618	0.0021	0.3604	0.0022	0.3630	-2.6537	-0.3888	1.4953	0.3221
34	0.0013	0.2909	0.0013	0.2897	0.0013	0.2919	-2.8521	-0.4131	1.5367	0.3374
35	0.0008	0.2327	0.0007	0.2316	0.0008	0.2335	-3.0618	-0.4383	1.5733	0.3528
36	0.0004	0.1851	0.0004	0.1842	0.0005	0.1858	-3.2834	-0.4645	1.6044	0.3683
37	0.0003	0.1465	0.0002	0.1458	0.0003	0.1470	-3.5174	-0.4917	1.6294	0.3839
38	0.0001	0.1153	0.0001	0.1147	0.0001	0.1158	-3.7643	-0.5200	1.6476	0.3996
39	0.0001	0.0903	0.0001	0.0898	0.0001	0.0906	-4.0249	-0.5494	1.6581	0.4152
40	0.0000	0.0703	0.0000	0.0699	0.0000	0.0706	-4.2997	-0.5800	1.6603	0.4309
41	0.0000	0.0544	0.0000	0.0541	0.0000	0.0547	-4.5895	-0.6116	1.6533	0.4465
42	0.0000	0.0419	0.0000	0.0417	0.0000	0.0421	-4.8948	-0.6445	1.6363	0.4621
43	0.0000	0.0321	0.0000	0.0319	0.0000	0.0323	-5.2165	-0.6786	1.6084	0.4775
44	0.0000	0.0245	0.0000	0.0243	0.0000	0.0246	-5.5551	-0.7140	1.5685	0.4929
45	0.0000	0.0186	0.0000	0.0184	0.0000	0.0187	-5.9115	-0.7507	1.5159	0.5080
46	0.0000	0.0140	0.0000	0.0139	0.0000	0.0141	-6.2865	-0.7887	1.4494	0.5229
47	0.0000	0.0105	0.0000	0.0104	0.0000	0.0105	-6.6808	-0.8280	1.3679	0.5376
48	0.0000	0.0078	0.0000	0.0078	0.0000	0.0079	-7.0951	-0.8688	1.2705	0.5520
49	0.0000	0.0058	0.0000	0.0057	0.0000	0.0058	-7.5304	-0.9110	1.1560	0.5661
50	0.0000	0.0043	0.0000	0.0042	0.0000	0.0043	-7.9874	-0.9547	1.0232	0.5798
51	0.0000	0.0031	0.0000	0.0031	0.0000	0.0032	-8.4671	-0.9999	0.8709	0.5930
52	0.0000	0.0023	0.0000	0.0023	0.0000	0.0023	-8.9701	-1.0467	0.6979	0.6059
53	0.0000	0.0017	0.0000	0.0016	0.0000	0.0017	-9.4975	-1.0951	0.5028	0.6182
54	0.0000	0.0012	0.0000	0.0012	0.0000	0.0012	-10.0501	-1.1452	0.2844	0.6300
55	0.0000	0.0009	0.0000	0.0008	0.0000	0.0009	-10.6286	-1.1969	0.0415	0.6412
56	0.0000	0.0006	0.0000	0.0006	0.0000	0.0006	-11.2341	-1.2504	-0.2276	0.6517
57	0.0000	0.0004	0.0000	0.0004	0.0000	0.0004	-11.8668	-1.3057	-0.5234	0.6615
58	0.0000	0.0003	0.0000	0.0003	0.0000	0.0003	-12.5301	-1.3629	-0.8505	0.6706
59	0.0000	0.0002	0.0000	0.0002	0.0000	0.0002	-13.2193	-1.4219	-1.2037	0.6789
60	0.0000	0.0002	0.0000	0.0001	0.0000	0.0002	-13.9360	-1.4828	-1.5856	0.6864

Table 8. Error Caused by Three Finite Difference Methods (1-day/1-mm)

Error (%)	Explicit Method			Implicit Method			Crank-Nicolson Method		
Depth (mm)	200-day	500-day	1000-day	200-day	500-day	1000-day	200-day	500-day	1000-day
0	0.0000	0.0000	0.0000	0.0000	0.0000	0.0000	0.0000	0.0000	0.0000
1	0.0130	0.0032	0.0011	0.0261	0.0064	0.0022	0.0062	0.0015	0.0005

2	0.0283	0.0067	0.0023	0.0557	0.0134	0.0046	0.0130	0.0032	0.0011
3	0.0463	0.0106	0.0036	0.0874	0.0209	0.0071	0.0196	0.0049	0.0017
4	0.0670	0.0150	0.0050	0.1193	0.0289	0.0098	0.0250	0.0067	0.0023
5	0.0905	0.0198	0.0065	0.1489	0.0370	0.0126	0.0279	0.0083	0.0029
6	0.1170	0.0250	0.0081	0.1732	0.0451	0.0154	0.0269	0.0096	0.0035
7	0.1467	0.0306	0.0098	0.1887	0.0529	0.0183	0.0202	0.0107	0.0041
8	0.1797	0.0368	0.0116	0.1914	0.0602	0.0211	0.0058	0.0113	0.0046
9	0.2161	0.0434	0.0135	0.1766	0.0666	0.0240	0.0187	0.0112	0.0050
10	0.2561	0.0505	0.0155	0.1392	0.0718	0.0267	0.0557	0.0103	0.0054
11	0.2999	0.0581	0.0177	0.0736	0.0755	0.0293	0.1082	0.0084	0.0056
12	0.3476	0.0663	0.0200	0.0267	0.0771	0.0317	0.1793	0.0052	0.0057
13	0.3994	0.0750	0.0224	0.1683	0.0763	0.0339	0.2724	0.0007	0.0055
14	0.4554	0.0842	0.0249	0.3586	0.0726	0.0357	0.3912	0.0056	0.0052
15	0.5158	0.0940	0.0275	0.6057	0.0653	0.0372	0.5398	0.0138	0.0046
16	0.5810	0.1045	0.0303	0.9180	0.0540	0.0382	0.7224	0.0242	0.0038
17	0.6509	0.1155	0.0332	1.3050	0.0381	0.0386	0.9437	0.0372	0.0026
18	0.7260	0.1271	0.0363	1.7764	0.0169	0.0385	1.2086	0.0530	0.0011
19	0.8063	0.1394	0.0395	2.3431	0.0103	0.0376	1.5224	0.0720	0.0009
20	0.8922	0.1523	0.0428	3.0164	0.0442	0.0360	1.8908	0.0946	0.0033
21	0.9839	0.1659	0.0463	3.8090	0.0855	0.0334	2.3198	0.1210	0.0062
22	1.0816	0.1802	0.0499	4.7342	0.1350	0.0299	2.8159	0.1518	0.0096
23	1.1858	0.1952	0.0536	5.8068	0.1936	0.0253	3.3860	0.1873	0.0136
24	1.2966	0.2110	0.0576	7.0427	0.2621	0.0195	4.0374	0.2280	0.0183
25	1.4144	0.2274	0.0616	8.4595	0.3415	0.0123	4.7782	0.2743	0.0237
26	1.5395	0.2447	0.0659	10.0763	0.4326	0.0038	5.6169	0.3266	0.0299
27	1.6724	0.2627	0.0703	11.9146	0.5366	0.0064	6.5626	0.3855	0.0369
28	1.8133	0.2816	0.0748	13.9979	0.6543	0.0182	7.6253	0.4515	0.0448
29	1.9627	0.3013	0.0796	16.3525	0.7869	0.0319	8.8158	0.5252	0.0537
30	2.1210	0.3218	0.0845	19.0078	0.9356	0.0475	10.1457	0.6069	0.0636
31	2.2886	0.3433	0.0895	21.9969	1.1014	0.0652	11.6278	0.6975	0.0746
32	2.4660	0.3656	0.0948	25.3572	1.2856	0.0852	13.2760	0.7973	0.0867
33	2.6537	0.3888	0.1002	29.1308	1.4895	0.1076	15.1055	0.9071	0.1002
34	2.8521	0.4131	0.1058	33.3657	1.7143	0.1325	17.1332	1.0275	0.1149
35	3.0618	0.4383	0.1116	38.1169	1.9615	0.1602	19.3775	1.1592	0.1311
36	3.2834	0.4645	0.1176	43.4470	2.2324	0.1908	21.8589	1.3027	0.1487
37	3.5174	0.4917	0.1238	49.4281	2.5286	0.2245	24.6000	1.4590	0.1679
38	3.7643	0.5200	0.1302	56.1434	2.8516	0.2614	27.6262	1.6286	0.1888
39	4.0249	0.5494	0.1368	63.6891	3.2031	0.3017	30.9655	1.8124	0.2115

40	4.2997	0.5800	0.1436	72.1768	3.5846	0.3457	34.6494	2.0111	0.2360
41	4.5895	0.6116	0.1506	81.7365	3.9979	0.3934	38.7132	2.2255	0.2624
42	4.8948	0.6445	0.1578	92.5202	4.4450	0.4452	43.1967	2.4566	0.2909
43	5.2165	0.6786	0.1652	104.7059	4.9276	0.5012	48.1446	2.7051	0.3216
44	5.5551	0.7140	0.1729	118.5032	5.4478	0.5617	53.6074	2.9720	0.3545
45	5.9115	0.7507	0.1808	134.1594	6.0078	0.6268	59.6426	3.2582	0.3897
46	6.2865	0.7887	0.1889	151.9675	6.6096	0.6967	66.3152	3.5648	0.4274
47	6.6808	0.8280	0.1972	172.2756	7.2557	0.7718	73.6994	3.8926	0.4676
48	7.0951	0.8688	0.2058	195.4991	7.9484	0.8521	81.8800	4.2428	0.5106
49	7.5304	0.9110	0.2147	222.1353	8.6903	0.9381	90.9539	4.6165	0.5563
50	7.9874	0.9547	0.2237	252.7820	9.4841	1.0298	101.0323	5.0148	0.6050
51	8.4671	0.9999	0.2331	288.1602	10.3326	1.1276	112.2436	5.4388	0.6567
52	8.9701	1.0467	0.2427	329.1432	11.2389	1.2317	124.7353	5.8899	0.7116
53	9.4975	1.0951	0.2525	376.7928	12.2060	1.3424	138.6784	6.3692	0.7698
54	10.0501	1.1452	0.2626	432.4052	13.2374	1.4599	154.2711	6.8782	0.8314
55	10.6286	1.1969	0.2730	497.5715	14.3365	1.5846	171.7448	7.4181	0.8965
56	11.2341	1.2504	0.2837	574.2467	15.5071	1.7166	191.3675	7.9905	0.9654
57	11.8668	1.3057	0.2947	664.8575	16.7532	1.8564	213.4567	8.5969	1.0380
58	12.5301	1.3629	0.3059	772.3861	18.0790	2.0041	238.3719	9.2389	1.1147
59	13.2193	1.4219	0.3175	900.6398	19.4891	2.1602	266.5692	9.9180	1.1954
60	13.9360	1.4828	0.3293	1054.3302	20.9881	2.3249	298.5621	10.6360	1.2805

Chapter 7: Physicochemical Diffusion Modeling

Table 1. Sulfate Concentration after Chemical Consumption by Explicit and Crank-Nicolson Method

mol/m^3	Explicit Method					Crank-Nicolson Method				
Depth (mm)	200-day	500-day	1000-day	3650-day	7300-day	200-day	500-day	1000-day	3650-day	7300-day
0	30	30	30	30	30	30	30	30	30	30
1	21.38188	22.81740	23.79335	25.41085	26.18289	21.38382	22.81811	23.79368	25.41093	26.18293

	226	546	171	6	476	165	851	289	487	204
2	14.13505261	16.44680126	18.11551784	21.03298758	22.48340648	14.13814576	16.44800762	18.11610009	21.03313426	22.48347738
3	8.739815365	11.27723007	13.26552094	17.01551857	18.99225698	8.743189387	11.27865065	13.26624329	17.01571559	18.99235539
4	5.092384529	7.379742248	9.357028557	13.45398189	15.77708609	5.095417069	7.381138372	9.357784235	13.45420921	15.77720447
5	2.816340007	4.62362732	6.36715079	10.3969809	12.88440028	2.818733524	4.624844393	6.367857641	10.39721909	12.88453061
6	1.48871819	2.78256457	4.186521147	7.853036991	10.340838	1.490430519	2.783533951	4.187129013	7.853269426	10.34097255
7	0.757106347	1.613881422	2.664619349	5.7985882	8.154620685	0.758238442	1.614599373	2.665107764	5.798802397	8.154752671
8	0.372692468	0.905103475	1.644802906	4.187032515	6.317685563	0.373393648	0.905603834	1.645173516	4.187220554	6.317809565
9	0.178553266	0.492403395	0.986592907	2.957994546	4.808620815	0.178964362	0.492734413	0.986860559	2.958152757	4.808732987
10	0.083658047	0.260657521	0.576178765	2.045765814	3.596212733	0.08388812	0.260866819	0.576363843	2.045893971	3.596310809
11	0.038494084	0.134646434	0.328248578	1.38606303	2.643224889	0.03861786	0.134773614	0.328371709	1.386163339	2.64330802
12	0.017457589	0.068054236	0.18275708	0.920675942	1.909980167	0.017521982	0.068128848	0.182836212	0.920752031	1.910048644
13	0.007826848	0.033738136	0.099616489	0.600026851	1.357387648	0.007859407	0.033780563	0.09966578	0.60008293	1.357442574
14	0.003477617	0.016442717	0.053246476	0.383992683	0.949198673	0.00349369	0.01646618	0.053276321	0.38403293	0.949241654
15	0.00153442	0.007894195	0.027952876	0.241495542	0.653434463	0.001542195	0.007906853	0.027970487	0.241523723	0.653467328
16	0.000673395	0.003740566	0.01443341	0.149371079	0.443058158	0.000677092	0.003747244	0.014443558	0.149390364	0.443082749
17	0.000294306	0.001752257	0.007340207	0.090932847	0.29604536	0.00029604	0.001755712	0.00734593	0.090945765	0.296063389
18	0.000128217	0.000812741	0.003681257	0.054523529	0.195037532	0.000129021	0.000814496	0.003684422	0.05453201	0.195050498
19	5.57E-05	0.00037376	0.001822837	0.032222084	0.12675338	5.61E-05	0.000374638	0.001824555	0.032227549	0.126762539
20	2.42E-05	0.000170628	0.000892163	0.018780752	0.081300772	2.43E-05	0.000171061	0.00089308	0.018784211	0.08130713

21	1.05E-05	7.74E-05	0.00043205	0.010802672	0.051490599	1.05E-05	7.76E-05	0.000432532	0.010804825	0.051494943
22	4.52E-06	3.49E-05	0.000207221	0.006135701	0.032214784	4.56E-06	3.50E-05	0.000207471	0.00613702	0.032217705
23	1.95E-06	1.57E-05	9.85E-05	0.003443146	0.019918819	1.97E-06	1.57E-05	9.87E-05	0.003443942	0.019920756
24	8.43E-07	7.02E-06	4.65E-05	0.001910015	0.012176756	8.50E-07	7.05E-06	4.65E-05	0.001910489	0.012178022
25	3.63E-07	3.13E-06	2.18E-05	0.001047924	0.007362571	3.66E-07	3.14E-06	2.18E-05	0.001048202	0.007363388
26	1.56E-07	1.39E-06	1.01E-05	0.000568913	0.004404736	1.58E-07	1.40E-06	1.01E-05	0.000569074	0.004405255
27	6.71E-08	6.19E-07	4.69E-06	0.000305764	0.002608301	6.77E-08	6.22E-07	4.69E-06	0.000305856	0.002608628
28	2.88E-08	2.75E-07	2.16E-06	0.000162759	0.001529296	2.91E-08	2.76E-07	2.16E-06	0.000162811	0.001529499
29	1.23E-08	1.22E-07	9.88E-07	8.58E-05	0.000888103	1.24E-08	1.22E-07	9.90E-07	8.59E-05	0.000888228
30	5.28E-09	5.37E-08	4.51E-07	4.49E-05	0.000510987	5.32E-09	5.39E-08	4.52E-07	4.49E-05	0.000511063
31	2.25E-09	2.37E-08	2.05E-07	2.33E-05	0.000291381	2.27E-09	2.38E-08	2.05E-07	2.33E-05	0.000291427
32	9.59E-10	1.05E-08	9.29E-08	1.20E-05	0.000164719	9.68E-10	1.05E-08	9.31E-08	1.20E-05	0.000164746
33	4.07E-10	4.62E-09	4.20E-08	6.11E-06	9.23E-05	4.11E-10	4.64E-09	4.20E-08	6.11E-06	9.24E-05
34	1.73E-10	2.04E-09	1.89E-08	3.09E-06	5.13E-05	1.74E-10	2.05E-09	1.90E-08	3.10E-06	5.14E-05
35	7.29E-11	8.97E-10	8.50E-09	1.56E-06	2.83E-05	7.36E-11	9.01E-10	8.52E-09	1.56E-06	2.83E-05
36	3.07E-11	3.95E-10	3.82E-09	7.78E-07	1.55E-05	3.10E-11	3.97E-10	3.83E-09	7.79E-07	1.55E-05
37	1.29E-11	1.74E-10	1.71E-09	3.86E-07	8.43E-06	1.30E-11	1.75E-10	1.71E-09	3.87E-07	8.43E-06
38	5.37E-12	7.65E-11	7.65E-10	1.91E-07	4.55E-06	5.43E-12	7.69E-11	7.67E-10	1.91E-07	4.55E-06
39	2.23E-12	3.37E-11	3.42E-10	9.37E-08	2.44E-06	2.26E-12	3.39E-11	3.43E-10	9.37E-08	2.44E-06
40	9.21E-13	1.48E-11	1.53E-10	4.57E-08	1.30E-06	9.36E-13	1.49E-11	1.53E-10	4.57E-08	1.30E-06
41	3.78E-13	6.52E-12	6.81E-11	2.22E-08	6.86E-07	3.86E-13	6.55E-12	6.83E-11	2.22E-08	6.86E-07
42	1.54E-13	2.87E-12	3.03E-11	1.07E-08	3.61E-07	1.58E-13	2.88E-12	3.04E-11	1.07E-08	3.61E-07
43	6.26E-14	1.26E-12	1.35E-11	5.16E-09	1.88E-07	6.43E-14	1.27E-12	1.35E-11	5.16E-09	1.88E-07
44	2.52E-14	5.54E-13	6.01E-12	2.47E-09	9.78E-08	2.60E-14	5.57E-13	6.03E-12	2.47E-09	9.78E-08
45	1.00E-14	2.43E-13	2.67E-12	1.18E-09	5.05E-08	1.05E-14	2.45E-13	2.68E-12	1.18E-09	5.05E-08
46	3.98E-15	1.07E-13	1.19E-12	5.60E-10	2.59E-08	4.18E-15	1.08E-13	1.19E-12	5.60E-10	2.59E-08

47	1.56E-15	4.70E-14	5.28E-13	2.65E-10	1.33E-08	1.66E-15	4.73E-14	5.30E-13	2.65E-10	1.33E-08
48	6.06E-16	2.06E-14	2.35E-13	1.25E-10	6.74E-09	6.51E-16	2.08E-14	2.35E-13	1.25E-10	6.74E-09
49	2.33E-16	9.07E-15	1.04E-13	5.87E-11	3.41E-09	2.54E-16	9.13E-15	1.05E-13	5.87E-11	3.41E-09
50	8.87E-17	3.98E-15	4.63E-14	2.75E-11	1.71E-09	9.84E-17	4.01E-15	4.65E-14	2.75E-11	1.71E-09
51	3.34E-17	1.75E-15	2.06E-14	1.28E-11	8.59E-10	3.78E-17	1.76E-15	2.06E-14	1.28E-11	8.59E-10
52	1.24E-17	7.67E-16	9.12E-15	5.97E-12	4.28E-10	1.44E-17	7.72E-16	9.16E-15	5.98E-12	4.28E-10
53	4.58E-18	3.37E-16	4.05E-15	2.77E-12	2.13E-10	5.42E-18	3.39E-16	4.06E-15	2.78E-12	2.13E-10
54	1.67E-18	1.48E-16	1.80E-15	1.28E-12	1.05E-10	2.03E-18	1.49E-16	1.80E-15	1.29E-12	1.05E-10
55	5.98E-19	6.48E-17	7.97E-16	5.94E-13	5.18E-11	7.52E-19	6.53E-17	8.00E-16	5.94E-13	5.18E-11
56	2.12E-19	2.84E-17	3.54E-16	2.74E-13	2.54E-11	2.76E-19	2.86E-17	3.55E-16	2.74E-13	2.54E-11
57	7.43E-20	1.25E-17	1.57E-16	1.26E-13	1.24E-11	1.00E-19	1.26E-17	1.58E-16	1.26E-13	1.24E-11
58	2.57E-20	5.46E-18	6.96E-17	5.78E-14	6.05E-12	3.62E-20	5.50E-18	6.99E-17	5.79E-14	6.05E-12
59	8.76E-21	2.39E-18	3.09E-17	2.65E-14	2.94E-12	1.29E-20	2.41E-18	3.10E-17	2.65E-14	2.94E-12
60	2.95E-21	1.05E-18	1.37E-17	1.21E-14	1.42E-12	4.56E-21	1.06E-18	1.38E-17	1.21E-14	1.42E-12

Table 2. Ettringite Formation after Chemical Consumption by Explicit and Crank-Nicolson Method

mol/m^3	Explicit Method					Crank-Nicolson Method				
Depth (mm)	200-day	500-day	1000-day	3650-day	7300-day	200-day	500-day	1000-day	3650-day	7300-day
0	100	100	100	100	100	100	100	100	100	100
1	90.83080634	94.81112789	96.73173155	98.76729184	99.33266688	90.83788771	94.81282384	96.73230102	98.7673621	99.33268908
2	81.4063896	89.39191506	93.29573082	97.46216225	98.62440182	81.42125304	89.3954294	93.29690624	97.46230704	98.62444757
3	71.77632921	83.66169943	89.60609011	96.03437725	97.84387657	71.80000405	83.66721461	89.60792635	96.03460341	97.84394819
4	62.17326731	77.65069194	85.64261669	94.45282328	96.96800311	62.20677283	77.65840509	85.64517364	94.45313889	96.96810346
5	52.8919132	71.45724636	81.43317511	92.70311869	95.98123595	52.93596691	71.46734015	81.4365091	92.70353188	95.98136814
6	44.2017053	65.20887618	77.03558473	90.78515888	94.87511865	44.25649289	65.22150204	77.03974426	90.78567706	94.87528572
7	36.30196973	59.03305951	72.52123408	88.71025053	93.64776386	36.36699459	59.04832789	72.52625876	88.71087984	93.64796859
8	29.31064272	53.03993625	67.96239168	86.49787295	92.30309007	29.38467202	53.05790948	67.96831286	86.49861813	92.30333478
9	23.27212	47.31526	63.42409	84.17236	90.84977	23.35323	47.33595	63.43093	84.17322	90.85005

	228	897	288	004	167	808	439	468	449	818
10	18.17266524	41.92020568	58.96026052	81.7598776	89.2999706	18.25841375	41.94354895	58.9680404	81.76086363	89.3003002
11	13.95677798	36.8944337	54.61295153	79.28600184	87.66798506	14.04439249	36.92031338	54.62168015	79.28711101	87.6683586
12	10.54185115	32.260333	50.41344055	76.77405195	85.96896878	10.62851143	32.28855787	50.42312091	76.77528538	85.96938671
13	7.830268014	28.02686575	46.3840745	74.24416903	84.21784849	7.913354189	28.05717598	46.39470072	74.24552765	84.21831102
14	5.718972059	24.19275267	42.54020645	71.71301591	82.4285168	5.796276125	24.22482524	42.55176248	71.71450064	82.42902399
15	4.106683265	20.74892453	38.89186125	69.19391742	80.61332099	4.176552494	20.78238274	38.90431976	69.19552929	80.61387285
16	2.898992069	17.68040248	35.44502503	66.69725904	78.7828217	2.960393597	17.71482895	35.45834665	66.69899916	78.78341825
17	2.01158608	14.96777893	32.20258128	64.2309947	76.94576647	2.064096154	15.00273099	32.21671428	64.23286428	76.94640779
18	1.371900864	12.58843109	29.16496903	61.80115988	75.10921237	1.415633237	12.62345746	29.17984948	61.80316013	75.10989862
19	9.20E-01	10.51755101	26.33064502	59.41232953	73.27873507	9.55E-01	10.55220854	26.34619742	59.41446163	73.27946652
20	6.06E-01	8.729037065	23.69641861	57.06799457	71.45867357	6.34E-01	8.762906499	23.71255694	57.07025954	71.45945056
21	3.92E-01	7.20E+00	21.25770892	54.77085303	69.6523742	4.14E-01	7.23E+00	21.27433802	54.7732517	69.65319716
22	2.49E-01	5.89E+00	19.00875681	52.52302455	67.86241191	2.66E-01	5.92E+00	19.02577415	52.52555748	67.86328132
23	1.56E-01	4.79E+00	1.69E+01	50.32620234	66.09077775	1.68E-01	4.82E+00	1.70E+01	50.32886975	66.09169414
24	9.56E-02	3.87E+00	1.51E+01	48.18175732	64.3390299	1.04E-01	3.90E+00	1.51E+01	48.18455906	64.3399938
25	5.76E-02	3.11E+00	1.33E+01	46.09080761	62.60841033	6.37E-02	3.13E+00	1.33E+01	46.09374312	62.6094223
26	3.42E-02	2.47E+00	1.18E+01	44.05426398	60.89993185	3.83E-02	2.50E+00	1.18E+01	44.05733223	60.90099243
27	1.99E-02	1.96E+00	1.03E+01	42.07285924	59.21444106	2.27E-02	1.98E+00	1.04E+01	42.07605874	59.21555079
28	1.14E-02	1.54E+00	9.07E+00	40.14716731	57.55266279	1.32E-02	1.56E+00	9.09E+00	40.15049609	57.55382216

29	6.38E-03	1.20E+00	7.93E+00	3.83E+01	55.91523057	7.58E-03	1.22E+00	7.95E+00	3.83E+01	55.91644004
30	3.52E-03	9.30E-01	6.90E+00	3.65E+01	54.30270727	4.27E-03	9.45E-01	6.92E+00	3.65E+01	54.30396726
31	1.91E-03	7.16E-01	5.99E+00	3.47E+01	52.71559861	2.37E-03	7.28E-01	6.01E+00	3.47E+01	52.7169095
32	1.02E-03	5.47E-01	5.18E+00	3.30E+01	51.15436205	1.30E-03	5.58E-01	5.20E+00	3.30E+01	51.15572415
33	5.31E-04	4.15E-01	4.47E+00	3.14E+01	4.96E+01	6.98E-04	4.24E-01	4.48E+00	3.14E+01	4.96E+01
34	2.73E-04	3.13E-01	3.84E+00	2.98E+01	4.81E+01	3.70E-04	3.20E-01	3.85E+00	2.98E+01	4.81E+01
35	1.38E-04	2.34E-01	3.29E+00	2.82E+01	4.66E+01	1.93E-04	2.40E-01	3.30E+00	2.83E+01	4.66E+01
36	6.81E-05	1.74E-01	2.80E+00	2.68E+01	4.52E+01	9.93E-05	1.79E-01	2.82E+00	2.68E+01	4.52E+01
37	3.32E-05	1.28E-01	2.38E+00	2.54E+01	4.37E+01	5.02E-05	1.32E-01	2.40E+00	2.54E+01	4.38E+01
38	1.59E-05	9.37E-02	2.02E+00	2.40E+01	4.24E+01	2.51E-05	9.71E-02	2.03E+00	2.40E+01	4.24E+01
39	7.45E-06	6.81E-02	1.71E+00	2.27E+01	4.10E+01	1.23E-05	7.08E-02	1.72E+00	2.27E+01	4.10E+01
40	3.44E-06	4.91E-02	1.44E+00	2.14E+01	3.96E+01	5.96E-06	5.13E-02	1.44E+00	2.14E+01	3.96E+01
41	1.56E-06	3.52E-02	1.20E+00	2.02E+01	3.83E+01	2.84E-06	3.69E-02	1.21E+00	2.02E+01	3.83E+01
42	6.93E-07	2.50E-02	1.01E+00	1.91E+01	3.70E+01	1.34E-06	2.64E-02	1.01E+00	1.91E+01	3.70E+01
43	3.03E-07	1.77E-02	8.37E-01	1.79E+01	3.58E+01	6.20E-07	1.87E-02	8.44E-01	1.80E+01	3.58E+01
44	1.30E-07	1.24E-02	6.95E-01	1.69E+01	3.46E+01	2.83E-07	1.32E-02	7.01E-01	1.69E+01	3.46E+01
45	5.50E-08	8.63E-03	5.74E-01	1.59E+01	3.34E+01	1.28E-07	9.22E-03	5.80E-01	1.59E+01	3.34E+01
46	2.28E-08	5.96E-03	4.73E-01	1.49E+01	3.22E+01	5.66E-08	6.41E-03	4.78E-01	1.49E+01	3.22E+01
47	9.28E-09	4.09E-03	3.88E-01	1.40E+01	3.10E+01	2.48E-08	4.42E-03	3.93E-01	1.40E+01	3.10E+01
48	3.72E-09	2.78E-03	3.18E-01	1.31E+00	2.99E+00	1.07E-08	3.03E-03	3.22E-01	1.31E+00	2.99E+00

				1	1				1	1
49	1.46E-09	1.88E-03	2.59E-01	1.23E+01	2.88E+01	4.57E-09	2.06E-03	2.62E-01	1.23E+01	2.88E+01
50	5.64E-10	1.26E-03	2.10E-01	1.15E+01	2.78E+01	1.92E-09	1.39E-03	2.13E-01	1.15E+01	2.78E+01
51	2.14E-10	8.41E-04	1.70E-01	1.08E+01	2.68E+01	7.98E-10	9.36E-04	1.73E-01	1.08E+01	2.68E+01
52	7.98E-11	5.56E-04	1.37E-01	1.01E+01	2.57E+01	3.27E-10	6.24E-04	1.39E-01	1.01E+01	2.58E+01
53	2.92E-11	3.65E-04	1.10E-01	9.39E+00	2.48E+01	1.32E-10	4.13E-04	1.12E-01	9.40E+00	2.48E+01
54	1.05E-11	2.38E-04	8.83E-02	8.76E+00	2.38E+01	5.28E-11	2.72E-04	8.99E-02	8.77E+00	2.38E+01
55	3.69E-12	1.54E-04	7.04E-02	8.16E+00	2.29E+01	2.08E-11	1.77E-04	7.18E-02	8.17E+00	2.29E+01
56	1.25E-12	9.90E-05	5.60E-02	7.60E+00	2.20E+01	8.10E-12	1.15E-04	5.72E-02	7.61E+00	2.20E+01
57	3.98E-13	6.31E-05	4.43E-02	7.07E+00	2.12E+01	3.10E-12	7.42E-05	4.53E-02	7.07E+00	2.12E+01
58	9.95E-14	4.00E-05	3.50E-02	6.57E+00	2.03E+01	1.17E-12	4.75E-05	3.58E-02	6.57E+00	2.03E+01
59	2.84E-14	2.51E-05	2.75E-02	6.10E+00	1.95E+01	3.84E-13	3.02E-05	2.82E-02	6.10E+00	1.95E+01
60	0.00E+00	1.57E-05	2.15E-02	5.66E+00	1.87E+01	1.42E-13	1.90E-05	2.21E-02	5.66E+00	1.87E+01

Table 3. Sulfate Concentration as Affected by External U_0

mol/m^3	T=500 days					T=10 years				
Depth (mm)	U300	U200	U100	U60	U30	U300	U200	U100	U60	U30
0	300	200	100	60	30	100	100	100	100	100
1	264.27039	171.81611	82.415711	48.354564	23.723523	99.779241	99.285773	97.774344	96.603435	95.420313
2	229.02421	144.37859	65.809265	37.563226	18.005058	99.467439	98.381172	95.269472	92.964229	90.693177
3	194.76034	118.3617	50.869746	28.151714	13.150163	98.967178	97.118845	92.301613	88.948462	85.754623
4	162.033	94.3967	38.0311	20.3691	9.26333	98.1599	95.3437	88.7704	84.5130	80.6063

	83	71	99	22	33	34	54	09	2	89
5	131.45637	73.038987	27.484618	14.241209	6.3070056	96.904793	92.923324	84.654183	79.68708	75.295636
6	103.65592	54.701379	19.200314	9.6327098	4.1592656	95.050896	89.768596	80.001807	74.550817	69.895155
7	79.197982	39.589093	12.973636	6.3130753	2.6624261	92.462797	85.855406	74.916871	69.212916	64.486693
8	58.486145	27.66571	8.4891254	4.0161314	1.6578375	89.052894	81.234993	69.535809	63.790255	59.148939
9	41.675439	18.669898	5.3879521	2.4849305	1.0063242	84.809719	76.027977	64.005037	58.392609	53.950401
10	28.634938	12.17815	3.3234852	1.4985336	0.5967205	79.810015	70.403112	58.462168	53.113486	48.94634
11	18.977746	7.6905718	1.9966465	0.8826296	0.3463477	74.208529	64.548513	53.024081	48.026457	44.178495
12	12.146868	4.7117297	1.1708536	0.5087983	0.1971472	68.209337	58.644667	47.781911	43.185376	39.676345
13	7.5231923	2.8072131	0.6716539	0.2876257	0.1102523	62.029984	52.845691	42.801258	38.626753	35.458992
14	4.5196963	1.6305056	0.3776969	0.1597488	0.0606786	55.870359	47.270602	38.125384	34.372905	31.537082
15	2.6408473	0.92554	0.2086219	0.0873248	0.0329168	49.893315	42.002818	33.779524	30.43505	27.914506
16	1.504838	0.5146681	0.1133971	0.0470582	0.0176266	44.217786	37.094609	29.775133	26.815953	24.589793
17	0.8385058	0.2809888	0.0607597	0.0250372	0.0093299	38.921107	32.573512	26.113486	23.51202	21.557225
18	0.4580222	0.1509311	0.0321431	0.0131702	0.0048874	34.046146	28.448706	22.788499	20.514902	18.807722
19	0.2458352	0.079913	0.0168133	0.0068581	0.0025368	29.609713	24.716411	19.788835	17.812709	16.329567
20	0.1299279	0.0417784	0.0087068	0.0035394	0.001306	25.610238	21.36403	17.099463	15.390949	14.109016
21	0.067748	0.0216001	0.0044694	0.0018123	0.0006675	22.033866	18.373173	14.702809	13.233265	12.130824
22	0.034912	0.0110595	0.0022766	0.0009216	0.0003339	18.858945	15.721799	12.57963	11.322042	10.378707
23	0.0178076	0.0056148	0.0011519	0.0004658	0.0001712	16.059181	13.385726	10.709694	9.638915	8.835744

24	0.0090029	0.0028296	0.0005794	0.0002342	8.61E-05	13.605786	11.339713	9.0723316	8.1651942	7.4848042
25	0.0045168	0.001417	0.0002899	0.0001172	4.31E-05	11.468951	9.5582417	7.6468746	6.882235	6.3087369
26	0.0022513	0.0007057	0.0001445	5.84E-05	2.15E-05	9.6188573	8.0161045	6.4130236	5.7717451	5.2907771
27	0.0011157	0.0003498	7.17E-05	2.90E-05	1.07E-05	8.026376	6.68884	5.3511414	4.8160391	4.4147078
28	0.0005503	0.0001727	3.55E-05	1.44E-05	5.29E-06	6.6635625	5.553064	4.4424854	3.9982428	3.6650585
29	0.0002703	8.50E-05	1.75E-05	7.10E-06	2.62E-06	5.5039974	4.5867113	3.6693859	3.3024501	3.0272473
30	0.0001323	4.17E-05	8.61E-06	3.50E-06	1.29E-06	4.5230173	3.7692039	3.0153714	2.7138357	2.4876833

Table 4. Sulfate Concentration as Affected by Inherent C_3A

C3A	T=500 days					T=10 years				
Depth (mm)	C150	C120	C90	C60	C30	C150	C120	C90	C60	C30
0	300	300	300	300	300	150	120	90	60	30
1	256.41105	261.03997	265.92772	271.05509	276.37381	149.36637	119.64299	89.833329	59.943801	29.990489
2	213.85346	222.74966	232.26213	242.3487	252.89619	148.47656	119.13984	89.597689	59.864173	29.977016
3	173.34159	185.81014	199.42459	214.12634	229.71563	147.07859	118.33931	89.218065	59.734389	29.954862
4	135.93628	150.96673	167.88487	186.6542	206.98171	144.90192	117.06609	88.601003	59.518904	29.917386
5	102.67276	119.00997	138.16689	160.22691	184.84615	141.68023	115.12595	87.631775	59.169898	29.854946
6	74.393935	90.692055	110.8244	135.16794	163.46388	137.20561	112.33247	86.181257	58.626314	29.753905
7	51.560178	66.598685	86.384851	111.81947	142.99347	131.39093	108.54878	84.124068	57.816542	29.595892
8	34.129669	47.021001	65.269688	90.518881	123.59629	124.30879	103.72944	81.3643	56.66566	29.357617
9	21.577488	31.883674	47.71338	71.56256	105.43316	116.18442	97.943793	77.861995	55.107039	29.011609

10	13.047681	20.765763	33.711063	55.163393	88.657721	107.34452	91.368573	73.650224	53.096198	28.528173
11	7.5649073	13.006703	23.017556	41.413237	73.406269	98.146419	84.252321	68.835203	50.623143	27.878632
12	4.2187007	7.8513083	15.199726	30.262965	59.785083	88.916632	76.867019	63.578803	47.718979	27.039529
13	2.2707238	4.5797167	9.7221002	21.527906	47.857404	79.915235	69.464914	58.070129	44.454203	25.997046
14	1.1838254	2.5891236	6.0356802	14.917764	37.63315	71.326547	62.251676	52.496185	40.928951	24.750618
15	0.5998209	1.4230274	3.645632	10.081666	29.064285	63.267056	55.376614	47.019707	37.258322	23.314743
16	0.2963079	0.7626321	2.1478437	6.6553428	22.047565	55.800478	48.937127	41.76748	33.557071	21.71842
17	0.143125	0.3996498	1.2374291	4.2994307	16.434466	48.953053	42.987454	36.828103	29.927344	20.002241
18	0.0677773	0.2053214	0.6988589	2.7233455	12.046185	42.725932	37.550261	32.255926	26.451274	18.213838
19	0.0315415	0.1036588	0.3877997	1.6947517	8.6905624	37.104059	32.626271	28.077809	23.18841	16.402724
20	0.0144557	0.0515374	0.211881	1.0381487	6.1777443	32.062116	28.201723	24.300243	20.176789	14.615558
21	0.006537	0.0252823	0.1142028	0.6271299	4.3323278	27.568381	24.253666	20.915558	17.436115	12.892582
22	0.0029218	0.0122584	0.0608292	0.3742285	3.0010198	23.587254	20.753555	17.906777	14.971723	11.265539
23	0.0012928	0.0058835	0.0320679	0.2209381	2.0559817	20.080966	17.669668	15.251172	12.778448	9.7569989
24	0.000567	0.0027991	0.0167552	0.1292306	1.39E+00	17.010795	14.968733	12.922763	10.843953	8.3807887
25	0.0002468	0.0013216	0.0086871	0.0749833	9.38E-01	14.337989	12.617062	10.894038	9.151371	7.1431191
26	0.0001067	0.0006199	0.0044743	4.32E-02	6.26E-01	12.024474	10.581362	9.1371359	7.681284	6.0440507
27	4.59E-05	0.0002892	2.29E-03	2.47E-02	4.15E-01	10.03342	8.8293263	7.6246467	6.413149	5.0790155
28	1.96E-05	0.0001342	1.17E-03	1.41E-02	2.74E-01	8.3296758	7.3300758	6.3301694	5.3262957	4.2402176
29	8.37E-06	6.21E-05	5.93E-04	8.00E-03	1.80E-01	6.88010	6.05447	5.22868	4.40060	3.51782

						66	56	56	27	31
30	3.56E-06	2.86E-05	3.00E-04	4.52E-03	1.17E-01	5.6538256	4.9753538	4.2968084	3.6169413	2.9009105

Table 5. Sulfate Concentration as Affected by Diffusion Coefficient D

D	T=500 days					T=10 years				
Depth (mm)	D-16.0	D-8.0	D-4.0	D-2.0	D-1.0	D-16.0	D-8.0	D-4.0	D-2.0	D-1.0
0	300	300	300	300	300	100	100	100	100	100
1	287.34472	282.10736	274.70914	264.27039	249.57501	99.926888	99.8956	99.849528	99.779241	99.665489
2	274.7111	264.27566	249.58969	229.02421	200.52262	99.849658	99.779666	99.666728	99.467439	99.071282
3	262.1203	246.56463	224.81237	194.76034	154.34668	99.764355	99.641023	99.419292	98.967178	97.907074
4	249.59347	229.0352	200.55786	162.03383	112.76978	99.667015	99.468025	99.071159	98.159934	95.776359
5	237.15211	211.75109	177.02202	131.45637	77.501993	99.553533	99.247979	98.580578	96.904793	92.267788
6	224.81839	194.77976	154.41615	103.65592	49.746596	99.419559	98.966801	97.89982	95.050896	87.115325
7	212.6153	178.19273	132.96218	79.197982	29.715654	99.260426	98.608867	96.976599	92.462797	80.356346
8	200.56685	162.06527	112.88255	58.486145	16.528872	99.071104	98.15708	95.757272	89.052894	72.363412
9	188.69804	146.47548	94.385465	41.675439	8.5979899	98.846172	97.593151	94.191597	84.809719	63.715613
10	177.03488	131.50267	77.647252	28.634938	4.2105978	98.579829	96.89811	92.238499	79.810015	55.004788
11	165.60426	117.22508	62.794565	18.977746	1.9562529	98.265921	96.053023	89.87183	74.208529	46.695497
12	154.43376	103.71714	49.890081	12.146868	0.8689294	97.897998	95.039896	87.085133	68.209337	39.080524
13	143.55138	91.046317	38.924811	7.5231923	0.3716365	97.469409	93.842694	83.89405	62.029984	32.303013
14	132.98514	79.269855	29.818957	4.5196963	0.1540175	96.973406	92.448402	80.336022	55.870359	26.401371
15	122.762	68.4317	22.4312	2.64084	0.06218	96.4032	90.8480	76.4671	49.8933	21.3502

	73	5	83	73	88	91	21	34	15	38
16	112.91093	58.560215	16.575034	1.504838	0.0245792	95.752576	89.037394	72.356803	44.217786	17.089343
17	103.4551	49.665964	12.037152	0.8385058	0.0095465	95.015159	87.017763	68.081383	38.921107	13.541478
18	94.418597	41.741511	8.5973226	0.4580222	0.0036558	94.185511	84.795991	63.717856	34.046146	10.623101
19	85.82222	34.76159	6.0440343	0.2458352	0.0013841	93.258867	82.384419	59.338529	29.609713	8.2505841
20	77.683634	28.684652	4.1860499	0.1299279	0.0005193	92.231399	79.800353	55.007284	25.610238	6.3439425
21	70.016891	23.455288	2.8589414	0.067748	0.0001934	91.100388	77.065263	50.777483	22.033866	4.8290729
22	62.832009	19.007314	1.9272854	0.034912	7.16E-05	89.86435	74.203748	46.691339	18.858945	3.6390355
23	56.134669	15.267207	1.2836307	0.0178076	2.64E-05	88.523139	71.242395	42.780367	16.059181	2.7146607
24	49.926035	12.157581	0.8454544	0.0090029	9.70E-06	87.078007	68.208625	39.066519	13.605786	2.0046647
25	44.202705	9.6004179	0.5511668	0.0045168	3.56E-06	85.531615	65.129629	35.56364	11.468951	1.4654018
26	38.956812	7.5198423	0.3559476	2.25E-03	1.30E-06	83.888001	62.031442	32.278992	9.6188573	1.060362
27	34.176258	5.8443176	2.28E-01	1.12E-03	4.74E-07	82.152496	58.938234	29.214659	8.026376	0.759503
28	29.845073	4.5082069	1.45E-01	5.50E-04	1.73E-07	80.331611	55.871798	26.368782	6.6635625	0.5384926
29	25.943876	3.45E+00	9.13E-02	2.70E-04	6.30E-08	78.432876	52.851248	23.736571	5.5039974	0.3779234
30	22.450421	2.63E+00	5.72E-02	1.32E-04	2.29E-08	76.464661	49.892898	21.311106	4.5230173	0.2625437

Table 6. Sulfate Concentration as Affected by Reaction Constant K

K	T=500 days					T=10 years				
Depth (mm)	K-1*10E7	K-1*10E8	K-1*10E9	K-1*10E10	K-1*10E11	K-1*10E7	K-1*10E8	K-1*10E9	K-1*10E10	K-1*10E11
0	300	300	300	300	300	100	100	100	100	100
1	263.608	264.270	271.888	279.8890	281.5922	99.9998	99.7792	97.2399	94.57302	94.00529

	54	39	19	4	3	57	41	74	6	6
2	227.42924	229.02421	244.25908	259.95037	263.29684	99.999096	99.467439	94.389147	89.158717	88.043228
3	191.67696	194.76034	217.52416	240.34308	245.22322	99.994972	98.967178	91.379239	83.772931	82.14622
4	156.58821	162.03383	192.02639	221.21109	227.47594	99.975144	98.159934	88.162415	78.434184	76.345901
5	122.49429	131.45637	168.04103	202.68163	210.1531	99.892152	96.904793	84.709907	73.163041	70.672551
6	90.020528	103.65592	145.77594	184.86425	193.34485	99.596025	95.050896	81.010888	67.981451	65.154583
7	60.431337	79.197982	125.37277	167.85022	177.13215	98.718346	92.462797	77.071202	62.912052	59.818076
8	35.785031	58.486145	106.90963	151.71241	161.58572	96.619932	89.052894	72.911733	57.977471	54.68637
9	18.109203	41.675439	90.405795	136.50565	146.76536	92.665131	84.809719	68.566267	53.199649	49.779745
10	7.7212566	28.634938	75.828334	122.26736	132.71946	86.781242	79.810015	64.078883	48.599207	45.115174
11	2.7944701	18.977746	63.100363	109.0187	119.48484	79.602954	74.208529	59.50099	44.194878	40.706166
12	0.8759874	12.146868	52.110346	96.76577	107.08679	71.966297	68.209337	54.888177	40.003036	36.562695
13	0.2432793	7.5231923	42.721762	85.501213	95.539488	64.456621	62.029984	50.297127	36.03731	32.691218
14	0.0610681	4.5196963	34.78246	75.205813	84.846461	57.356568	55.870359	45.782771	32.30832	29.094771
15	0.0140844	2.6408473	28.133141	65.850239	75.001394	50.768902	49.893315	41.395884	28.823517	25.773132
16	0.0030242	1.504838	22.614568	57.396782	65.989012	44.71839	44.217786	37.181209	25.587137	22.723061
17	0.0006111	0.8385058	18.073281	49.801059	57.786102	39.200406	38.921107	33.176183	22.600256	19.938576
18	0.0001172	0.4580222	14.365762	43.013636	50.362621	34.198781	34.046146	29.410232	19.860941	17.411279
19	2.15E-05	0.2458352	11.361161	36.98155	43.682842	29.691651	29.609713	25.904605	17.364475	15.130711
20	3.80E-06	0.1299279	8.9427526	31.649682	37.706512	25.653547	25.610238	22.67263	15.103654	13.08471

21	6.50E-07	0.067748	7.0083668	26.961991	32.389989	22.056448	22.033866	19.720326	13.069118	11.259785
22	1.08E-07	0.034912	5.4700492	22.862578	27.687323	18.870583	18.858945	17.047233	11.249723	9.6414751
23	1.75E-08	0.0178076	4.2531825	19.296592	23.551269	16.065117	16.059181	14.647399	9.6329199	8.2146943
24	2.79E-09	0.0090029	3.2952777	16.210973	19.934208	13.608787	13.605786	12.510361	8.2051293	6.964051
25	4.35E-10	0.0045168	2.5445935	13.555045	16.78896	11.470457	11.468951	10.622259	6.9521084	5.8741368
26	6.70E-11	0.0022513	1.958726	11.280962	14.069484	9.6196077	9.6188573	8.966699	5.859287	4.9297798
27	1.02E-11	0.0011157	1.5032278	9.344028	11.731461	8.0267479	8.026376	7.525672	4.9120718	4.1162608
28	1.53E-12	0.0005503	1.1503399	7.7029001	9.7327663	6.6637459	6.6635625	6.2802993	4.0961125	3.4194905
29	2.28E-13	0.0002703	0.8778497	6.3196884	8.0338162	5.5040875	5.5039974	5.2114709	3.3975247	2.8261488
30	3.37E-14	0.0001323	0.6680946	5.1599734	6.5978228	4.5230614	4.5230173	4.3003632	2.8030703	2.3237871

Table 7. Sulfate Concentration as Affected by Proportional Constant L

L Depth (mm)	T=500 days						T=10 years					
	L-2	L-2.2	L-2.4	L-2.6	L-2.8	L-3	L-2	L-2.2	L-2.4	L-2.6	L-2.8	L-3
0	300	300	300	300	300	300	100	100	100	100	100	100
1	269.75288	268.5986	267.46954	266.36975	265.30253	264.27039	99.960272	99.937166	99.907401	99.870958	99.828088	99.779241
2	239.73144	237.45877	235.24463	233.09699	231.02206	229.02421	99.895331	99.838278	99.766353	99.679911	99.579851	99.467439
3	210.17465	206.85936	203.65084	200.5602	197.59518	194.76034	99.77179	99.657998	99.518687	99.355467	99.170703	98.967178
4	181.35359	177.12092	173.0635	169.19308	165.51597	162.03383	99.53722	99.329196	99.082822	98.802427	98.493053	98.159934
5	153.58806	148.62282	143.92319	139.49657	135.34288	131.45637	99.110447	98.753861	98.346036	97.895949	97.412681	96.904793
6	127.2573	121.80778	116.73128	112.02333	107.671	103.65592	98.374932	97.79985	97.165191	96.486424	95.777612	95.050896

7	102.79536	97.163485	92.015918	87.327654	83.066718	79.197982	97.179974	96.3082	95.379924	94.417806	93.440516	92.462797
8	80.660301	75.17279	70.264582	65.883411	61.974868	58.486145	95.355194	94.114876	92.839901	91.55837	90.291119	89.052894
9	61.272669	56.235554	51.835007	47.990202	44.62605	41.675439	92.74058	91.085649	89.441303	87.836187	86.288711	84.809719
10	44.933701	40.582441	36.873004	33.70197	30.980727	28.634938	89.226893	87.154793	85.160617	83.26616	81.481699	79.810015
11	31.750424	28.213925	25.271748	22.809729	20.736099	18.977746	84.792843	82.352559	80.071355	77.956428	76.004924	74.208529
12	21.6003	18.892912	16.692578	14.888026	13.394381	12.146868	79.522716	76.808477	74.335339	72.090459	70.055238	68.209337
13	14.153661	12.196282	10.639547	9.3860719	8.3647405	7.5231923	73.595312	70.72808	68.171784	65.892126	63.855225	62.029984
14	8.9452401	7.603673	6.5572297	5.7282739	5.0621225	4.5196963	67.248536	64.352878	61.816861	59.587352	57.618199	55.870359
15	5.4649875	4.5892227	3.9176285	3.3930945	2.9765764	2.6408473	60.734503	57.91915	55.487952	53.374222	51.523877	49.893315
16	3.2362422	2.6889817	2.2753798	1.9562189	1.705333	1.504838	54.281127	51.627933	49.361248	47.40696	45.707472	44.217786
17	1.8630927	1.5340638	1.2884331	1.1007996	0.9545482	0.8385058	48.069215	45.630691	43.563838	41.792656	40.259721	38.921107
18	1.0458572	0.8546059	0.7132846	0.6062349	0.5233773	0.4580222	42.225596	40.02833	38.17647	36.596331	35.233286	34.046146
19	0.5741317	0.4661798	0.3870803	0.3275752	0.2817814	0.2458352	36.827507	34.878242	33.241832	31.849642	30.651439	29.609713
20	0.3090479	0.2496409	0.2064096	0.1740696	0.1492971	0.1299279	31.912411	30.204356	28.774237	27.559948	26.516426	25.610238
21	0.1635266	0.1315414	0.1083939	0.0911561	0.0780012	0.067748	27.488797	26.00692	24.76834	23.718038	22.816321	22.033866
22	0.0852446	0.0683441	0.0561673	0.0471319	0.0402571	0.034912	23.545606	22.270532	21.206002	20.304038	19.530154	18.858945
23	0.0438656	0.0350785	0.0287695	0.0241012	0.0205575	0.0178076	20.059464	18.970103	18.06127	17.291626	16.631529	16.059181
24	0.0223216	0.0178156	0.0145891	0.0122069	0.0104017	0.0090029	16.999823	16.075014	15.303807	14.650922	14.0911	13.605786
25	0.0112498	0.0089663	0.0073346	0.0061317	0.0052214	0.0045168	14.332446	13.551919	12.901208	12.350441	11.878251	11.468951
26	0.0056	0.0044	0.0036	0.0030	0.0026	0.0022	12.021	11.366	10.820	10.358	9.9622	9.6188

	231	775	601	583	032	513	698	592	534	401	354	573
27	0.0027909	0.0022211	0.0018149	0.0015161	0.0012903	0.0011157	10.032039	9.485147	9.0293352	8.6436069	8.3129567	8.026376
28	0.0013769	0.0010955	0.0008951	0.0007477	0.0006363	0.0005503	8.3289939	7.8748381	7.4963412	7.1760542	6.9015096	6.6635625
29	0.0006758	0.0005377	0.0004394	0.0003671	0.0003125	0.0002703	6.8797715	6.5045863	6.1919154	5.9273377	5.7005505	5.5039974
30	0.0003303	0.0002629	0.0002149	0.0001796	0.0001529	0.0001323	5.6536616	5.3453167	5.0883545	4.8709201	4.6845447	4.5230173

Table 8. Data Fitting to the Experimental Results (Type GU)

Ratio	0.08	0.17	0.2	0.25	0.3
352.112676	28.169014	59.859155	70.422535	88.028169	105.6338
Depth (mm)	1w	2w	4w	8w	12w
0	28.169	59.8592	70.42254	88.0282	105.6338
1	20.199547	46.226235	57.018837	73.828638	90.307966
2	13.404166	34.011634	44.638032	60.414176	75.659453
3	8.2767418	23.949751	33.887739	48.307529	62.16929
4	4.7778492	16.207055	25.017135	37.79724	50.140623
5	2.5879796	10.578362	18.007534	28.978488	39.721831
6	1.3192389	6.6795704	12.670905	21.800872	30.934161
7	0.634644	4.0896265	8.7365852	16.116895	23.702219
8	0.2890321	2.4316358	5.9156548	11.72559	17.884742
9	0.1250883	1.4053796	3.9410864	8.4075622	13.302888
10	5.17E-02	0.7898825	2.5874249	5.9499285	9.7638993
11	2.05E-02	0.4317872	1.6760944	4.1615992	7.0789447
12	7.80E-03	0.2295755	1.0722677	2.8805945	5.074998
13	2.87E-03	1.19E-01	0.6778621	1.9756111	3.6014049
14	1.03E-03	5.97E-02	0.4235965	1.3439825	2.5322621
15	3.57E-04	2.92E-02	0.2616831	0.9077814	1.7658655
16	1.21E-04	1.39E-02	1.60E-01	0.6093015	1.2223787
17	4.02E-05	6.47E-03	9.64E-02	0.4066859	0.8406448
18	1.31E-05	2.93E-03	5.75E-02	0.2700974	0.5747879
19	4.19E-06	1.29E-03	3.39E-02	0.178576	0.3910123
20	1.32E-06	5.58E-04	1.97E-02	0.1175777	0.2648069
21	4.09E-07	2.35E-04	1.13E-02	7.71E-02	0.1786335
22	1.25E-07	9.72E-05	6.40E-03	5.04E-02	0.1200881

23	3.78E-08	3.93E-05	3.57E-03	3.28E-02	8.05E-02
24	1.13E-08	1.56E-05	1.97E-03	2.13E-02	5.38E-02
25	3.34E-09	6.07E-06	1.07E-03	1.38E-02	3.59E-02
26	9.76E-10	2.32E-06	5.72E-04	8.86E-03	2.39E-02
27	2.83E-10	8.75E-07	3.02E-04	5.68E-03	1.59E-02
28	8.15E-11	3.24E-07	1.57E-04	3.63E-03	1.05E-02
29	2.33E-11	1.18E-07	8.05E-05	2.31E-03	6.96E-03
30	6.59E-12	4.26E-08	4.07E-05	1.46E-03	4.60E-03

Table 9. Data Fitting to the Experimental Results (Type HS)

	0.14	0.148	0.155	0.166	0.19
352.11268	49.295775	52.112676	54.577465	58.450704	66.901408
	1w	2w	4w	8w	12w
0	50	52.1127	54.577	58.4507	66.901
1	36.181996	41.572768	46.388423	51.792076	60.364582
2	24.065311	31.766684	38.53635	45.302379	53.952002
3	14.670466	23.229049	31.287342	39.121987	47.769116
4	8.1903373	16.245049	24.825852	33.360082	41.902739
5	4.1929005	10.861259	19.252799	28.093869	36.420086
6	1.974964	6.9412197	14.593575	23.369715	31.368891
7	0.8605624	4.240306	10.812581	19.205991	26.778249
8	0.3492859	2.4766341	7.830867	15.597208	22.660184
9	0.1330622	1.3836502	5.5437487	12.518913	19.011784
10	4.79E-02	0.7399387	3.8361762	9.9328112	15.817749
11	1.64E-02	0.3791295	2.5946185	7.7916563	13.053124
12	5.40E-03	0.1863488	1.715152	6.0435632	10.686033
13	1.71E-03	8.80E-02	1.1080552	4.6355521	8.6802254
14	5.24E-04	4.00E-02	0.6995724	3.5162497	6.9973183
15	1.56E-04	1.75E-02	0.4316299	2.6377777	5.5986527
16	4.52E-05	7.40E-03	2.60E-01	1.9569251	4.45E+00
17	1.28E-05	3.03E-03	1.53E-01	1.4357334	3.51E+00
18	3.55E-06	1.20E-03	8.83E-02	1.041631	2.75E+00
19	9.69E-07	4.62E-04	4.98E-02	0.7472479	2.13E+00
20	2.60E-07	1.73E-04	2.74E-02	0.5300197	1.65E+00
21	6.85E-08	6.32E-05	1.48E-02	3.72E-01	1.26E+00
22	1.78E-08	2.25E-05	7.77E-03	2.58E-01	9.60E-01
23	4.58E-09	7.83E-06	4.01E-03	1.77E-01	7.26E-01

24	1.16E-09	2.67E-06	2.02E-03	1.20E-01	5.44E-01
25	2.93E-10	8.90E-07	1.00E-03	8.00E-02	4.05E-01
26	7.28E-11	2.91E-07	4.85E-04	5.30E-02	3.00E-01
27	1.80E-11	9.38E-08	2.30E-04	3.46E-02	2.20E-01
28	4.39E-12	2.97E-08	1.07E-04	2.24E-02	1.60E-01
29	1.07E-12	9.24E-09	4.90E-05	1.43E-02	1.16E-01
30	2.57E-13	2.84E-09	2.20E-05	9.01E-03	8.31E-02

Table 10. Data Fitting to the Experimental Results (Blend IC)

		0.12	0.16	0.31	0.56	0.82
352.11268		42.253521	56.338028	109.15493	197.1831	288.73239
		1w	2w	4w	8w	12w
0		42.253	56.338	109.155	197.183	288.73239
1		30.162349	43.65626	89.320762	168.78005	254.2629
2		19.834882	32.231366	70.831461	141.53686	220.65233
3		12.058689	22.750143	54.54407	116.322	188.62163
4		6.8001322	15.400322	40.869161	93.725815	158.76221
5		3.5675948	10.025242	29.857885	74.076354	131.52955
6		1.7465157	6.2894495	21.311635	57.467085	107.23293
7		0.8006467	3.8084669	14.890379	43.798256	86.0298
8		0.3452149	2.2280848	10.201967	32.828095	67.93003
9		0.1407238	1.2600755	6.8643485	24.226798	52.812176
10		5.45E-02	0.6890872	4.5411958	17.625979	40.449962
11		2.02E-02	0.3644668	2.956499	12.658278	30.544991
12		7.19E-03	0.1864939	1.8952683	8.9847774	22.760608
13		2.47E-03	9.24E-02	1.1966861	6.3105794	16.752296
14		8.22E-04	4.43E-02	0.7442874	4.3907053	12.191551
15		2.66E-04	2.06E-02	0.4559457	3.0291569	8.7819634
16		8.39E-05	9.28E-03	2.75E-01	2.0739103	6.2678495
17		2.59E-05	4.07E-03	1.63E-01	1.4100466	4.4367674
18		7.83E-06	1.73E-03	9.55E-02	0.9525413	3.1177039
19		2.33E-06	7.18E-04	5.49E-02	0.6396056	2.1766472
20		6.80E-07	2.90E-04	3.11E-02	0.4270067	1.5109609
21		1.96E-07	1.15E-04	1.73E-02	2.83E-01	1.043561
22		5.56E-08	4.42E-05	9.45E-03	1.87E-01	0.7175125
23		1.56E-08	1.67E-05	5.09E-03	1.23E-01	4.91E-01
24		4.32E-09	6.17E-06	2.69E-03	8.02E-02	3.35E-01

25	1.19E-09	2.24E-06	1.40E-03	5.21E-02	2.28E-01
26	3.22E-10	7.97E-07	7.15E-04	3.36E-02	1.55E-01
27	8.67E-11	2.79E-07	3.60E-04	2.15E-02	1.05E-01
28	2.31E-11	9.61E-08	1.78E-04	1.37E-02	7.05E-02
29	6.13E-12	3.26E-08	8.65E-05	8.68E-03	4.74E-02
30	1.61E-12	1.09E-08	4.14E-05	5.45E-03	3.18E-02

APPENDIX B-CODES AND REPORTS

MATLAB Codes-Physical Diffusion Modeling

Explicit Method:

```
%==================Pure Diffusion=================
format compact
U0=30;%The sulfate concentration of the aggressive solution (mol/m^3)
D=1.296e-7;%Diffusion coefficient (m^2/d)
dX=0.001; %Space step(m)
dT=1; %Time step(d)
M=7300; %Number of subdomain of simulated time
N=100; %Number of subdomain of space of diffusion field
%==================Solving Z======================
r=D*dT/dX^2; %Variable substitution
Z=zeros(N+1,1); %Z initial linear array
for j=[ 1:M] %Iteration for time field
        Z(1,j+1)=U0; %Boundary condition
        for i=[2:N] %Iteration for space field
           Z(i,j+1)=r*Z(i+1,j)+(1-2*r)*Z(i,j)+r*Z(i-1,j);
        end
    Z(N+1,j+1)=(1-2*r)*Z(N+1,j)+2*r*Z(N,j);
end
%=========OUTPUT Z IN DIFFERENT TIME======================
for n=[1:101]
    VZ(n,1)=Z(n,201);
    VZ(n,2)=Z(n,501);
    VZ(n,3)=Z(n,1001);
    VZ(n,4)=Z(n,3651);
    VZ(n,5)=Z(n,7301);
```

end

%=================END=================

Implicit Method:

%====================BASIC PARAMETERS========================

U0=30;%The sulfate concentration of the aggressive solution(mol/m^3)

D=1.728e-7;%Diffusion coefficient(m^2/d)

dX=0.001;%Space step(m)

dT=1;%Time step(d)

M=7300;%Number of subdomain of simulated time

N=100;%Number of subdomain of space of diffusion field

%======================SOLVING Z=========================

r=D*dT/dX^2;%Variable substitution

Z=zeros(N+1,1);%Z initial linear array

U=[U0;zeros(N,1)];%Sulfate concentration U linear array

az=(1+2*r)*ones(N,1);%Diagonal element of Matrix AZ

bz=(-r)*ones(N-1,1);

AZ=sparse(diag((bz),1)+diag((bz),-1)+diag(az));

AZ(N,N-1)=-2*r;

dz(1)=r*U0;

dz(2:N)=zeros(N-1,1);   %Linear array dz

for j=[1:M]%Iteration solution of Z

    Z(2:N+1,j+1)=AZ\(Z(2:N+1,j)+dz');

    Z(1,j+1)=U0;

end

%=========OUTPUT Z IN DIFFERENT TIME====================

```
for n=[1:101]

VZ(n,1)=Z(n,201);

VZ(n,2)=Z(n,501);

VZ(n,3)=Z(n,1001);

VZ(n,4)=Z(n,3651);

VZ(n,5)=Z(n,7301);

end
```

Crank-Nicolson Method:

```
%====================BASIC PARAMETERS=======================

U0=30;%The sulfate concentration of the aggressive solution(mol/m^3)

D=1.296e-7;%Diffusion coefficient(m^2/d)

dX=0.001;%Space step(m)

dT=1;%Time step(d)

M=7300;%Number of subdomain of simulated time

N=100;%Number of subdomain of space of diffusion field

%======================SOLVING Z==========================

r=D*dT/dX^2;%Variable substitution

Z=zeros(N+1,1);%Z initial linear array

U=[U0;zeros(N,1)];%Sulfate concentration U linear array

az=-2*(1+1/r)*ones(N,1);%Diagonal element of Matrix AZ

bz=2*(1-1/r)*ones(N,1);%Diagonal element of Matrix BZ

dz(1)=-2*U0;

dz(2:N)=zeros(N-1,1);    %Linear array dz

%   Matrix AZ and BZ

AZ=sparse(diag(ones(N-1,1),1)+diag(ones(N-1,1),-1)+diag(az));

AZ(N,N-1)=2;
```

```matlab
BZ=sparse(-diag(ones(N-1,1),1)-diag(ones(N-1,1),-1)+diag(bz));

BZ(N,N-1)=-2;

for j=[1:M]%Iteration solution of Z

    Z(2:N+1,j+1)=AZ\(BZ*Z(2:N+1,j)+dz');

    Z(1,j+1)=U0;

end

%==========OUTPUT Z IN DIFFERENT TIME=========================

for n=[1:101]

VZ(n,1)=Z(n,201);

VZ(n,2)=Z(n,501);

VZ(n,3)=Z(n,1001);

VZ(n,4)=Z(n,3651);

VZ(n,5)=Z(n,7301);

end
```

MATLAB Codes-Physicochemical Diffusion Modeling

Explicit Method:

```matlab
%====================Basic Parameters===================

format compact

U0=30;%The sulfate concentration of the aggressive solution(mol/m^3)

C0=100;%The initial concentration of CA(mol/m^3)

G=2.8;%Lamda,the weighted average stoichiometric coefficient of the lumped reaction for CSH2

D=1.296e-7;%Diffusion coefficient(m^2/d)

k=8.64e-4;%The rate constant of reaction(mol/(m^3*d))

dX=0.001;%Space step(m)
```

```
dT=1;%Time step(d)

M=7300;%Number of subdomain of simulated time

N=100;%Number of subdomain of space of diffusion field

%==================Solving Z============================

r=D*dT/dX^2;%Variable substitution

b=k*dT/G;%Variable substitution

Z=-G*C0*ones(N+1,1);%Z initial linear array

for j=[1:M]%Iteration for time field

        Z(1,j+1)=U0;%Boundary condition

        for i=[2:N]%Iteration for space field

            Z(i,j+1)=r*Z(i+1,j)+(1-2*r)*Z(i,j)+r*Z(i-1,j);

        end

    Z(N+1,j+1)=(1-2*r)*Z(N+1,j)+2*r*Z(N,j);

end

%======================SOLVING U============================

U=[U0;zeros(N,1)];%Sulfate concentration U initial linear array

for j=[1:M]%Iteration for time field

    U(1,j+1)=U0;%Boundary condition

    for i=[2:N]%Iteration for space field

        U(i,j+1)=r*U(i+1,j)+(1-2*r-b*U(i,j)+b*Z(i,j))*U(i,j)+r*U(i-1,j);

    end

    U(N+1,j+1)=(1-2*r-b*U(N+1,j)+b*Z(N+1,j))*U(N+1,j)+2*r*U(N,j);

end

%=====================SOLVING C============================

C=(U-Z)/G;%Calculation of C

C(1,1)=C0;
```

```
%==========OUTPUT Z IN DIFFERENT TIME============================
for n=[1:101]
    VZ(n,1)=Z(n,201);
    VZ(n,2)=Z(n,501);
    VZ(n,3)=Z(n,1001);
    VZ(n,4)=Z(n,3651);
    VZ(n,5)=Z(n,7301);
end
save VZ.mat VZ
%======OUTPUT SULFATE CONCENTRATION U IN DIFFERENT TIME======
for n=[1:101]
    VU(n,1)=U(n,201);
    VU(n,2)=U(n,501);
    VU(n,3)=U(n,1001);
    VU(n,4)=U(n,3651);
    VU(n,5)=U(n,7301);
end
%========OUTPUT CA CONCENTRATION C IN DIFFERENT TIME=========
for n=[1:101]
    VC(n,1)=C(n,201);
    VC(n,2)=C(n,501);
    VC(n,3)=C(n,1001);
    VC(n,4)=C(n,3651);
    VC(n,5)=C(n,7301);
end
%======OUTPUT ETTRINGITE PRODUCTION E IN DIFFERENT TIME========
```

```
for n=[1:101]

VE(n,1)=C0-C(n,201);

VE(n,2)=C0-C(n,501);

VE(n,3)=C0-C(n,1001);

VE(n,4)=C0-C(n,3651);

VE(n,5)=C0-C(n,7301);

end
```

%===================END=================

Crank-Nicolson Method:

```
%====================BASIC PARAMETERS========================

U0=30;%The sulfate concentration of the aggressive solution(mol/m^3)

C0=100;%The initial concentration of CA(mol/m^3)

G=2.8;%Lamda,the weighted average stoichiometric coefficient of the lumped reaction for
CSH2

D=1.296e-7;%Diffusion coefficient(m^2/d)

k=8.64e-4;%The rate constant of reaction(mol/(m^3*d))

dX=0.001;%Space step(m)

dT=1;%Time step(d)

M=7300;%Number of subdomain of simulated time

N=100;%Number of subdomain of space of diffusion field

%=====================SOLVING Z===========================

r=D*dT/dX^2;%Variable substitution

Z=-G*C0*ones(N+1,1);%Z initial linear array

U=[U0;zeros(N,1)];%Sulfate concentration U linear array

C=C0*ones(N+1,1);%CA concentration C linear array
```

az=-2*(1+1/r)*ones(N,1);%Diagonal element of Matrix AZ

bz=2*(1-1/r)*ones(N,1);%Diagonal element of Matrix BZ

dz(1)=-2*U0;

dz(2:N)=zeros(N-1,1);   %Linear array dz

%   Matrix AZ and BZ

AZ=sparse(diag(ones(N-1,1),1)+diag(ones(N-1,1),-1)+diag(az));

AZ(N,N-1)=2;

BZ=sparse(-diag(ones(N-1,1),1)-diag(ones(N-1,1),-1)+diag(bz));

BZ(N,N-1)=-2;

for j=[1:M]%Iteration solution of Z

   Z(2:N+1,j+1)=AZ\(BZ*Z(2:N+1,j)+dz');

   Z(1,j+1)=U0;

end

%=====================SOLVING U=============================

for j=[1:M]%Iteration for time field

BN(N)=k*dT/G*(U(N+1,j)+(D/dX^2*(U(N,j)-2*U(N+1,j)+U(N,j))-k/G*U(N+1,j)*(U(N+

1,j)-Z(N+1,j)))*dT/2);%Calculation of beta

   au(N)=-2*(1+1/r+BN(N)/2/r);%Diagonal element of Matrix AU

   bu(N)=2*(1-1/r+BN(N)/2/r);%Diagonal element of Matrix BU

   for i=[2:N]%Iteration for space field

BN(i-1)=k*dT/G*(U(i,j)+(D/dX^2*(U(i+1,j)-2*U(i,j)+U(i-1,j))-k/G*U(i,j)*(U(i,j)-Z(i,j)))*

dT/2);%Calculation of beta

     au(i-1)=-2*(1+1/r+BN(i-1)/2/r);%Diagonal element of Matrix AU

     bu(i-1)=2*(1-1/r+BN(i-1)/2/r);%Diagonal element of Matrix AU

```
    end

    du(1)=-2*U0-BN(1)*Z(2,j+1)/r-BN(1)*Z(2,j)/r;

    du(2:N)=-Z(3:N+1,j+1).*BN(2:N)'/r-Z(3:N+1,j).*BN(2:N)'/r;%Linear array d

    %    Matrix A and B

    AU=sparse(diag(ones(N-1,1),1)+diag(ones(N-1,1),-1)+diag(au));

    AU(N,N-1)=2;

    BU=sparse(-diag(ones(N-1,1),1)-diag(ones(N-1,1),-1)+diag(bu));

    BU(N,N-1)=-2;

    U(2:N+1,j+1)=AU\(BU*U(2:N+1,j)+du');%Solution of U

    U(1,j+1)=U0;

end

%========================SOLVING C============================

C=(U-Z)/G;%Calculation of C

C(1,1)=C0;

%==========OUTPUT Z IN DIFFERENT TIME========================

for n=[1:101]

VZ(n,1)=Z(n,201);

VZ(n,2)=Z(n,501);

VZ(n,3)=Z(n,1001);

VZ(n,4)=Z(n,3651);

VZ(n,5)=Z(n,7301);

end

%======OUTPUT SULFATE CONCENTRATION U IN DIFFERENT TIME=======

for n=[1:101]

VU(n,1)=U(n,201);

VU(n,2)=U(n,501);
```

```
VU(n,3)=U(n,1001);

VU(n,4)=U(n,3651);

VU(n,5)=U(n,7301);

end

%========OUTPUT CA CONCENTRATION C IN DIFFERENT TIME=========

for n=[1:101]

VC(n,1)=C(n,201);

VC(n,2)=C(n,501);

VC(n,3)=C(n,1001);

VC(n,4)=C(n,3651);

VC(n,5)=C(n,7301);

end

%======OUTPUT ETTRINGITE PRODUCTION E IN DIFFERENT TIME=======

for n=[1:101]

VE(n,1)=C0-C(n,201);

VE(n,2)=C0-C(n,501);

VE(n,3)=C0-C(n,1001);

VE(n,4)=C0-C(n,3651);

VE(n,5)=C0-C(n,7301);

end

%==================END=================
```

MIP TEST REPORTS

Blend IC after Sulfate Exposure

micromeritics®

MICROMERITICS INSTRUMENT CORPORATION

AutoPore IV 9500 V1.09	Serial: 445	Port: 2/1	Page 1

Sample ID: Sample IC
Operator: Ong
Submitter: Chiqian
File: D:\MERCURY\9500\DATA\NAM\CHIQIAN\CHI04-IC.SMP

LP Analysis Time: 9/9/2015 2:34:06PM
HP Analysis Time: 9/9/2015 4:10:13PM
Report Time: 9/9/2015 4:10:13PM

Sample Weight: 10.4100 g
Correction Type: Blank
Show Neg. Int: No

Summary Report
Penetrometer parameters

Penetrometer:	[05-0128] 15cc Bulb, 1.836cc Stem, Solid		
Pen. Constant:	27.820 µL/pF	Pen. Weight:	68.2700 g
Stem Volume:	1.8360 mL	Max. Head Pressure:	4.4500 psia
Pen. Volume:	16.4910 mL	Assembly Weight:	235.9800 g

Hg Parameters

Adv. Contact Angle:	130.000 degrees	Rec. Contact Angle:	130.000 degrees
Hg Surface Tension:	485.000 dynes/cm	Hg Density:	13.5335 g/mL

User Parameters

Param 1:	0.000	Param 2:	0.000	Param 3:	0.000

Low Pressure:

Evacuation Pressure: 50 µmHg
Evacuation Time: 5 mins
Mercury Filling Pressure: 2.01 psia
Equilibration Time: 10 secs

High Pressure:

Equilibration Time: 10 secs

Blank Correction Sample: D:\MERCURY\9500\DATA\BLANK-~1\05-0128.SMP
Blank Correction ID: [05-0128] 15cc Bulb, 1.836cc Stem, Solid, 23C

(From Pressure 0.10 to 60000.00 psia)

Intrusion Data Summary

Total Intrusion Volume =	0.0613 mL/g
Total Pore Area =	12.083 m²/g
Median Pore Diameter (Volume) =	484 A
Median Pore Diameter (Area) =	74 A
Average Pore Diameter (4V/A) =	203 A
Bulk Density at 2.01 psia =	2.1385 g/mL
Apparent (skeletal) Density =	2.4609 g/mL
Porosity =	13.1032 %
Stem Volume Used =	35 %

Pore Structure Summary

Threshold Pressure:	5.66 psia (Calculated)
Characteristic length =	319512 A
Conductivity formation factor =	0.001
Permeability constant =	0.00442
Permeability =	2.6594 mdarcy
BET Surface Area =	230.0000 m²/g
Pore shape exponent =	1.00
Tortuosity factor =	0.006
Tortuosity =	6.2723
Percolation Fractal dimension =	2.459
Backbone Fractal dimension =	2.555

Mayer Stowe Summary

Interstitial porosity =	47.6300 %
Breakthrough pressure ratio =	3.3512

Type GU after Sulfate Exposure

MICROMERITICS INSTRUMENT CORPORATION

AutoPore IV 9500 V1.09   Serial: 445   Port: 2/1   Page 1

Sample ID: Sample G
Operator: Ong
Submitter: Chiqian
File: D:\MERCURY\9500\DATA\NAM\CHIQIAN\CHI02-G.SMP

LP Analysis Time: 9/2/2015 6:26:05PM   Sample Weight: 10.7400 g
HP Analysis Time: 9/2/2015 8:41:02PM   Correction Type: Blank
Report Time: 9/3/2015 6:44:32PM   Show Neg. Int: No

Summary Report
Penetrometer parameters

Penetrometer:	[05-0128] 15cc Bulb, 1.836cc Stem, Solid		
Pen. Constant:	27.820 µL/pF	Pen. Weight:	68.2700 g
Stem Volume:	1.8360 mL	Max. Head Pressure:	4.4500 psia
Pen. Volume:	16.4910 mL	Assembly Weight:	234.4300 g

Hg Parameters

Adv. Contact Angle:	130.000 degrees	Rec. Contact Angle:	130.000 degrees
Hg Surface Tension:	485.000 dynes/cm	Hg Density:	13.5335 g/mL

User Parameters

Param 1:	0.000	Param 2:	0.000	Param 3:	0.000

Low Pressure:

Evacuation Pressure: 50 µmHg
Evacuation Time: 5 mins
Mercury Filling Pressure: 2.01 psia
Equilibration Time: 10 secs

High Pressure:

Equilibration Time: 10 secs

Blank Correction Sample: D:\MERCURY\9500\DATA\BLANK-~1\05-0128.SMP
Blank Correction ID: [05-0128] 15cc Bulb, 1.836cc Stem, Solid, 23C

(From Pressure   0.10 to 60000.00 psia)

Intrusion Data Summary

Total Intrusion Volume –	0.0635 mL/g
Total Pore Area –	3.327 m²/g
Median Pore Diameter (Volume) –	1089 A
Median Pore Diameter (Area) –	457 A
Average Pore Diameter (4V/A) –	763 A
Bulk Density at 2.01 psia –	2.1450 g/mL
Apparent (skeletal) Density –	2.4833 g/mL
Porosity –	13.6200 %
Stem Volume Used –	38 %

Pore Structure Summary

Threshold Pressure:	5.21 psia (Calculated)
Characteristic length –	347396 A
Conductivity formation factor –	0.000
Permeability constant –	0.00442
Permeability –	2.2701 mdarcy
BET Surface Area –	230.0000 m²/g
Pore shape exponent –	1.00
Tortuosity factor –	0.000
Tortuosity –	6.8125
Percolation Fractal dimension –	2.738
Backbone Fractal dimension –	2.293

Mayer Stowe Summary

Interstitial porosity –	47.6300 %
Breakthrough pressure ratio –	3.3512

Type HS after Sulfate Exposure

mi micromeritics®

MICROMERITICS INSTRUMENT CORPORATION

AutoPore IV 9500 V1.09	Serial: 445	Port: 2/1	Page 1

Sample ID: Sample H
Operator: Ong
Submitter: Chiqian
File: D:\MERCURY\9500\DATA\NAM\CHIQIAN\CHI03-H.SMP

LP Analysis Time: 9/3/2015 7:08:49PM
HP Analysis Time: 9/4/2015 1:15:47PM
Report Time: 9/8/2015 2:30:33PM

Sample Weight: 12.4900 g
Correction Type: Blank
Show Neg. Int: No

Summary Report

Penetrometer parameters

Penetrometer:	[05-0128] 15cc Bulb, 1.836cc Stem, Solid		
Pen. Constant:	27.820 µL/pF	Pen. Weight:	68.2700 g
Stem Volume:	1.8360 mL	Max. Head Pressure:	4.4500 psia
Pen. Volume:	16.4910 mL	Assembly Weight:	224.3200 g

Hg Parameters

Adv. Contact Angle:	130.000 degrees	Rec. Contact Angle:	130.000 degrees
Hg Surface Tension:	485.000 dynes/cm	Hg Density:	13.5335 g/mL

User Parameters

Param 1:	0.000	Param 2:	0.000	Param 3:	0.000

Low Pressure:

Evacuation Pressure: 50 µmHg
Evacuation Time: 5 mins
Mercury Filling Pressure: 2.01 psia
Equilibration Time: 10 secs

High Pressure:

Equilibration Time: 10 secs

Blank Correction Sample: D:\MERCURY\9500\DATA\BLANK-~1\05-0128.SMP
Blank Correction ID: [05-0128] 15cc Bulb, 1.836cc Stem, Solid, 23C

(From Pressure 0.10 to 60000.00 psia)

Intrusion Data Summary

Total Intrusion Volume =	0.0664 mL/g
Total Pore Area =	4.655 m²/g
Median Pore Diameter (Volume) =	857 A
Median Pore Diameter (Area) =	348 A
Average Pore Diameter (4V/A) =	570 A
Bulk Density at 2.01 psia =	2.1230 g/mL
Apparent (skeletal) Density =	2.4712 g/mL
Porosity =	14.0901 %
Stem Volume Used =	46 %

Pore Structure Summary

Threshold Pressure:	23.48 psia (Calculated)
Characteristic length =	77043 A
Conductivity formation factor =	0.002
Permeability constant =	0.00442
Permeability =	0.4560 mdarcy
BET Surface Area =	230.0000 m²/g
Pore shape exponent =	1.00
Tortuosity factor =	0.001
Tortuosity =	18.6994
Percolation Fractal dimension =	2.637
Backbone Fractal dimension =	2.599

Mayer Stowe Summary

Interstitial porosity =	47.6300 %
Breakthrough pressure ratio =	3.3512